UNIVERSITY OF BIRMINGHAM

The Effect of Casting Parameters on the Fluidity and Porosity of Aluminium Alloys in the Lost Foam Casting Process

By

Kiavash Siavashi

A thesis submitted to the Faculty of Engineering of

The University of Birmingham

For the degree of

Doctor of Philosophy

School of Metallurgy and Materials
College of Engineering & Physical Sciences
Birmingham B15 2TT
United Kingdom
September 2011

Abstract

The Lost Foam Casting process has been firmly established for Aluminium and ferrous alloys. This process offers many advantages over conventional casting processes but its full potential has yet to be reached due to the many defects introduced to the casting associated with decomposition of the foam pattern during mould filling. The foam pattern commonly used in this process is Expanded Polystyrene (EPS) which degrades to liquid and vapour byproducts. The liquid decomposition byproducts travel to the metal/mould interface, where the globules of liquid foam can become trapped against the coating and their molecular weight is reduced due to the heat from the molten metal. At the same time, they release bubbles of gas into the castings. These globules can wick into the refractory coating only if their molecular weight is sufficiently reduced to below a critical molecular weight.

In this study, to improve the quality of Aluminium alloys made by Lost Foam Casting, easier removal of the decomposition byproducts was obtained by using low molecular weight foam patterns. The molecular weight of expanded Polystyrene was not reduced when it was exposed to γ-rays because of cross-linking while the molecular weight of Poly Methyl Methacrylate (PMMA) was significantly due to chain session. Therefore, plates of Probead-70™ (a copolymer of Polystyrene 30 wt %-Poly Methyl Methacrylate 70 wt %) were exposed to γ-rays and reduced their molecular weight by up to about 85% below the critical molecular weight value. With low molecular weight foam patterns the decomposition byproducts require less reduction to reach the critical molecular weight to become absorbed by the coating, and consequently less defects are introduced into the casting. γ-radiation was employed to reduce the molecular weight of the foam. The porosity content of the castings was significantly reduced leading to an improvement of their mechanical properties such as their fatigue life which was increased by 100%.

Lost Foam Casting has also been reported to experience complexities with fluidity. Misrun is likely to occur in Lost Foam Casting due to the formation of a large amount of gas at the metal/foam interface, increasing the back pressure, compared to the conventional castings. This reduces the velocity of the molten metal which might lead to solidification of the molten metal before filling the mould entirely.

In the current work, a reproducible fluidity test was designed and the effects of different casting parameters on fluidity were examined. In some of the castings inserted thermocouples were employed to study the filling behaviour to determine the velocity of molten metal, thickness of the metal/foam interface and the time of freezing. It was concluded that it is not recommended to alter the coating thickness in order to improve fluidity, because the effect of coating thickness depends on the pouring temperature of the castings and permeability of the coating. The metallostatic pressure was found to affect the fluidity insignificantly (within the values in the current work, 2600-2700 Pa). Instead, increasing coating permeability, decreasing the density of the foam pattern and increasing the pouring temperature were found to increase the fluidity in Lost Foam Casting. However the effect of increasing pouring temperature and decreasing foam density may be detrimental to the quality of castings. The molecular weight of the foam pattern and the use of brominated foam patterns did not have a considerable effect on fluidity in Lost Foam Casting.

It was also found that solidification in the Lost Foam Casting occurs at the metal/foam interface. A heat balance between the molten metal and the mould, and the foam pattern, was developed to give a fluidity equation to aid interpretation of the fluidity results.

In summary, this research has provided a better understanding of the effect of casting parameters on the fluidity of Lost Foam Casting and the heat transfer from the molten metal to the foam pattern and to the mould. In addition, the quality of AL alloys castings was improved by reducing the molecular weight of the foam pattern used in the Lost Foam Casting process.

DEDICATION;

To my parents,

For their unwavering support through times of adversity.

ACKNOWLEDGMENTS

I offer my sincerest gratitude to my supervisor, Dr W.D. Griffiths, who has supported me throughout my thesis with his patience and knowledge. I attribute the achievement of my PhD degree to his encouragement and effort and without him this thesis, too, would not have been completed or written. One simply could not wish for a better or friendlier supervisor.

In the various experiments I have been aided in running the equipment by Adrian Caden, a fine technician. Peter Cranmer has also inadvertently, and without fail, provided something much greater in all the years I've known him: a friendly smile and a hello every time we met. I would also like to express my thanks to other staff at the School of Metallurgy and Materials.

The author wishes to express his gratitude to Dr. Clare Topping of Isotron (Daventry, UK) for her assistance in irradiation processing of the foam patterns. Deepest gratitude is also due to Dr. Steve Holding of Smithers RAPRA for Gel Permeation Chromatography work.

Special thanks are also due to Professor Robert Hill of Imperial College for sharing his novel ideas.

Finally, I would like to express my deepest thanks to my parents for supporting me graciously and providing me the conditions before and throughout all my studies at University.

Contents

1 INTRODUCTION

Lost Foam casting (LFC) is a relatively new casting process using an expanded foam pattern which degrades during the casting process, because of the heat provided by the liquid metal. Therefore, the foam pattern does not require removal from the mould; this offers many advantages such as freedom in design, allowing complex parts to be easily made and removing the need for the cores [1].

This process depends upon a variety of independent processes such as pattern making, moulding and casting. Depending upon the alloy cast the foam pattern used in the LFC process can differ. The most commonly used foam is expanded polystyrene (EPS) and copolymers of polystyrene (PS) and poly methyl methacrylate (PMMA) [2]. The pattern segments are glued together and then glued to the running and gating system to make a cluster. The cluster is then coated with a slurry to give a refractory coating when dry, and placed in the mould container and surrounded by dry, loose sand. Compaction of the sand is brought about by vibration [3]. The liquid metal is then poured onto the cluster and the heat from the molten metal decomposes the foam pattern and replaces its shape in the mould. This casting process facilitates casting of a complex casting with several components in a single large casting to avoid subsequent machining and assembly operations.

Lost Foam Casting (LFC) is used in the automotive industry for products such as cylinder heads, exhaust manifolds, pumps and valve bodies. LFC process can be carried out with aluminium, ferrous and copper based alloys [4]. While the LFC process has many advantages, such as being a readily automated process, allowing a reusable sand system, freedom in design and freedom from cores, etc, the production of high quality castings is difficult [5]. In conventional casting methods the liquid metal flows into an empty cavity but in the case of

LFC the flowing liquid metal interacts with the foam pattern and the liquid metal flow is controlled by the rate of pattern decomposition [6]. As the foam pattern has to eliminate ahead of the molten metal stream, the decomposition byproducts can easily become trapped inside the flowing molten metal and cause a variety of defects such as folds, pores and surface blisters; thus the removal mechanism of the decomposition byproducts from the mould is the key parameter in having a high quality casting [5, 7]. Davies and Griffiths put forward a mechanism suggesting that the liquid byproducts of the foam pattern decomposition are drawn to the casting/coating interface but then their average molecular weight (M_w) has to reduce to reach a critical M_w (which depends on the coating permeability) in order to be wicked into the coating and leave the mould [8].

Another issue in the LFC process is misrun, as the heat required to degrade the foam pattern is supplied by the liquid metal and this endothermic reaction takes place constantly during the casting process at the metal/foam interface [9] this causes a reduction in the temperature and the velocity of the liquid metal front. This may result in solidification of the flowing liquid metal before complete filling of the foam pattern.

Unfortunately, the effect of casting parameters on the fluidity of LFC is not very well known despite previous work [10-13]. A fluidity model is still required to address the fluidity of LFC as there have been contradictory reports about the effect of different casting conditions on the fluidity of LFC.

The current work is aimed at two main objectives; firstly, to explain the effect of different parameters on the fluidity of LFC, in parallel developing a fluidity equation for the LFC process. Secondly, it was also aimed at investigating and bringing about easier removal of the decomposition byproducts from the mould to improve the quality of Lost Foam Castings.

2 LITERATURE REVIEW

2.1 The Lost Foam Casting process

In the Lost Foam Casting (LFC) process, expanded polystyrene (EPS) and copolymers of polystyrene (PS) and poly methyl methacrylate (PMMA) are commonly used. Pieces of foam pattern are assembled together to make a cluster, which is then coated, dried and finally surrounded by unbonded dry sand, compacted by vibration. Once the molten metal is poured into the mould, heat from the liquid metal decomposes the foam pattern and the decomposition byproducts are removed from the mould. The foam pattern is therefore completely replaced with the liquid metal. This process has become established for some aluminium automotive parts as well as some ferrous and copper based alloys. The stages of the Lost Foam Casting (LFC) process are shown in Figure 2-1.

It has been claimed that the Lost Foam Casting process offers many advantages, such as simplicity of operation, dimensional accuracy, high casting yield, readily automated production, great versatility, a reusable sand system, excellent surface finish and good Ultimate Tensile Strength (UTS) [14]. The process also does not require cores as intricate interior channels can be incorporated into the foam patterns.

Production of foam patterns is a three-step process: pre-expansion of expandable polystyrene (PS) beads to make a pre-puff of correct density, followed by stabilization or aging and finally moulding of the foam beads into the desired pattern shape [15].

The pieces of expanded polystyrene (EPS) pattern are joined together using hot melt glue to make a cluster then coated with a refractory slurry with a typical thickness of 0.5 mm (the coating thickness is variable). When the coating is dried, the cluster is subsequently invested with dry sand which is vibrated around the cluster to fill all internal passages and maintain the

shape of the cluster during the process. The molten metal is then poured into the pattern, where it decomposes the foam and replaces the volume that the foam originally occupied in the sand. The molten metal stream pushes the liquid and gaseous byproducts of the polymer degradation to escape into and through the refractory coating, but the main task of the coating is to support the surrounding sand during the brief interval of gasification of the pattern and its replacement by the molten metal [16]. The coating is a region where a complex combination of mass flux of the foam degradation byproducts and heat flux occur [17].

Although this is a readily automated process with many advantages, LFC can be associated with poor mechanical properties because the foam degradation byproducts are trapped in the advancing liquid metal and cause porosity and other defects [18]. Fluidity is also an issue in LFC (i.e. misrun), because of the heat energy supplied by the liquid metal to degrade the foam. Therefore, a model to understand the fluidity of LFC is required in order to minimise the misrun failures [19].

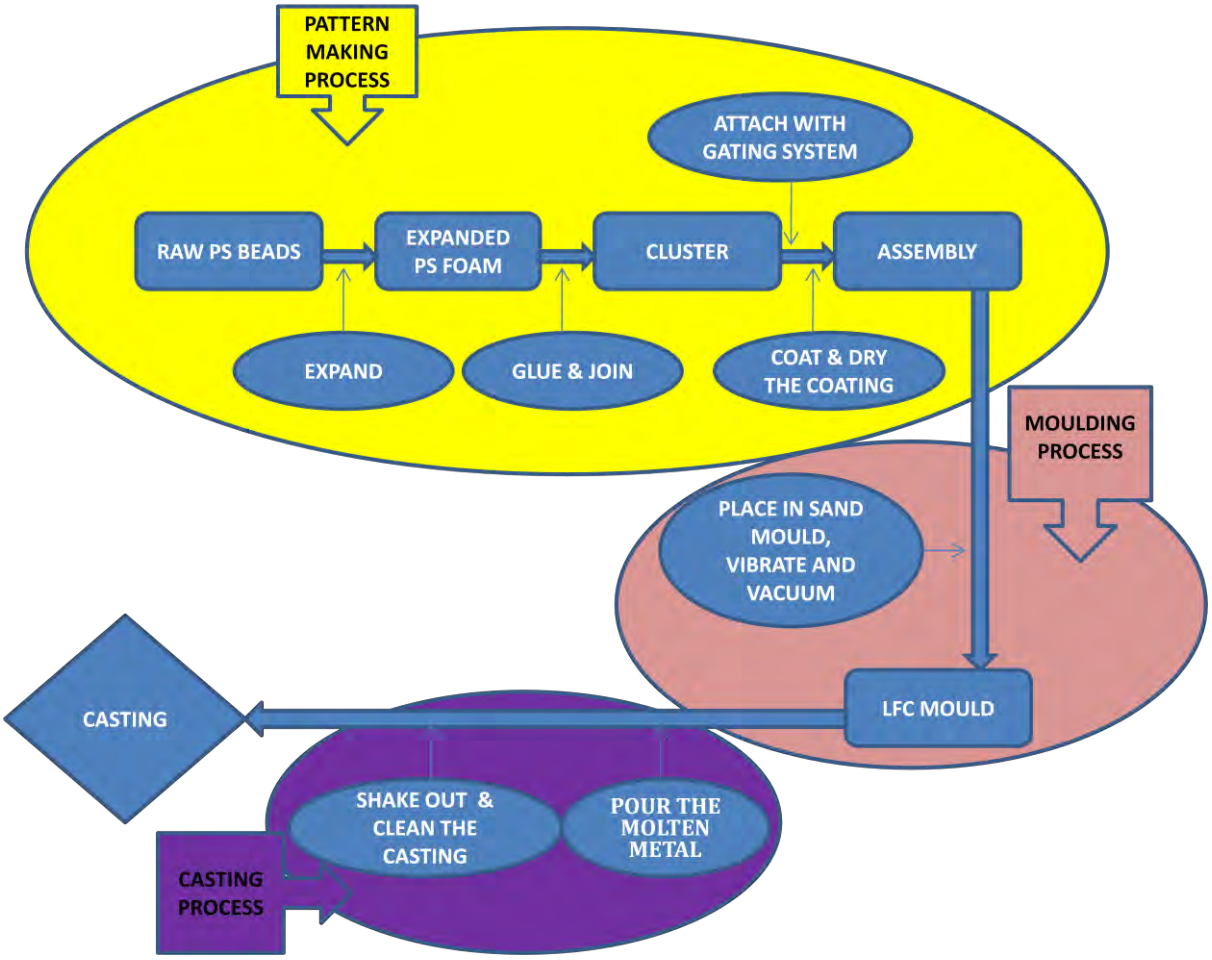

Figure 2-1. Steps of Lost Foam Casting process.

2.1.1 Foam patterns in LFC

As was mentioned EPS is one of the foam pattern materials used in the LFC process. The styrene monomer is a colourless aromatic liquid of molecular formula C_8H_8. Styrene is one of the few substituted alkenes that will readily polymerise by free radical and anionic mechanisms as a result of the ability of the aromatic ring to stabilise the propagating species. Polymerisation of styrene monomers is a highly exothermic reaction (71 $kJmol^{-1}$). In the polymerization of styrene, one carbon-carbon double bond is replaced by a stronger carbon-carbon single bond, resulting in difficult depolymerisation of polystyrene. Typically a chain of polystyrene consists of about a few thousand monomers, giving a M_w of 100,000-400,000

$gmol^{-1}$. The styrene monomer and the product of its polymerization (polystyrene) is shown in Figure 2-2 [20].

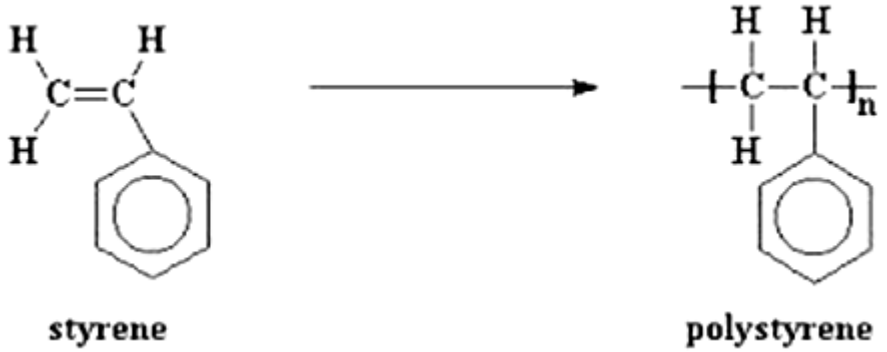

Figure **2-2. The chemical composition of polystyrene and the results of its polymerization.**

The M_w of the expanded polystyrene foam pattern used in LFC was measured using Gel Permeation Chromatography (GPC) and has an approximate value of 280,000 $gmol^{-1}$ ± 5,000 [21].

Poly methyl methacrylate (PMMA) is normally used to make a copolymer used in LFC (normally with polystyrene). PMMA is formed from the free radical addition polymerisation of methyl methacrylate. The glass transition temperature of commercial grades of PMMA varies from about 80 to 160 °C. N unit of PMMA is shown in Figure 2-3 [22].

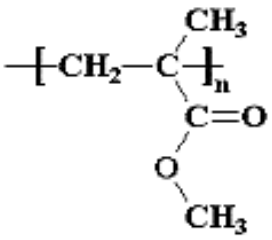

Figure 2-3. Chemical formula of PMMA.

Two copolymers produced by Foseco plc are Probead-70™ and Probead-30™. Copolymer Probead-70™ consists of 70wt.% PMMA and 30wt.% PS and copolymer Probead-30™ consists of 30wt.% PMMA and 70wt.% PS. Copolymer Probead-30™ is produced in two

different densities, (Copol 1.3 and Copol 1.5, having densities of 1.3 and 1.5 $lbft^{-3}$ (or 21 and 24 kgm^{-3}) respectively). These are normally used for cast iron LFC. The molecular weight of the expanded copolymers can occur over a range depending on the copolymerization process.

2.1.2 Foam Pattern Production

Styrenic polymer foams are produced commercially by extrusion and moulding of the molten polymer or by expansion moulding of polymer particles. Due to concern over the volatile organic compounds, a reduction in the level of blowing agents is aimed at during foam pattern production. Polystyrene particles can be prepared by polymerizing styrene in aqueous suspension in the presence of chain-transfer agents or styrene oligomers [23]. Production of expanded polystyrene is started by stirring the solution of styrene with an initiator and a suspension agent finely distributed in water, in a reactor, at about 90 ^{o}C. This can result in production of polystyrene foam with a variety of bead sizes. Different bead sizes are produced subject to the required application; closed beads with a typical diameter of 2 to 4 mm; (‘’T’’ grade beads) are mostly used in the LFC process [24], [2]. However different grades of beads are used when certain properties are demanded [25]. For example “X” and “D” grades beads are used for thinner section and large part casting, respectively [25].

During the moulding of the pattern, the pre-expanded beads are injected into the mould and heated above the glass transition temperature of the polymer [26, 27]. Expansion of the polystyrene beads is carried out using a blowing agent at about 115 ^{o}C, the polystyrene beads become expanded by as much as forty times their initial size [2]. The remaining blowing agent in the beads leads to further expansion of the beads. The bead fusion process affects the properties of the castings significantly, such as the formation of fold defects. The moulding

conditions determine the degree of fusion between the beads and can be controlled to produce different foams [26, 27].

Since easy degradation of the foam pattern is desirable in the LFC process, organic brominated additives have been included in EPS patterns in recent years. These release hydrogen bromide gas at high temperatures [28] (during casting) which speeds up degradation of the foam pattern and increases the quality of castings [25, 29] probably because of reduction in entrapment of the decomposition byproducts into the advancing molten metal. Chemical structure of some organic brominated foam patterns are shown in Figure 2-4.

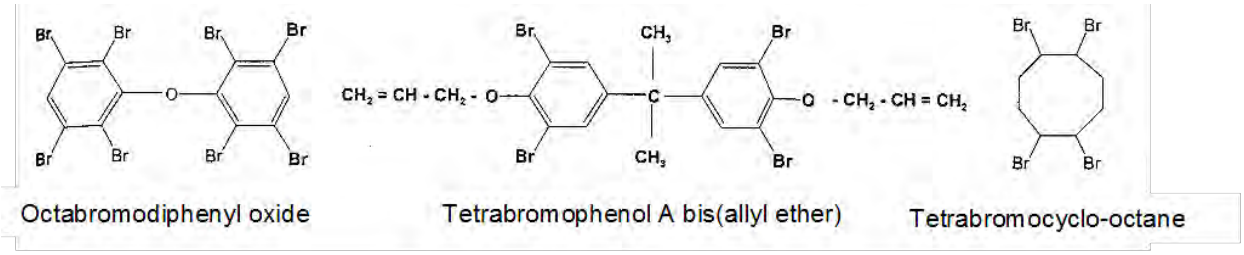

Figure 2-4. The chemical structures of some organic brominated additives [25].

2.1.3 The pattern coating

In the LFC process, the manufactured pattern is given a layer of a permeable refractory coating.

The coating layer can be applied to the surface of the foam pattern by dipping the cluster into a slurry of refractory particles such as alumina, silica and mica, with binders of polyvinyl acetate, dextrines, acrylics, etc [30]. The coating thickness after drying depends on the viscosity of the coating slurry [30-32], normally measured by a "Baume meter" which determines the Baume scale. Commercial coatings are presented as pre-mixed slurries and can be diluted by adding water. It is suggested that the coated pattern assembly should then be

completely dried at a temperature of up to 66 ^{o}C as air drying does not completely remove the internal moisture [33].

Assuming the interface between the molten metal flow and the foam pattern to be smooth and convex, most of the decomposition byproducts are carried ahead of the molten metal stream and gradually drawn to the sides of the mould, where they can become absorbed by the permeable pattern coating. The gaseous byproduct of decomposition also passes through the permeable coating [34].

Previous work has shown that most of the defects found in LFC are associated with the removal mechanisms of the foam decomposition byproducts from the casting section [16, 19, 35-37]. Therefore the refractory coating is expected to have certain characteristics of permeability to ease removal of the byproducts.

2.1.3.1 Coating permeability

The rate of byproduct escape from the mould is determined by the permeability of the applied coating. Decomposition byproducts of the foam pattern pass through the coating layer easier if the coating has higher permeability [30].

A method to measure the coating permeability was developed which employed a layer of coating applied to a mesh disc, obtained by dipping in the slurry coating. A flow of air was then passed through the disc and the permeability of the coating was measured based on the pressure drop across the coating using Darcy's law [38, 39].

Davies measured the permeability of commercial coating types using this method. He found a value of 9.3×10^{-14} m^2 for a medium permeability coating and a permeability value of 1.5×10^{-13} m^2 for an identical thickness of low permeability coating (0.33 mm). However, in thicker coatings (0.6 mm thickness), the permeability values obtained for the medium

permeability coating and the low permeability coating were very similar, 6.7×10^{-14} and 6.3×10^{-14} m^2, respectively [21].

The permeability values obtained for a high permeability coating were considerably higher than those of the low and medium permeability coatings. For example, when the thickness of the high permeability coating was 0.33 mm, a permeability value of 1.2×10^{-12} m^2 was obtained, approximately thirteen and eight times higher than the value obtained for the low and medium permeability coatings [21].

2.1.4 Moulding

Dry unbonded silica sand is normally used in the LFC process for moulds. Once the coated assembly is placed into a moulding box, it is surrounded by dry loose sand. The mould is fixed on a vibrating table with an adjustable vibration frequency, and the sand is compacted against all surfaces [38, 40]. The best compaction is suggested to occur using both horizontal and vertical vibration with a 90^o phase difference [41]. Distortion of the cluster, especially in the case of thin foam patterns, is a potential problem which might occur during the sand compaction process [40, 41].

2.2 Mould filling in LFC vs. conventional casting methods

In this section, the difference in mould filling behaviour of LFC and other casting methods is briefly reviewed.

A transparent window has been used to study flow in the LFC process and the interaction between the foam pattern and the molten metal to obtain a visual understanding of the metal/foam interface. However this does not reflect the actual interface in LFC as the transparent window is not a porous layer and will change the nature of the interface because

the gaseous byproducts of foam degradation are not able to pass through or the liquid byproducts be absorbed by the glass. Therefore, a large thickness of the metal/foam interface has been reported when a transparent window was used to observe the filling behaviour of LFC [42].

During the casting process, the molten metal flows into the cluster due to the difference in pressure between the pouring cup and the ingates. For conventional empty cavity gravity castings the flow does not encounter a high back pressure compared to LFC [43]. Tseng and Askeland measured the velocity of the flow in the LFC process and compared it with conventional casting [44]. This was also carried out by Shivkumar and Gallois, [34, 45] and they established that the typical metal flow velocity for LFC was of order of 0.1 ms^{-1}, compared to 1 ms^{-1} in conventional castings.

LFC has also a higher cooling rate compared to empty cavity casting methods. An endothermic reaction takes place constantly during the casting process at the metal/foam interface which produces a chilling effect by the foam pattern degradation on the metal flow [9].

In recent years, real time X-ray observation has been used to clarify features of mould filling in the LFC process [1, 18, 46]. For example, Figure 2-5 shows the filling of an EPS plate by Al alloy 2L99.

Inserting a series of thermocouples in the foam pattern and recording their changes in temperature is another method used to determine the position of the metal flow front and study the flow characteristics in LFC. In this method, the position of the metal flow front is identified when the temperature recorded by a thermocouple shows a sudden increase [7, 34].

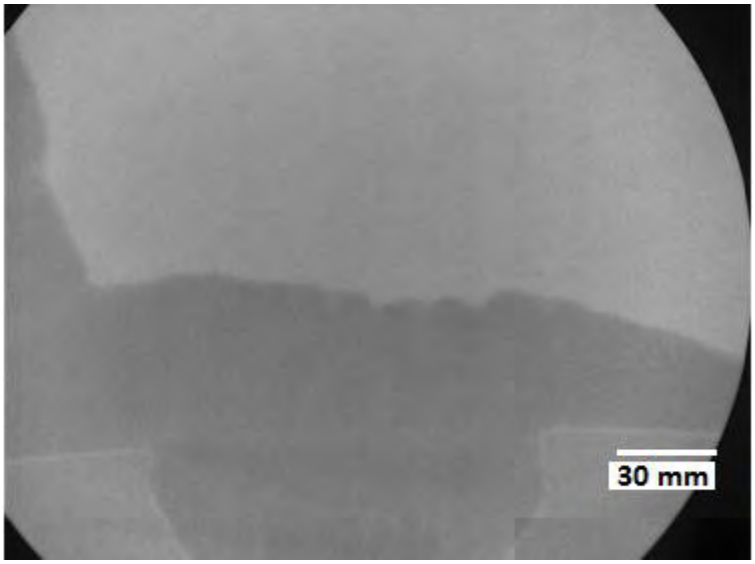

Figure 2-5. The real-time X-ray image showing filling of an EPS plate with molten Al alloy 2L99.

2.3 Polystyrene decomposition

The term decomposition is referred to the breakdown of the polymer chains into simpler fragments. A reduction in average molecular weight of the product is a common result of any polymer degradation process. The agencies which can cause degradation reactions in polymers are mainly categorized into physical factors (heat, light, etc) and chemical factors (oxidation, hydrolysis, etc).

Physical or chemical factors lead to either chain scission reactions (depolymerisation) or non chain scission reactions (separation of volatile and non-volatile fragments). Thermal reaction in linear polymers is suggested to be due to random scission of interunit bonds or the exact reverse of polymerization (depolymerisation). The products of thermal depolymerisation (at 350-420 ^{o}C) have been divided into four fractions. The most volatile fraction is present in a gaseous form at room temperature and consists mostly of carbon dioxide. Secondly, the non-volatile fraction is a residue consisting of large fragments of polystyrene chains which reduce in size as the degradation process continues. The third fraction, also non-volatile, consists of mainly monomers of styrene with smaller quantities of toluene and traces of ethyl-benzene

and methyl-styrene. Finally the fourth fraction is volatile at degradation temperatures, but non-volatile at room temperature, and has an average molecular weight of about 250 $gmol^{-1}$. Volatile materials are rapidly produced in the early stages of degradation at temperatures higher than 340 ^{o}C. This then reduces the production rate of monomers in the later stages of the degradation process [47].

There has been much research carried out on the degradation of EPS foam patterns [42, 48-56].

When solid EPS is heated to more than 100 ^{o}C chain scission starts to occur. Further heating then causes reduction in the molecular weight of the foam accompanied by a collapse and reduction in the volume of almost 4000% [34]. This is in agreement with Shivkumar [57] who also determined the physical changes during degradation of EPS and PMMA foam patterns during mould filling. He stated that, in the case of EPS, the foam had a glass transition at 80 to about 100 ^{o}C, and collapsed at a temperature of about 110 to 120 ^{o}C. At about 160 ^{o}C the collapsed polystyrene started to melt. The peak volatilization temperature started at about 275-300 ^{o}C, peaked at 400-420 ^{o}C and ended at 460-500 ^{o}C. The heat of degradation for EPS foam pattern material was calculated to be 912 Jg^{-1}. It was also claimed that the amount of gas produced during vaporization of the foam pattern was not changed at different temperatures and had a value of 205 ± 25 cm^{3} (STP) per gram of polystyrene.

Further investigation of the decomposition of EPS was continued by Shivkumar et al. to understand the physical form of the decomposition byproducts at higher temperatures. They reported that at 750 ^{o}C, the fraction of liquid viscous residue formed upon degradation of the polymer pattern was about 60% for casting with EPS and 30% for casting with PMMA foam patterns. Only a fraction of polymer degraded to gaseous byproducts and a significant amount

was not decomposed and remains in the mould even after it is filled, (in the case of casting with aluminium alloys) [55].

Shivkumar and Gallois also reported that the liquid byproducts appeared glassy when cooled to room temperature and had a brownish colouring depending on the degree of pyrolysis. Formation of liquid residue of PS from foamed EPS was claimed to occur mainly at the metal front, however it can also happen due to contact between gaseous byproducts and solid EPS because of incomplete decomposition of foamed EPS due to the relatively low temperature of the gaseous byproduct (compared to liquid metal). Therefore, the amount of liquid residue of PS formed during the casting process is proportional to the area of the metal front. Liquid byproducts form at a significant distance from the molten metal front and survive for periods of the order of seconds at lower temperatures (up to 400 ^{o}C) compared to gaseous byproducts [34].

They also established that the enthalpy of the transformation from foamed EPS to the gaseous byproduct of decomposition was more than 1350 Jg^{-1}. The transformation of solid to liquid residue of polystyrene (consisting totally of monomers) required 965 Jg^{-1} of heat energy (this was significantly found to be about 912 Jg^{-1} by Shivkumar [57]). However the heat of vaporization had a value of 385 Jg^{-1} if the gaseous byproduct of polystyrene degradation consisted entirely of monomers [34]. It was also claimed that the thermal energy is transported into the sand by both heat and mass transfer, however the rate of this transfer depended on the nature of the sand, coating and polymer [54].

Shivkumar et al. [55] also determined that the volume of gases produced at 750°C and 1300°C was about 220 cm^3 (STP)/g and 760 cm^3 (STP)/g respectively. They carried out casting experiments with thermocouples inserted into the foam pattern connected to data acquisition system. The foam patterns were also covered by a transparent glass window to

study the flow behaviour. The fraction of liquid viscous residue increased with temperature in the interface but was essentially constant above about 650 °C. During the filling of EPS patterns with liquid metal, nearly 60% of the polymer was converted to a viscous residue and 40% was transformed to gaseous products. In the case of PMMA, almost 60% of the polymer undergoing degradation at the metal front was transformed to gaseous products. They also reported that the molten metal velocity in LFC with PMMA patterns was lower than that with EPS. In the case of casting with EPS patterns, no gas layer was detected at the metal front up to about 525°C. The thickness of the gas layer with PMMA patterns was larger than that of the casting with EPS patterns, presumably because of the greater evolution of gas.

2.4 Removal mechanisms of decomposition byproducts

Significant effort has been put into studying the removal mechanisms of the degradation byproducts over the last 20 years, for example, by Zhao et al. [42], Shivkumar and Gallois [34], Liu et al. [49], Caulk [53], Barone and Caulk [48], Molibog and Littleton [52], Sun et al. [58], Hill et al. [59] and Davies and Griffiths [8]. As was mentioned in the last section, the foam decomposition by-products consist of vapour and liquid polymer. It is intended that the permeable refractory coating on the pattern allows the vapour byproducts to escape and also absorbs the liquid polymer residue.

In the case of Al casting, an EPS pattern breaks down predominantly to a viscous liquid residue which is transported to the metal-coating interface where it is thought to be wicked into the permeable coating [58], although alternative suggestions have been put forward [42].

Sun et al. [58] suggested that at a critical temperature of the liquid decomposition byproducts and the coating, the liquid polystyrene can wet the coating surface. They determined temperatures of 370 ^{o}C and 510 ^{o}C for wetting the high and low permeability coating,

respectively. When the temperature is increased further, the liquid residue can become absorbed by the coating.

Zhao et al. [42] cast EPS foam pattern at about 790 ^{o}C and reasoned that, because the boiling temperature of the foam is at least 300 ^{o}C below the pouring temperature (about 440 ^{o}C), the liquid polystyrene cannot exist in direct contact with the molten metal and gasification is unavoidable. They suggested that liquid polystyrene globules become trapped against the coating, and then vaporize to reduce their M_w when liquid metal passes over them and heats the globules until they reduce their size until they disappear completely from the casting channel as they convert completely to vapour, as shown in Figure 2-6. The gasification theory was supported by the results of interrupted casting experiments; SEM images of the coating near the interrupted metal front revealed continuous carbon-rich plastic globules which they claimed indicated that the liquid polymer was vaporized and released gas to the coating, with no evidence of liquid polymer transportation to the coating. This contradicts the results of the experiments performed by Davies who observed low molecular weight decomposition byproducts attached to and absorbed by the coating [21].

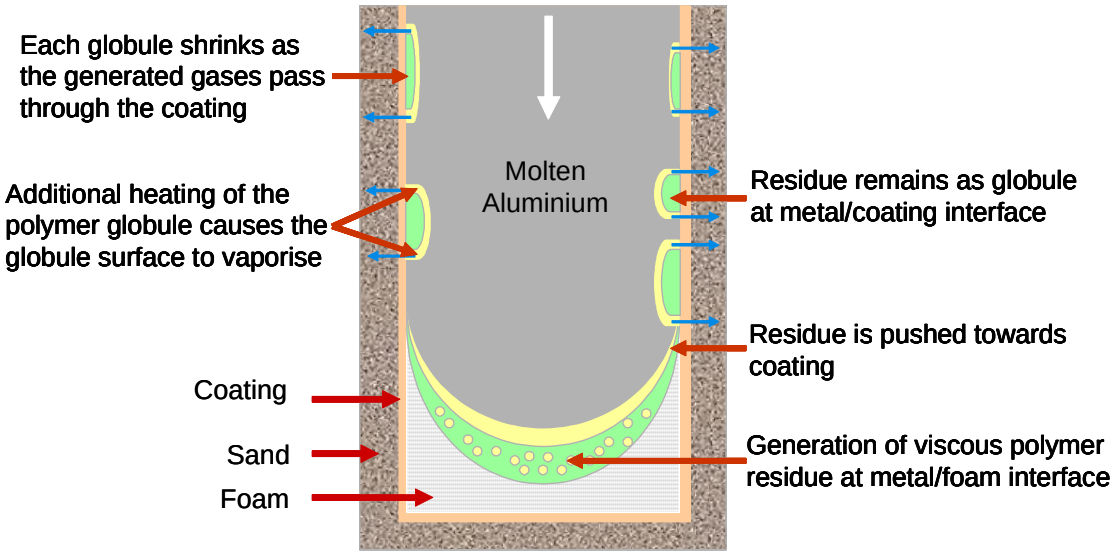

Figure 2-6. Gasification-driven foam removal mechanism [21]. (Re-drawn from Zhao et al [42]).

Davies [21] carried out a detailed investigation to understand the absorption of the liquid foam pattern decomposition byproducts into the coating. They measured the molecular weight of degradation by-products attached to and absorbed by the coating and concluded that a critical molecular weight, and hence critical viscosity, was necessary for its absorption into the pattern coating. For example, for a coating permeability of 1.2 x 10^{-12} m^2 (high permeability coating), the polystyrene foam pattern, with initial M_w of 325,000 $gmol^{-1}$, was wicked into the coating once the M_w of the liquid degradation byproduct had reduced to 70,000-75,000 $gmol^{-1}$, while a M_w value of 10,000 to 15,000 $gmol^{-1}$ was needed for absorption by a low permeability coating. Therefore, it was suggested that the rate of degradation of the expanded polystyrene in the LFC process depended on the temperature of the polymer and the time period for which the polymer had been heated, and that wicking occurred after sufficient degradation, in that the viscosity and the M_w of the liquid residue were reduced sufficiently to become wicked into the coating pores.

2.5 Metal/foam interface

The interaction between the flowing metal and the foam pattern has also been studied. Some models assume the formation of a narrow zone between the molten metal and the pattern in the LFC process [38, 60, 61] while Barone and Caulk [48] have suggested different models for the metal/foam interaction.

Barone et al. [48] suggested four different physical mechanisms for foam decomposition in the LFC process, affected by the shape of the interface between the foam pattern and the molten metal. The “contact mode” occurs when the molten metal is initially in contact with the foam pattern directly leading to ablation. Ablation is when the boundary cells are collapsed and creates an undercut in the pattern next to the casting/coating interface.

Secondly, a “gap mode” is suggested, in which a gaseous layer forms between the foam pattern and the molten metal, due to melting and vaporization of the foam pattern. The “collapse mode” is when the foam pattern collapses and releases air ahead of the metal front with the air passing into the pattern through the foam porosity. As was described, a convex metal front profile is desirable in filling of the LFC process. A concave metal front leads to the entrapment of pieces of foam into the metal advance described as the “engulfment mode”. Barone and co-workers did not analyse the ”collapse” and “engulfment” modes as they referred to them as random occurrences which are difficult to model [49].

As was mentioned in previous sections, the collapse of the EPS foams occurs at about 110-120 ^{o}C, releasing a large amount of air between the liquid metal and the rest of the foam which may slow down the heat transfer from the molten metal to the foam pattern [62]. At about 160 ^{o}C, polystyrene starts melting [57] the viscous liquid residue of polystyrene is driven ahead of the molten metal flow [55, 63], and/or becomes drawn to the mould wall if the molten metal front forms a convex profile [7, 60]. In the case of formation of a concave metal front the decomposition byproduct (the liquid fraction mostly) is inclined to gather at the metal/foam interface; hence, there is a good chance that the decomposition byproducts can become trapped in the liquid metal flow and form a variety of defects such as porosity [21].

The amount of released gas and air during decomposition of the foam pattern is an important parameter affecting the size and shape of the metal/foam interface. Most of the foam vaporization starts at temperatures above 300 ^{o}C [34], the viscous liquid polystyrene starts to vaporize before becoming trapped against the pattern coating, close to the hot liquid metal [17]. Shivkumar et al. [34] and Molibog et al. [60] performed experiments to determine the production rate and fraction of viscous liquid residue byproduct. As was mentioned Shivkumar [57] measured the volume of the evolved gas from complete degradation of 1

gram of polystyrene to be 205 $\pm 25\ cm^3$ (STP). Therefore, it can be assumed that a large amount of gas is evolved from the decomposition of the polystyrene foam pattern. The rate of gas evolution per time is increased at higher temperatures; for example, the fraction of gaseous byproducts is much higher in the case of ferrous alloy LFC compared to Al alloys [63, 64].

The metal/foam interface can also be influenced by casting parameters such as the molten metal velocity, the casting temperature, etc. The effect of the velocity of flowing metal on the metal/foam interface was studied by Ainsworth and Griffiths [46]. They filled some foam plates from the bottom under the influence of gravity and in counter gravity filling conditions. Filling of the foam plates was observed using real time X-ray to study the effect of different casting conditions, especially velocity of filling on the metal/foam interface and castings quality. They concluded that when the plates were filled with a velocity of 12 mms^{-1}, the advancing liquid metal front (in the case of aluminium alloys) divided into short fingers which led to entrapment of pattern degradation byproducts into the metal stream. But when the filling velocity was 5 mms^{-1} the liquid metal stream advanced with a planar interface with the foam pattern and less or no entrapment occurred.

The effect of temperature on the physical properties of the interface was investigated by Yang et al [63]. They carried out experiments to test if the temperature at which the foam decomposition occurred affected the gas fraction of decomposition byproducts and concluded that the gas fraction was increased by increasing the temperature of decomposition. They also obtained some values for interfacial pressure in the metal/foam interface; the interfacial pressure for an aluminium casting using EPS foam pattern coated with a high permeability coating was less than half of the interfacial pressure in the case of an iron casting with the

same casting design, condition indicating that the pressure at the metal/foam interface of the LFCs with a high melting point alloys is higher.

The length and the morphology of the interface was also investigated by Yang et al. [63] who proposed a transformation zone to exist between the foam pattern and the advancing liquid metal, having a length of 3.1 mm and consisting of two different layers, so that the EPS decomposition underwent different stages (i.e. collapse, melting and vaporization), as shown in Figure 2-7. Firstly, there is a zone of collapsed foam which has shrunk but has not decomposed yet, with a length of 1.1 mm, and secondly a melt zone [63]. This is in agreement with other work [52, 60] that suggested that the melt zone (with a length of 2 mm) contained decomposition byproducts in the form of a mixture of gaseous byproducts (bubbles) and liquid polystyrene. The length of the melt zone was found by Sand et al. [65], to vary from 1 to 2 mm have verified by some experiments which used a series of thermocouples inserted into the foam pattern.

It was also reported that a convex interface provided a constant heat and mass transfer from the casting channel to the surrounding sand. Fu et al. [54] have suggested that condensation of the gas which passed through the coating is likely to occur. They suggested that once the gaseous byproducts passed through the coating, with further heat from the molten metal the temperature of the sand was increased and the condensed byproducts revapourize and travel further into the sand until reaching a region of lower temperature where they condense once again.

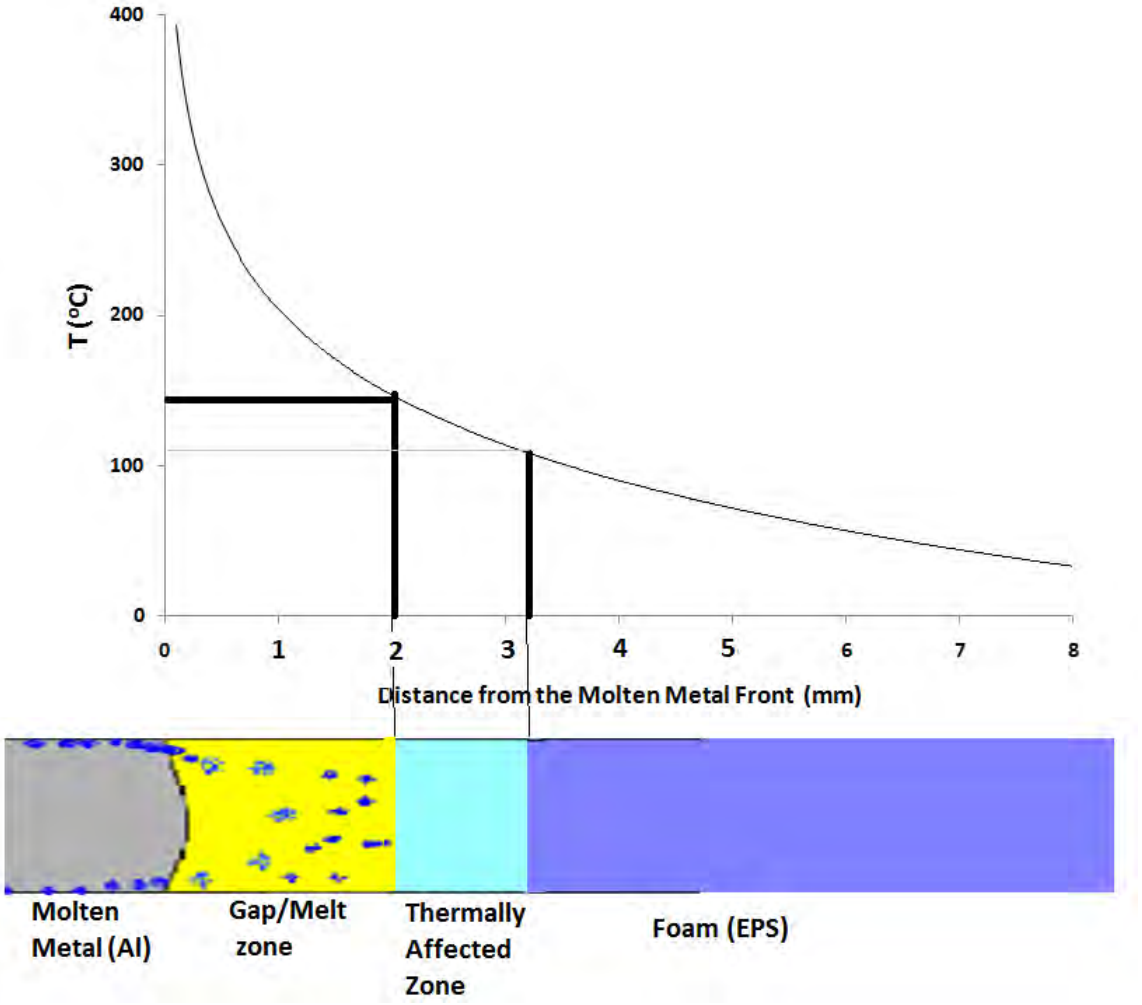

Figure 2-7. Lengths and temperatures of the metal/foam interface in LFC[63].

Therefore, there is a close association between the shape of the interface, the velocity of the molten metal and the quality of Lost Foam Castings. To increase the quality of the castings, the gaseous byproduct has to be removed from the mould as soon as possible or may become engulfed in the molten metal stream and cause porosity; the evolved gas has to pass through the coating to the sand [55]. This necessitates the gaseous byproduct to pass through the coating at a suitable time and place ahead of the metal/foam interface as the liquid polymer viscous residue wets and spreads across the coating surface [66]. Once wetted, the passage of gas through the coating will not be easy and will cause accumulation of gas ahead of the molten metal stream and reduce the metal velocity, as the rate of the heat transfer to the foam

pattern would be reduced by the increased thickness of the interface [62]. If the gas produced is eliminated from the melt zone easily, again the velocity of the molten metal increases up to a point that a thick layer of gas forms and insulates the foam pattern and consequently also reduces the molten metal velocity [67].

Other parameters such as the level of bead fusion of the pattern, the permeability of the coating and orientation of the filling should also be optimised in order to prevent formation of a concave metal flow front. For example increasing the bead fusion of the foam pattern reduces the thermally affected zone in the foam pattern next to the metal/foam interface and increases the temperature drop at the metal front resulting in an increase in the mould filling time [6, 27, 29, 46, 66].

2.6 Lost Foam Casting Defects

There are a variety of defects to be found in castings made by LFC, such as porosity, misrun, laps/folds, surface defects and metal penetration defects. These defects are introduced to the casting because of either entrapment of the decomposition byproducts into the molten metal stream or solidification before filling the pattern completely due to the rapid reduction in the temperature and the velocity of the advancing molten metal.

2.6.1 Porosity

Porosity of Al 2L99 alloy castings produced by LFC can vary from 1 to 1.5%. The porosity content of LFCs varies from high to as good as in conventional castings (if the process is well controlled) [1]. Studying the morphology of the pores in the LFC process shows that the shape of the pores are different from those found in green sand casting which are more irregular, forming as interdendritic porosity, rather than being spherical, while both shapes are found in the LFC process [21].

An unstable metal front profile, which is normally caused by a high velocity of the molten metal, prevents the liquid byproducts from reaching the coating surface. Instead, they become entrapped in the metal flow and because of the heat from the surrounding hot metal they decompose further and leave a pore in the casting [68]. Hill et al. [59] also suggested that large pores are introduced to the LFC process as a result of this. Wang et al. [69] examined internal pores with different velocities of the liquid metal and established that no pore was found in thin aluminium castings (0.48 cm thickness) with a velocity of less than 23 mms^{-1}. This was probably because the metal/foam interface tends to become unstable in higher molten metal velocity and entrapment of the decomposition byproducts is easier in such an interface. Shivkumar et al. [70] found that the porosity content of a casting can increase up to 5% near the metal front which may be due to shrinkage as well as the decomposition byproducts entrapment.

2.6.2 Misruns

While high velocity filling can cause porosity related defects and failures in LFC (as was described in 2.5.1), low velocity filling can cause incomplete castings as the liquid metal flow might freeze before filling the pattern completely (misrun). The metal front temperature and the removal mechanisms of decomposition byproducts from the mould can affect fluidity of LFC [19].

2.7 Fluidity

Fluidity length is defined as the maximum distance to which the molten metal flows in a standard mould [71]. The fluidity length can be measured by casting the molten metal in a long horizontal channel; however this is inconvenient as it requires a long heavy mould. A long horizontal channel can be replaced by a spiral channel as the mould for the latter is

lighter and occupies less volume [72]. However a spiral test may not be appropriate for LFC as the heat from the flowing metal may affect the foam pattern in the outer radii before the metal flow reaches it.

The parameters affecting fluidity are related to the molten metal, and the mould and test conditions. The molten metal variables are the liquidus and solidus temperatures of the cast alloy, the viscosity of the flowing liquid metal and its latent heat of fusion. The mould variables are back pressure, (giving resistance to metal flow), mould thermal conductivity, the size of the casting channel and the sand type. Finally, the test variables are the applied metal head height and the pouring temperature [73].

Lost Foam Casting is different from conventional empty cavity casting in many features such as the heat transfer and solidification behaviour; the heat for the foam decomposition is supplied by the molten metal and this has a quenching effect on the flowing liquid metal at the metal/foam interface. Secondly, the presence of foam ahead of the flowing liquid metal makes the filling behaviour of LFC different from that of conventional casting methods, as different back pressure mechanisms occur in LFC compared to other casting methods, due to the decomposition of the foam pattern.

2.7.1 Fluidity and solidification behaviour in an open cavity casting

Solidification of pure metals occurs at a single temperature while alloys have a range of solidification temperature. The solidification manner of pure metals is called “skin freezing” while alloys have a "pasty freezing" solidification.

In the skin freezing solidification mode (pure metals and eutectic alloys), as the metal loses its initial superheat, solidification starts with a planar growth front from the walls of the mould. The liquid channel therefore becomes thinner and subsequently makes the flow passage

tighter. The flow of metal is stopped when the two edges of the solidification fronts meet and close the channel, as shown schematically in Figure 2-8.

Figure 2-8. Schematic choking in skin freezing materials.

This is the case for when remelting and refreezing solidified regions downstream is overlooked. Normally, the passage of molten metal through the choke point causes remelting at points A and B (see Figure 2-8). Likewise, due to the heat lost from the molten metal as it passes the choking point, solidification occurs at points C and D, to some extent. The solidified region therefore migrates downstream. If the channel is short enough, the migration of the growing choke point might reach the end of the channel before the channel is closed, resulting in complete remelting of the choke point and uninterrupted continuation of the flow. This phenomenon is called continuous fluidity and the continuous fluidity length is denoted as L_c [72].

Alloying reduces the fluidity of the pure metal (at a given superheat) [74]. For non-eutectic alloys solidification no longer takes place with a planar front. Dendrites grow from the mould wall at an early stage. The flowing metal consists of a slurry of tumbling crystals; the existence of dendrites in the flow creates more resistance against the movement of the flow at an early stage of solidification. At some critical point, the dendrite arms interlock and stop the liquid metal from flowing further [71]. This is the coherency point and has been estimated to occur at a fraction solid of between 20 and 50% [72].

Eutectic alloys and pure metals have the same solidification behavior at a constant superheat. For a constant superheat, a eutectic alloy's fluidity is more than 1.5 times that of its constituent pure elements [71] because of lower melting point.

In the case of casting with grain-refined alloys, some fine grains can be carried along with the tip of the liquid metal stream. As the liquid metal temperature decreases, the fraction solid in the liquid metal flow increases. When a sufficient amount of solid is formed (to stop the flow) and gathered at the tip of the flow, the metal stream stops flowing as shown in Figure 2-9 schematically.

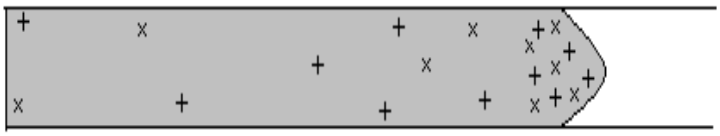

Figure 2-9. Fine grains carried along with the tip of stream finally cause the flow stoppage.

For aluminium-silicon alloys, the peak observed in the fluidity diagram (Figure 2-10) implies that the fluidity of the eutectic alloys is a maximum. Most of the Al-Si alloys are in the range of 4 to 10 percent Si. For hypereutectic alloys, due to less friction in the liquid because of the formation of primary Si, fluidity is higher as dendritic interlocking does not take place in these alloys [72].

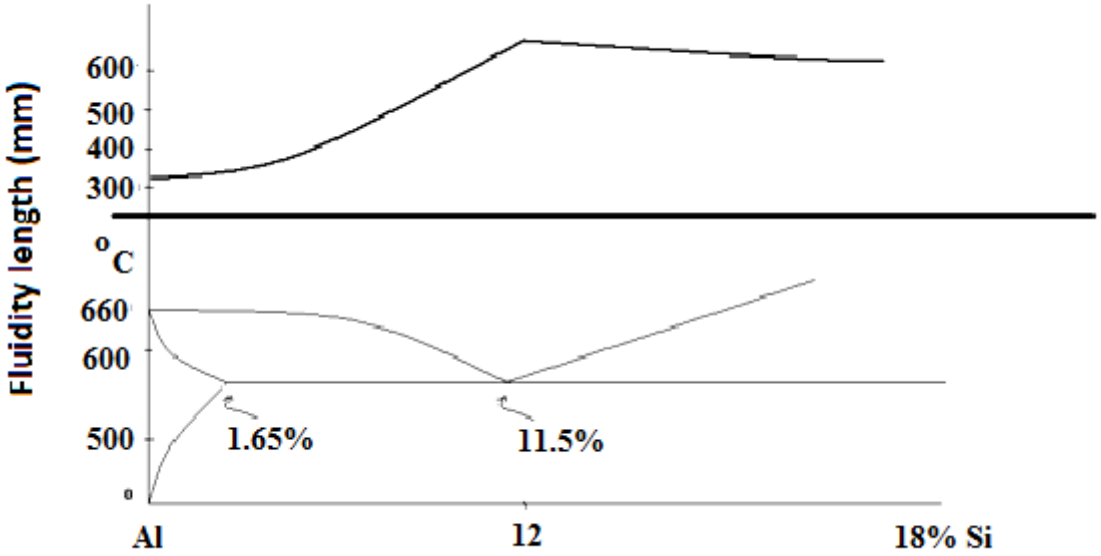

Figure 2-10. Fluidity vs. Chemical composition for Al-Si alloys [75]

Two aspects of filling thin sections are "flowability", which is limited by heat transfer, and "fillability", which is limited by surface tension. Evidence for solidification occurring whilst the metal was still flowing is to be found in the direction of the columnar grains growing into the direction of the flow. As the liquid metal stream passes along the casting channel, remelting of the newly solidified dendrites occurs at the side facing the stream and refreezing occurs at the other side resulting in directional growth of the dendrites as shown in Figure 2-11.

Figure 2-11. Schematic dendritic growth in direction of the flow

The second aspect, fillability, occurs at higher mould and/or metal temperature where the heat content of the system is high and solidification is delayed until after the mould has filled.

Studies in the microstructure of this kind of solidification show that the liquid metal was static during freezing in thin sections. [72].

2.7.1.1 The coherency point

At a certain point during solidification, dendrites start to interlock and form a coherent network and the system (fluid) starts to behave more like a solid than a liquid before the solidification process is accomplished. The volume fraction of solid at this point is called the coherency point (f_s^{coh}) [71] [76]. Many researchers have shown that the coherency point depends on the alloy and solidification parameters such as cooling rate [76-79]. Chavez et al. [80] determined the coherency point of Al-Si-Cu alloys based on determination of their thermal diffusivity using solidification data obtained from thermocouples placed at different points of a casting. Veldman et al. [81] showed that increasing the silicon content of aluminium alloys reduced the coherency point; however for a certain alloy, the coherency point depends on the cooling rate of any solidifying point. They also calculated the coherency point of aluminium A356 solidifying with a cooling rate of 0.7 and 2.7 Ks^{-1} to be 0.22 and 0.14 respectively.

2.7.1.2 Fleming's analysis of fluidity

Fleming's fluidity model was derived for an empty cavity casting. To simplify the analysis of the fluidity length (L_f), Fleming assumed no separation of the molten metal stream. He also neglected the effects of friction and acceleration.

He developed a formula for the time of freezing (t_f) as shown in Equation 2-1.

$$t_f = \frac{\rho_s H a}{2h(T_M - T_0)} \qquad \textbf{Equation 2-1}$$

Where;

a: Modulus of the casting channel (m) (the ratio of an element volume to its surface area).

H: Latent heat of fusion (Jkg^{-1})

h: Heat transfer coefficient from the molten metal to the mould ($Wm^{-2}K^{-1}$)

T_0: Mould temperature (K)

T_M: Melting point of the cast metal (K)

ρ_s: Density of solid (kgm^{-3})

The fluidity length as a function of metal velocity and other casting parameters was determined as shown in Equation 2-2 [72].

$$L_f \cong \frac{\rho_s a V}{2h(T_M - T_0)}(H + c'\Delta T) \qquad \textbf{Equation 2-2}$$

Where;

c′: Specific heat capacity of the molten metal ($Jkg^{-1}K^{-1}$)

ΔT: Superheat (^oC)

V: velocity (ms^{-1})

The velocity of the molten metal can be written as a function of casting head height as $V^2 = 2gh$, however this is an overestimation because it is reported that the velocity can be reduced by 20%, when being turned through 90°. Secondly, the velocity of a fluid changes when it passes through a channel in which the area changes according to the Law of

Continuity [82] which states that the flow rate of a fluid is constant. Therefore, the velocity of a flowing fluid multiplied by the cross-sectional area of the channel is constant as shown by Equation 2-3 [82].

$$Q = V_1A_1 = V_2A_2 \qquad \textbf{Equation 2-3}$$

Where;

V_1 and V_2: Velocity, A: channel cross-sectional area (m^2) and

Q: flow rate (m^3s^{-1}).

2.7.2 Fluidity in Lost Foam Casting

The velocity of molten metal during mould filling in LFC is of the order of cms^{-1} while it is of the order of ms^{-1} in the case of empty cavity castings [34]. The metal velocity depends on the metallostatic pressure ($V^2 = 2gh$) and the heat transfer rate from the molten metal to the foam in the casting. In the case of LFC, due to the presence and decomposition of the foam pattern ahead of the metal flow, the temperature of the molten metal is reduced faster at the metal front compared to the case of an empty cavity casting. In addition, the casting head height should be high enough to overcome the back pressure caused by vaporization and gas evolution from the foam pattern decomposition. The back pressure in LFC depends on the gas generation rate and gas escape rate which themselves depend on metal temperature, pattern density, casting section modulus and the thickness and permeability of the coating [19, 69, 83].

The fluidity in LFC also depends on other properties of the molten metal such as surface tension, oxide film content, inclusion content and solidification mode as well as casting

conditions such as the geometry of the casting, mould materials, coating, pouring rate and pouring temperature [10].

The fluidity of LFC has been investigated by casting experiments and by computer simulations. Tschopp [10] listed all the variables affecting the fluidity of LFC and analysed the effect of casting parameters on the fluidity of Aluminium A356 LFC. He concluded that, in order to increase fluidity, filling rates should be increased, the thermal conductivity of the sand has to decrease or the area to perimeter ratio of the section needs to increase. The effect of metal temperature, metallostatic pressure, coating permeability and foam type (different foam densities, different molecular weight and different copolymers) will increase the fluidity length where they increase the metal velocity and reduce the time interval in which the molten metal is losing heat. It was suggested that section thickness was the most effective parameter affecting the fluidity of LFC. Coating permeability, foam type and metallostatic head pressure were other parameters controlling the fluidity length. Tschopp also claimed that the role of pouring temperature on fluidity of LFC was not very clear. Increasing casting temperature increased the temperature gradient between the molten metal and the foam pattern which increased the foam decomposition rate which increased the volume of gas evolved and subsequently increased back pressure in the mould causing a reduction in velocity of the molten metal, therefore reducing the fluidity length. In general, Tschopp did not suggest increasing pouring temperature to increase the fluidity as it may also cause surface oxidation and increasing surface tension. Instead, to avoid misrun, increasing the coating permeability was suggested [10].

Many researchers aimed at deriving a fluidity equation for the LFC process.

Ajdar et al. [11] evolved a model based on Chvorinov's rule. Chvorinov's rule states that solidification time is proportional to the casting modulus, as shown by Equation 2-4 [84].

$$t = C\left(\frac{V}{A}\right)^n \qquad \textbf{Equation 2-4}$$

Where;

C: Chvorinov's constant

t: time of solidification

V and A are the volume and surface area of the casting channel respectively and "n" is an experimental exponent derived from cooling curves obtained from different moulds and different casting conditions [84].

The heat balance in a narrow chill zone (at the metal/foam interface) located at the front of the molten metal can be stated by Equation 2-5.

$$L_C W t_p \rho_L C_L \Delta T = L_f W t_P \rho_P H_E \qquad \textbf{Equation 2-5}$$

Where;

C_L: Specific heat capacity of the molten metal ($Jkg^{-1}K^{-1}$).

H_E: Decomposition energy of the EPS foam pattern (Jkg^{-1}).

L_c: Length of the characteristic chill zone (m).

L_f: Fluidity length (m).

t_p: Thickness of the foam pattern (m).

ΔT: Superheat, (K).

W: Width of the foam pattern (m).

ρ_L=density of the molten metal (kgm^{-3}).

ρ_p: Foam density (kgm^{-3}).

Therefore, leading to a model of the fluidity of LFC, Equation 2-6 [11].

$$\frac{\Delta T}{L_f} = \frac{\rho_p H_E}{C_L 2.2 t_p \rho_L} \qquad \textbf{Equation 2-6}$$

Pan and Liao also developed a model based on Fleming's model taking into account the endothermic nature of the foam pattern decomposition, as shown by Equation 2-7 [85].

$$L_f = \frac{\rho_L a v}{2h\ (T_M - T_0)} (c_L \Delta T + \frac{H}{2} - \frac{H_E \rho_P}{\rho_L}) \qquad \textbf{Equation 2-7}$$

Where;

H_E: Decomposition energy of the foam pattern (Jkg^{-1}).

H: Latent heat of the molten metal, (Jkg^{-1}).

h = heat transfer coefficient to the mould ($Wm^{-2}K$)

Mirbagheri et al. [13] developed a new mathematical model to simulate mould filling in the cast iron LFC process using a finite difference method, as shown by Equation 2-8. An algorithm was developed to calculate the gas pressure of the evaporated foam during mould filling.

$$p_s = p_0 nm \rho_{FB} \left[1 + \left(\frac{1 - \sum \Delta V_{gap}}{V_{cav}} \right)^r \right] \left(V_{gap} + V_M \right) / V_{gap} \qquad \textbf{Equation 2-8}$$

When $1<r<2$ $3.5<n<4.5$

Where;

m: the "gasified latent capacity" of the foam (the volume of gas evolved from decomposition of 1 gram of foam), which for polystyrene foam was 300 cm^3g^{-1}

V_M: the volume of grey iron flowing into the mould cavity (at each time step of the filling period).

V_{Cav}: the mould cavity volume

V_{gap}: the volume of the gap

P_S: the gas pressure in the metal/foam interface (gap)

ρ_{FB}: the density of the foam pattern

"r" and "n" are thermal radiation and coating permeability factors respectively (a value of 2 was used for "r" a high melting point alloy and high superheat, but for "n" 4.5 was used for minimum permeability). Results from this simulation are shown in Figure 2-12 [13].

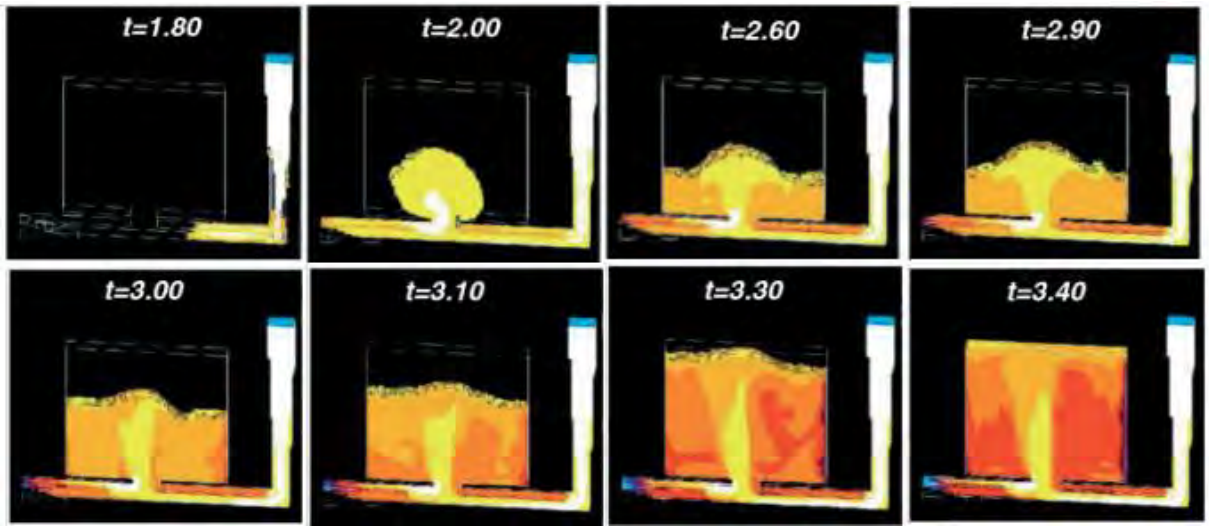

Figure 2-12. Simulation of mould filling in the LFC process. Molten metal: grey iron, Mould materials: unbonded silica sand [13].

2.8 Properties of molten metal

2.8.1 Reynolds number

Reynolds number is a dimensionless characteristic of a fluid, defined as the ratio of inertial forces to viscous forces [86]. It describes and defines different flow regimes, normally laminar or turbulent flow. Laminar flow occurs at low Reynolds numbers, where viscous forces are dominant, and is characterized by smooth, constant fluid motion, while high Reynolds numbers produce chaotic flows [45]. The Reynolds number can be calculated by Equation 2-9 [87].

$$R_e = \frac{Dynamic\ pressure}{shear\quad stress} = \frac{\rho \upsilon^2{}_S \big/ L}{\mu \upsilon_S \big/ L^2} = \frac{\rho \upsilon_S L}{\mu} = \frac{\upsilon_S L}{\nu} \qquad \textbf{Equation 2-9}$$

Where:

υ_s: Mean fluid velocity (s^{-1}).

L: Characteristic length (m).

μ: (Absolute) dynamic fluid viscosity (Pa·s).

ν: Kinematic fluid viscosity ($m^2\ s^{-1}$).

ρ: Density of the fluid ($kg\ m^{-3}$).

A flow is laminar when its Reynolds number is less than about 2000 to 3000 and turbulent flow occurs when the Reynolds number is about 5×10^5 [88] . Reynolds numbers between the mentioned values describe a transition from surface turbulence to bulk turbulence. Bulk turbulence is the chaotic eddying flow of the bulk liquid while surface turbulence is when the chaos is in the surface and causes the surface to break up [89].

2.8.2 Heat transfer coefficients measured in Lost Foam Casting

Shivkumar [90] proposed a value of 420 $Wm^{-2}K^{-1}$ for the heat transfer coefficient from solidifying aluminium to silica sand when the polystyrene foam pattern was coated with a 1 mm thickness of coating and a value of 570 $Wm^{-2}K^{-1}$ was also determined for the same coefficient when the foam pattern was not coated. It was then concluded that the coating has an insulation effect on the heat flux from the molten metal to the foam and therefore increases the fluidity of LFC.

Venkataramani et al. [91] developed a computer simulation to estimate the heat transfer coefficient from molten metal to the mould in a cylindrical casting with different thicknesses of coating. The initial value of 420 $Wm^{-2}K^{-1}$ was used to carry out the simulation with. The results showed that the heat transfer coefficient from the molten metal to the mould varied drastically during the casting experiment and the actual values can be estimated accurately, for example a very high value of 18000 was also reported for a very short period of time at the middle of the experiment. It was also reported that the heat transfer coefficient from the molten metal to the foam pattern decreased with increasing pouring temperature and increasing coating thickness.

Molibog et al. [92] measured thermal conductivity of the coating from thermal diffusivity, density and specific heat capacity values which were measured by Differential Scanning Calorimeter (DSC) at a range of temperatures (from room temperature to 1025 ^{O}C). They developed graphs explaining changes in thermal conductivity for four different coatings at different temperatures, as shown in Figure 2-13.

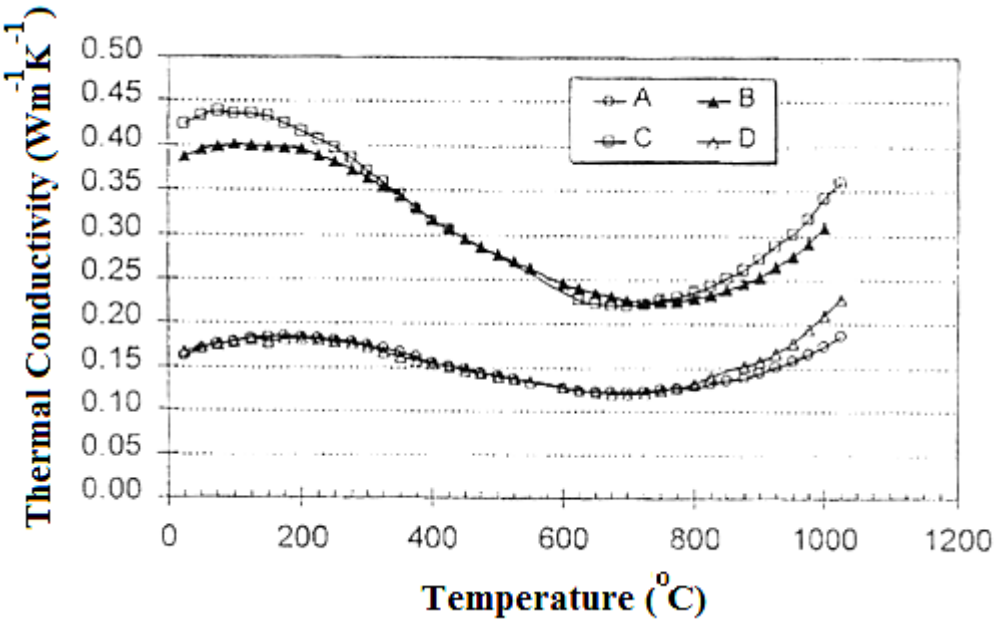

Figure 2-13. Thermal conductivity of coatings used in LFC, where A and D are mica based coatings and B and C are Silica based coatings [92].

It was concluded that the mica based coating had an average thermal conductivity of 0.15 $Wm^{-1}K^{-1}$ which results in a heat transfer coefficient of 450 $Wm^{-2}K^{-1}$ for a coating thickness of 0.3 mm [92].

The fluidity equation derived by Pan and Liao [12] (Equation 2-7Equation 2-7) was derived from Flemings' flow equation based on the fact that depolymerisation of the polymer is an endothermic reaction.

Evaluation of this model, suggested that the calculated fluidity length was higher than the experimental values by almost one order magnitude. Pan and Liao assumed that heat exchange was confined to a small zone at the metal front the "characteristic zone" denoted as l_c. Therefore, Equation 2-7 was developed to Equation 2-10 (see Equation 2-7 for parameters guide).

$$L_f = \frac{\rho_L a V_E}{2H(T_M - T_0)(1 + \frac{L_f \rho_P}{l_c \rho_L} H_E)} (\frac{H}{2} + C_L \Delta T) \qquad \textbf{Equation 2-10}$$

Liu et al. (2002) [61] suggested that part of the heat loss from liquid Al passed through the refractory coating in the LFC process, but most of the heat passes through the gas in the metal/foam interface to degrade the solid foam pattern. Therefore, a complicated heat transfer mechanism governs the LFC process, involving conduction, convection and radiation. They developed an algorithm to model flow in LFC which included calculating the speed of the foam pattern degradation, gas pressure, fluid velocity and height and length of the gap interface, etc. The values of heat transfer coefficients from the molten metal to the sand and to the metal/foam interface to start the simulation with were assumed to be 1300 and 3300 $Wm^{-2}K^{-1}$ respectively. Although these values seem to be too high and conflict with values mentioned in other reports [92], they claimed that the result of the simulation was in good agreement with the results of casting experiments, for example, the velocity of the molten metal, (shown in Figure 2-14) [61]. Although they have claimed an agreement between the actual and simulated results, Figure 2-14 shows that the measured velocity had a constant value of between 7 to 12 cms^{-1} while the simulated values started from 20 cms^{-1} and ended to a constant value which made the simulation unlikely to some extent.

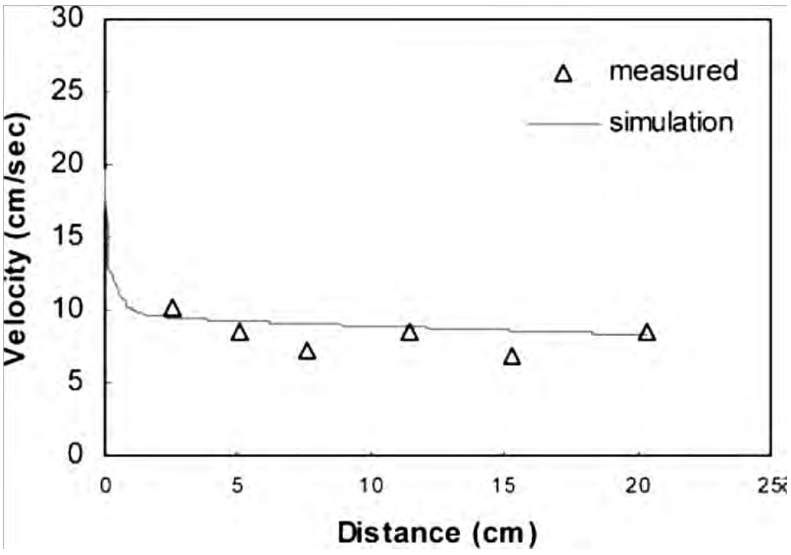

Figure 2-14. Flow simulation results compared to the actual velocity of the molten metal [61].

Liu et al. [49] carried out a series of LFC experiments with thermocouples connected to a data acquisition system. They also carried out simulation of flow in the LFC process, when the EPS foam pattern was coated with 0.7 mm of coating and velocity of liquid metal was about 1.5 cms^{-1}. Figure 2-15 shows the result of estimation of the heat transfer coefficient from the molten metal to the foam and how it increased with time.

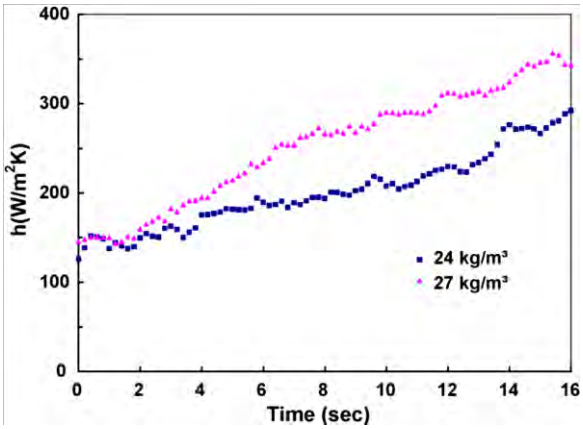

Figure 2-15. Simulation of heat transfer coefficient from the molten metal to the pattern for different foam densities for Al alloys LFC [49].

Liu et al. (2007) carried out some experiments to understand the effect of pattern density variation on the mould filling process. A foam pattern was surrounded by a compacted sand mould and a heated steel block was pushed toward the foam. Corresponding simulation results are shown in Figure 2-17.

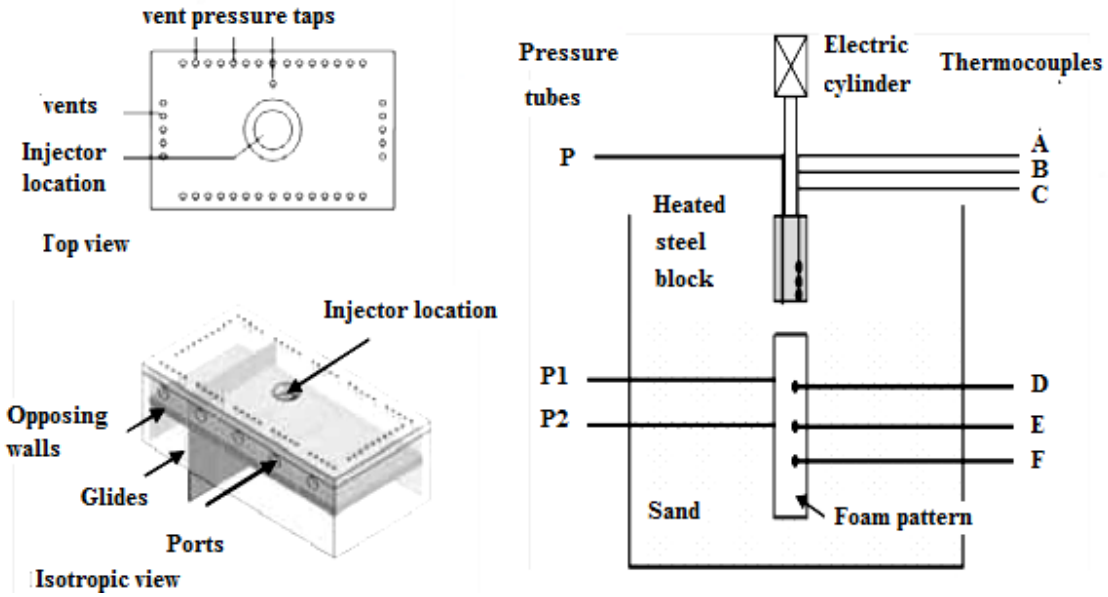

Figure 2-16. Experimental set up [93]

The heat flux from the heated steel to the foam was measured over a period of time to obtain a heat transfer coefficient as shown in Figure 2-17.

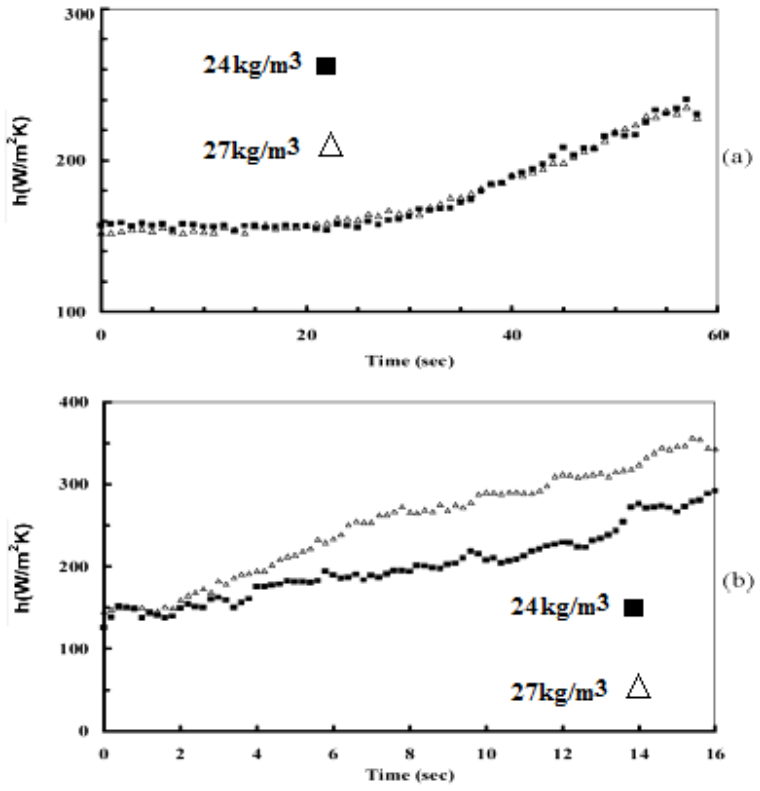

Figure 2-17. Simulated heat transfer coefficient for a metal front velocity of (a) 0.44 cm/s, and (b) 1.5 cm/s [93].

The average peak pressure of the gap was also measured for different metal velocities and different foam densities, as shown in Table 2-1.

Table 2-1. Measured values for average pressure in the metal/foam interface for different densities of foam pattern [93].

Metal front velocity (cm/s)	Average peak pressure for EPS foam density of 24 kg/m^3 (kPa)	Average peak pressure for EPS foam density of 27 kg/m^3 (kPa)
0.36	0.39	0.46
0.44	0.96	2.5
0.95	4.5	8.1
1.5	19.1	19.8

In this experiment the average temperature of the kinetic zone (gap zone) was found to be approximately 200 °C and to have a length of 1 to 4 cm. This length (1 to 4 cm) for the metal/foam interface appears very high but this may be a result of the limited vents in the mould [93]. These allow ventilation for the decomposition gaseous byproducts but this is unlikely to simulate the actual LFC process precisely, see Figure 2-16.

Liu et al. [94] suggested a mechanism for the effects of temperature on thermal conductivity of the coating; increasing the temperature of the coating may result in shrinking the coating in volume which creates a gap between the metal and the coating which reduces the thermal conductivity and heat transfer from the molten metal to the mould. This mechanism explains why the cooling rate during solidification in the LFC process is very small. This was stated based on the results of LFC with Mg alloys but could also apply to Al alloys.

Wang et al. [14] developed a computer program to simulate the fluid flow using the data acquired from thermocouples inserted in the foam pattern used in the LFC process. They used initial values of 117 and 0.5 $Wm^{-1}K^{-1}$ for the thermal conductivity of aluminium alloy 319 and

the sand mould, respectively. They also computed a value of 1,003,000 Jkg^{-1} for heat of degradation of EPS foam pattern.

Tsai et al. [95] implied that the coating in LFC prevents the sand collapsing, increasing metal fluidity by an insulation effect and reducing the surface tension between the molten metal and the sand wall. They also listed the parameters affecting fluidity in the LFC process accompanied by a description of corresponding physical phenomena. Furthermore, a mathematical model for Lost Foam plate casting was developed based on some simplifying assumptions. This resulted in an estimation of the heat transfer coefficients from the molten metal to the mould and to the foam pattern which were 100 and 1300 $Wm^{-2}K^{-1}$ respectively.

They claimed that the heat flow to the foam pattern was much more than the heat flow to the sand mould at any instant of time. The transient heat loss to the sand mould was proportional to the available surface area through which heat transfer takes place, while the transient heat loss to the pattern was proportional to the decomposed pattern volume. The results show that the heat loss to the foam pattern increased over time while the increase in the heat loss to the sand mould was very slow, as shown in Figure 2-18.

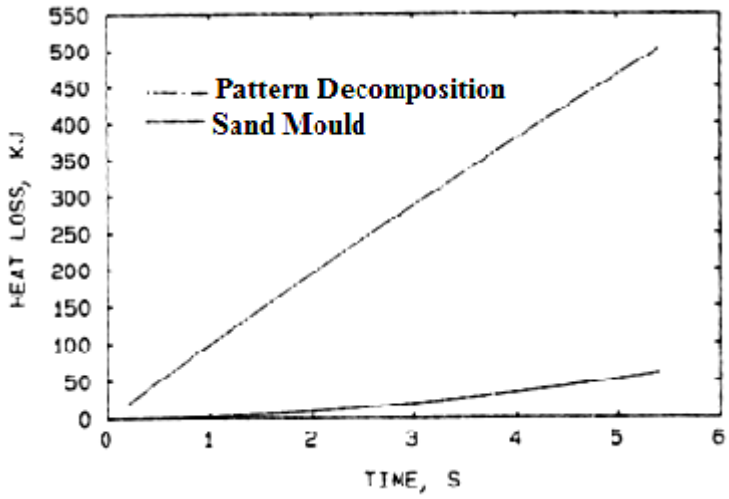

Figure 2-18. Heat loss from molten metal to the pattern decomposition and to the sand mould vs. time [95].

Finally, it was concluded that for any coating material there is a critical coating thickness corresponding to a critical heat transfer coefficient at which maximum heat loss to the mould occurs. It was implied that when the coating thickness was less than the critical value, an increase in the coating thickness increased the heat loss from the metal to the sand mould, however if the coating thickness was greater than the critical value an increase in the coating thickness reduced the heat loss to the mould, as shown in Figure 2-19. Therefore, the critical thickness should always be exceeded in order to achieve insulation.

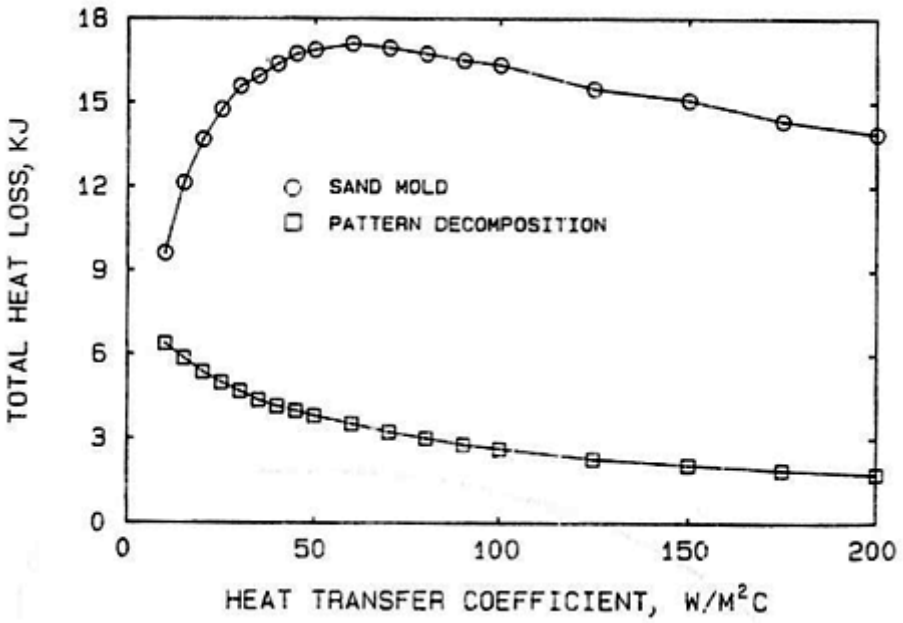

Figure 2-19. Heat loss from the molten metal to the sand mould and the degrading foam pattern in the LFC process with Al alloys [95].

In addition, they claimed that the key point to having a successful controlled LFC process is the casting section thickness; when a casting is thicker than a critical thickness the heat loss from the molten metal to the degrading foam pattern is greater than that to the mould. Otherwise, a reverse trend occurs [95]. This is in agreement with the statement made by Tschopp suggesting that casting thickness is the most effective parameter on the fluidity of LFC [10].

Caulk [53] suggested a foam melting model for the LFC of aluminium (gap mode). He carried out a bubble flux analysis and possible fates of any residual polymer liquid left behind was discussed in likely scenarios which mainly corresponds to how the pattern decomposes at a particular location. He assumed the thermal conductivity of the gas in the metal/foam interface to have a value of 0.04 $Wm^{-1}K^{-1}$ (i.e. assuming the gap length to be 2 mm the heat transfer coefficient from the molten metal to the foam pattern is $20Wm^{-2}K^{-1}$; which seems an order of magnitude smaller than was suggested in most of the references, such as [93]).

Houzeaux et al. [83] developed a model based on some assumptions which seem to be rather simplifying:

- Metal and foam properties are not varied.
- There is no solidification during filling.
- There is no source of contaminant, like viscous residues.
- No gas is trapped between the metal and the foam.

For a two dimensional aluminium plate casting, they computed a value of 6000 $kgs^{-3}K^{-1}$ ($Wm^{-2}K^{-1}$) for the heat transfer coefficient from the molten metal to the foam pattern which seems to be far too high.

Venkataramani et al. [91] claimed that at the beginning and at the end of the solidification of a casting section, increasing pouring temperature and coating thickness caused a reduction in the heat transfer coefficient from the molten metal to the mould however they reported that the accurate values could not be estimated as the results showed drastic oscillation. They carried out aluminium LFC experiments with thermocouples inserted and the data was used to develop a program to estimate the heat transfer coefficient based on the cooling curves at

different locations of the castings. The value they used to start the simulation was 420 $Wm^{-2}K^{-1}$.

Summary

The computed, measured, simulated or calculated values for heat transfer coefficients are summarized in Table 2-2.

Table 2-2. Summary of heat transfer coefficients in the LFC process reported in the literatures.

Reference	Heat transfer coefficient to	Value $Wm^{-2}K^{-1}$	Heat transfer coefficient to	Value $Wm^{-2}K^{-1}$
Venkataramani et al. [91]	Air (Top surface of the casting)	150	Sand mould	420
T.Molibog et al. [92]	----	----	Coating	4666*
Liu et al. [49] [93]	Foam	250 (average)	---	----
Liu et al. [61]	Decomposition gas	3300	Sand mould	1300
Tsai et al. [95]	Foam	1300	Sand mould	100
Caulk [53]	Decomposition gas	20	----	-----
Guillaume et al. [83]	Foam	6000	----	----

The value of 4666 seems to be very high for the heat transfer coefficient of the casting/coating interface. This value was calculated from the thermal conductivity values (k) in the literature when the coating thickness was assumed to be 0.3 mm (as they are assumed to be in the current work), using Equation 2-11 [63];

$$k = h \times x \qquad \textbf{Equation 2-11}$$

Where x is the length of the gap between the molten metal and the foam pattern (the thickness of the material through which the heat is passing), k is the thermal conductivity.

The value range of 150-450 $Wm^{-2}K^{-1}$ for the heat transfer coefficient from the molten melt to the foam pattern seems to be reasonable as this range was in agreement with several other reports [49] and [91, 93].

2.9 Effect of irradiation on foams

As was emphasized in section 2.4, the molecular weight of the degradation byproducts has an important role in their ease of removal from the mould in the LFC process. Radiation was known to affect the properties of foams and plastics, however irradiation processes are also commonly used to polymerize and crosslink monomers (using high energy radiation such as γ-rays) [96] for example to prepare lubricants and coatings for pots and pans, Perfluorinated polymers such as polytetrafluoroethylene can be degraded using γ-irradiation [97, 98].

In order to ensure satisfactory results with minimum costs, the irradiating source should meet some criteria such as delivering a desirable dose, while the size, shape and density of the product are important parameters which determine throughput rate [99].

The absorbed dose is defined as the energy absorbed per unit mass in a small volume at a particular location of the product. The international unit of dose is the gray (Gy) which is 1 Joule per kilogram. The Rad was the previous used unit which is 100 times smaller than a gray [100].

Radiation processing involves mainly the use of either electron beams from electron accelerators, or γ-radiation from cobalt-60 (Co-60) sources [99]. While some synthetic polymers crosslink during radiation processing, others degrade [96]. For example PMMA degrades under the effect of irradiation whereas PS responds to radiation by cross-linking. One of the mechanisms of cross-linking when polystyrene is exposed to irradiation is the loss

of two hydrogen atoms from adjoining chains and consequent bonding between the two carbon- centred free radical sites leading to interchain bonding [101-103].

The effect of irradiation on polymer blends such as Probead-70™ and Probead-30™ which are blends of EPS and PMMA has not been extensively studied. Polymer blends can be divided into two groups in terms of their response to irradiation processing. (1) The cross-linkable blends such as ethylene vinyl acetate; this type of blends of polymers show increased elongation and tensile strength when exposed to γ-radiation. (2) The degradable blends reduce molecular weight under exposure to γ-radiation with consequent reduction of their strength [99]. In the case of PS-PMMA blends, as PS is a cross-linkable polymer and PMMA is a degradable polymer, it is suggested that PS prevents reduction in molecular weight of the blend (i.e. a protective role) and prevents reductions in mechanical properties overall [99]. However Shultz et al. [104] suggested that the rate of chain scission in the PS-PMMA blend would be closer to that of pure PMMA under the effect of irradiation therefore the mention blend is thought to reduce its M_w under effect of irradiation. They also suggested that the presence of PS would reduce the rate of chain scission corresponding to its weight percentage in PS-PMMA blends. It is not therefore possible to say whether protection (against reducing strength) occurs in polymer blends with PS due to exposure to irradiation [99].

2.10 Summary

The nature of LFC is more complex than conventional casting methods; for example the filling behaviour is strongly affected by the presence of the foam pattern and its degradation. There are many parameters involved in the quality of the castings and the operation of the process, such as thickness and permeability of the coating, type of foam pattern, density of the foam pattern, etc, apart from those factors also relevant in open cavity castings. Defects

introduced in the LFC process (such as porosity, misrun and laps) mostly originate from decomposition of the foam pattern. A reduction in porosity and misrun are objectives of the current research.

The shape of the metal/foam interface is a determining parameter in the quality of the castings in LFC. Generally, convex metal front profiles are aimed at. Such profiles naturally push the degradation byproducts to the sides of the casting channel. The liquid polymer byproducts can be absorbed by the permeable coating, once their molecular weight is sufficiently reduced by the action of heat. Therefore using a lower molecular weight pattern may lead to higher quality castings because less reduction in M_w will be required before absorption of the liquid polymer byproduct into the pattern coating. The M_w of expanded copolymer foam patterns may be reduced by exposure to γ-radiation. The properties of castings made with irradiated foam patterns, such as porosity content and fatigue properties may also improve due to modifying the foam pattern used in LFC.

As was discussed misrun is also an issue in LFC. A great amount of heat is taken from the molten metal during the process which may lead to solidification of the liquid metal before filling the pattern completely.

The mechanisms of heat/mass transfer in LFC were reviewed. The complex heat and mass flux through the coating in addition to the poorly-known nature of the metal/foam interface make fluidity and heat transfer coefficients is the LFC process difficult to determine and understand. It was also suggested that there was little agreement in the literature about the value of heat transfer coefficients from the molten metal to the mould and to the foam pattern. Current work is aimed at a better understanding of this, to determine the heat transfer coefficients governing the LFC process.

A review of previous models for the fluidity of LFC showed that an inclusive model to explain and relate the fluidity of LFC changes in casting parameters is still required. While the accuracy of the models reviewed will be examined by experiments, this work will also attempt to develop a fluidity model for LFC based on the results of fluidity tests which will verify the effect of different casting parameters on fluidity.

3 EXPERIMENTAL METHODS

3.1 Materials

3.1.1 Foam patterns

The foam patterns used in the fluidity tests were Expanded Polystyrene (EPS) of "normal" bead fusion levels having density of 27 and 16 kgm^{-3}, untreated copolymers of EPS and poly methyl methacrylate (PMMA), Probead-70™ with density of 24 kgm^{-3}, in addition to the brominated EPS with density of 30 kgm^{-3}.

For irradiation processing of the foam patterns, plates of copolymers Probead-70™ (70wt% PMMA-30wt% PS) with density of 24 kgm^{-3}, Probead-30™ (30wt% PMMA-70wt% PS) with density of 20 kgm^{-3} and blocks of PMMA with density of 20 kgm^{-3} were used. All of the foam patterns were supplied by Foseco (FS) Ltd. (Tamworth, UK).

3.1.2 Coatings

Three coatings were used in the LFC experiments. Davies [21] examined three different coatings and their permeability for a thickness of 0.33 mm, has been shown in Table 3-1.

Table 3-1. Different types of coatings used in the current work and their permeability values.

Coating	Permeability (m^2)	Commercial name
A/ Low permeability	9.3×10^{-14}	PID 1095/1
B/ Medium permeability	1.5×10^{-13}	Styromol 169.23
C/ High permeability	1.2×10^{-12}	Styromol MTR7733

In addition to these coatings some Probead-30™ foam patterns that were used in cast iron LFC were coated with "SEMCO®Perm c2™" by Foseco (FS) Ltd. (Tamworth, UK).

To control the coating thickness a Baume stick was used to measure the dilution of the slurry coating. The dilution of the slurry coatings was maintained to be 40 ^{o}Baume which resulted in formation of 0.3 mm thickness of coating when foam pattern was dipped into the coating. The thickness of the coating was measured using a digital micrometer along the length of the foam strip. Twice dipping resulted in 1.3 mm of coating layer on the foam pattern.

3.1.3 Cast metals

The alloys cast in the LFC process were commercially pure aluminium (CP Al), 2L99 alloy (see Table 3-2 for the chemical composition) and grey flake cast iron of grade 250.

Table 3-2. The chemical composition of the cast alloy (Al 2L99) used in the LFC process in the current work [105].

Element	Wt%
Copper	0.10 max.
Magnesium	0.35
Silicon	6.5-7.5.
Iron	0.20 max. (0.15)
Manganese	0.10 max.
Nickel	0.10 max.
Zinc	0.10 max.
Lead	0.05 max.
Tin	0.05 max.
Titanium	0.20 max.
Aluminium	Remainder
Others:	total - (0.15)

3.1.4 Moulding materials

AFS grade 60 silica sand was used for the mould in the LFC experiments. In order to make pouring basins a sand binder was required, and PEPSET® 5112 and 5230 were employed and mixed with sand with an addition rate of 0.06 wt%. In the fluidity tests, boards of Kalmin 50A (supplied by Foseco (FS) Ltd) were employed to make the downsprue. To attach the fluidity strips to the downsprue, a hot melt glue was used and the joint lines were sealed with CORFIX 21™ (also supplied by Foseco (FS) Ltd).

3.1.5 Melting process

A high-frequency (10 kHz) induction furnace was employed to melt the charge. Ingots of metal were placed in a clay-graphite crucible and heated until the temperature of the melt was approximately 50 ºC above the required pouring temperature. This was to allow sufficient time for the crucible to be removed safely.

3.2 Fluidity in open cavity casting

To examine Fleming's fluidity equation for prediction of the fluidity of liquid Al alloys in an open cavity mould, 2L99 alloy was cast at 720 ^{o}C into a die (a simple tool steel mould), covered with a transparent window, as shown in Figure 3-1. The transparent glass window was graduated to allow the measurement of the velocity of the flowing molten metal using a high speed camera, (30 frames per second), see Figure 3-2.

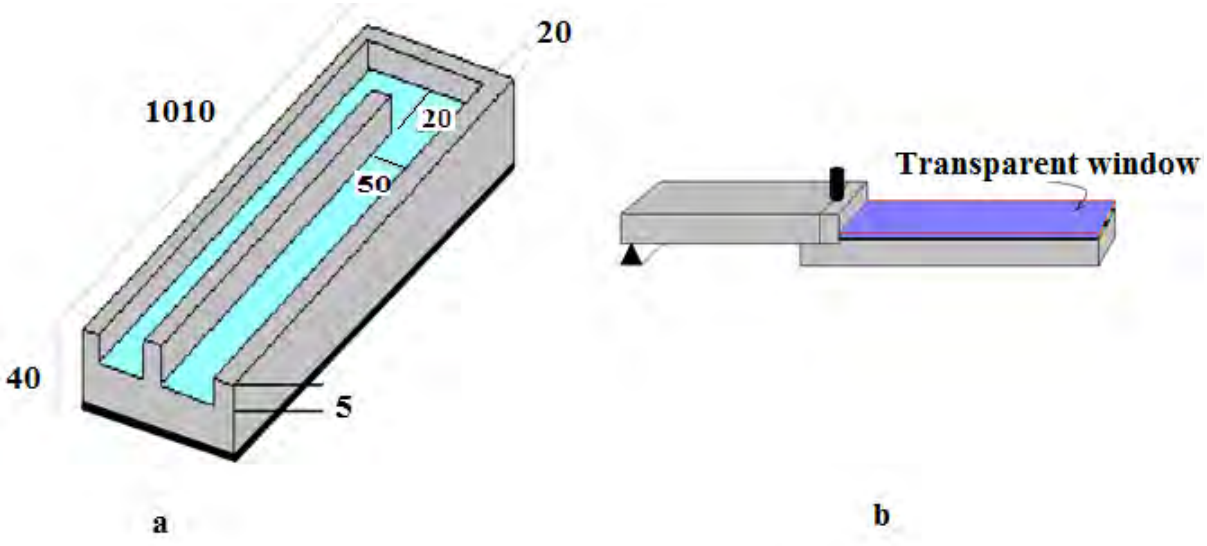

Figure 3-1. The die mould placed with a transparent window on top of the mould, shown schematically; a) the bottom level of the mould, b) the mould set up.

After shot blasting and cleaning for 30 minutes the mould was coated with a commercial coating, DYCOTE-140™ (supplied by Foseco (FS) Ltd. Tamworth, UK). A pouring cup with

an overflow was used to give a constant head height of 100 mm was used in this experiment to deliver the molten metal to the fluidity strips.

Figure 3-2. The experimental set up for 2L99 Al die casting observed with a high speed camera.

3.3 Casting trials to determine the flow properties in the LFC process

Plates of EPS foam pattern were coated with a high permeability coating of 0.3 mm and attached to a pouring cup using hot melt glue, sealed with CORFIX21™ applied to the external surface of the pattern and the pouring cup. The pouring cup had an overflow fitted to give a constant head height of 140 and 280 mm for horizontally and vertically positioned plate, respectively (the dimensions are given in Figure 3-3).

The assembly was positioned horizontally (see Figure 3-3) in a moulding box (two sides of the moulding box were removed and replaced with medium density fibreboard (MDF) in order to improve the image resolution in the real time X-ray) surrounded with sand when the

mould was half-filled, the moulding box was clamped to a compaction table and vibrated for 2 minutes to compact the sand. After filling the mould box completely, vertical vibration was again applied for another 2 min to complete the compaction process. The filled moulding box was placed in a real time X-ray which was equipped with a 225 keV X-ray tube and a 0.3 m diameter image intensifier combined with a high speed digital camera.

The mould was then cast with 2L99 alloy at 825 ^{o}C (± 5 ^{o}C) to determine the width of the molten metal stream.

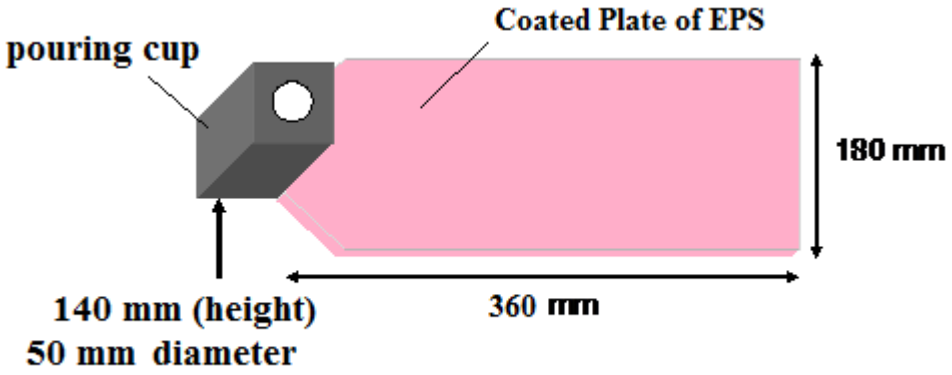

Figure 3-3. The foam pattern attached to the pouring cup, shown schematically.

This experiment was repeated with the plate attached to a longer pouring cup (280 mm) and positioned vertically, as shown in Figure 3-4.

Approximately 6 kg 2L99 alloy was melted using a high-frequency (10 kHz) induction furnace in a clay-graphite crucible.

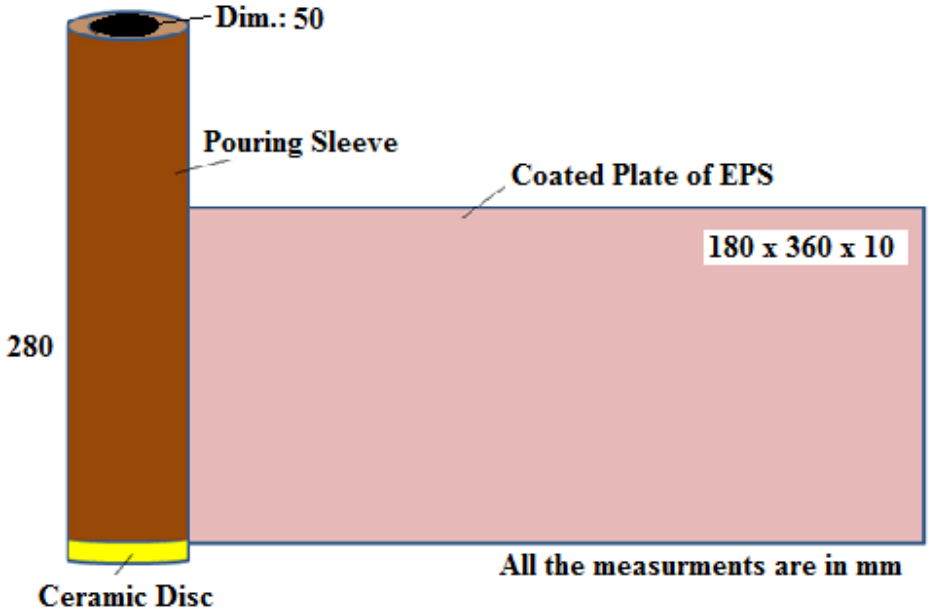

Figure 3-4. The foam pattern attached to the pouring cup to determine the thickness of the molten Al stream in the LFC process.

A top view of the experimental set up is shown in Figure 3-5, in which the plate is positioned vertically.

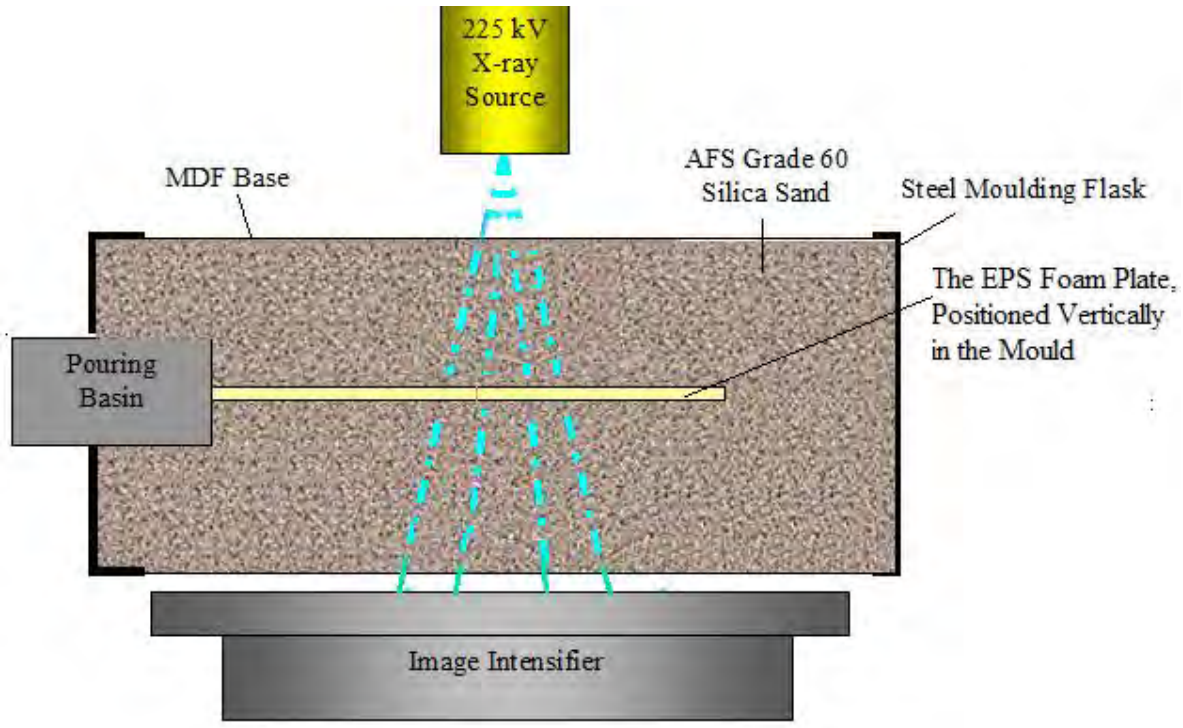

Figure 3-5. Schematical top view of the real time X-ray observation of the LFC.

The pouring arm was automatically driven into the X-ray facility and the molten metal was poured into the pouring basin continuously when the metal reached the temperature of 825 ^{o}C.

The image intensifier, X-ray source and the camera moved along with the flowing liquid metal to record the flow behaviour filling the entire foam pattern.

3.3.1 Experiments to determine the flow regime in the LFC process

The measured liquid metal velocity of Al alloys LFC in the literature [34, 45] was low enough to suggest that the metal flow in the LFC process was laminar rather than turbulent, as is normally the case in conventional open-cavity casting. Therefore a set of experiments were carried out in the real time x-ray to obtain a more accurate value of the liquid metal velocity at several points along the casting. For these tests, a thermocouple was placed in the running system in the middle of the pouring sleeve to monitor the pouring temperature (in this test a completely filled casting was desirable to obtain the Reynolds number).

Strips of EPS foam pattern were cut from the plates to have dimensions of 50×450×10 mm, and then coated with a high permeability coating. Different casting head heights of 145, 290 and 500 mm were provided using fibre pouring sleeves of different head heights and the molten metal was cast at 820, 850, 860, 880 and 890 ^{o}C. A variety of LFC conditions were created to determine if any casting condition produces a turbulent flow. The pattern assembly is schematically shown in Figure 3-6.

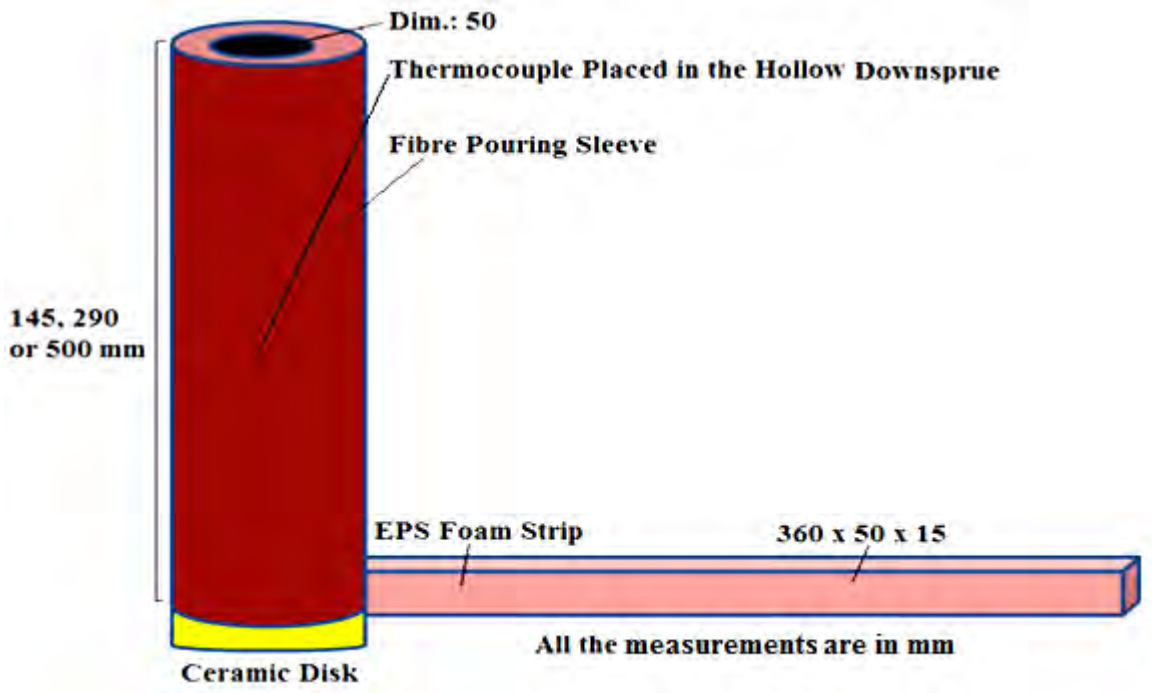

Figure 3-6. The pattern assembly for the casting experiment to determine the flow regime in the LFC process.

3.4 Fluidity testing of LFC

The characteristics of the molten AL 2L99 flow were examined in section 3.3. As a result of these observations, a fluidity test model was designed to examine the effect of different casting parameters on the fluidity of LFC. Five parameters were varied; pouring temperature, casting head height, coating thickness, coating permeability and foam type, as shown in Table 3-3. This variation created 12 different combinations and some of them carried out more than once to examine reproducibility of the tests, therefore, totally 17 fluidity tests were carried out as shown in Table 4-4.

Table 4-4. Summary of the fluidity test results.

The model was designed to consist of 4 levels of foam strips, to produce a more compact mould more easily used. The width and height of the foam strips was selected so as to avoid branching of the molten metal flow, as was determined by the experiments in section 3.3, see Figure 3-7.

Table 3-3. The casting parameters varied to test their effects on the fluidity of LFC.

Parameter	**Casting conditions**			
Pouring temperature (^{o}C)	680		780	
Coating thickness (mm)	0.3		1.3	
Coating permeability	Low		High	
Foam type	EPS	Reduced M_w Probead-70™	Brominated EPS	Low density EPS
Head height	Automatically tested as the model consisted of 4 levels of fluidity strips			

A height of 100 mm between the top of the highest foam strips and the top of the mould was left to avoid failure of the coating due to an insufficient mass of compacted sand above the foam strips. The number of branches was selected to be 16 in order to reduce the heat content of the liquid metal rapidly, by increasing the metal/foam interface area again making for a shorter, more convenient test. This mould also increases the number of results obtained from a test. Finally, a space of 80 mm was placed at the bottom of the downsprue of the casting to reduce the surface turbulence of the liquid metal flow before entering the fluidity strips. As was mentioned, the downsprue was made of Kalmin 50A boards.

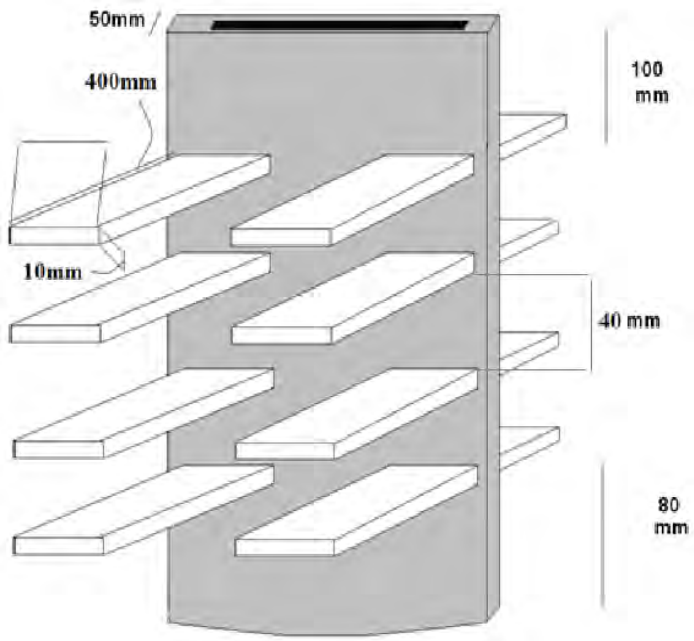

Figure 3-7. Schematic of the fluidity model.

The melting process was carried out as described in section 3.1.5. A pouring basin was placed above the downsprue. Since the casting head height should be kept constant during the casting process a graphite stopper was used to block the downsprue. The molten metal was then poured slowly into the pouring basin and the stopper pulled out when the molten was reached 20 ^{o}C above the desired temperature.

3.4.1 Recording the temperature at different points of the fluidity test

To learn about the solidification behaviour of LFC, some of the fluidity experiments (3) were carried out with thermocouples embedded in the foam patterns. This was to show the position of the liquid metal front at any time, its velocity and the reduction in the temperature of the liquid metal with flow to help interpret the flow behaviour of LFC. The thermocouple arrangement is shown in Figure 3-8.

As the pattern was filled by the molten 2L99 alloy, the temperatures in the patterns was recorded every 0.1 s using a standard computer-based data acquisition system. This was carried out for five different casting conditions.

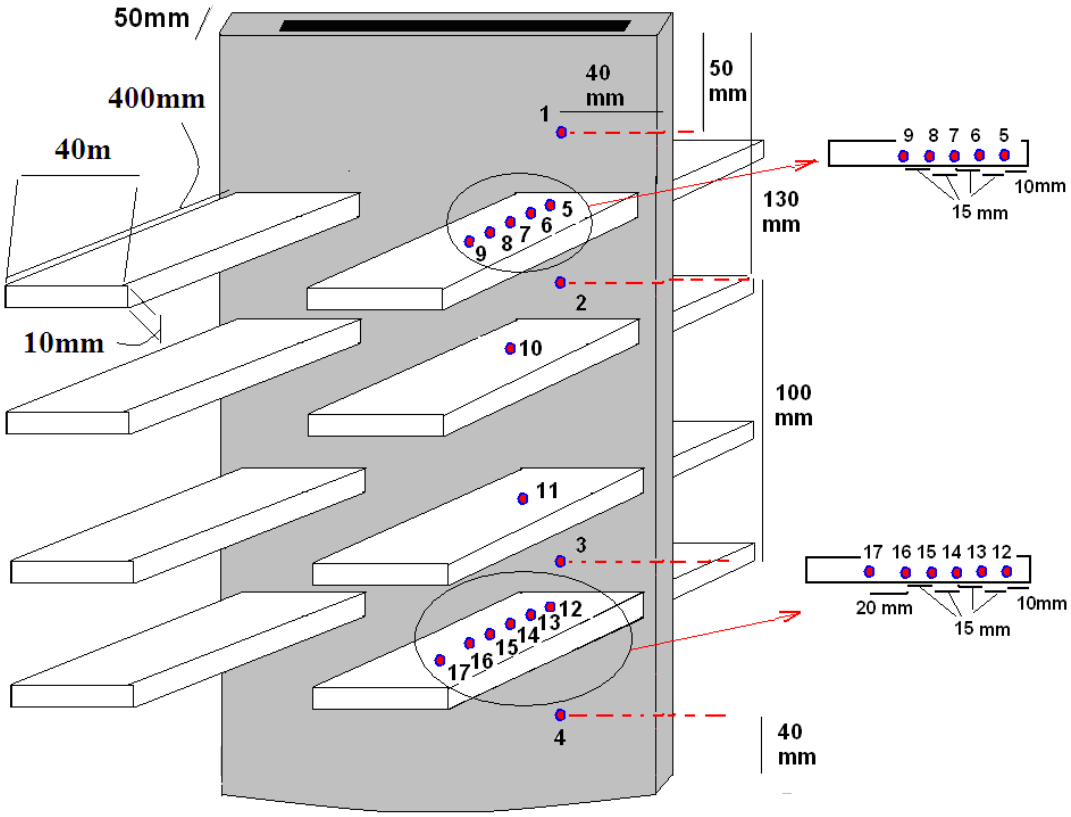

Figure 3-8. The map of thermocouples inserted in the fluidity strips. Red dots show the thermocouple positions (perpendicular to the metal flow direction and in the downsprue).

3.4.2 Experiment to compare the effect of the coating permeability on the flow behaviour of LFC

Parallel to the fluidity tests which included an examination of the effect of the coating permeability on the flow behaviour in the LFC process, another test was carried out to clarify the latter. Two fluidity strips were coated with 0.3 mm of high and low permeability coatings and cast at the same time at 680 ^{o}C, attached to the same pouring sleeve, as shown in Figure 3-9a.

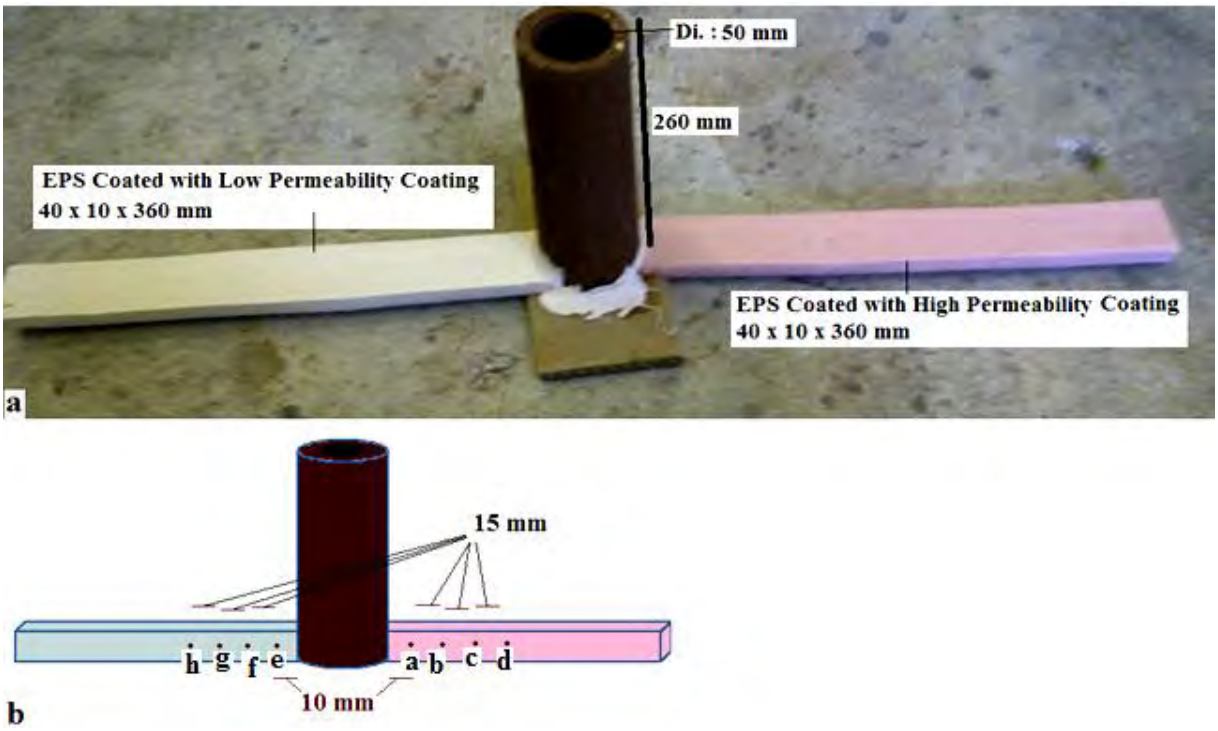

Figure 3-9. Assembly of the casting to compare the effect of low and high permeability coatings on the flow behaviour in the LFC process.

To obtain cooling curves from different points of the casting, thermocouples were again embedded in the foam pattern in both strips as shown schematically in Figure 3-9b. The temperature change was recorded at a rate of 0.1 Hz to measure the velocity of the molten metal to estimate the thickness of the metal/foam interface, the time of freezing and finally the heat transfer coefficients from the molten metal to the foam pattern and to the mould for each fluidity strip. This experiment was carried out to compare the effect of LFC with different coating permeabilities on the fluidity of LFC in the same casting (one strip coated with high permeability and the other coated with low permeability coating) and the fluidity lengths of this experiment cannot be compared to the actual fluidity tests.

3.5 Thermogravimetric analysis of EPS decomposition

To learn about the decomposition byproducts of EPS foam pattern, an experiment was arranged for the thermogravimetric analysis of the decomposition temperatures and

byproducts of EPS performed by NETZSCH-Group (Bavaria, Germany) using Discovery TGA™, coupled with mass spectrometry. EPS samples were analysed under pure Ar with the temperature increased from 25 ^{o}C to 800 ^{o}C with a rate of 10 Kmin^{-1} (the temperature range of Al alloys LFC) [106].

3.6 Irradiation processing

The degradation byproducts from the foam can only become absorbed by the coating when their M_w is reduced to a critical value [8]. Therefore using a lower molecular weight pattern may lead to higher quality castings because less reduction in M_w will be required before absorption of the liquid polymer byproduct into the pattern coating. The M_w of expanded copolymer foam patterns may be reduced by exposure to γ-radiation.

Plates of EPS and PMMA (10 mm of thickness), and the EPS-PMMA copolymers of Probead-70™ (10 mm thickness of) and Probead-30™ (15 mm of thickness) were irradiated by a Cobalt-60 γ-ray source in order to reduce their M_w. The foam plates were exposed to dosages of up to about 190 MRad. In addition to this, the effect of different radiation sources, (γ-rays or an electron beam), were also compared at dosages of up to about 180 MRad. All radiation processing was performed by Isotron (Daventry, UK). The effect of irradiating the foam patterns on their M_w was determined using Gel Permeation Chromatography (GPC).

The foam patterns sealed in polyethylene bags under a vacuum of 0.5 bar to attempt to minimize the presence of oxygen and reduce cross-linking. Some of the plates were also processed in air to examine the effect of irradiation under vacuum.

3.6.1 Gel Permeation Chromatography

Gel Permeation Chromatography (GPC) determines the complete molar mass distribution of a polymer. In GPC, a dilute polymer solution passed into a column containing a porous gel. The

small molecules of the solvent in the solution pass through carrying the polymer molecules however the largest polymer molecules are excluded and can only pass through the largest pores of the column and consequently have a much shorter path to follow. The polymer molecules elute from the chromatography column in order of decreasing molecular size in solution. The concentration of polymer is plotted against the elution volume providing a qualitative indication of the molar mass distribution [107].

Gel Permeation Chromatography (GPC) was used to determine the extent of reduction in the M_w of the foam patterns due to irradiation processing and the average molecular weight (M_w) of the irradiated foam plates.

All GPC work was carried out by Rapra Technology (Shrewsbury, UK). A single solution of each sample was prepared by the addition of 10 ml of tetrahydrofuran (THF) to approximately 20 mg of each polystyrene sample. The solutions were left for at least 4 hours to dissolve. After thorough mixing, the solutions were filtered through a 0.2 μm polyamide membrane [108].

The GPC system used for this work was calibrated with polystyrene and the results of the GPC measurements were expressed as 'polystyrene equivalent' M_w rather than absolute values of M_w, it was therefore necessary to show that comparisons between results obtained within this work and the critical M_w values obtained by Davies and Griffiths [8] would be valid, see section 4.5.3.

3.6.2 The effect of irradiation on the strength of the foam patterns

In order to ascertain the effect of γ-irradiation on the mechanical properties of the irradiated foams, 3 point bending tests were carried out on samples of irradiated Probead-70™ of dimensions of 80 x 50 x 10 mm, subjected to a 30 kg load applied at 5 mm min^{-1}.

3.6.3 Casting trials

The resulting foam patterns from irradiation processing were cut to make strips of dimensions of 10 x 40 x 300 mm and then coated with a 0.3 mm high permeability coating in the case of 2L99 casting and 0.5 mm of "SEMCO®Perm C2™".in the case of cast iron casting. They were then attached to a pouring sleeve of 145 mm height with inner diameter of 50 mm. The moulding process and the pattern assembly were similar to section 3.1. Strips of Probead-70™ were cast with 2L99 alloy while the irradiated plates of Probead-30™ were cast with cast iron. The pouring temperature was 780 ^{o}C for 2L99 LFC and 1450 ^{o}C for cast iron LFC.

3.6.4 Porosity measurement

Defects such as internal porosity and surface cavities are considered to be associated with the entrapment of liquid polymer degradation byproducts at the casting-coating interface. To characterize the quality of the castings obtained, their porosity was measured using image analysis, carried out on polished samples (to 1 μm) taken from the centre line of the castings. The internal porosity was characterised by measurement of the total porosity area on a surface of 25×10 mm. About 35 images were taken and analysed to measure the area percentage occupied by porosity.

In addition, surface cavities on the bottom casting surface, were characterised by measurement of their total length and frequency.

3.6.5 Mechanical properties of the castings

The mechanical properties of the castings were examined to investigate any improvement associated with reduced M_w foam patterns. Hardness (Vickers), tensile and fatigue properties were examined.

3.6.5.1 *Tensile*

After cooling, the strips cast with 2L99 alloy were removed from the flask, cleaned, and then examined for any surface defects. Strips were then sectioned from their length and machined into tensile test samples (with dimensions given in Figure 3-10). The tensile testing was performed on a Zwick tensile testing machine at a strain rate of 1 $mm.min^{-1}$. A gauge length of 70 mm was used.

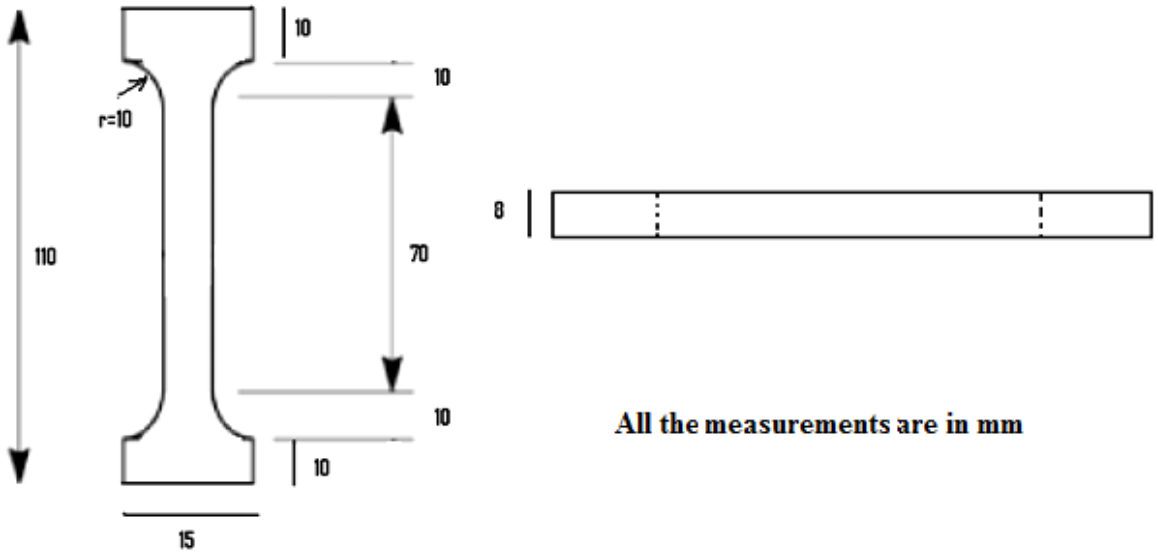

Figure 3-10. Dimensions of the specimens used in the tensile tests.

3.6.5.2 *Fatigue*

To establish the effect of using reduced M_w foam patterns on fatigue properties, test bars of dimensions 10 × 10 × 70 mm were taken from the centre line of the 2L99 strip castings with dimensions of 200 × 40 × 10 mm, cast at 780 ^oC with head height of 100 mm, and given a T6 heat treatment, (solutionized at 535 °C for 12 hours, aged at 135 °C for 6 hours). These samples were subjected to a high cycle fatigue test using 4 point bending, with maximum and minimum forces of 2.5 and 0.25 kN, frequency of 67 Hz, and loading span on the top and bottom of the specimens of 20 mm and 60 mm, respectively.

The samples were placed in the fatigue test machine with their as-cast surfaces intact, arranged so that the base of the casting faced downwards. This meant that the surface containing the cavities that were suspected of being associated with liquid polymer degradation byproducts trapped at the casting-coating interface experienced the maximum stress. Following this a JEOL 6060 scanning electron microscope (SEM) was used to examine the fracture surface and the crack initiation point.

3.6.6 X-ray observation of the castings with irradiated plates

To determine any difference in the metal/foam interface in LFC with untreated foam patterns and irradiated foam patterns, plates of untreated Probead-30™ (M_w 271,000 $gmol^{-1}$) and irradiated plates of Probead-30™ with 80 and 140 MRad (having M_w of 178,000 and 113,000 $gmol^{-1}$ respectively) were coated with high permeability coating of 1 mm thickness and cast with 2L99 alloy. The thickness of the foam plates was 10 mm. The plates were fitted with a bottom-gated casting system, as shown in Figure 3-11.

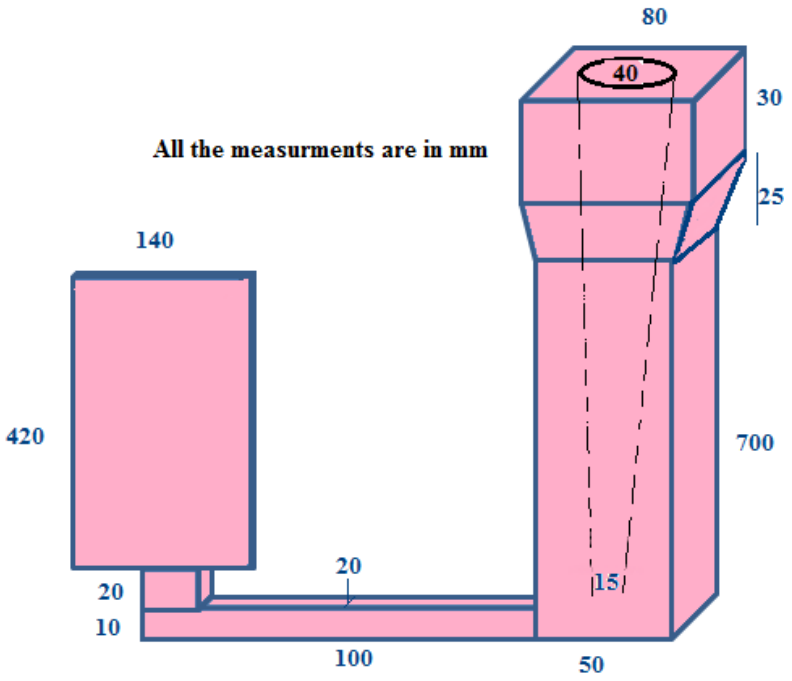

Figure 3-11. Pattern assembly for the bottom filled LFC with irradiated and untreated foam patterns.

The melting process and delivery of the molten metal to the X-ray facility proceeded as described in section 3.3. When the desired temperature of 820 ^{o}C was reached, the molten metal was poured into the pouring basin. The camera moved upward with the flow of the metal filling the plate to maintain a view point at the metal/foam interface.

4 RESULTS

4.1 Characteristics of flow in LFC

4.1.1 Real-time X-ray observation of filling of lost foam castings

To learn about the characteristics of molten 2L99 Al flow in LFC, a series of experiments were cast with different conditions to reveal such features as the width, thickness and velocity of the flowing molten 2L99 Al in the LFC process.

When a flat horizontal section was cast, the liquid aluminium split into two streams. It was observed that the narrower stream had a width of about 50 mm, indicating that the design of the fluidity test should be narrower than 50 mm to prevent flow splitting obscuring the fluidity test results. Therefore in the LFC fluidity test the width of the foam pattern strip was selected to be 40mm. to view the video of the foam plate filling see APPENDIX I.

Three plates were positioned vertically (see section 3.3), to determine the natural height (thickness) of the molten metal flow. In these experiments, the filling of the foam patterns was observed in real time X-ray, as shown in Figure 4-1.

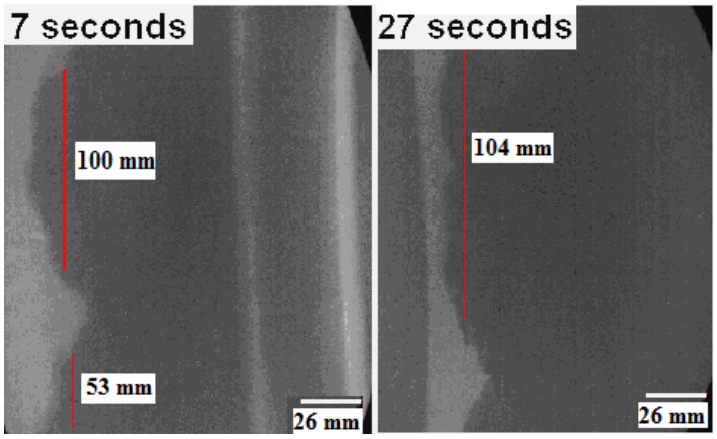

Figure 4-1. The molten aluminium filling EPS plate positioned vertically coated with high permeability coating of 0.3 mm thickness, cast at 825°C, test 3.

The results show that there were two liquid metal streams filling the vertically positioned foam pattern, one at the bottom of the plate, moving ahead of the molten metal front and the other stream filling the top of the pattern. The metal stream at the bottom of the casting had a varying height while the flow at the top of the casting had an approximately constant height of about 100 mm.

Therefore, it was deduced that in LFC of a vertical plate, the molten metal flow often branched at the bottom of the casting and a secondary stream could advance ahead of the main stream with a height of between 35 to 55 mm at the bottom which obscured the measured fluidity length. Therefore to avoid having the pattern filled by more than one layer of molten metal stream, the thickness of the pattern should be less than 35 mm.

4.1.1.1 Laminar or turbulent flow in the LFC process?

To determine whether the metal velocity during mould filling in the LFC process would produce laminar or turbulent flow in the bulk liquid, several EPS foam pattern strips were cast horizontally (with 2L99 and pure Al) while observing the metal front velocity using real-time X-ray. Casting head height and pouring temperature were varied in order to alter the conditions in LFC and influence the velocity of the molten metal. A high pouring temperature was deliberately selected (820°C to 890°C) to produce a high velocity of filling. The different casting head heights were 145, 290 and 500 mm.

The velocity of molten metal was measured at three points, the beginning, middle and end of the casting strip, from observation of the distance moved from frame to frame in the real-time X-ray. Table 4-1 shows the Reynolds numbers calculated for different pouring temperatures while

Table 4-2 shows the Reynolds numbers calculated for the velocities of castings cast with a high pouring temperature (890 ^{o}C), but with varying casting head heights.

The characteristic length, L, is required to calculate the Reynolds number and was defined to be 4 times the cross-sectional area, divided by the wetted perimeter for the rectangular casting channel. According to the dimensions of the casting channel (10×360×50 mm) L has a value of 0.017 m. The dynamic fluid viscosity, μ, was taken to be 0.0012 Pa·s at 800 °C and ρ, the density of the liquid metal, is 2436 kg m^{-3} [109].

In the case of 2L99 alloy, the measured velocities varied from 5.1 mms^{-1} to 13.6 mms^{-1} while the fluidity length varied from 165 mm to 396 mm. In the case of commercially pure aluminium (CP Al), the velocity varied from 9.2 mms^{-1} to 16.2 mms^{-1} and the length of the foam strip, 450 mm, was filled completely.

Table 4-1. The Reynolds numbers calculated for different flow velocities in the LFC process cast with 2L99 alloy and CP Al, casting head height=145 mm.

When the casting head height was 145 mm.										
Cast Metal	Pouring temperature (°C)	At the beginning of strip		At the middle of strip		At the end of strip		Mean		Fluidity length (mm)
		V (mms^{-1})	Re	V (mms^{-1})	Re	V (mms^{-1})	Re	V (mms^{-1})	Re	
2L99	820	13.6	553	13.5	530	12	488	12.1	491	229
2L99	820	13.5	548	9.2	374	5.5	223	9	366	165
2L99	850	9.2	376	7	285	5.1	207	8.2	333	235
CP Al	860	15.7	638	9.7	394	9.2	374	10.1	411	242
CP Al	860	16.2	658	10.1	410	9.7	394	11.3	459	263

Table 4-2. The Reynolds numbers calculated for different flow velocities in the LFC process cast with 2L99 alloy, pouring temperature =890 °C .

When the pouring temperature was 890 °C.									
Head height (mm)	At the beginning of strip		At the middle of strip		At the end of strip		Mean		Fluidity length (mm)
	V (mms^{-1})	Re	V (mms^{-1})	Re	V (mms^{-1})	Re	V (mms^{-1})	Re	
290	13.6	553	12.8	520	6.6	268	10.6	430	275
500	13.1	532	9.7	431	5.7	251	11.25	495	396

Reynolds numbers for the measured velocities varied from 207 to 553 for 2L99 alloy, and from 374 to 658 for pure aluminium. A flow is laminar when its Reynolds number is under 2,000 to 3,000, and the transition from laminar to turbulent flow is usually taken as 5×10^5 [88] All of the calculated Reynolds numbers were therefore well inside the laminar flow region, and it can be concluded that the LFC process has a laminar flow trait.

4.2 Fluidity in LFC

4.2.1 Fluidity in an empty cavity casting

To check if Fleming's fluidity equation predicts well the fluidity of casting in an open cavity mould, 2L99 aluminium was cast as was described in section 3.2.

The predicted fluidity length was determined using Equation 2-2, $L_f \cong \frac{\rho_s a V}{2h(T_M - T_0)}(H + c'\Delta T)$.

Where [109];

ρ= density of liquid metal, 2435 kgm-^{3}

H= latent heat of solidification, 389,000 Jkg $^{-1}$

c'= the specific heat capacity, 910 Jkg^{-1}K^{-1}

h= heat transfer coefficient from the liquid metal to the mould, 1800 Wm^{-2}K^{-1} (heat transfer coefficient of the die mould)

a= mould cross section modulus, the ratio of the volume element to the surface element of the casting channel calculated to be 0.00227 m.

The mean velocity of the molten metal (2L99 alloy) in the left channel of the mould was measured to be 0.46 ms^{-1} (three tests were carried out). According to Fleming's equation (Equation 2-2) and assuming the heat transfer coefficient was not affected by replacing the upper half of the mould by glass, the predicted fluidity length for the left strip should have been 567 mm while the mean measured fluidity length for the left strip was 610 mm. The mean velocity of the molten metal in the right channel was 0.43 ms^{-1} which gave a predicted fluidity length of 529 mm while the mean measured fluidity length was 520 mm.

The precision of the velocity measurement was ± 0.006 ms^{-1} according to the camera speed (60 frames per second) causing a $\pm 1.6\%$ error in velocity measurement. The results show that Fleming's equation predicted the fluidity length of flowing metal accurately in the case of open cavity casting. In the next section Fleming's equation was tested for the case of LFC.

4.2.2 Fluidity of lost foam casting

To examine Fleming's fluidity equation for LFC, EPS foam strips were cast with commercial purity (CP) aluminium and aluminium 2L99 alloy at 720 ^{o}C and 660 ^{o}C respectively. The lower pouring temperature was used to ensure that the foam strip was not filled completely (a

filled length of foam does not give a measurable fluidity length). A 0.3 mm layer of high permeability coating was applied to the surface of the EPS foam pattern in each case.

For a foam strip with dimensions of 50×15×360 mm, the ratio of the volume to the area (a) was calculated to be 0.00577 m. And the heat transfer coefficient from the molten metal to the mould is taken to be 420 $Wm^{-1}K^{-2}$ [90].

The predicted values for the fluidity lengths obtained by Fleming's equation can be calculated as follows;

a) CP Aluminium, cast at 675 ^{o}C (15 K superheat)

$$L_f = \frac{2436 * 0.00577 * 0.012}{2 * 420 * (660 - 20)} * (396000 + 897 * 15) = 0.01425m$$

b) CP Aluminium, cast at 670 ^{o}C (10 K superheat)

$$L_f = \frac{2436 * 0.00577 * 0.012}{2 * 420 * (660 - 20)} * (396000 + 897 * 10) = 0.01395m$$

c) 2L99 alloy, cast at 678 ^{o}C (15 K superheat)

$$L_f = \frac{2436 * 0.00577 * 0.01}{2 * 420 * (617 - 20)} * (396000 + 897 * 15) = 0.126m$$

d) 2L99 alloy (Al-7Si-0·4Mg), cast at 678 ^{o}C (10 K superheat)

$$L_f = \frac{2436 * 0.00577 * 0.01}{2 * 420 * (617 - 20)} * (396000 + 897 * 10) = 0.125m$$

Each of these casting conditions (a to d) were cast twice and their fluidity lengths, mean fluidity length and standard deviations are shown in Table 4-3. The predicted fluidity lengths were calculated using the velocity values determined from the casting experiments observed

by real-time X-ray in section 3.3.1. In the case of 2L99 alloy the actual casting temperature measured in the pouring basin was 687 ^{o}C, and a length of 270 mm was filled in 28.8 seconds suggesting that the mean velocity of metal flow was 0.01 ms^{-1}.

Table 4-3. Comparison between the predicted fluidity lengths by Fleming's equation and the actual fluidity lengths of LFC.
*** The length of filled foam strip was 450 mm.**

Casting material	Superheat (K)	Predicted fluidity length (mm)	Fluidity length test l (mm)	Fluidity length test 2 (mm)	Mean measured fluidity length; (mm)	Standard deviation of (mm)	Fleming's predict fluidity
2L99	15	126	191	199	195	4	35% shorter
	10	125	216	228	222	6	43% shorter
	70	142	262	278	270	8	47% shorter
CP aluminum	15	119	Filled*	Filled*	Filled*	Filled*	More than 73% shorter
	10	116	Filled*	Filled*	Filled*	Filled*	More than 74% shorter

Table 4-3 shows the fluidity lengths of the castings with commercially pure aluminium and 2L99 alloy, cast at different temperatures, and compares the predicted and measured fluidity lengths. The measured fluidity length of the casting was significantly longer than the predicted fluidity length. This is also shown in Figure 4-2. The difference varied from 25% to 33% of the fluidity length for 2L99 alloy, and more than 140% in the case commercial purity aluminium. The pure aluminium casting fluidity length reached a length of 450 mm while, Fleming's equation predicted the fluidity length to be about 120 mm.

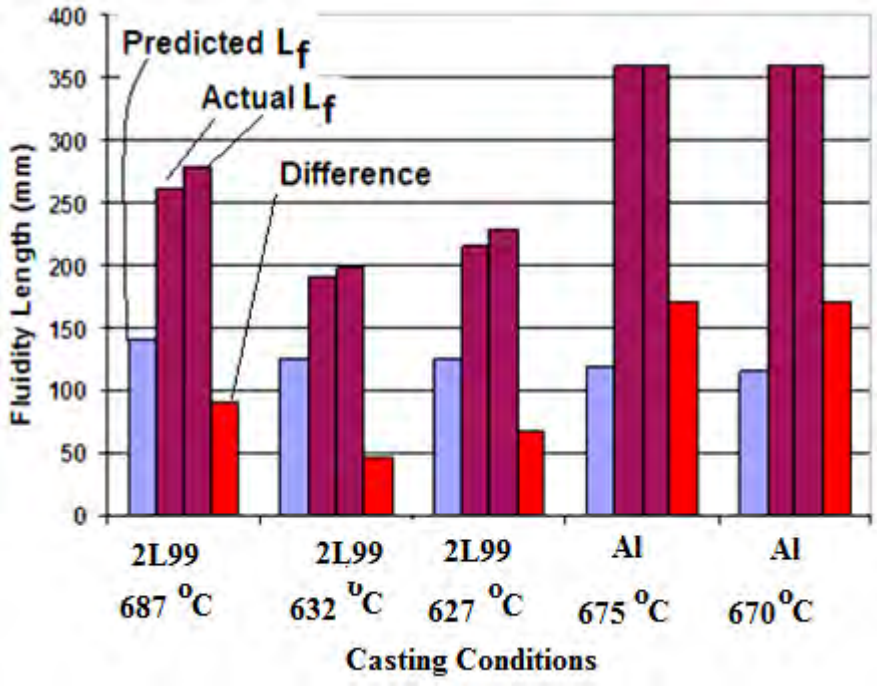

Figure 4-2. Comparison between the predicted fluidity lengths (by Fleming's) and the actual casting results.

4.2.2 Fluidity test results

To examine the effect of varying casting parameters on the fluidity of LFC, five parameters were chosen. Casting head height was included automatically, as the model consisted of four levels of foam strips. The other variables examined were the effect of pouring temperature, coating thickness and coating permeability. Effect of foam type was also examined by using low density EPS, brominated EPS and reduced M_w Probead-70™. Table 10-1 to Table 10-17 in Appendix II show the results of the fluidity tests, giving the fluidity lengths of the castings for each branch, the total and mean fluidity length and the casting front curvature with their standard deviation. Figure 4-3 shows one example of the fluidity tests (casting D2).

Figure 4-3. One of the fluidity tests, (casting D2)

The pouring temperatures were 680 ^{o}C and 780 ^{o}C (± 10 ^{o}C). In the case of coating thickness, the applied coating had nominal thicknesses of 0.3 mm and 1.3 mm, however up to ± 0.1 mm was recorded in the actual coating thickness. The values recorded in the experiments are given in Table 10-1 to Table 10-17.

L_1 to L_4 are the fluidity lengths of the cast strips at each level of castings. R_1 to R_4 are the radii of the curvatures at the front tip of the cast strips, calculated by measuring the length of the arch. The results have been summarized in Table 4-4 which shows all of the mean fluidity lengths, and the standard deviations where the casting was repeated.

Table 10-1 shows the results of fluidity test A1, cast at 780 ^{o}C using an EPS foam pattern and high permeability coating of 0.3 mm. This experiment was repeated twice to check reproducibility (see Table 10-2 and Table 10-3). Comparing these tests shows that the fluidity was very reproducible as the standard deviation of the three tests was 5 mm. This is low compared to the mean fluidity lengths of the tests (274 mm).

Similarly, Table 10-5 and 10-6 show results of fluidity tests cast at 780 ^{o}C, with low permeability coating and coating thickness of 0.3 mm, (C1 and C2), to verify the reproducibility of the fluidity test. It is also the case for Table 10-7 and 10-8 (D1 and D2) and Table 10-12 and 10-13 (H1 and H2).

Figure 4-5 compares the standard deviations and the mean fluidity lengths of the fluidity tests when the test was performed more than one time to judge reproducibility (castings A, C, D and H).

In Figure 4-4 and Figure 4-5, the standard deviation of the fluidity tests compared with the fluidity lengths and the mean fluidity length of the castings respectively, indicated that the standard deviation was negligible compared to their fluidity lengths. Therefore, the fluidity test design was reproducible and the results obtained did not show considerable scatter.

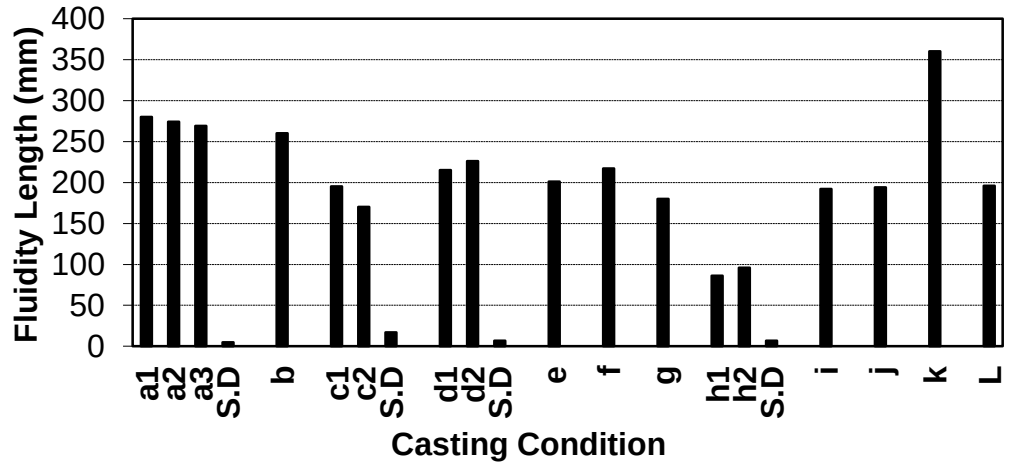

Figure 4-4. Summary of the fluidity results of casting in the different casting conditions, see Table 4.4.

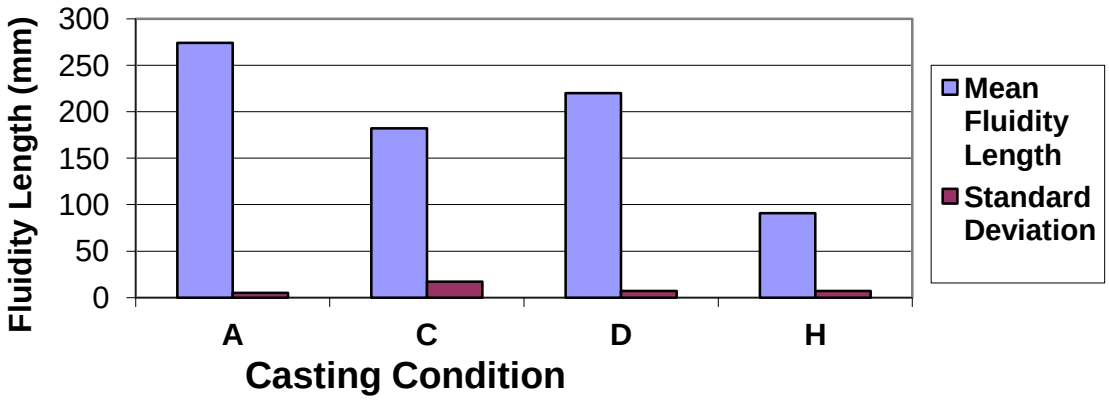

Figure 4-5. Reproducibility of the fluidity test. S.D is significantly small compared to the mean Lf, see Table 4-4.

	No. of tests	Coating permeability	Foam type	Casting temp. ^{o}C	Coating thickness (mm)	Fluidity length(s) (mm)	Mean fluidity length (mm)	Standard Deviation (mm)
A	3	High	EPS	784	0.33	280	274	5
				783	0.36	274		
				778	0.3*	269		
B	1	High	EPS	783	1.40	260	260	N.A
C	2	Low	EPS	776	0.3*	195	182	17
				780	0.32	170		
D	2	Low	EPS	784	1.37	215	220	7
				787	1.45	226		
E	1	High	EPS	685	0.3*	201	201	N.A
F	1	High	EPS	681	1.3	217	217	N.A
G	1	Low	EPS	680	0.37	180	180	N.A
H	2	Low	EPS	677	1.36	86	91	7
				676	1.3	96		
I	1	High	Low M_w Probead-70™	685	0.36	192	192	N.A
J	1	High	Brominated EPS	683	0.28	194	194	N.A
K	1	High	Low density	683	0.3	360	360	N.A
L	1	High	Probead-70™	683	0.32	196	196	N.A

Table 4-4. Summary of the fluidity test results.
*** The nominal coating thickness (according to the dilution).**

4.2.3 Effect of casting head height on the fluidity of LFC

The mean and standard deviation of the fluidity lengths for the four levels of fluidity strips (having head heights of 260, 210, 170, 110 mm) were calculated and compared for each

fluidity test in order to establish the effect of casting head height on fluidity (see Table 4-5), shown in Figure 4-6, also. S.D.S is the standard deviation within the fluidity lengths of the four casting strips with the same head height, while S.D.L is the standard deviation of the mean fluidity lengths for the 16 strips of each casting with different casting head heights.

Table 4-5. The effect of casting head height on fluidity length of LFC.

Casting	Head height (mm)	Mean L_f (mm)	S.D.S (mm)	S.D.L (mm)	Casting	Head height (mm)	Mean L_f (mm)	S.D.S (mm)	S.D.L (mm)
A	**260**	293	14	16	G	**260**	77	32	8
	210	283	9			**210**	97	4	
	160	260	17			**160**	92	8	
	110	257	10			**110**	94	4	
B	**260**	278	22	13	H	**260**	188	15	10
	210	257	25			**210**	183	11	
	160	246	13			**160**	200	9	
	110	261	24			**110**	205	17	
C	**260**	183	10	5	I	**260**	188	15	10
	210	187	25			**210**	183	11	
	160	175	22			**160**	200	9	
	110	180	15			**110**	205	17	
D	**260**	229	4	8	J	**260**	191	29	7
	210	212	26			**210**	200	24	
	160	215	4			**160**	193	17	
	110	225	14			**110**	183	21	
E	**260**	205	7	12	L	**260**	206	33	5
	210	217	29			**210**	205	24	
	160	196	27			**160**	197	27	
	110	187	20			**110**	187	20	
F	**260**	182	12	4					
	210	178	12						
	160	188	26						
	110	185	19						

This shows that the fluidity lengths of the casting strips with different head heights were similar, although there may be a weak dependence. The highest S.D.L belonged to casting A

(16 mm), but this was smaller than the maximum standard deviation of the fluidity length of the strips with the same head height (17 mm). In other words, head height has no strong effect on the fluidity lengths of LFC at the values of head height investigated in this work.

For example, the mean fluidity lengths of casting strips with different head heights are shown in Figure 4-6 for the castings made with condition A (EPS foam pattern coated with high permeability coating of 0.3 mm and cast at 780 ^{o}C). This demonstrates that there is no clear trend observed in the mean fluidity lengths of the casting strips with different head heights. Figure 4-6 also indicates that the standard deviations of the fluidity lengths compared to their mean fluidity lengths, were negligible.

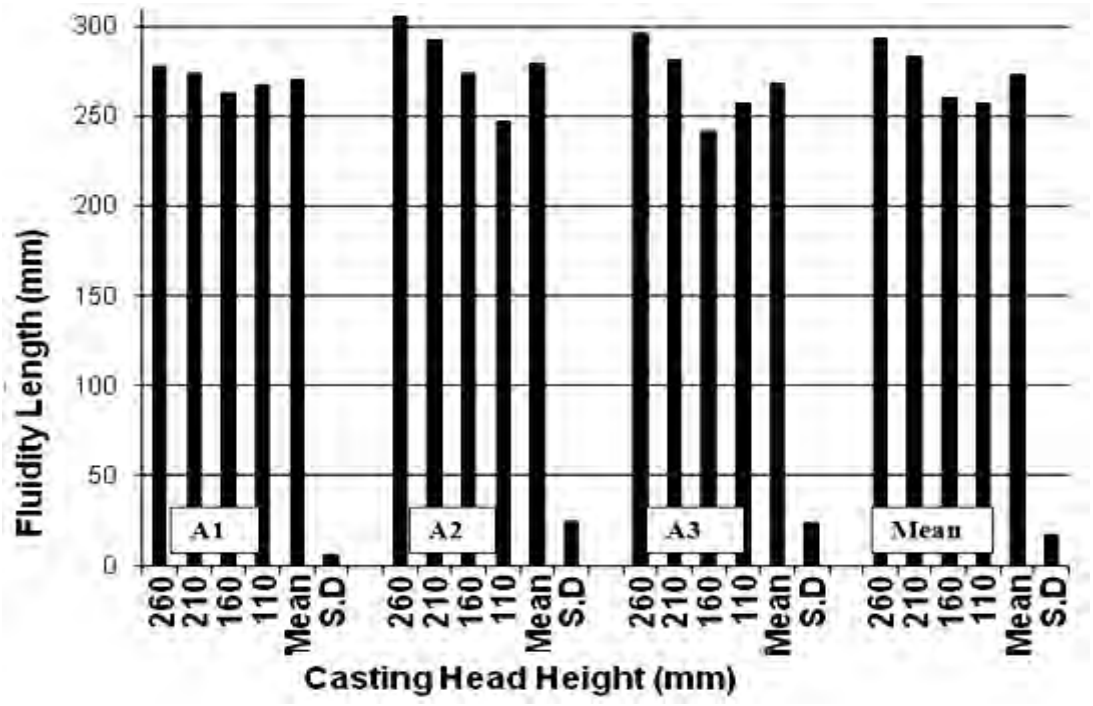

Figure 4-6. The mean fluidity lengths of different levels of fluidity strips, test A.

However, Table 4-5 suggests a weak relationship between head height and fluidity length, with the individual castings suggesting that the highest strip may give longer fluidity lengths, eg, in casting A2, but this is not consistently the case.

An F-test was carried out to check if the mean fluidity lengths of the cast strips with different head heights were significantly different. The parameters calculated in this test were:

Table 4-6. The parameters calculated for an F-test to verify if the fluidity length of the cast strips with different head heights are different.

S_B	f_b	MS_B	Sw	fw	MS_W
3496	3	1165	3050	8	381

$F = MS_B / MS_W = 3.05$, $F_{5\%}(3,8) = 4.06 > 3.05$

Where;

S_B = Between-group sum of squares.

f_b = Between-group degrees of freedom.

MS_B = Between-group mean square.

Sw = Within-group sum of squares.

fw = Within-group degrees of freedom.

MS_W = Within-group mean square.

This means that the fluidity lengths of the cast strips with different casting head heights were not significantly different at the 95% confidence level.

4.2.4 Effect of coating thickness on the fluidity of LFC

Increasing the coating thickness from 0.3 mm to 1.3 mm had different effects on fluidity at different casting temperatures and with different coating permeability. As shown in Figure 4-7, the effect of increasing thickness from 0.3 mm to 1.3 mm, when 2L99 alloy was cast at 780 ^{o}C with a high permeability coating, was a 5% reduction (Figure 4-7a) but a 20% increase with a low permeability coating. The effect of increasing the coating thickness from 0.3 mm

to 1.3 mm at 680 ^{o}C was a 8% increase and a 50% reduction in the fluidity length for high and low permeability coatings, respectively.

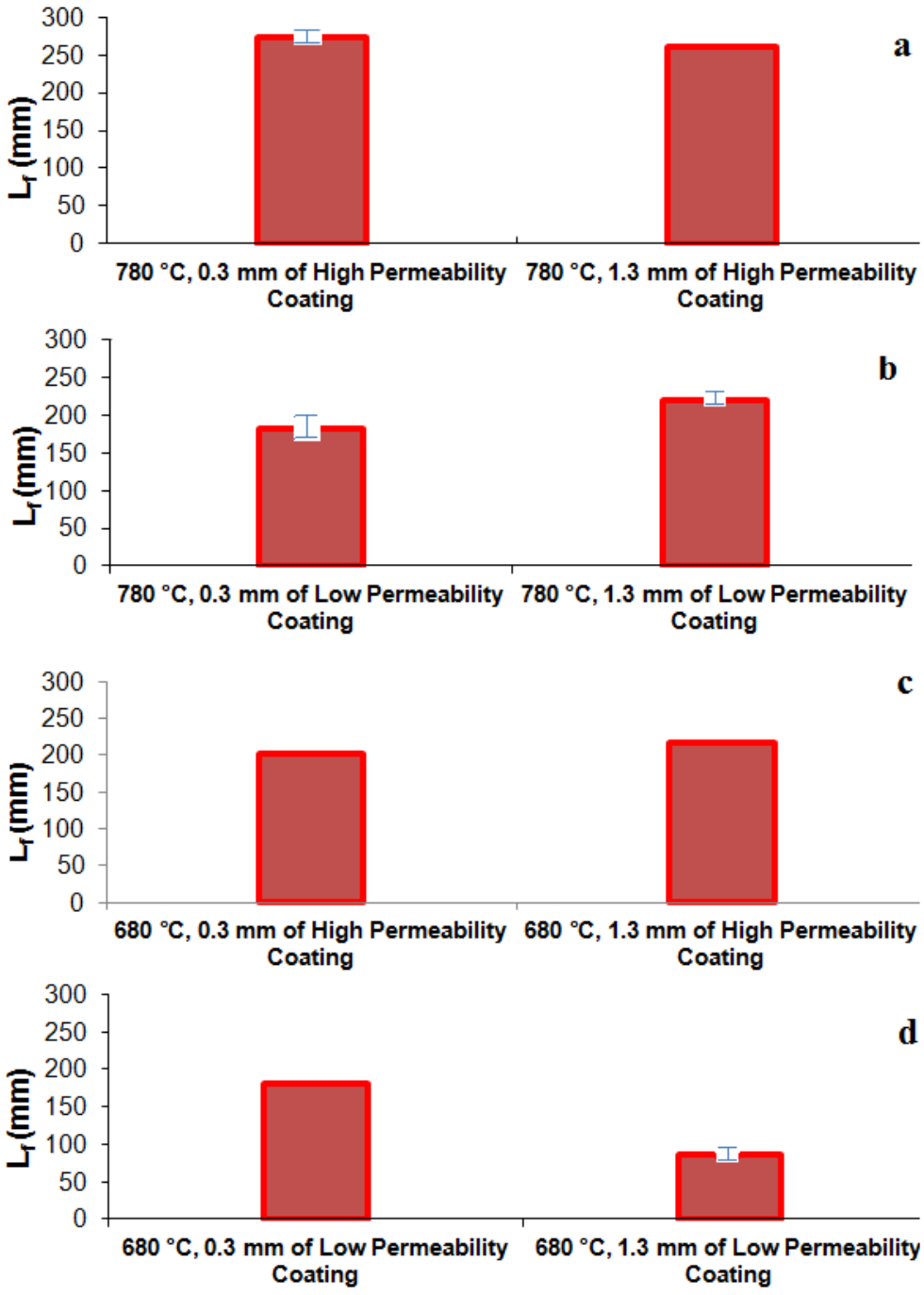

Figure 4-7. The effect of increasing the coating thickness on fluidity of LFC in different casting conditions.

The effect of coating thickness on the fluidity of LFC is obscure. The fluidity of LFC was increased with increased coating thickness only when the foam pattern was cast at a high

temperature and coated with a low permeability coating. Increasing the thickness of a low permeability coating (cast at 680 ^{o}C), resulted in a considerable decrease in fluidity length (Figure 4-7d). Changing the coating thickness of a high permeability coating did not affect the fluidity of LFC considerably (see Figure 4-7 a and c).

4.2.5 Effect of coating permeability on the fluidity of LFC

Similar to the coating thickness, the effect of coating permeability depended on casting conditions, (see Figure 4-8). When cast at 680 ^{o}C, with the foam pattern having a thick layer of coating (1.3 mm), decreasing the permeability of the coating decreased the fluidity length. When cast at 780 ^{o}C, with the foam pattern having a thin layer of coating (0.3 mm), changing the permeability of the coating from high to low reduced the fluidity length by 34%, (see Figure 4-8a). Changing coating permeability (from high to low) had the least effect on fluidity length (a 10% reduction) when a thin layer of coating was given to the foam pattern and it was cast at 680 ^{o}C (see Figure 4-8b). Changing coating permeability from high to low affected fluidity length the most when it was cast at 680 ^{o}C and the foam pattern was coated with thick layer of coating.

Hence, it can be concluded that coating permeability affected the fluidity length more when the coating was thicker. In addition, in contrast to the coating thickness, changing the coating permeability affected the fluidity of LFC at both casting temperatures (680 and 780 ^{o}C).

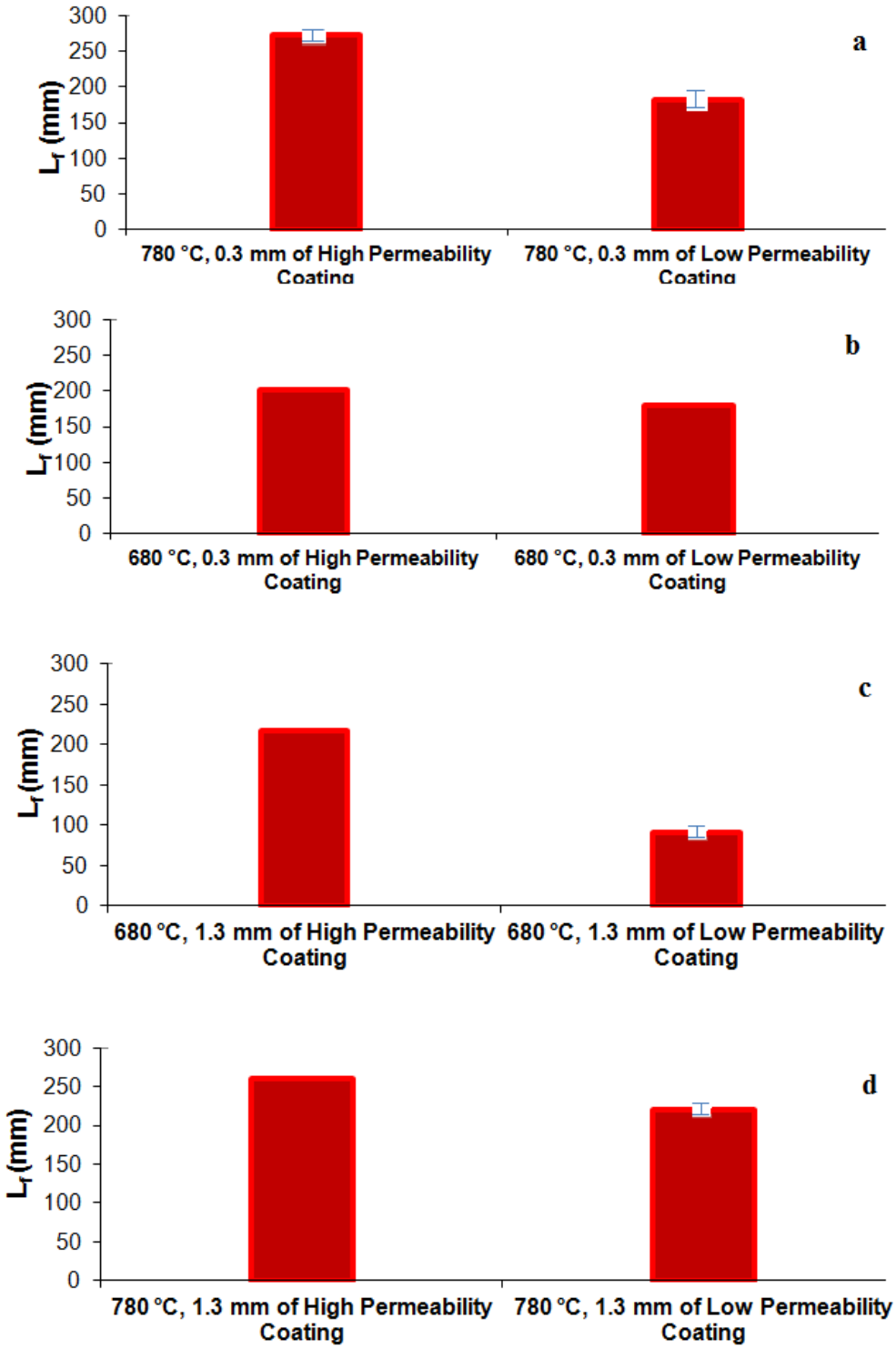

Figure 4-8. Effect of reducing the permeability of the coating on fluidity of LFC in different casting conditions.

4.2.6 Effect of casting temperature on the fluidity of LFC

Casting temperature, or in other words superheat, affects the fluidity of pure metals and alloys as was discussed in section 2.7. In the case of LFC, changes in casting temperature affect fluidity as it affects the decomposition of the foam pattern, and also other parameters similar to the conventional casting process (such as heat transfer to the mould and solidification). It was claimed that the role of pouring temperature on fluidity of LFC is not very clear [10].

In three of the four casting conditions, shown in Figure 4-9, reducing the pouring temperature reduced the fluidity length. A 58% reduction in fluidity length was recorded when reducing the pouring temperature from 780 ^{o}C to 680 ^{o}C with a pattern coating of 1.3 mm of low permeability coating, shown in Figure 4-9d. In contrast, a casting with a low permeability coating of 0.3 mm was indifferent to the change in the casting temperature, (see Figure 4-9b).

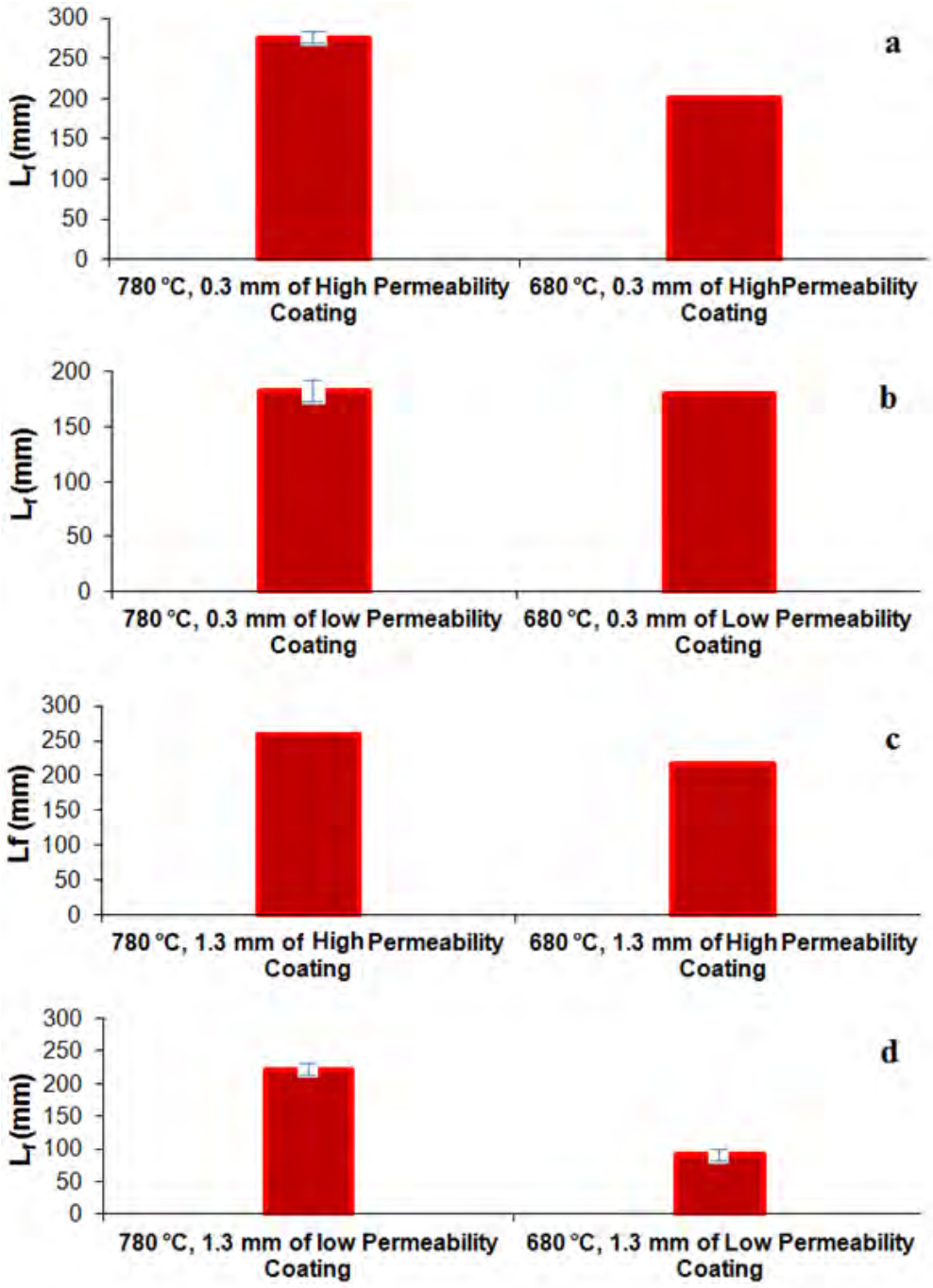

Figure 4-9. Effect of the pouring temperature on fluidity of LFC (reduced from 780 ^{o}C to 680 ^{o}C) in different casting conditions.

4.2.7 Effect of foam pattern type on fluidity

Figure 4-10 shows that the fluidity of LFC did not depend on the molecular weight of the foam pattern. Strips of Probead-70™ were exposed to ɣ−radiation which reduced their M_w to 71,000 $gmol^{-1}$. A fluidity test was then made using the irradiated foams and cast at 680 ^oC when the foams were coated with a high permeability coating of 0.3 mm thickness. Results of the fluidity test were compared with the casting of an untreated Probead-70™ foam pattern of 320,000 $gmol^{-1}$ M_w. This shows that the Mw of the foam pattern did not affect the fluidity length of LFC.

It is also demonstrated that using brominated foam pattern instead of conventional EPS did not affect the fluidity of LFC significantly. However combustion of the brominated foam pattern may be easier than untreated ones which lead to production of higher quality castings but it has not affected the fluidity length (see Figure 4-10b).

Using low density EPS (16 kgm^{-3}) increased the fluidity of LFC considerably. As the length of the foam pattern strips in the fluidity test was 360 mm and they were filled completely, the increase in the fluidity length of LFC due to using a low density foam was more than 80%, as shown in Figure 4-10a.

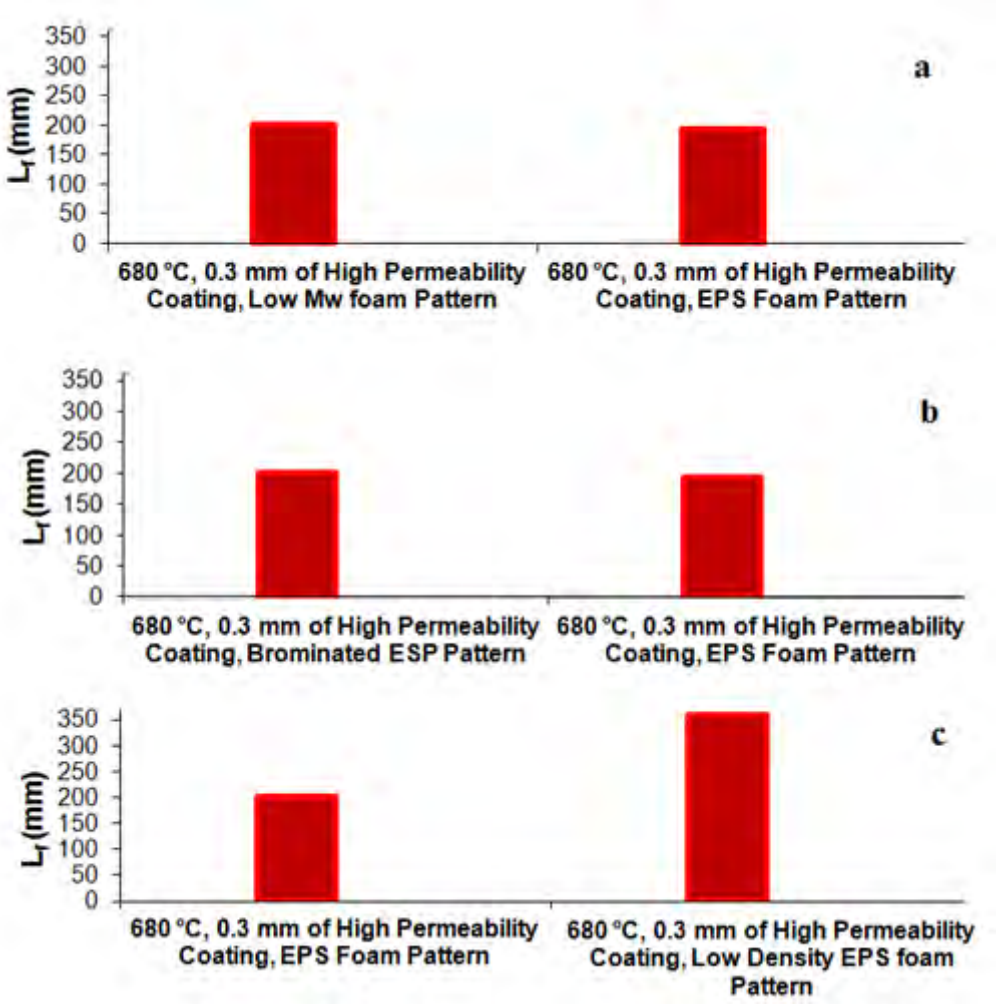

Figure 4-10. Effect of using different foam patterns (instead of conventional EPS) on fluidity of LFC.

4.3 Cooling curves measured in the fluidity tests

As was mentioned before, some of the fluidity tests (castings D2, H2 and J) were carried out with thermocouples inserted to determine the position of the liquid metal front, its velocity and the reduction in temperature of the liquid metal during filling of the foam pattern to help interpret the fluidity behaviour, (as shown in Figure 4-11).

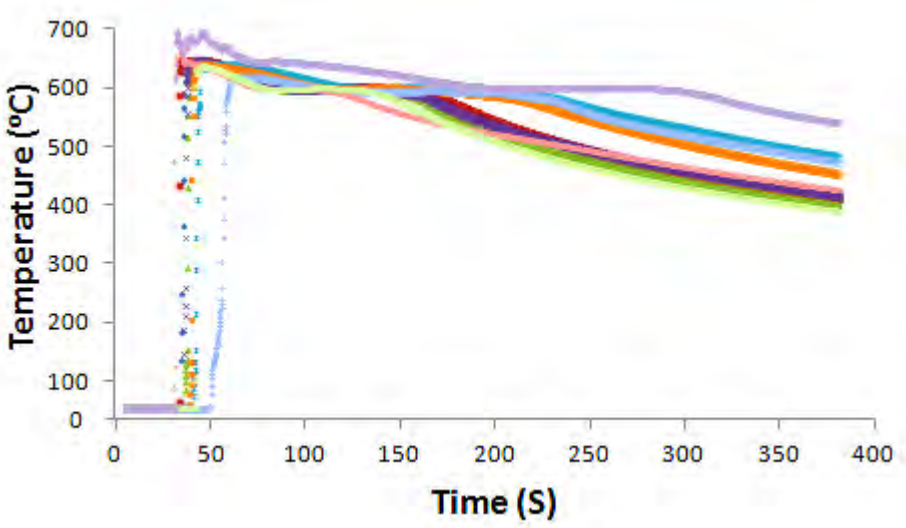

Figure 4-11. Cooling curves of different points of casting H2.

The thermocouples were inserted at points 1, 4, 6, 7, 10, 11, 12, 13, 14 and 16 (see Figure 3-8). Figure 4-12 to Figure 4-16, show part of the cooling curves of the cast alloy (2L99) at these different points of the casting.

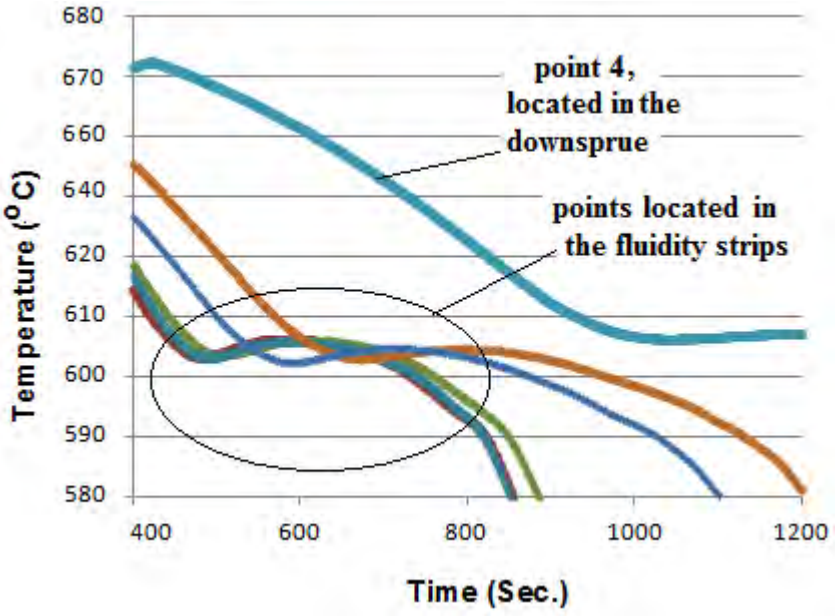

Figure 4-12. Comparison between the cooling curves of the points in the fluidity strips and the downsprue for casting H2.

Figure 4-12 shows that point 4 (located at the bottom of the downsprue) solidified after all of the points in the fluidity strips, (its cooling curve is above the cooling curves of the other

points). This is also the case for casting D2, as shown in Figure 4-13. The latest point to solidify in the fluidity strips solidified earlier than the earliest point to solidify at the downsprue and, therefore, it can be concluded that the metal in the fluidity strips solidified before the downsprue.

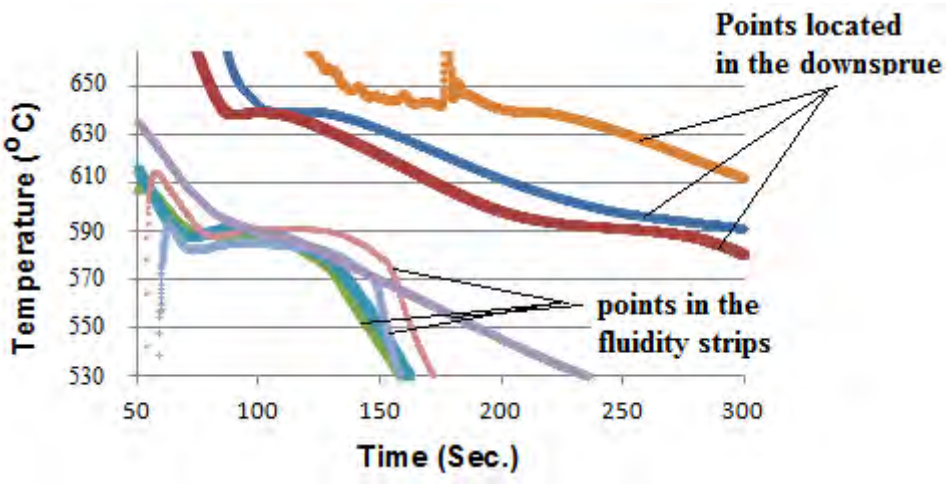

Figure 4-13. Comparison between the cooling curves of the points located in the downsprue and the points located in the fluidity strips.

The cooling curves of points 12, 13, 14, 16 located in the bottom fluidity strip of casting H2 are shown in Figure 4-14. This indicates that the closer the point was to the beginning of the fluidity strip the longer it took to solidify. Point 16 (70 mm from the beginning of the strip) was the first point to solidify while the last point to solidify was point 12 located just 10 mm from the beginning of the fluidity strip. This is also the case for the upper fluidity strips shown in Figure 4-15, point 7 (40 mm from the beginning of the strip) solidified before point 6 (30 mm from the beginning of the strip).

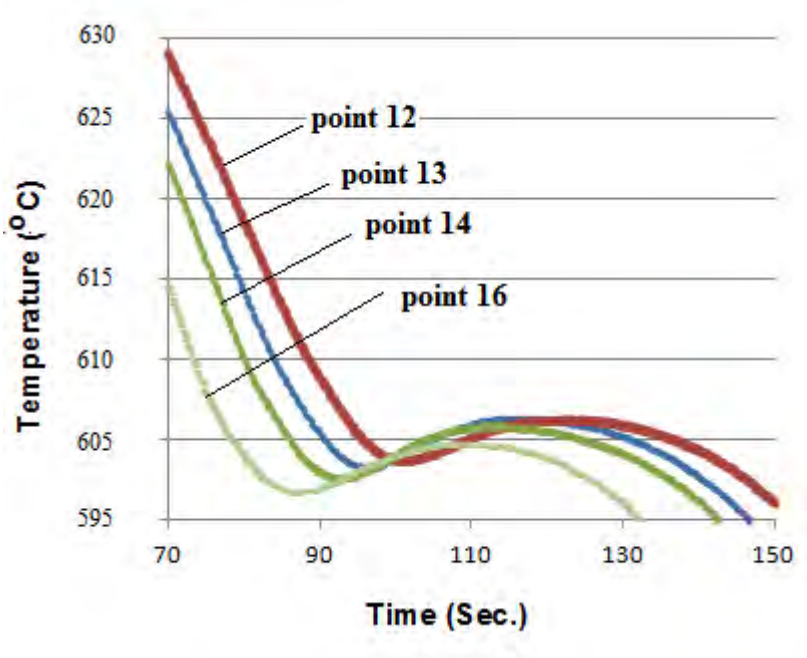

Figure 4-14. Cooling curves of points 6 and 7 located at the top fluidity strip of casting H2.

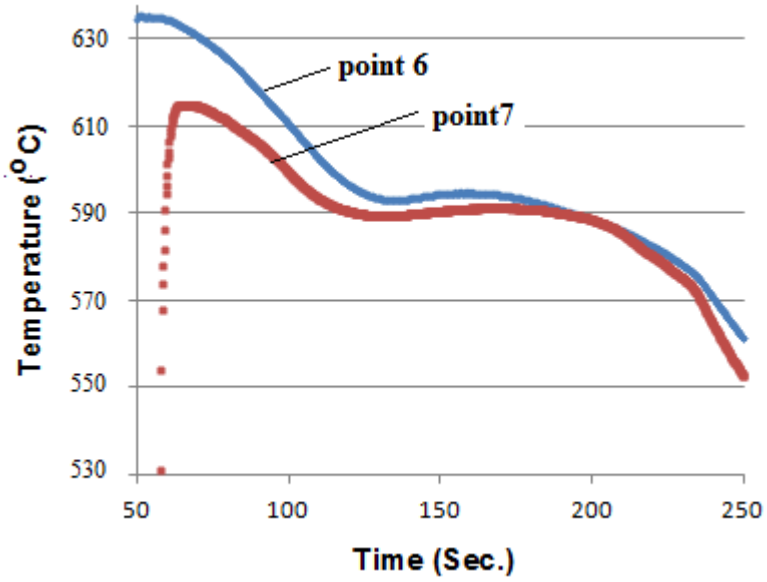

Figure 4-15. Comparison between the solidification behaviour of the points in the top fluidity strips of casting D2.

This is also confirmed by the cooling curves of the points located in the same fluidity strip of casting D2 and J.

To compare the solidification behaviour and cooling curves of different branches and downsprue in casting H2, the temperature at one point in each fluidity strip (at 40 mm distance from the downsprue) was determined and their recorded temperatures were plotted against time and compared in Figure 4-16.

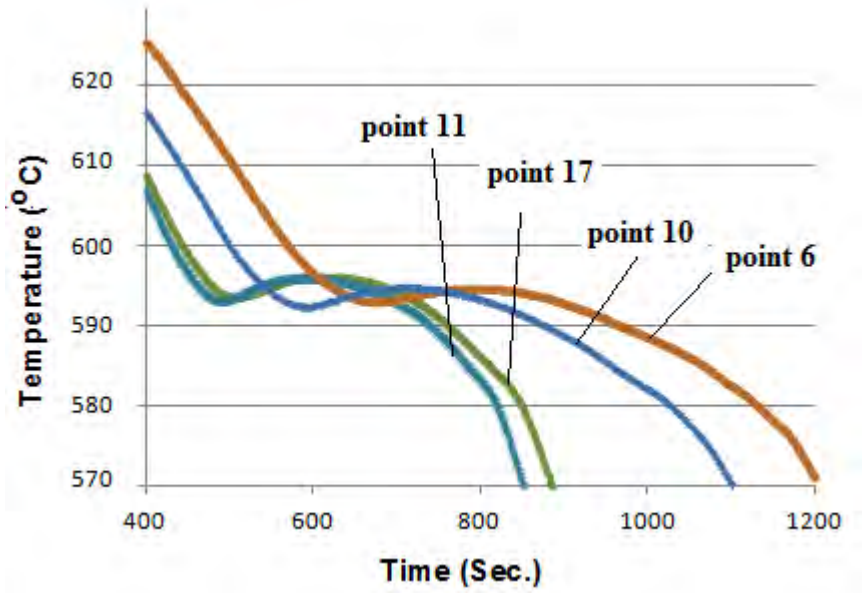

Figure 4-16. Cooling curves of different points with different casting head heights (casting H2).

This shows that the fluidity strips with different casting head heights solidified with no particular order; in other words, the solidification behaviour in the LFC was irrespective of the pouring head height.

Therefore, it can be concluded that solidification occurs at the tip of the molten metal flow at the metal/foam interface in LFC.

Data from these cooling curves were also analysed to determine the coherency temperature, cooling rate, coherency point, flow time, velocity of molten metal and the thickness of the metal-pattern gap.

4.3.1 Coherency point

As was described in section 2.7.1, once the molten metal reaches a certain temperature the volume fraction of solid is such as to cause the individual dendrites to interlock with their neighbours [76]. The liquid metal stops flowing when the liquid metal stream tip reached its coherency point. Therefore, in order to find the temperature at which the metal flow stops the coherency point of the casting should be determined. It was also reported by Veldman et al. [81]that for a certain alloy, the coherency point depends on the cooling rate during solidification. The cooling rate at different points of fluidity test H2 was calculated from the data obtained from the thermocouples inserted in the foam pattern strips.

4.3.2 Estimated cooling rate for the different points of the fluidity test in casting H2

Cooling rates at points 4, 6, 10, 11, 13, 14 and 16, located at different levels of the casting and within the downsprue, were calculated from the temperature at each point (recorded four times per second) of casting H2 (cast at 680 ^{o}C with a low permeability coating of 1.3 mm thickness), (see Table 4-7).

Table 4-7. Cooling rates of different points of casting H2.

Point	Located at	Cooling rate (Ks^{-1})	Mean cooling rate (Ks^{-1})
6	Top branches	0.59	0.6
10		0.65	
11		0.56	
13	Bottom branches	0.94	0.74
14		0.73	
16		0.7	
4	Downsprue	0.36	0.36

The mean cooling rate of the fluidity strips was close to 0.7 Ks^{-1} which suggested the fraction of solid for coherency in 2L99 alloy to be around 0.22 [81].

4.3.2.1 Calculating the coherency point temperature (T_c)

The temperature at which the coherency point is was reached calculated using the Scheil equations (assuming equilibrium conditions and no diffusion in solid respectively).

The Scheil equation assumes conditions of no diffusion in the solid but complete diffusion in the liquid phase [110].

$$x_S = kx_0(1-f_s)^{(k-1)} \qquad \text{And} \qquad x_L = x_0 f_L^{(k-1)}$$

Equation 4-1

Where;

x_0 = percentage of Si in 2L99 alloy (7%)

x_s = percentage of Si in solid at the coherency point

x_l = percentage of Si in liquid at the coherency point

k = the partition coefficient

f = the volume fraction of solid or liquid.

And;

$$f_s = 1-\left(\frac{T_m - T_c}{T_m - T_{liq}}\right)^{\left(\frac{1}{k-1}\right)}$$

Equation 4-2

Where T_m is the melting point of pure Al and T_{liq} is the liquidus temperature of the alloy, (617^oC) [109].

Given;

k=0.13 [111] and $f_s = 0.22$;

$x_S = 1.12\%$ Si and $x_l = 8.8\%$ Si (approximately similar to the equilibrium condition).

Using Equation 4-2 to calculate T_c:

$$0.22 = 1 - \left(\frac{660 - T_c}{660 - 617} \right)^{\left(\frac{1}{0.13-1} \right)}$$

$$\sqrt[-1.14]{0.78} = \frac{660-T_c}{660-617} \rightarrow \sqrt[1.14]{1.28} = \frac{660-T_c}{660-617}$$

Then $T_c = 606\,^0C$.

Therefore 606 ^oC was considered to be the temperature at which the flow of liquid metal stops (T_c) due to reaching the coherency point.

4.3.2.2. Flow time

The time interval for the molten metal flow to reach a point at which the temperature at that point is reduced to the coherency temperature is considered to be the flow time, the time interval within which the molten metal is flowing.

Table 4-8 shows when the temperature at different points of the fluidity strips reached T_c (606^{o}C) for casting H2 and demonstrates that solidification began in the fluidity strips before the downsprue, as the point located in the downsprue at the bottom (point 4) reached its T_c temperature later than the points located in the fluidity strips.

Table 4-8. Temperature of different points of casting H2 reached the coherency temperature.

Point	4	6	10	11	12	13	14
Time (s)	109	52	49	53	54.2	52.2	47.6

There was also no priority observed for solidification in the different casting strips at different head heights. Solidification occurred in the branches randomly regardless of the head height of the fluidity strips, as points 6, 10, 11 and 14 (located in the fourth, third, second and the first level of the casting respectively) reached temperature T_c with no order observed. This is to be expected, as it was shown in section 4.2.3 that the average fluidity lengths of the strips with different head heights were approximately the same.

These results also show that the molten metal starts to solidify at the flow tip rather than the entrance of the branches. Because point 14 reaches temperature T_c earlier than point 13 and point 13 reaches temperature T_c earlier than point 12, on the same fluidity strip (see Table 4-8), it is demonstrated that the liquid metal solidified sooner in the points located closer to the downsprue.

The temperature recorded at point 17 shows that this point never reached a temperature above 606 ^{o}C, but the casting result showed that the metal stream tip just reached this point. The maximum temperature reached at this point was 603 ^{o}C at 46 sec; at this time the temperature of point 12 (just at the entrance of the channel) was 611 ^{o}C.

4.3.2.3. Velocity of the molten metal

The recorded temperatures for the different points located on the same casting strip of casting H2 were analysed to measure the velocity of the liquid metal front. A sudden rise in the temperature of points with inserted thermocouples was recorded and this rise was assumed to

correspond to the moment when the molten metal reached the thermocouple tip. For example, this temperature was reported to be 619 ^{o}C for point 14, see Figure 4-17. The velocity of the flow tip between different thermocouple points in the casting branches was used to estimate the liquid metal velocity at which this temperature (T_c or greater) was reached between two adjacent thermocouples (ignoring the effect of any temperature loss between thermocouples because they are just 15 mm apart). The velocity at the beginning of the casting channel was about 15 mms^{-1} (at a point 15 mm from the downsprue), in the middle of the channel it was reduced to 6 mms^{-1}, and just before the coherency of the molten 2L99 a value of 34 mms^{-1} was determined. The mean velocity of the liquid metal throughout the casting channel was therefore about 5.7 mms^{-1}.

4.3.2.4. The thickness of the metal/foam interface

Once the liquid metal entered the mould, heat from the liquid metal caused a collapse in the foam pattern at about 110-120 ^{o}C [57]. According to the literature the temperature of a boiling polystyrene foam mixed with air released from the foam degradation process can increase to more than 400 ^{o}C [34, 47]. The temperatures recorded by the thermocouples showed a sudden increase from about 120 ^{o}C to about 620 ^{o}C. As was mentioned, this sudden increase is likely to correspond to the moment at which the liquid metal reached the thermocouple. For example, the temperature is plotted against time for point 14 in Figure 4-17.

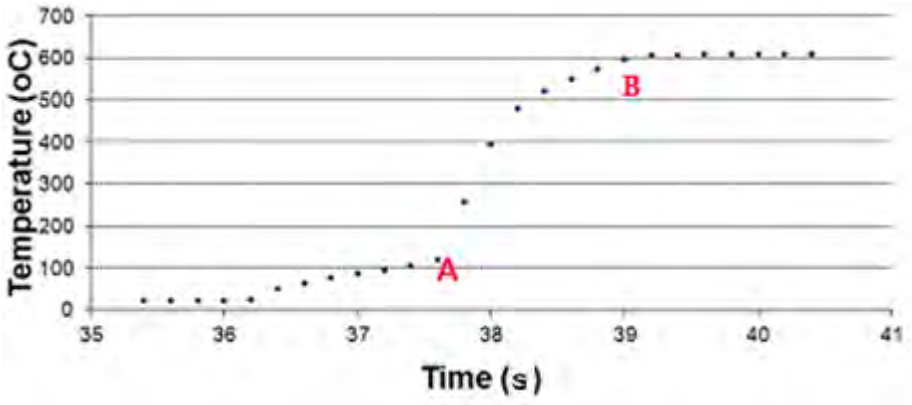

Figure 4-17. The molten metal reached point 14 located at the first level of fluidity strips, cause a sudden increase in the recorded temperature, casting H2.

Figure 4-18. Schematic position of point 14, A) Position of point 14 at time A, B) Position of point 14 at time B, see Figure 4-17.

The time interval from A to B was assumed to be the time interval in which the interfacial gap reached point 14 (point A in Figure 4-18) followed by the liquid metal reaching this point, (point B in Figure 4-18), just over a second later, corresponding to point B in Figure 4-17. This time interval (t_g) is the time required for the metal flow front to travel the gap length (the gap moves ahead of the molten metal flow but this time interval is the time needed for the metal flow to traverse that length).

The velocity of the molten metal between points 12, 13, 14 and 15 was about 15, 6.2 and 4.6 mms^{-1}, respectively and t_g at these points was calculated to be 0.5, 1.1 and 0.8 seconds.

Since,

$$l_g = t_g \times V_{liq}$$ **Equation 4-3**

Where l_g and V_{liquid} are the length of the gap between the flowing liquid metal and the foam pattern and the velocity of the liquid metal respectively. This gives the length of the gap zone between points 12, 13, 14 and 15 to be 6, 5 and 3 mm, respectively, i.e., the gap length decreases as the metal flow proceeds and decrease its temperature, as is to be expected.

4.3.2.5. Time of freezing

The fluidity length of the branch with inserted thermocouples was 95 mm (in casting H2) and the measured metal velocity was 6 mms^{-1}. Therefore, the freezing time of the molten metal was calculated to be 15 seconds.

Casting J was cast at 680 ^{o}C using a brominated EPS foam pattern coated with low permeability coating of 0.3 mm thickness. Table 4-9 shows that the mean cooling rate of the fluidity strips was close to 0.7 Ks^{-1} which gave a value of 0.22 for the coherency fraction of solid, similar to casting H2 [81] (see Table 4-7). It also indicated that the coherency temperature (T_c) calculated for casting H2 was still valid for this casting (606 ^{o}C) despite the fact that a different foam type was used.

Table 4-9. Cooling rates of different points of casting I.

Point	Located in	Cooling rate (Ks^{-1})	Mean cooling rate (Ks^{-1})
6	Top branch	0.69	0.66
7		0.63	
12	Bottom branch	0.61	0.64
13		0.65	
15		0.67	
16		0.67	

Table 4-10 shows when the temperature at different points of the fluidity strips reached T_c (606 ^{o}C) for casting J.

Table 4-10. Temperature of different points of casting J reached the coherency temperature.

Point	**6**	**7**	**12**	**13**	**15**	**16**
Time (s)	42.3	38	24.2	23.6	17.5	16.5

Table 4-10 also confirms that point 16 was the first point to solidify, as the molten metal reached temperature of $606\,^{0}C$ (coherency temperature) at 16.5 s (from the time the molten metal entering the cast strip).

The velocity at the beginning of the fluidity strip was about 17 mms^{-1} (from point 12 to 13). Further into the strip, it was reduced to 5 mms^{-1} (point 13 to15) and a value of 3-4 mms^{-1} was determined (between points 15 and 16). The mean velocity of liquid metal throughout the casting channel was therefore about 6.26 mms^{-1} (from point 12 to 16).

4.3.3.6 Thermocouple displacement

To check if the thermocouples recorded the liquid metal temperature precisely, and that the recorded temperatures were from the centre of the fluidity strips, the solidified casting strips were observed by X-ray to determine any displacement of the thermocouple tip due to the liquid metal flow. Figure 4-19 and Figure 4-20 show the filled casting strips with thermocouples for casting H2 (cast at 680 ^{o}C using EPS foam pattern with low permeability coating of 1.3 mm.

None of the thermocouples were displaced horizontally while points 12, 13, 14, 15 and 16 (on the first level from the bottom) were 1, 0.6, 0.8, 0.6 and 1.4 mm away from the vertical axis of the casting strip, respectively. Points 10 and 11 (on the third and second level from the bottom respectively) were 0.8 and 0.5 mm away from the vertical axis of the cast strip. In the fourth casting strip (with the least head height), Point 6 was not displaced in any direction and point 7 was displaced 1.3 mm from the vertical axis of the fluidity strip.

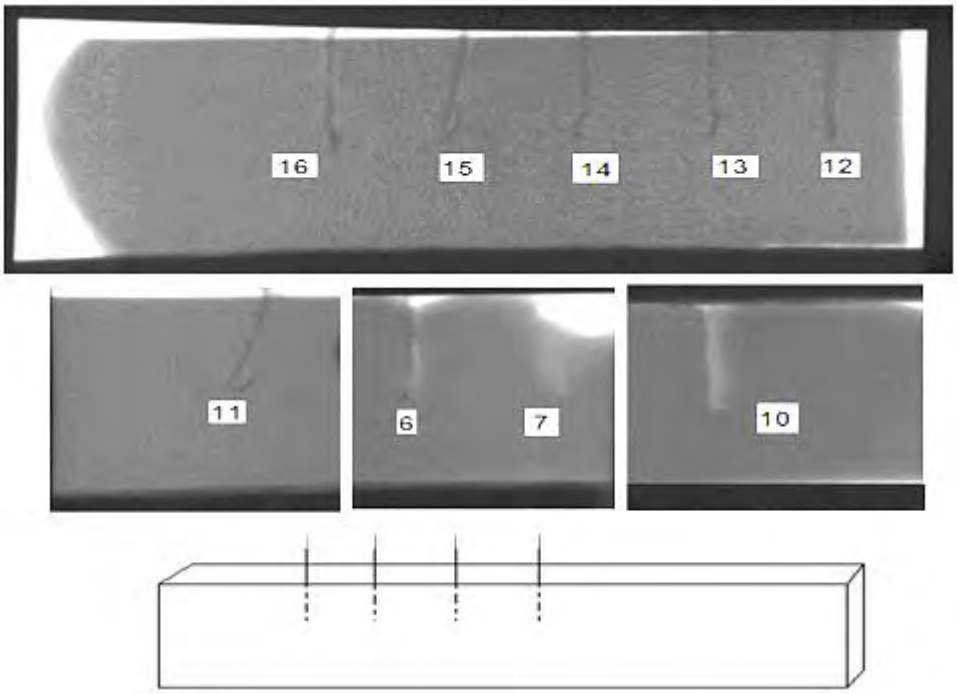

Figure 4-19. X-ray images taken from the fluidity strip of casting H2, inserted with thermocouples.

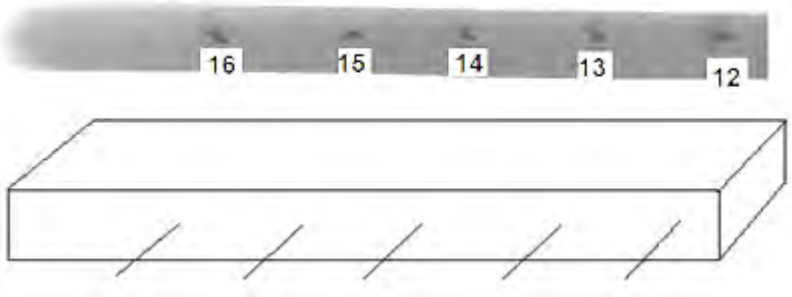

Figure 4-20. X-ray images taken from the fluidity strip of casting D2, inserted with thermocouples.

In casting D2, point 15 was displaced by 1.9 and 0.7 mm horizontally and vertically respectively. Point 11 was 0.8 mm away from the vertical axis of the fluidity strip.

It can be concluded that, despite the slight displacement of the thermocouples on some occasions, the recorded temperatures should be representative of the temperature of the points at the centreline of the fluidity strips.

4.4 Thermogravimetric analysis of EPS decomposition

Figure 4-21 depicts the temperature-dependent mass change of an EPS sample with a heating rate of 10 $Kmin^{-1}$. The spectrometry result reported a mass number of 28 and 14. At 107 ^{o}C a mass loss step was observed which probably corresponded to the release of N_2 trapped in the foam beads. At about 107 ^{o}C a release of a small amount of cubane was reported (C_8H_8) which reduced the mass of the foam by 0.73%. A second peak was observed to correspond to the release of butane gas (C_4H_{10}) at about 403 ^{o}C. This caused a 99.42% reduction in the foam mass; or in other words, the foam was decomposed completely at about 425 ^{o}C [106].

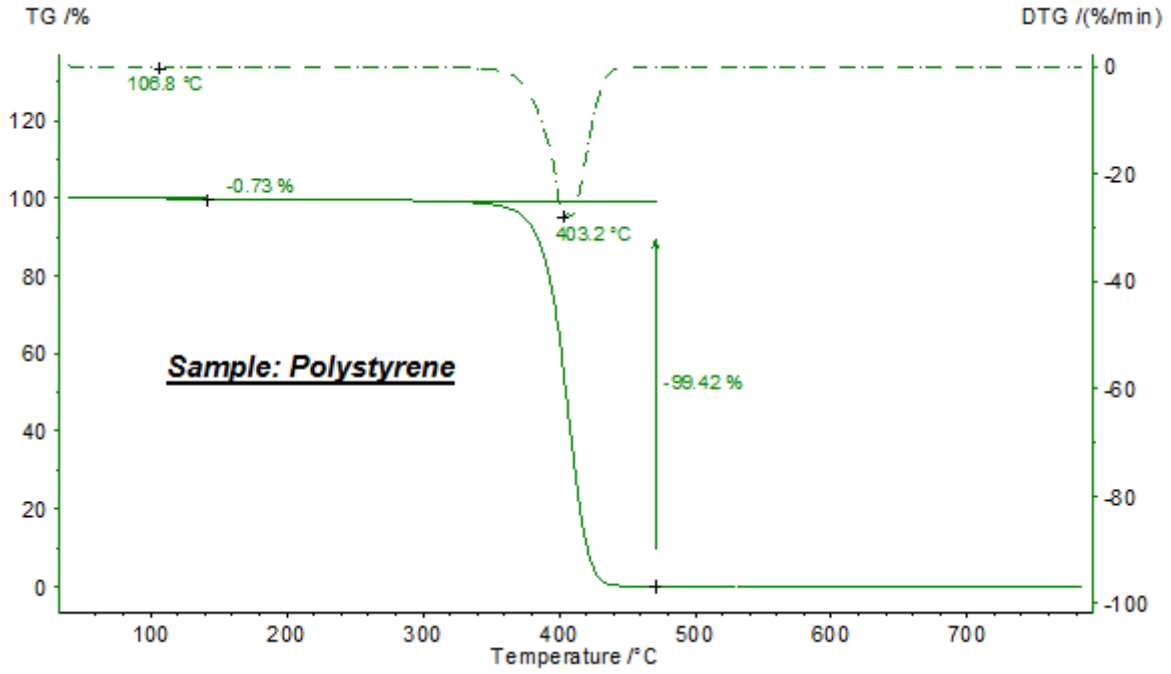

Figure 4-21. Temperature-dependent mass change (TG) and rate of mass change (dashed line) for the EPS foam sample.

Figure 4-21 also shows that there was no significant reduction reported in the mass of the foam until a temperature of about 310 ^{o}C. According to the literature [57], up to this temperature the foam decomposition occurs by collapse, and releases gas and produces liquid residue from the EPS. Therefore, it can be concluded that the formation of the liquid polymer

does not change the mass of the foam pattern during the LFC process, until a considerable amount of foam is converted to the gaseous byproducts, and this only occurs above a temperature of 310 ^{o}C. This temperature would be reached at the region close to the metal front in the metal/foam interface (see Figure 2-7) [63]. This is in agreement with the literature, which suggested that most of the foam vaporization starts at temperatures above 300 ^{o}C and liquid byproducts form a significant distance from the molten metal front and survive for periods of seconds at lower temperatures, compared to the gaseous byproducts [34].

4.5 Mathematical modelling of molten metal flow in LFC

4.5.1 Basis of the model

A model was derived based on an analysis of the heat loss in LFC, taking into account the heat loss from the molten metal to decompose the foam pattern and lateral heat transfer in the strip through the coating to the mould. Figure 4-22 shows the heat transfer to the mould and to the foam pattern from the molten metal stream schematically.

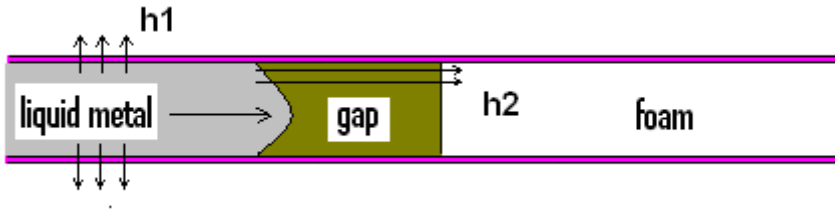

Figure 4-22. Heat transfer to the mould and to the foam from the molten metal is shown schematically.

The heat transferred to the mould is governed by the heat transfer coefficient h_1 . The heat transfer to the foam pattern can be split into two parts. Firstly, heat transfer increases the foam temperature from room temperature to the collapse temperature (about 117 ^{o}C [55]). Secondly, the heat transfer rate from the molten metal to the foam pattern is h_2 which causes degradation of the collapsed foam. A mean rate of the interfacial heat transfer can be estimated from the mass of the decomposing foam, which is determined by the product of the foam density, the fluidity length and the fluidity channel surface area. On the other side of the heat balance, the heat loss from the molten metal depends on the mass of the metal that filled the cast strip which is the product of the liquid metal density, the fluidity length and the fluidity channel surface area.

Hence, equating the heat loss from the molten metal to the heat absorbed by the foam pattern and the mould should result in an equation including the fluidity length. Solving the equation for the fluidity length, a fluidity equation may be derived.

4.5.2 Data to develop the flow equation

The fluidity equation requires data obtained from the thermocouples inserted in the cast strips of the fluidity tests, the data to estimate the heat transfer coefficients, estimates of the size of the gap between the metal flow and the foam pattern, and finally data to test the fluidity equation such as metal flow velocity.

As was stated in previous section, cooling curves of the horizontally cast strips in the fluidity tests were measured for different test conditions. The temperature at which the metal flow stops was assumed to be the coherency point (see section 4.3.1), which was also shown to be dependent on the cooling rate of the casting, for a particular alloy [81]. Table 4-7 shows the calculated cooling rates at different points in casting H2 which led to the calculation of the coherency point to be about 0.22. The coherency temperature of casting H2 was calculated to be 606 ^{o}C in section 4.3.1. Therefore, the flow times (the time interval in which the flowing molten metal tip reaches the coherency temperature) at different points of casting H2 within the fluidity strip are shown in Table 4-8.

The velocity of the molten metal was found to varry from 15 to 3 mms^{-1} while the thickness of the metal/foam interface (gap zone) reduced from 6 to 1 mm within the length of the fluidity strip (located at the bottom of casting H2, see sections 4.3.2.4). The mean velocity of the molten metal and the thickness of the metal/foam interface for the bottom fluidity strip of casting H2 were estimated to be 5.7 mms^{-1} and 1.5 mm respectively, with the mean values obtained from 95 mm of the casting strip length. Therefore the time of freezing, according to

the fluidity length of the casting strip and the velocity of molten metal determined from the thermocouples, was calculated to be 15 seconds ($t_f = L_f \times V$).

Table 4-11. Parameters calculated for casting H2 to use in modelling of the flow.

Coherency Point Temperature (^{0}C)	Velocity (mms^{-1})	The Mean Velocity (mms^{-1})	Gap Length(mm)	The Mean Gap Length (mm)	Time of Freezing (s)
606	15-3	5.7	6-1	1.5	15

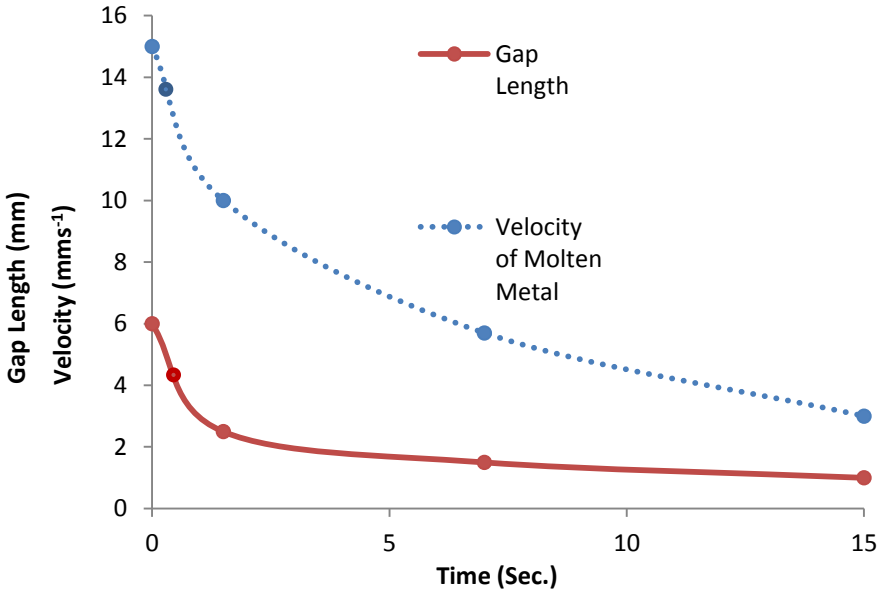

Figure 4-23. The velocity of the molten metal and the length of the metal/foam interface for the bottom fluidity strip of casting H2.

Figure 4-23shows the change in velocity of the molten metal and the size of the gap between the flowing metal and the foam pattern for the bottom fluidity strip of casting H2. Although the metal flow entered the casting strip with a high velocity, this was reduced to 3 mms^{-1} just before flow stopped. This is also the case for the gap between the liquid metal and the foam pattern; however, the reduction in the latter was more rapid, presumably because a thermal equilibrium was quickly reached as the molten metal filled the strip (see section 4.3.2.4).

4.5.3 Fleming, Ajdar et al. and Pan-Liao equations for LFC

The fluidity length (L_f) is the product of the velocity of the flowing metal and the time taken for the flow to stop, i.e., the fluidity length is given by;

$$L_f = V \times t_f \qquad \textbf{Equation 4-4}$$

Where V is the mean velocity of the flowing metal, and t_f is the time to reach the coherency point for the advancing liquid metal front. It was also denoted as the time of freezing in section 4.3.2.5 for casting H2.

Some other fluidity models, discussed in section 2.7.2, were evaluated to determine how they predicted the fluidity length of LFC. Table 4-12 shows the results and compares actual and predicted fluidity lengths of LFC. The fluidity tests against which these models were compared, was cast at 620 ^{o}C and used EPS foam pattern coated with 0.3 mm of high permeability coating.

These strip castings were carried out, and measured fluidity lengths varied within 10 mm. The fluidity lengths were 193, 199 and 222 mm; the mean pouring temperature and mean fluidity length were T_{av} = 620.3 ^{o}C and $L_{f\,av}$ = 204.6 mm respectively. The superheat for the castings was deliberately selected to be extremely low in order to provide a partially filled casting to make a comparison with the predicted lengths.

The casting properties of 2L99 and the casting conditions used were as follows [109];

ρ = 2436 kg/m^3, T_M=617 ^{o}C, T_0=20 ^{o}C

H = 389000 J/kg (latent heat of solidification)

C_L = 897 J/kg (specific heat capacity)

h = 200 $Wm^{-2}K^{-1}$ (for the LFC process, see section 2.8.2)

a = 0.00577 m (calculated by the ratio of the volume to the area)

V = 0.011 ms^{-1} (measured by real time X-ray observation obtained as described in section 3.3.1)

ΔT = 3 ^oC (620 ^oC was the mean pouring temperature)

H_E = heat of the degradation of the EPS foam pattern 1,350,000 J/kg (see section 2.3)

ρ_P = 27 kgm^{-3} (measured)

1. Fleming model (Equation 2-2)

$$L_f \cong \frac{\rho_s a V}{2h(T_M - T_0)}(H + c'\Delta T)$$

$$L_f = \frac{2436*0.00577*0.011}{2*200*(617-20)}*(389000+897*3) = 0.25m$$

2. Ajdar et al. model (Equation 2-5)

$$\frac{\Delta T}{L_f} = \frac{\rho_p H_E}{C_L 2.2 t_p \rho_L},$$

Therefore,

$$L_f = \frac{897*2.2*0.015*2436*3}{27*1350000} = 0.006m$$

3. Pan and Liao model (Equation 2-7)

$$L_f = \frac{\rho_L a V}{2h\ (T_M - T_0)}(c_L \Delta T + \frac{H}{2} - \frac{H_{_E}\rho_P}{\rho_L})$$

$$L_f = \frac{2436*0.0057*0.011}{2*200*(617-20)}*(897*3+\frac{389000}{2}-\frac{1350000*27}{2436}) = 0.12m$$

The same foam pattern (EPS) was also filled with commercially pure aluminium and a length of 360 mm was filled completely. The results of prediction of the fluidity length for the case of CP Al are also presented in Table 4-12 when the casting conditions were as follow [109];

$T_M = 660\ ^oC$

$V = 0.013\ ms^{-1}$ (measured in real x-ray time)

$H = 396000\ Jkg^{-1}$ (latent heat of solidification)

$c' = 897\ Jkg^{-1}$ (specific heat capacity)

Pouring temperature (T_p) = 670 ^oC

Table 4-12. Comparison between actual fluidity length and the predicted length by different fluidity models.

	Fleming Model (m)	Ajdar et al. Model (m)	Pan-Liao Model (m)	Actual Fluidity length (m)
2L99 alloy	0.25	0.006	0.12	0.20
Error	25%	97%	40%	--
CP Al	0.28	0.021	0.14	--
Error	> 23%	> 94%	> 61%	--

This shows that the Fleming model predicted the fluidity length with about a 25% difference to the actual fluidity length, although the Fleming equation is for an open cavity casting and does not take into account any effect associated with LFC. The other two models (by Ajdar et al. [11] and Pan and Liao models [85]) predicted the fluidity length of LFC poorly despite their consideration for a foam pattern. This suggests that the principal heat transfer mechanism in Fleming's simple fluidity model of heat loss to the mould, may be the significant factor in LFC also.

4.5.4 Heat of foam degradation and the heat transfer coefficient of the liquid metal-foam interface

The heat necessary for foam pattern degradation is the sum of the heat required to increase the foam temperature from room temperature to the collapse temperature ($117\,^{o}C$ [55]), the heat required for the collapsed foam to turn into a liquid viscous residue, and finally the heat of vaporisation which vaporises the liquid globules of PS to gaseous byproducts, a total of $1350\,Jg^{-1}$ [34].

It can be assumed that the rate of heat loss from the molten metal to the foam pattern (q) in the fluidity strip is related to the volume of the foam decomposed (i.e. the volume replaced with metal in the fluidity length), which equals the cross-sectional area of the fluidity strip multiplied by the fluidity length. In the case of the bottom fluidity strip of casting H2 this is;

Volume of decomposed foam = $L_f \times w \times t = 95 \times 10 \times 40 = 38{,}000\ mm^3$

Where w and t are the width and thickness of the casting channel (m).

All of the heat consumed to decompose this volume of foam passed through the metal/foam interface with the governing heat transfer coefficient of h_2. The rate of heat transfer per time (q) through this interface can be written as;

$$q = A\ h_2(T_1 - T_2) \qquad \textbf{Equation 4-5}$$

Where A is the area of the metal/foam interface, T_1 and T_2 are the temperatures of the environments at both sides of the interface;

T_1 = the mean temperature of the flow front of the liquid metal.

T_2 = the temperature of the collapsed foam ($117\,^{o}C$).

The mean temperature of the metal flow tip for casting H2 was recorded by a series of thermocouples to be about 614 ^{o}C (see section 4.3). The metal/foam interface for the fluidity strips was assumed to be plane (width × thickness) with an area of 400 mm^{2}.

The heat of degradation, H, can also be written as;

$$Q_f = \mathrm{H} \times \mathrm{M} \qquad \textbf{Equation 4-6}$$

Where;

Q_f = Energy required to decompose the volume of foam consumed.

M = Mass of consumed foam (the mass of foam replaced by the liquid metal in the fluidity length);

and M = Volume × density of foam = $L_f \times w \times t \times \rho_f = 95 \times 10 \times 40 \times 27 \times 10^{-6}$ =1.08 g

Where ρ_f is the density of the foam pattern (27 kgm^{-3}).

As was stated earlier in this section, to decompose 1 gram of polystyrene, 1350 J energy is required (H=1350 Jg^{-1}); hence, for the bottom fluidity strip of casting H2, the heat taken from the molten metal to decompose the foam pattern is calculated to be;

Q_f= 1.08 × 1350=1458 J

Having the value for the time of freezing (15 seconds) for the bottom fluidity strip of casting H2 (derived from the cooling curves, see section 4.3.2.5), the mean rate of heat flow passing through the metal/foam interface is calculated to be;

$$q = {Q_f}/{t_f} = 97.2 \text{ W}$$

Therefore the heat flux through the metal/foam interface is estimated to be;

$^{q}/_{A}$= 97.2 / (4×10^{-4}) =243,000 Wm^{-2}

Inserting in Equation 4-5;

$$^{q}/_{A} = 243{,}000 = h_2\,(614 - 117)$$

Therefore a mean heat transfer coefficient for the metal/foam interface can be determined to be 485 $Wm^{-2}K^{-1}$.

4.5.5 The heat transfer coefficient from the metal to the mould

The parameters to be used in this section are defined below [109];

Q = Heat from the liquid metal (J).

q = Rate of heat flow = $^{Q}/_{t_f}$ (W).

A_1 = Surface area of the fluidity channel (m^2).

A_2 = Surface area of the metal/foam interface (m^2).

h_1 = Heat transfer coefficient from the molten metal to the mould ($Wm^{-2}K^{-1}$).

h_2 = Heat transfer coefficient from the molten metal to the foam pattern ($Wm^{-2}K^{-1}$).

C_f = Specific heat capacity of the foam pattern, ($Jkg^{-1}K^{-1}$) = 1500 $Jkg^{-1}K^{-1}$

C_{al} = Specific heat capacity of the alloy ($Jkg^{-1}K^{-1}$) = 910 $Jkg^{-1}K^{-1}$

m_f = Mass of degraded foam in the fluidity length of the fluidity strip

m_{al} = Mass of solidified aluminium along the fluidity length

H = Latent heat of solidification (for Al, H= 389000 J/kg)

T_p = Pouring temperature (686 ^oC for casting H2)

T_{fs} = The coherency temperature at which the metal flow stops (606 ^oC for 2L99 alloy, calculated in 4.3.1).

T_r = Room temperature (17 ^oC)

T_{fc} = Temperature at which foam collapses ($117\,^0C$) (see section 2.3)

T_{mo} = Mould temperature (17 ^oC)

T_{mf} = Metal front temperature (617 ^oC, measured from cooling curves of casting H2 on average)

q, rate of heat flow to the surrounding mould and the foam pattern from the molten metal, which consists of q_1 (rate of heat transfer to the mould), q_2 (rate of heat transfer to the foam to increase foam temperature to the collapse temperature) and q_3, (rate of heat transfer to the collapsed foam to cause decomposition).

$$q_1 = A_1 h_1 \left(T_p - T_{mo}\right) \qquad \textbf{Equation 4-7}$$

$$q_2 = A_2 h_2 \left(T_{mf} - T_{fc}\right) \qquad \textbf{Equation 4-8}$$

$$q_3 = \frac{c_f m_f (T_{fc} - T_r)}{t_f} \qquad \textbf{Equation 4-9}$$

$$q = q_1 + q_2 + q_3 \qquad \textbf{Equation 4-10}$$

q, (Q/t_f), is also the rate of heat loss from the molten metal from the moment of pouring until after the metal flow stopped. It consists of the heat lost in reducing the temperature from the pouring temperature to the coherency point temperature and the latent heat lost due to solidification of 0.22% of the metal (to reach the coherency point). Therefore;

$$q = \frac{c_{al} \times m_{al} \times (T_p - T_{fs}) + H \times m_{al} \times f_s^{coh}}{t_f} \qquad \textbf{Equation 4-11}$$

To calculate the mass of metal in the fluidity length and the mass of foam degraded in the casting process (m_{al} and m_f respectively), A_1 (the surface area of the fluidity length) is required to calculate, as shown in Figure 4-24.

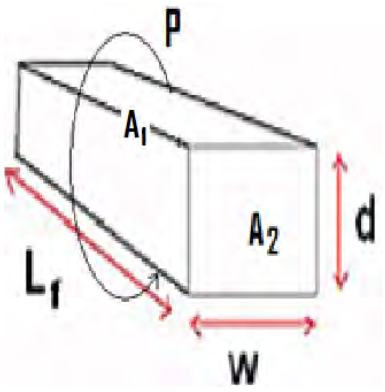

Figure 4-24. A schematic of the fluidity strip, the surface area of the casting channel is a function of the fluidity length (L_f).

For casting H2, of fluidity length 95mm;

$A_1 = 95 \times 10 \times 2 + 95 \times 40 \times 2 = 10{,}000\ mm^2 = 0.01\ m^2$

And the surface area of the metal/foam interface;

$A_2 = 400 \times 10^{-6}\ m^2$

Hence Equation 4-11 becomes;

$$q = \frac{[910 \times 0.12 \times (677-606) + 389000 \times 0.12 \times 0.22]}{15} = 1211 \text{ W}$$

And, Equation 4-10 can be written as;

$$q = 0.01 \times h_1 \times (677 - 17) + 400 \times 10^{-6} \times 485 \times (617 - 117) + \frac{1500 \times 1.08 \times 10^{-3} \times (117-17)}{15}$$

$$= 6.6\, h_1 + 108$$

Equating this to the heat loss from the molten metal (1211 W) gives a mean value for the heat transfer coefficient of the metal/mould interface, h_1, to be about 170 $Wm^{-2}K^{-1}$.

It has to be noted that the heat transfer coefficient at the metal/mould interface (h_1) is more complex to determine in the LFC process due to the existence of the refractory coating and entrapment and vaporization of liquid viscous residue into the refractory coating. Globules of liquid EPS absorbed by the coating should change the heat transfer coefficient of metal to the mould.

4.5.6 The fluidity equation

Having derived heat transfer coefficients h_1 and h_2 from temperature measurements in specific castings, these applied to create a fluidity equation for LLFC.

Substituting Equation 4-7, 4-8 and 4-9 in Equation **4-10**, the time of freezing can be written as;

$$t_f = \frac{c_{al} \times m_{al} \times (T_p - T_{fs}) - c_f m_f (T_{fc} - T_r) + H \times m_{al} \times f_s^{coh}}{A_1 h_1 (T_p - T_{mo}) + A_2 h_2 (T_{mf} - T_{fc})}$$

Equation 4-12

Furthermore, Equation 4-4 stated that the fluidity length is a function of the velocity of the molten metal and time of freezing. A_1 (the surface area of the casting channel along the fluidity length), is a function of the fluidity length (see Figure 4-24). In addition, m_{al} and m_f are functions of the fluidity length as they are the mass of aluminium and foam consumed in the fluidity length, respectively. Then;

$$A_1 = P\ L_f$$

$$m_{al} = L_f\ A_2\ \rho_{al}$$

$$m_f = L_f\ A_2\ \rho_f$$

Where P is the perimeter of the casting channel.

Replacing these parameters in Equation 4-12 and solving for the fluidity length, gives;

$$L_f = \frac{v \times A_2[c_{al} \times \rho_{al} \times (T_p - T_{fs}) - c_f \rho_f (T_{fc} - T_r) + H \times \rho_{al} \times f_s^{coh}] - A_2 h_2 (T_{mf} - T_{fc})}{P \times h_1 (T_p - T_{mo})}$$

Equation 4-13

All of the parameters used in Equation 4-13 are feasible to measure or to calculate, except for the temperature of the molten metal tip. However the term associated with this value, $A_2 h_2 (T_{mf} - T_{fc})$, is small compared to the rest of the numerator in Equation 4-13 and the fluidity length should not be very sensitive to changes in this parameter. As long as the only parameter which can change the temperature of the metal flow is the pouring temperature, which does not change more than 100-200 ^{o}C, it is suggested to replace the temperature of the metal flow tip with a constant value such as the liquidus temperature of the alloy (617 ^{o}C).

Equation 4-12 can be tested with casting D2 of fluidity length 225 mm, (the bottom fluidity strip);

$h_1 \sim 170 Wm^{-2}K^{-1}$

$h_2 \sim 485 Wm^{-2}K^{-1}$,

$A_1 = 225 \times 10 \times 2 + 225 \times 40 \times 2 = 29{,}600 \text{ mm}^2 = 0.0225 \text{ m}^2$

$A_2 = 400 \times 10^{-6} \text{ m}^2$

$T_p = 787\ ^{o}\text{C}$

$m_{al} = 225 \times 10 \times 40 \times 10^{-9} \times 2436 = 0.218 \text{ kg}$

$m_f = 225 \times 10 \times 40 \times 10^{-9} \times 27 = 0.0024 \text{ kg}$

Equation 4-12 gives a value of 17.8 seconds for the time of freezing for casting D2 which is in agreement with the time of freezing measured by the data acquired from thermocouples inserted in the fluidity strip, 19 seconds (a difference of 6%).

4.5.7 Effect of coating permeability on the flow behaviour of LFC

To learn more about the effect of coating permeability on the fluidity length, velocity of molten metal, thickness of the gap zone and the heat transfer coefficients from the molten metal to the foam pattern and mould, the cooling curves of different points in a casting with two fluidity strips, one coated with low permeability coating and the other with high permeability coating, were obtained and the results are shown in Table 4-13. The estimation of mean heat transfer coefficients was carried out in a similar way to the procedure developed in section 4.4.6 and 4.4.7.

Table 4-13. Comparison between the flow behaviour of LFC coated with high and low permeability coatings.

Coating Permeability	L_f (mm)	V_{mean} (mms^{-1})	t_f (s)	Mean l_g (mm)	h_1 ($Wm^{-2}K^{-1}$)	h_2 ($Wm^{-2}K^{-1}$)
High	240	8.8	34	1.3	60	515
Low	155	5	31	1.8	70	365

As was expected, the fluidity length of the casting with high permeability coating was higher than that with the low permeability coating. This also shows that the velocity of molten metal and the time of freezing are slightly higher when a high permeability coating is used. However it was found that the thickness of the metal/foam interface was not greatly changed, (the error in the measurement of the latter was ± 0.5 mm, with a rate of temperature recording (10 times per seconds) and the velocity of molten metal obtained.

The heat transfer coefficient from the molten metal to the mould (h_1) was similar in the case of casting with high and low permeability coatings, but the heat transfer coefficient from the molten metal to the foam pattern (h_2) was markedly higher when the foam was coated with a high permeability coating. This is probably because the decomposition byproducts were removed from the metal/foam interface through the coating and this provides a higher rate of heat transfer from the molten metal, due to a reduction in the thickness through which the heat is transferred. A 0.5 mm reduction in the metal/foam interface (38% of 1.3 mm) causes a 38% increase in the heat transfer coefficient (see Equation 2-11). A 38% increase in the heat transfer coefficient in the casting with the low permeability coating (365 $Wm^{-2}K^{-1}$) suggests a heat transfer coefficient for the casting with a high permeability coating of 505 $Wm^{-2}K^{-1}$ which is reasonably close to the measured value (515 $Wm^{-2}K^{-1}$).

It should be noted that the value of these heat transfer coefficients are not comparable with the results of the fluidity tests, as they were carried out with different conditions (different assembly, coating thickness and the pouring temperature, see section 3.4.2), purely to provide a comparison between two different permeability coatings.

4.6 Effect of γ-irradiation on PS-PMMA copolymer foam pattern material for Lost Foam casting

4.6.1 Gel Permeation Chromatography (GPC) and the Polystyrene Equivalent

The wetting and wicking theory cited in section 2.4 explains how globules of liquid polystyrene degradation byproducts can become trapped against the coating surface in LFC. In addition, the critical M_w of degradation byproducts to wet and wick into the coating was measured by Davies [21]. The GPC technique applied for this analysis used polystyrene calibrants and therefore all of the results are expressed as "polystyrene equivalent" molecular weight, and there might be significant differences between these "polystyrene equivalents" and the true molecular weights of the samples [108].

The first concern is the solvent/column used to measure the M_w of polystyrene samples by Davies [21], which was carried out in 2007 and might now have a different behaviour from the solvent/column used to measure the M_w of the foam pattern in this work. Therefore the M_w of samples of conventional EPS were remeasured using the GPC technique. The measured M_w of foam samples (EPS) had a value of 327,000 $gmol^{-1}$ ±1000 while the M_w of the foams measured in 2007 was 324,000 $gmol^{-1}$ ±5000 [21]. Therefore, it was still valid to make comparison between the solvent/column used to measure the M_w of the foam pattern in this work and the work carried out by Davies [21].

Secondly, despite the fact that different foam types were used and studied, the comparisons between their critical M_w would still be valid because as was mentioned 'polystyrene equivalent' molecular weight was used in the presentation of the results of GPC measurements.

4.6.2 The effect of irradiation on the M_w of foam patterns

As was mentioned in section 3.6, plates of foamed polymers (PS and PMMA) and copolymers (Probead-70™ and Probead-30™) were exposed to γ-irradiation.

Figure 4-25 shows typical results of molecular weight distributions produced by Rapra Technology, showing an overlay of the computed molecular weight distributions for three samples of Probead-70™ having received different dosages of γ-radiation. These plots were all normalised with respect to area, the y-axis being a function of weight fraction. This Figure demonstrated that the M_w distribution of the foam samples irradiated with higher doses of γ-rays was shifted to the left on the M_w axis, also, the average M_w of foam samples was reduced by exposure to higher γ-ray doses.

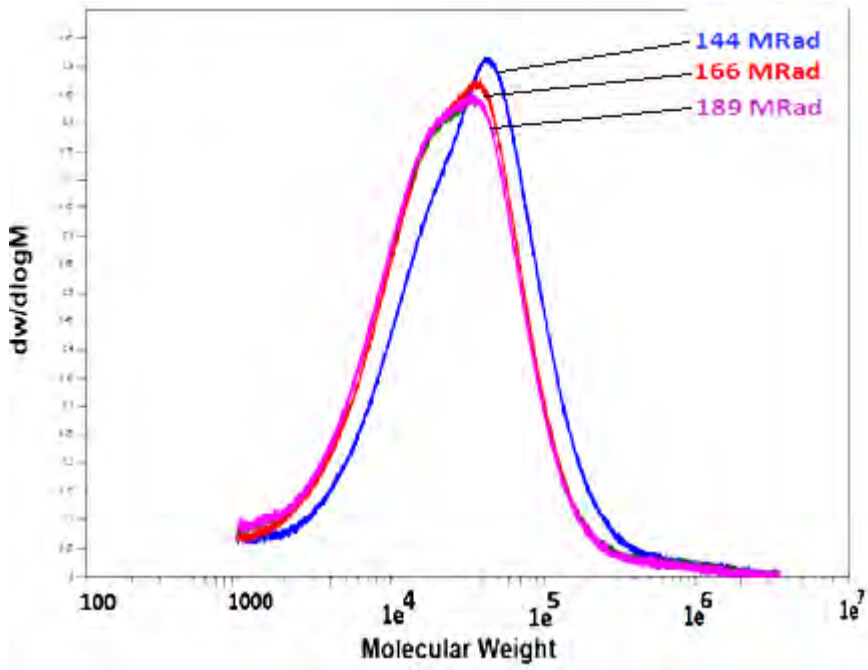

Figure 4-25. Overlay of the computed molecular weight distributions for irradiated copolymer of Probead-70™ (70wt.% PMMA and 30wt.% PS) with different doses of γ-rays. M = molecular weight.

The foam pattern (Probead-70™) had an original M_w of about 327,000 $gmol^{-1}$, which was reduced according to the amount of irradiation received, to values as low as about 45,000

gmol^{-1} with the maximum γ-irradiation (a dosage of 189 MRad). This has been plotted against irradiation dosage in Figure 4-26, which shows that the copolymer Probead-70™ had its molecular weight reduced by up to 85% when exposed to 189 MRad of γ-rays.

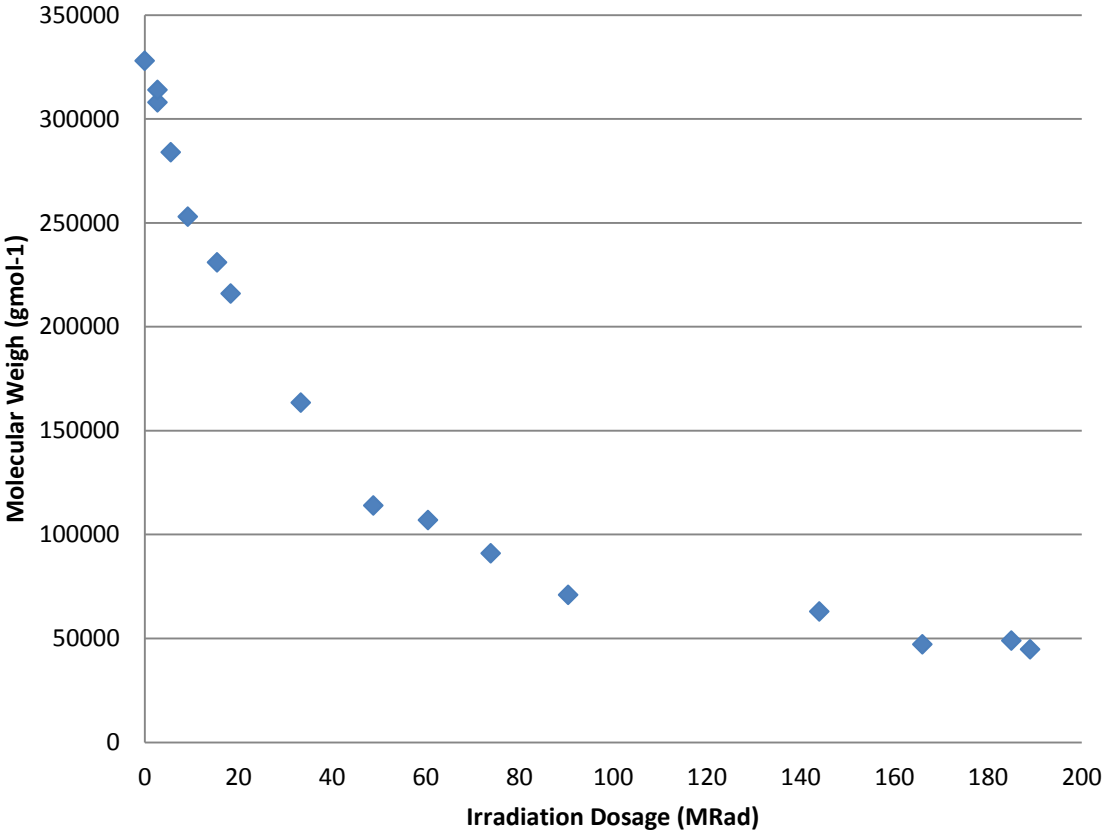

Figure 4-26. Effect of γ-irradiation on the M_w of foam pattern Probead-70™ (70wt.% PMMA and 30wt.% PS).

4.6.2.1 Difference between γ-ray irradiation processing and E-beam exposure

To examine the effect of electron beam irradiation on molecular weight of the foam pattern, plates of copolymer Probead-70™ were exposed to 80 MRad of electron beam. GPC indicated that the molecular weight was reduced to about 86,000 gmol^{-1}, a reduction to 32% of the original M_w (327,000 gmol^{-1}). In contrast, when the same exposure was delivered by γ-radiation, the M_w of the foam pattern was reduced to 26% of the original M_w (reduced to about 106,000 gmol^{-1}), (extrapolated from Figure 4-26 from the suggested trend).

To further compare the effect of γ-ray and electron beam in reducing the molecular weight of expanded foams, samples of granulated expanded pure PMMA (poly methyl methacrylate) were exposed to 100 MRad of γ-ray and electron beam, respectively. The molecular weight of the untreated pure PMMA foam granules was determined to be 370,000 ± 3,000 $gmol^{-1}$, but after irradiation with 100 MRad of γ-ray had its molecular weight reduced to about 10,250 $gmol^{-1}$ (a 97% reduction). On the other hand, this reduction due to the exposure to 100 MRad of electron beam was 94% (M_w was reduced to about 18,550 $gmol^{-1}$). Figure 4-27 compares the effect of γ-ray and electron beam on molecular weight for the two different types of foam (PMMA and Probead-70™).

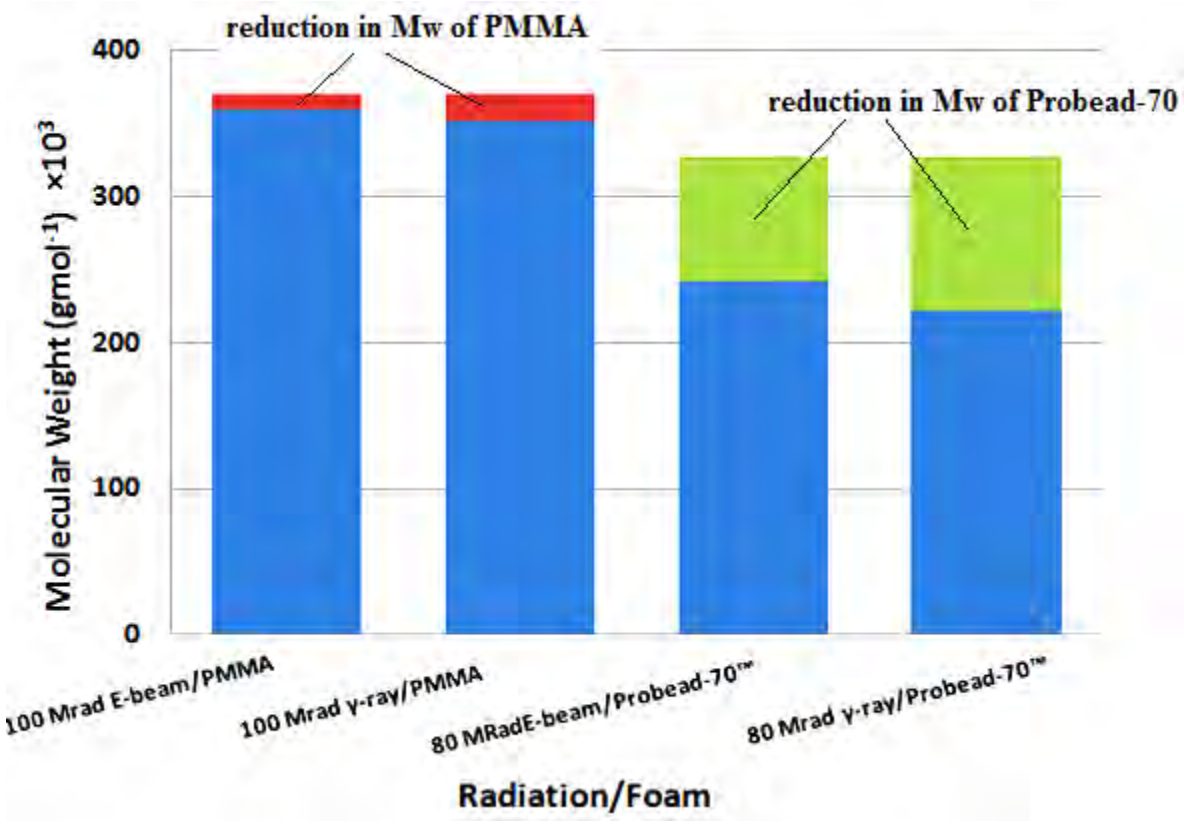

Figure 4-27. Comparison between γ-ray and electron beam in reducing the M_w of PMMA and Probead-70™. In both cases, the reduction due to irradiating with γ-ray was slightly higher.

This implies that the effect of the electron beam was slightly less than that of the γ-irradiation. According to Isotron Ltd, 80 MRad from the electron beam process can be obtained much

more quickly than by irradiation with the γ source (by about 25 times faster) [112]. A shorter irradiation time reduces the amount of ozone initiated oxidation [97] and therefore the opportunity for chain scission and cross-linking reactions. In the case of the electron beam treatment, a shorter time is required to deliver the same dosage than by γ-irradiation which leads to less reduction in M_w as there is less time for chain scission, however in a shorter time of irradiation less cross linking occurs which offsets the latter to some extent. Therefore, irradiating the foam samples using the electron beam approach is slightly less effective in reducing the M_w compared to γ-irradiation; however it is a significantly shorter process.

4.6.2.2 The effect of irradiation processing under reduced pressure

The GPC results also revealed that irradiating the polymer while in a partial vacuum (0.5 bar) had no effect on preventing cross linking of newly cut chains of polymer/copolymer due to the presence of oxygen. However it was recommended to perform the irradiation processing in vacuum to reduce the cross linking of newly cut chains as this was thought to occur at higher rate in the presence of oxygen [113]. Plates of Probead-70™ exposed to 100 MRad of γ-radiation showed approximately the same amount of reduction in their molecular weight when irradiated in an envelope containing 1 or 0.5 bar pressure, as shown in Figure 4-28. The M_w of the foam samples irradiated by 100 MRad of γ-ray in 0.5 bar air was about 72,600 $\pm$ 800gmol^{-1}, the same as the M_w of the foam samples irradiated in 1 bar air (having M_w of 73,300 $\pm$ 800 gmol^{-1}).

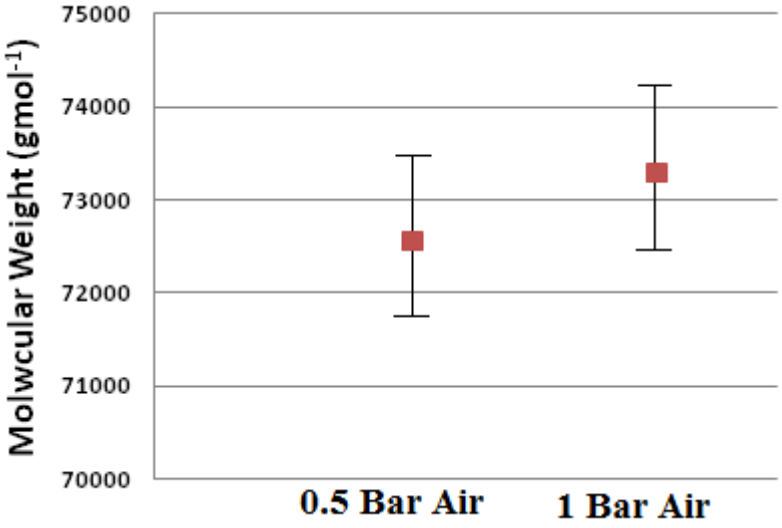

Figure 4-28. Comparison between the reduced M_w of the copolymer Probead-70™ irradiated by 100 MRad of γ-ray in air and under vacuum of 0.5 bar.

4.6.2.3 The effects of irradiation processing on Probead-30™

As mentioned, another copolymer Probead-30™ (70wt.% PMMA and 30wt% PS), was also exposed to different doses of electron beam irradiation. Figure 4-28 shows how the molecular weight of the copolymer Probead-30™ responded to irradiation.

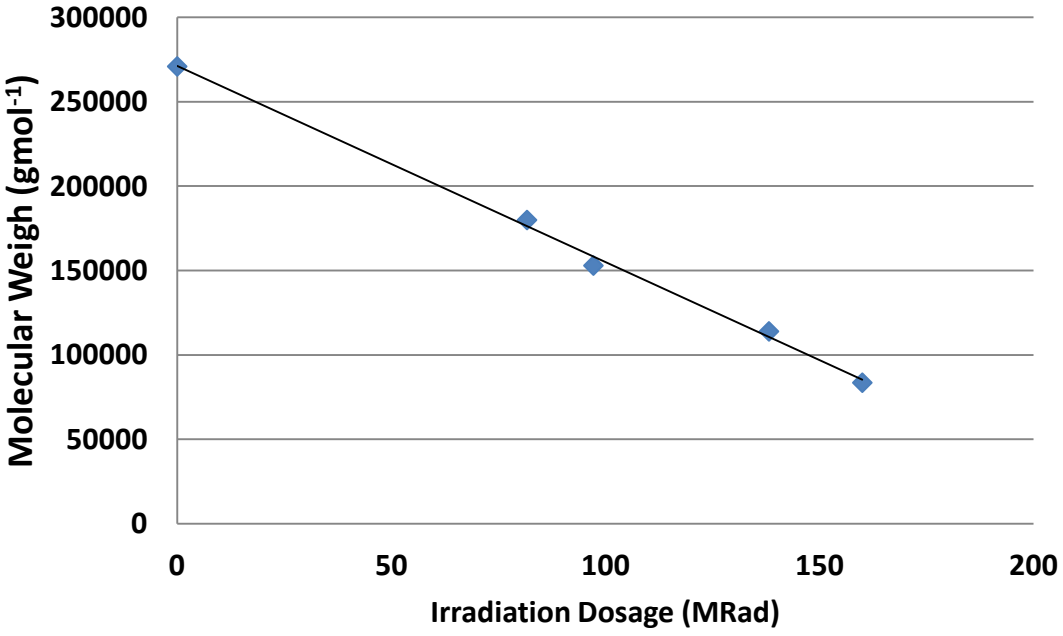

Figure 4-29. Effect of irradiation on the M_w of the foam pattern Probead-30™ (70wt.% PS and 30wt.% PMMA) using electron beam.

This shows that the foam pattern (Probead-30™) had an original M_w of 271,000 $gmol^{-1}$, also reduced according to the amount of irradiation received, to values as low as about 83,000 $gmol^{-1}$ with the maximum irradiation, (a dosage of 160 MRad). The foam pattern therefore had its molecular weight reduced by up to about 70% of its original molecular weight.

4.6.2.4 The effects of irradiation processing on pure polymers and copolymers

To study the effect of irradiation on the molecular weight of the pure polymers, plates of expanded polystyrene (EPS) and granules of expanded Poly methyl methacrylate (PMMA) were exposed to 100 MRad of γ-irradiation. GPC revealed that pure EPS showed only about a 1-2% reduction in its molecular weight (original M_w of 320,000 ±3,000 $gmol^{-1}$) while the expanded granules of pure PMMA had their molecular weight reduced to 10,250 $gmol^{-1}$ (about 96% reduction in its original M_w).

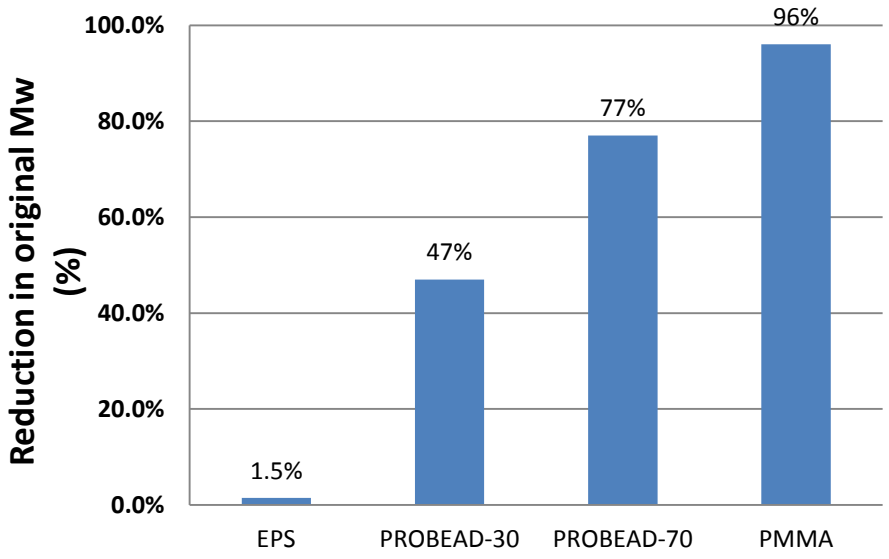

Figure 4-30. Comparing the effect of γ-ray on the Mw of different foam types.

With the copolymers, the reduction in M_w was greater in the case of 70% PMMA- 30% PS copolymer (Probead-70™), than in the case of the 30% PMMA- 70% PS copolymer

(Probead-30™), i.e., the effectivness of irradiation increased with increasing amounts of PMMA in the foam patterns.

4.6.3 The effect of irradiation on mechanical properties of the foam pattern used for Lost Foam casting

The effect of radiation processing on mechanical properties of foam patterns used in the LFC process was determined using a 3-point bend test on irradiated Probead-70™. A typical result is shown in Figure 4-31.

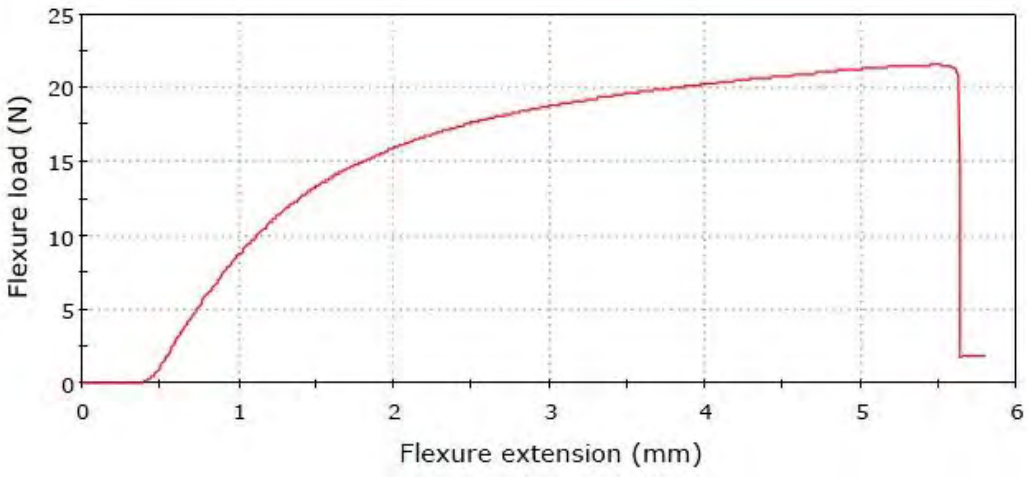

Figure 4-31. Force-displacement curve obtained from 3 point bending test of irradiated foam pattern Probead-70™ with 33 MRad of γ-ray (163,500 gmol^{-1}).

This shows that the maximum load at fracture of the foam pattern, (in this case irradiated with 33 MRad of γ-ray), was 21.75 N and the sample failed at 4.8 mm flexural extension.

Figure 4-32 shows the relationship between load at failure and molecular weight and shows a reduction in maximum load at failure with increasing irradiation and decreasing M_w.

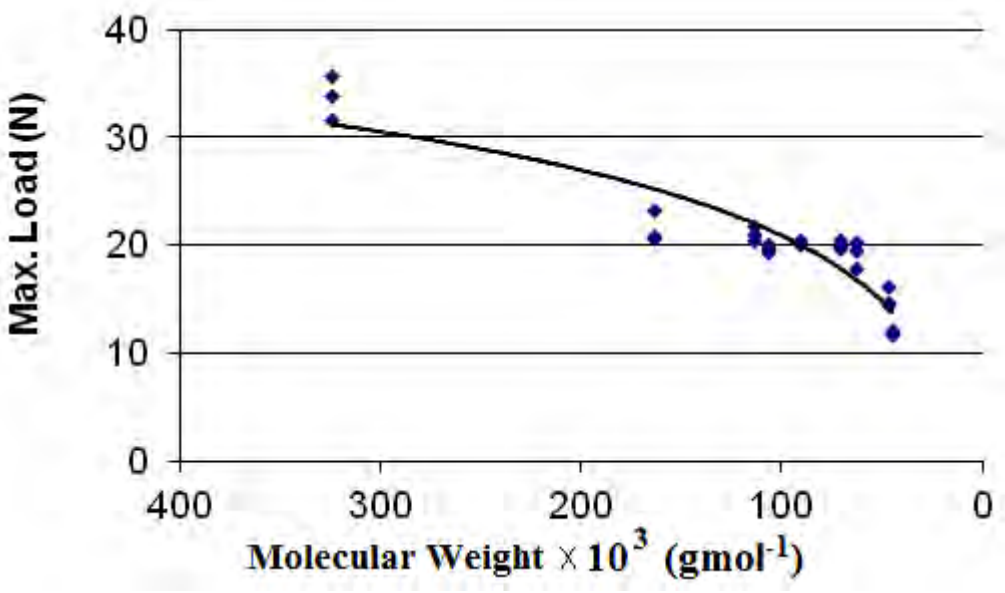

Figure 4-32 . Results of 3 point bending tests on the irradiated foam patterns, showing that foam strength was reduced by reduction of its molecular weight by γ-irradiation.

The maximum reduction of foam strength, (in the most irradiated foam pattern, 189 MRad), was about 60%. This significant reduction in mechanical properties of the foam pattern caused some difficulties in the pattern, assembly and moulding processes, as the foam patterns irradiated with 189 MRad of γ-ray became too friable and fragile to make a pattern with successfully. However, the foam patterns irradiated with γ-radiation below 166 MRad (144, 100,90,75,60, 45 and 30 MRad) were still rigid enough to carry out the moulding process with.

4.6.4 The effect of irradiating the foam pattern on casting quality

4.6.4.1 Effect of irradiating the foam pattern on porosity of aluminium alloy LFC

Strips of dimensions 10 x 40 x 300 mm were cut from the irradiated foam patterns, coated with a high permeability coating of thickness 0.3 mm, and cast horizontally with 2L99 Al alloy, (Al-7wt.%Si-0.3wt.%Mg), with a pouring temperature of 780°C and 150 mm head height. All castings filled completely. Porosity of the castings was measured using image

analysis on the cross sections of the casting centreline. Figure 4-33 shows a picture from castings with different M_w foam patterns (irradiated with different dose of γ-rays), the pictures are focused to capture the porosities rather than the microstructure. This shows that the castings with lower M_w foam are less porous.

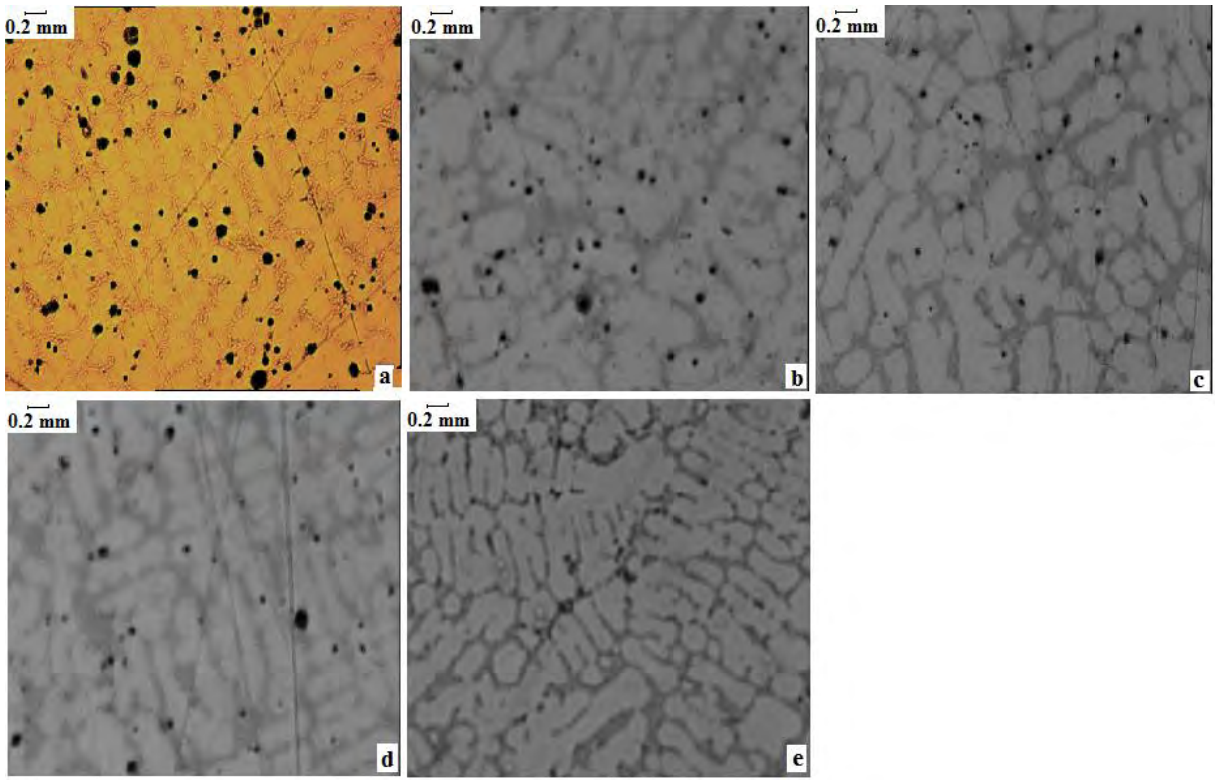

Figure 4-33. Images taken from the centreline of the casting made with different M_w foam patterns (Probead-70™) showing that the porosity content of the castings was reduced due using lower M_w foam patterns. The foam patterns used in these castings were: a) untreated Probead-70™ b) Probead-70™ irradiated with 30 MRad c) Probead-70™ irradiated with 75 MRad d) Probead-70™ irradiated with 90 MRad e) Probead-70™ irradiated with 185 MRad

Figure 4-34 shows the porosity content of castings made with irradiated foam patterns with different doses of γ-radiation, for the foam pattern material, Probead-70™.

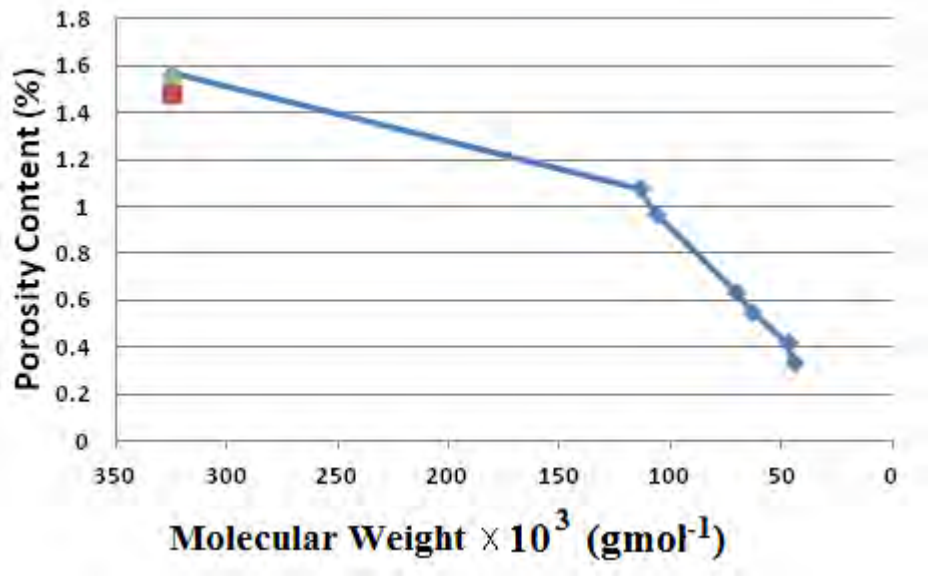

Figure 4-34. Relationship between the porosity content of the castings made with irradiated foam patterns and the molecular weight of the foam pattern (Probead-70™).

The porosity content was reduced, as the foam pattern molecular weight was reduced, from about 1.5% in the casting made with the unirradiated foam to about 0.4% in the casting made with the most irradiated foam (189 MRad, M_w of about 45,000 $gmol^{-1}$). The porosity content of the castings was decreased by up to 85% due to irradiation of the foam patterns.

An F-test was carried out to determine if the measured porosity contents were significantly different in castings made with unirradiated patterns and fully irradiated (189 MRad) foam patterns. The parameters calculated in this test were:

Table 4-14 shows the parameters calculated for an F-test to verify if the porosity content of the castings with irradiated and untreated foam patterns were different.

S_B	f_b	MS_B	Sw	fw	MS_W
1.92	1	1.92	0.1066	4	0.026

$F = MS_B / MS_W = 73.8$, $F_{1\%}(1,4) = 21 << 73.8$

Where;

S_B = Between-group sum of squares.

f_b = Between-group degrees of freedom.

MS_B = Between-group mean square.

Sw = Within-group sum of squares.

fw = Within-group degrees of freedom.

MS_W = Within-group mean square.

This means that the porosity content of the castings made from untreated and fully irradiated foams were significantly different at the 99% confidence level.

The internal porosity of the castings was characterised by measuring the parameters of surface cavities found at the base of the castings, thought to be associated with the entrapment of liquid polymer degradation byproducts at the casting-coating interface. Figure 4-35 shows some of the defects found at the base of the castings made with different M_w foam patterns and their relationship with porosity in the casting.

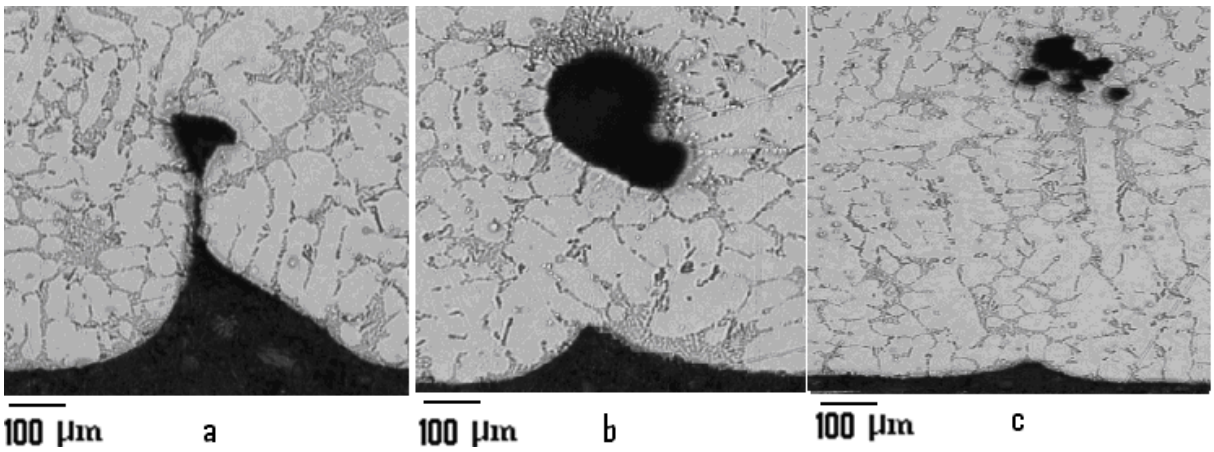

Figure 4-35. Defects occurring at the base of the castings. (a) made with untreated foam pattern, (b) and (c) made with irradiated foam patterns, (30 and 75 MRad respectively).

The total length of the defects at the bottom surface of the castings (which were assumed to correspond to the entrapment of liquid polymer globules by the casting/coating interface) was measured on a dimension of 25 ×10 mm from the centreline of the castings made with different M_w foam patterns (Probead-70™).

Figure 4-36 shows the total length of defects plotted against M_w, suggesting that they were eliminated at about 60,000 $gmol^{-1}$, i.e. the castings that were made using foam patterns (Probead-70™) with M_w of less than 60,000 $gmol^{-1}$ did not contain defects related to globules of liquid polymer at the casting/coating interface, at the base of the castings. The critical M_w for wicking of the polystyrene residue was 70,000-75,000 $gmol^{-1}$ [21], and 60,000 $gmol^{-1}$ was lower than this critical molecular weight. This suggests that globular defects at the bottom of the castings should not be observed when the initial M_w of the foam is lower than the critical value, see Figure 4-36.

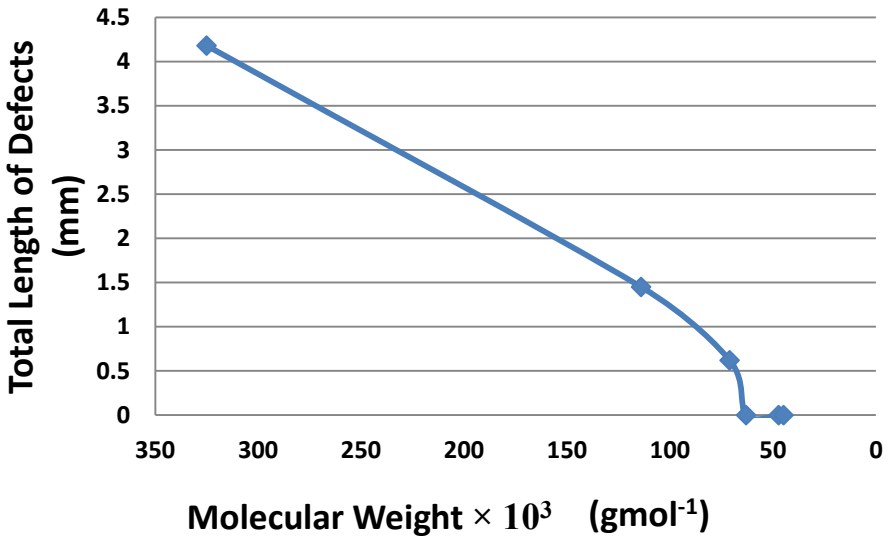

Figure 4-36. Graph showing the relationship between the M_w of the foam patterns (Probead-70™) related to the total length of the defects found on the bottom surface of the horizontally cast plates.

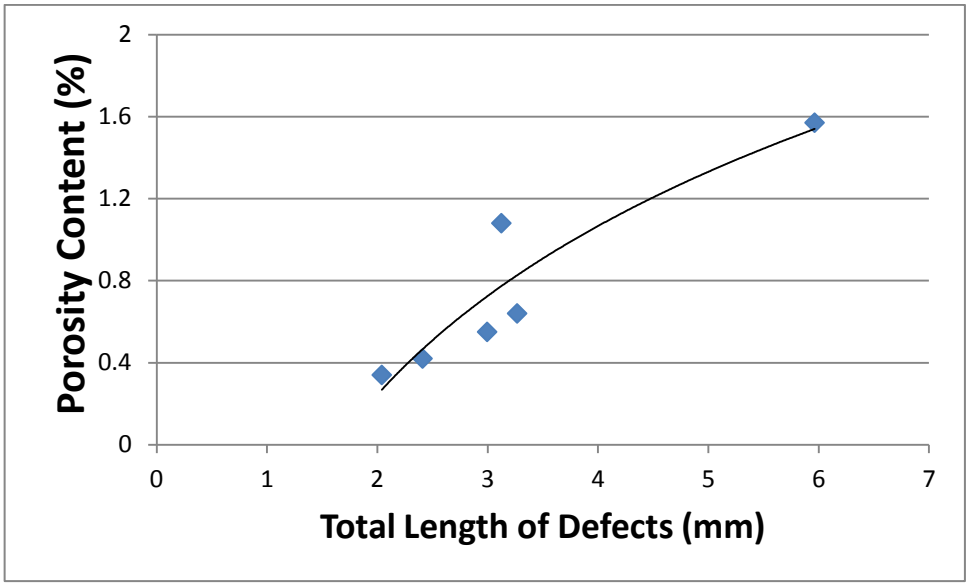

Figure 4-37. The relationship between the porosity content of the castings made with irradiated foam patterns (Probead-70™) and the total length of the defects found on the bottom surface of the horizontally cast plates.

Figure 4-37 shows that the castings with shorter and less defects at the base of the castings were also less porous. This is thought to be due to the fact that the polystyrene residues (degradation byproducts) trapped at the casting/coating interface, release gas bubbles that rise up through the liquid metal above and become trapped in the solidifying casting, as shown in Figure 4-35. Therefore, having smaller or less frequent globules, trapped against the coating during casting, leads to less porosity.

4.6.4.2 Effect of irradiating the foam pattern on mechanical properties of aluminium alloy LFC

The results of the tensile tests are shown in Figure 4-38. This shows that the UTS of the castings made with γ-irradiated foam patterns increased slightly with decreasing M_w. A Fisher test confirmed that the UTS of the castings made with the unirradiated foam, and made with the most irradiated foam (189 MRad), were statistically different at the 99.9% confidence limit.

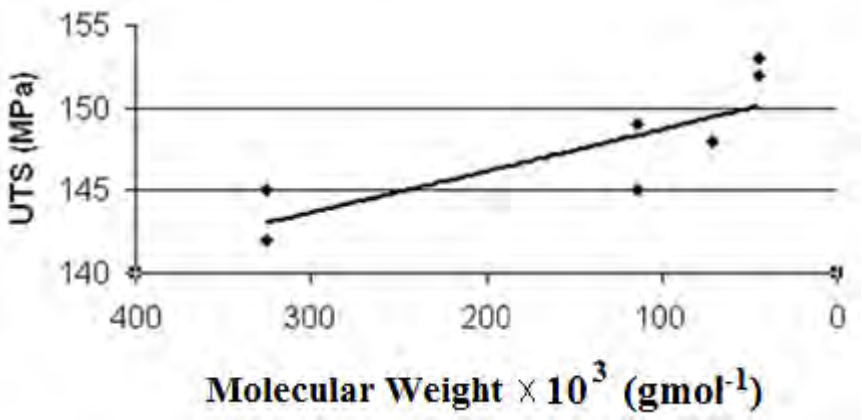

Figure 4-38. Ultimate Tensile Strength of test bars of Al-7Si-0.3Mg alloy related to the M_w of the patterns used.

To study further the improvement in the mechanical properties of the castings made with lower M_w foam patterns fatigue tests were carried out on the heat treated test bars of 2L99 alloy, of dimensions 10 x 40 x 300 mm. The samples were placed in a fatigue test with their as-cast surfaces intact, arranged so that the lower surface of the casting faced downwards. This meant that the surface containing the cavities suspected of having defects associated with liquid polymer degradation byproducts trapped at the casting-coating interface experienced the maximum stress in the test.

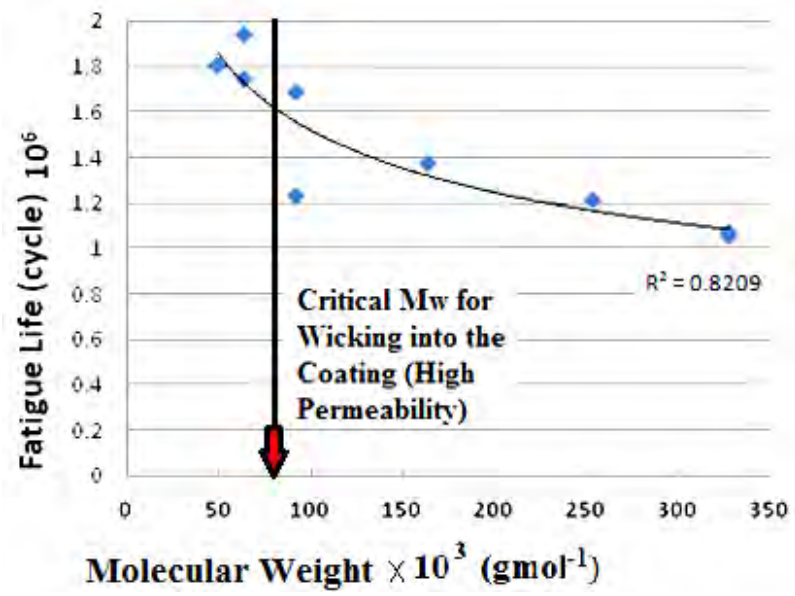

Figure 4-39. Fatigue properties of the heat treated alloy improved by irradiation of the foam patterns (Probead-70™) used in the casting process.

When the M_w of the foam pattern was lower than the critical value for wicking of the polystyrene residue (which was about 70,000 $gmol^{-1}$ in the case of the high permeability coating) [21], the fatigue life was increased to nearly twice that of castings made with the untreated foam patterns, as shown in Figure 4-39. This shows that fatigue properties of the heat treated alloy improved by reducing the M_w of the foam patterns used in the casting process. This also shows that the improvement in the fatigue properties was observed only when the M_w of the pattern was reduced below the critical value for wicking into the refractory coating. In other words, when the M_w of the pattern was not sufficiently reduced (i.e. still was greater than the critical value for wicking into the coating), the fatigue life of the casting was not greatly increased.

The fracture surfaces of the fatigue samples were inspected using a scanning electron microscope (SEM), (see Figure 4-40). The fracture surface of the specimens illustrated that the failure of the casting made with an irradiated foam pattern with M_w of 63,000 $gmol^{-1}$, occurred due to a small surface-breaking defect (a pore broke through the bottom surface), see Figure 4-40b. However the initiation of the fatigue failure of the casting made with an untreated foam pattern was due to a near-surface pore with a diameter 4 times greater than that of the former defect (Figure 4-40a).

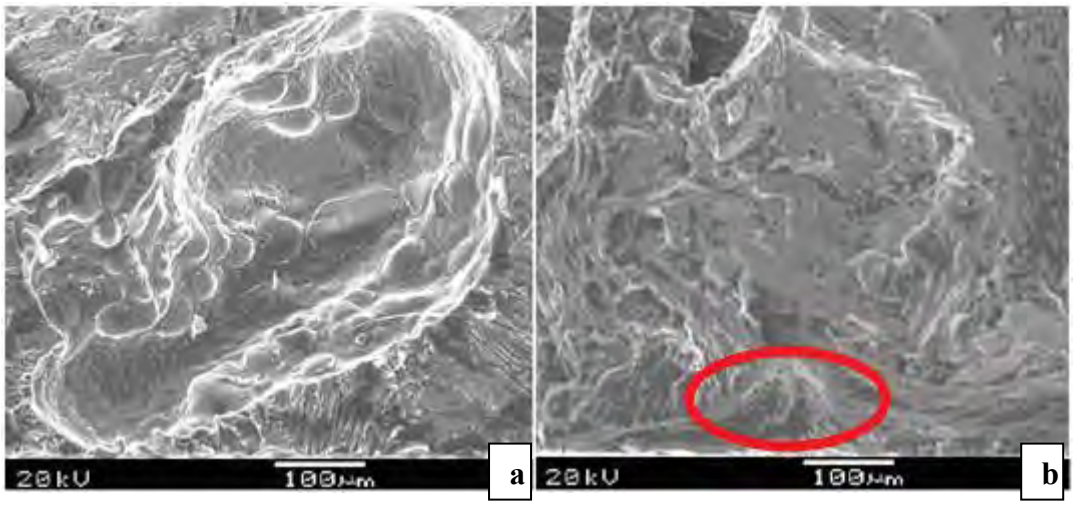

Figure 4-40. SEM micrographs of fracture surfaces from the fatigue tests (a) casting with an untreated EPS (M_w of 325,000 $gmol^{-1}$) and (b) casting with an irradiated foam pattern (144 MRad, M_w of 63,000 $gmol^{-1}$).

Finally, to study the effect of irradiating the foam pattern used in the LFC process on the hardness of the castings, this was measured on the cross section cut from the centreline of the casting strips, (see Figure 4-41).

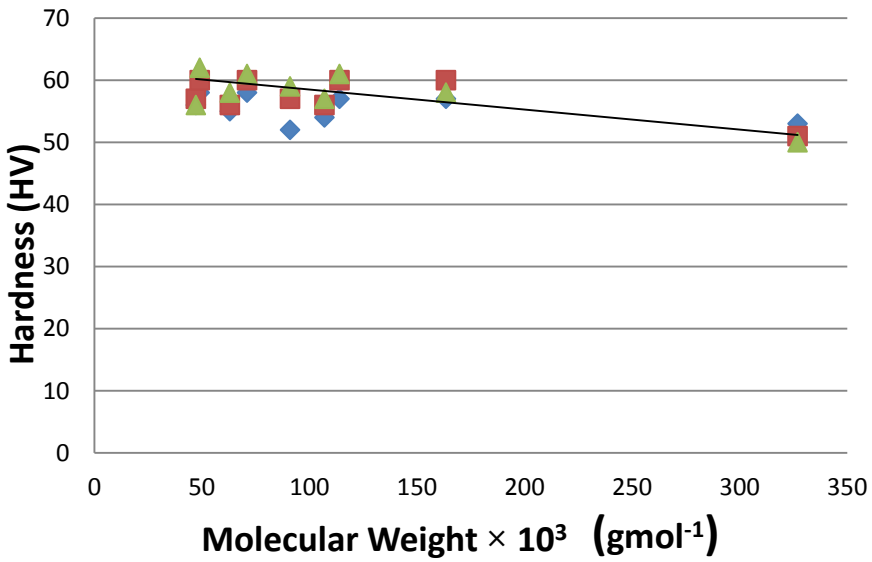

Figure 4-41. Results of hardness test, castings with irradiated foam patterns (different M_w)

This shows that the hardness of the castings produced in LFC was not greatly affected by the molecular weight of the foam pattern (57 HV on average).

4.6.4.3 *Effect of irradiating the foam pattern on quality of cast iron LFC*

To study the effect of molecular weight of the foam pattern on the quality of cast iron castings (in this case, made with Probead-30™), castings were made with irradiated foam patterns with 0, 80, 100, 140 and 180 MRad electron beam. Image analysis was performed to measure their porosity content, and Figure 4-42 shows typical images taken from the centreline cross section of castings made with Probead-30™ irradiated with 100 MRad of electron beam. This figure shows the base of the horizontally cast strip.

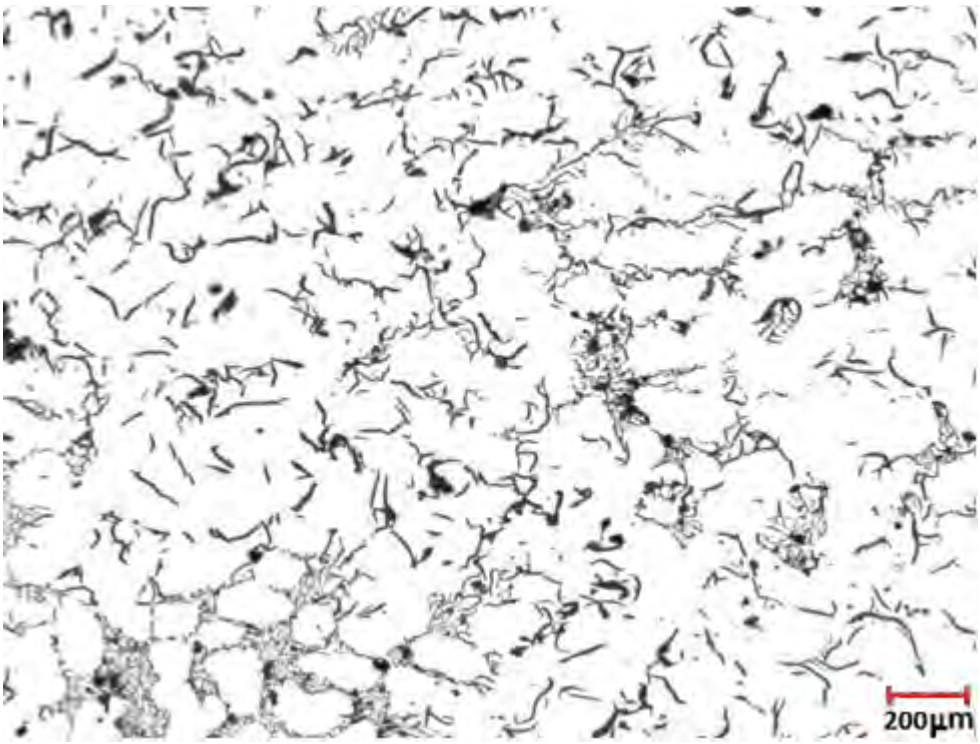

Figure 4-42 shows an image taken from the centreline of cast iron casting with Probead-30™; foam pattern irradiated with 100 MRad of electron beam (M_w of about 178,000 $gmol^{-1}$).

An area of 25×10 mm taken from the centreline cross section of the cast iron castings was analysed for porosity content, with between 20 to 30 images taken.

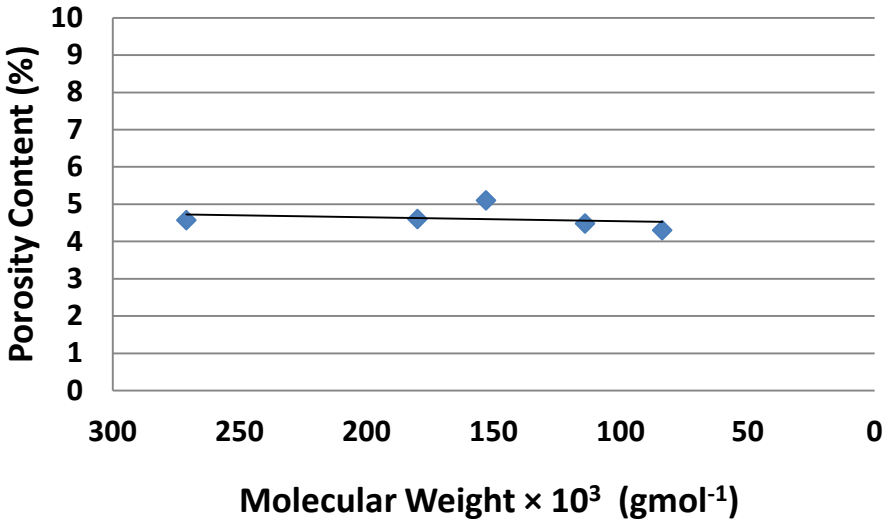

Figure 4-43. Relationship between porosity content of cast iron castings made with irradiated foam patterns and the molecular weight of used foam pattern (Probead-30™)

Figure 4-43 shows that casting with reduced M_w foam patterns of Probead-30™, with M_w of between 271,000 to 83,000 $gmol^{-1}$, had no effect on porosity content. This is probably because of the high temperature of cast iron casting. The rate of foam pattern decomposition was probably higher with that casting temperature (1450 ^oC) so that reduction in M_w of the decomposition byproducts was quickly reached and subsequently they became absorbed by the coating vaporized quickly and initial M_w of the foam pattern was much less important.

This is also supported by the fact that there were no globular-shaped defects found on the lower surface of the castings, regardless of the cast iron castings irrelevant to the M_w of the foam pattern used. In contrast, in the case of Al castings, these defects were reduced by reducing the M_w of the foam pattern (see section 4.5.6).

4.6.5 The effect of irradiating the foam pattern on counter-gravity filling behaviour and the interface in Lost Foam Casting of Al alloy (2L99)

Some casting experiments were carried out using irradiated plates of copolymer Probead-30™, irradiated with 0, 80,140 MRad of electron beam; having M_w of 271,000, 178,000 and

113,000 $gmol^{-1}$ respectively. Therefore, 2L99 alloy was cast at 820^{o}C, with a bottom-filling running system in a real time X-ray system in order to see the shape of the advancing metal front (see the videos of the castings at the end of this thesis).

Casting with an un-irradiated foam pattern, Probead-30™ (M_w of 271,000 $gmol^{-1}$) was found to have a velocity of 16 mms^{-1}. Figure 4-44 shows sequences of filling the untreated plate foam pattern.

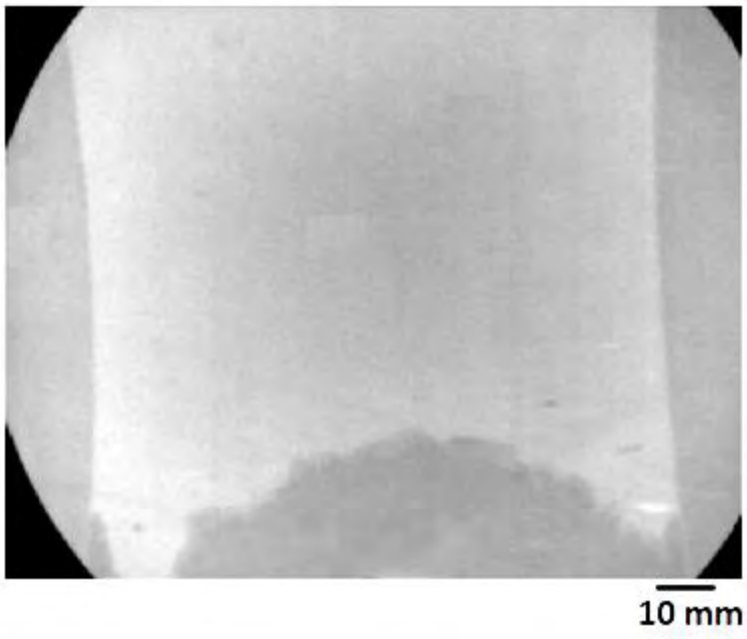

Figure 4-44. The sequences of filling the untreated foam pattern (Probead-30™) in the LFC process.

a. 7.26 seconds, The liquid metal started branching (left corner).

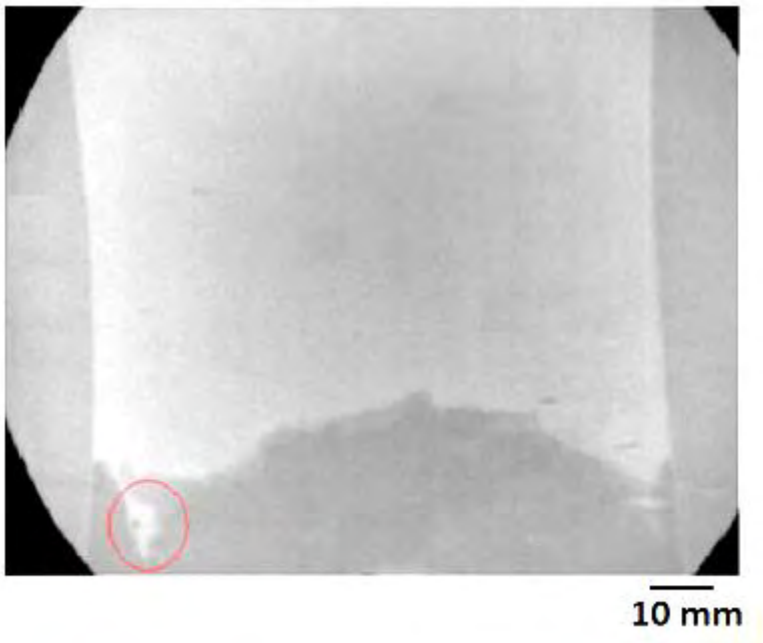

Figure 4-44. The sequences of filling the untreated foam pattern (Probead-30™) in the LFC process.

b. 7.88 seconds, advancing liquid metal stream entrapping the degrading foam pattern.

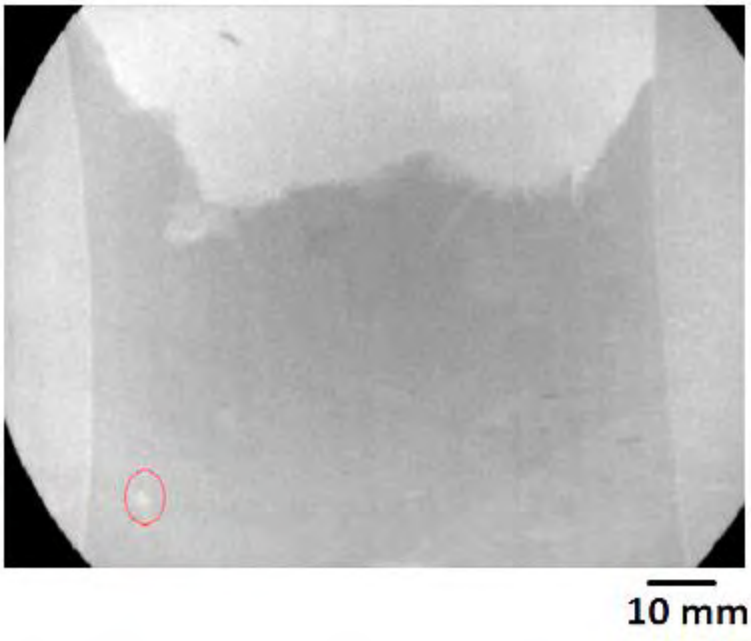

Figure 4-44. The sequences of filling the untreated foam pattern (Probead-30™) in the LFC process.

c. 10.43 seconds, the left bubble is almost diminished.

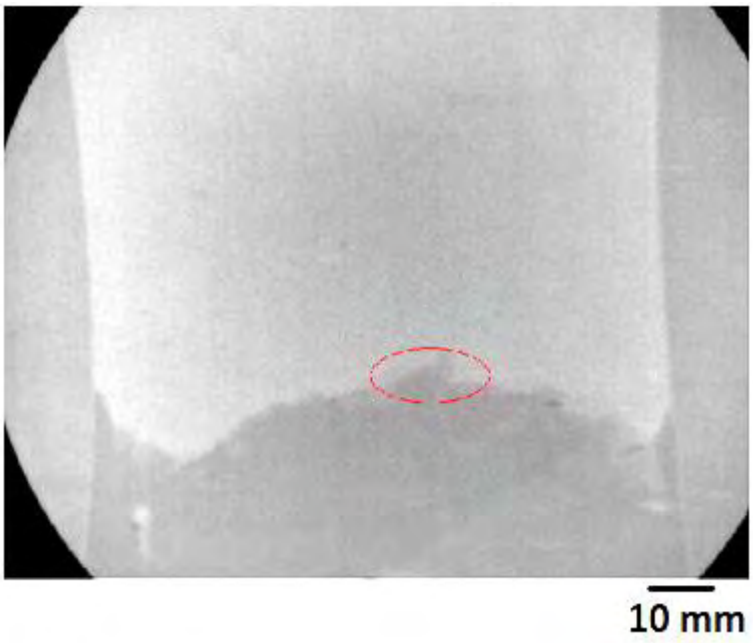

Figure 4-44. The sequences of filling the untreated foam pattern (Probead-30™) in the LFC process.

d. 7.15 seconds, the metal/foam interface became irregular.

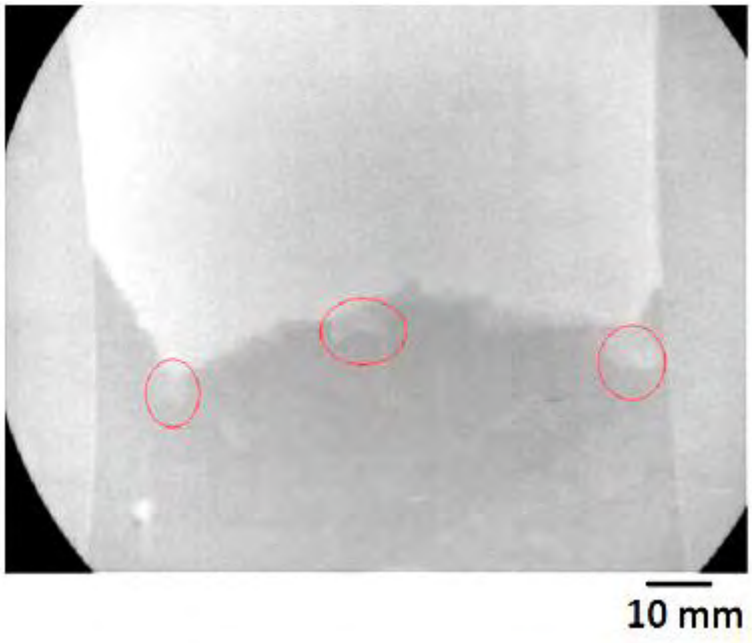

Figure 4-44. The sequences of filling the untreated foam pattern (Probead-30™) in the LFC process.

e. 9 seconds, pieces of foam pattern were ablated and entrapped between the streams of flowing metal where they joined together.

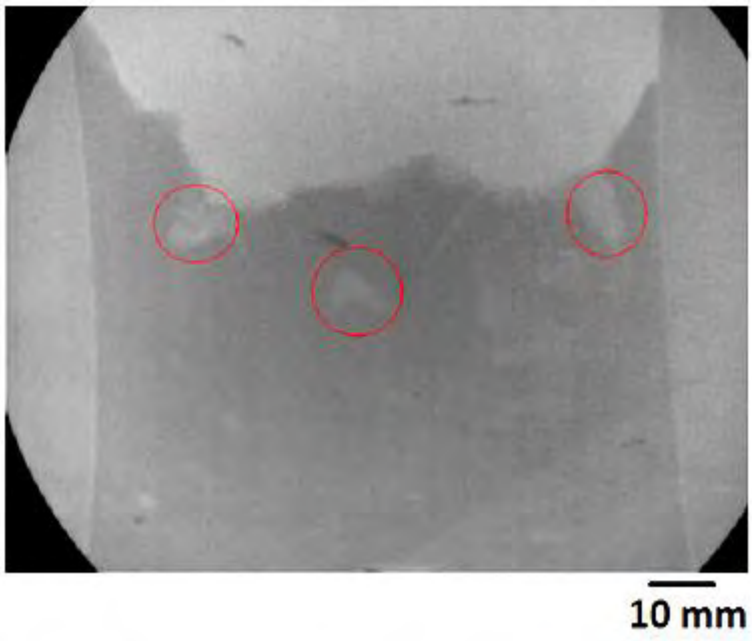

Figure 4-44. The sequences of filling the untreated foam pattern (Probead-30™) in the LFC process.

f. 10.53 seconds, the ablated pieces of foam in decomposition and released bubbles of gas.

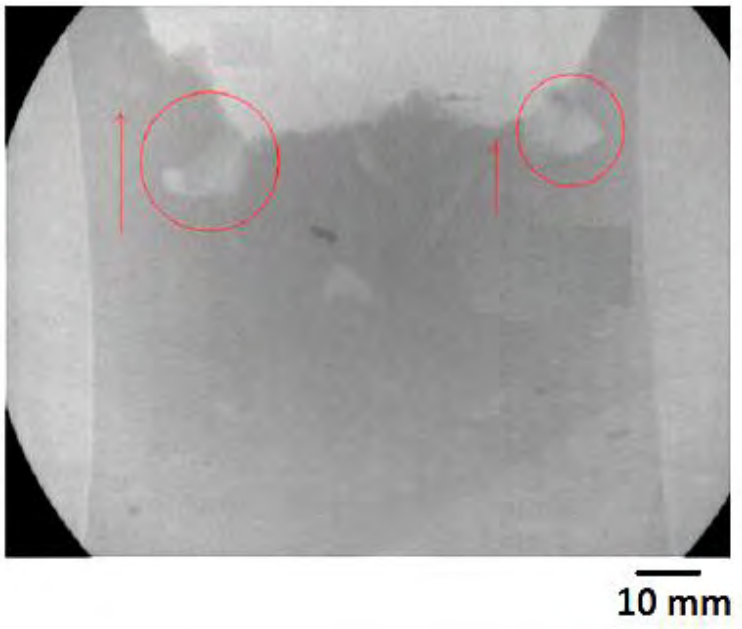

Figure 4-44. The sequences of filling the untreated foam pattern (Probead-30™) in the LFC process.

g. 11.28 seconds, the created bubbles expanded and tend to moved upward with the stream.

X-ray images from the casting with an irradiated foam pattern of Probead-30™, (M_w of 178,000 $gmol^{-1}$), produced a filling velocity of 19.6 mms^{-1}. Figure 4-45 shows images of the plate being filled with 2L99 alloy at 820 ^oC.

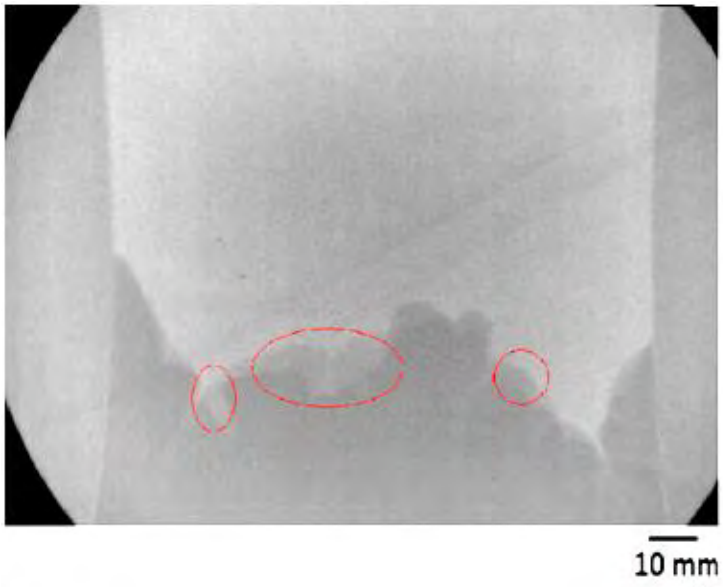

Figure 4-45. Real time X-ray observation of filling the plate of Probead-30™ irradiated with 80 MRad of γ-ray (M_w of 178,000 g mol^{-1}).

a) 11 seconds, there was no bubble or ablated piece of foam observed at the beginning of filling. A gap seemed to form ahead of the liquid metal front as the contrast of the image is different.

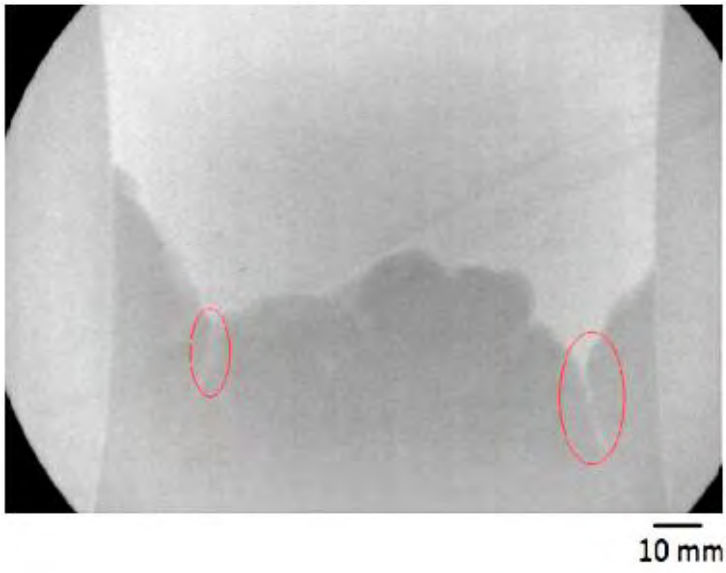

Figure 4-45. Real time X-ray observation of filling the plate of Probead-30™ irradiated with 80 MRad of γ-ray (M_w of 178,000 g mol^{-1}).

b) 12.5 seconds, branching was occurred while the stream started to find a finger shape front.

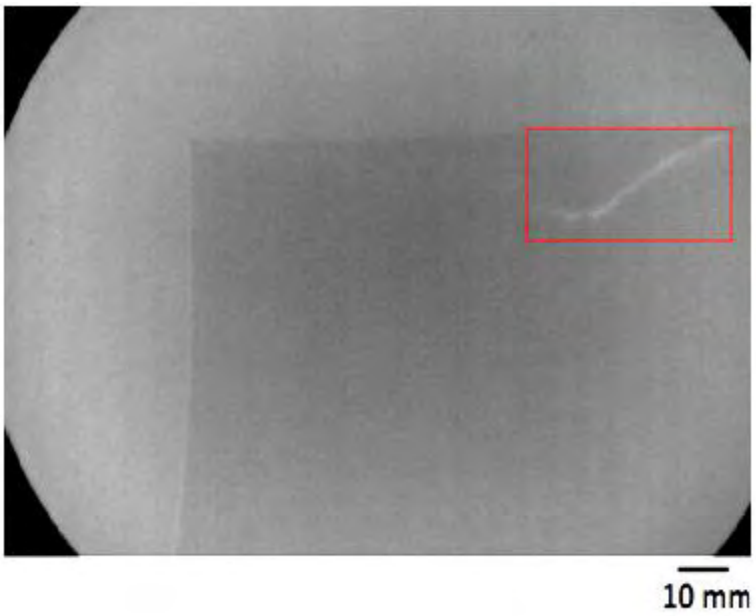

Figure 4-45. Images taken from Real time X-ray observation of filling the plate of Probead-30™ irradiated with 80 MRad of γ-ray (M_w of 178,000 g mol $^{-1}$).

c) 30 seconds, the streams adjoined at the end of the casting and caused the failure of cold joint which might be dependent to the size of the pattern.

Casting a plate of foam pattern Probead-30™ irradiated with 140 MRad of γ-ray (M_w of 113,000 $gmol^{-1}$) has been shown in Figure 4-46. The velocity of liquid metal during filling this plate was 24 mms^{-1}.

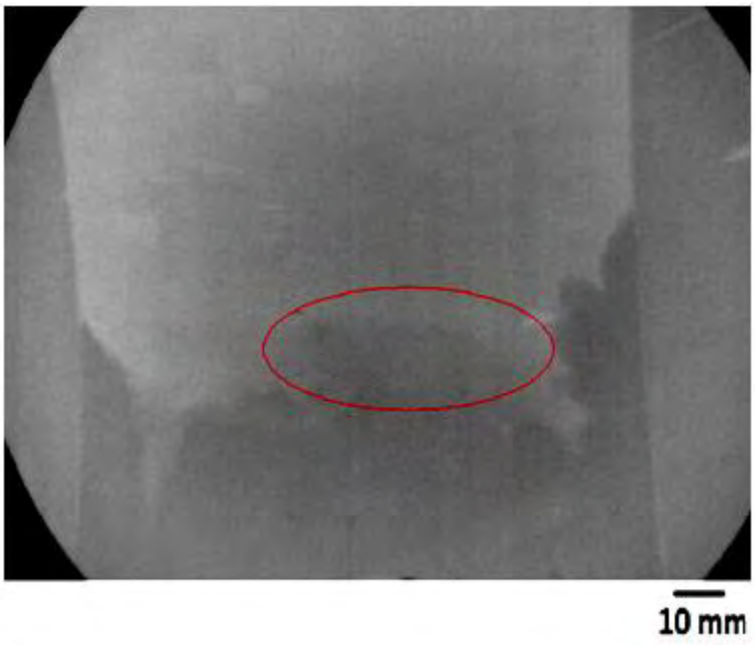

Figure 4-46. Images of real time X-ray observation of LFC with irradiated foam patterns (irradiated with 140 MRad of γ-ray, M_w of 113,000 $gmol^{-1}$).

a) 12 seconds, A big gap ahead of the liquid metal stream is found at the metal/foam interface.

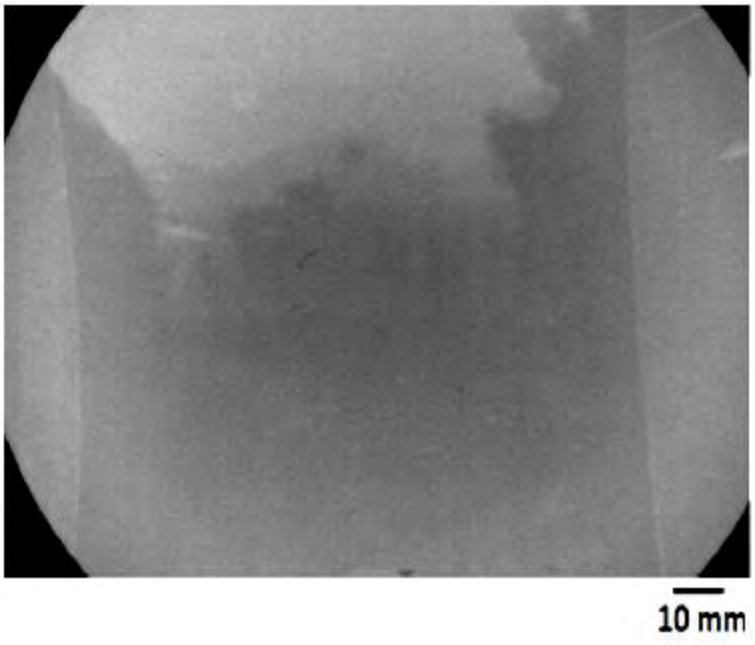

Figure 4-46. Images of real time X-ray observation of LFC with irradiated foam patterns (irradiated with 140 MRad of γ-ray, M_w of 113,000 $gmol^{-1}$).

b) 14 seconds, irregularity in the metal/foam interface, however no big bubble left behind the liquid metal flow.

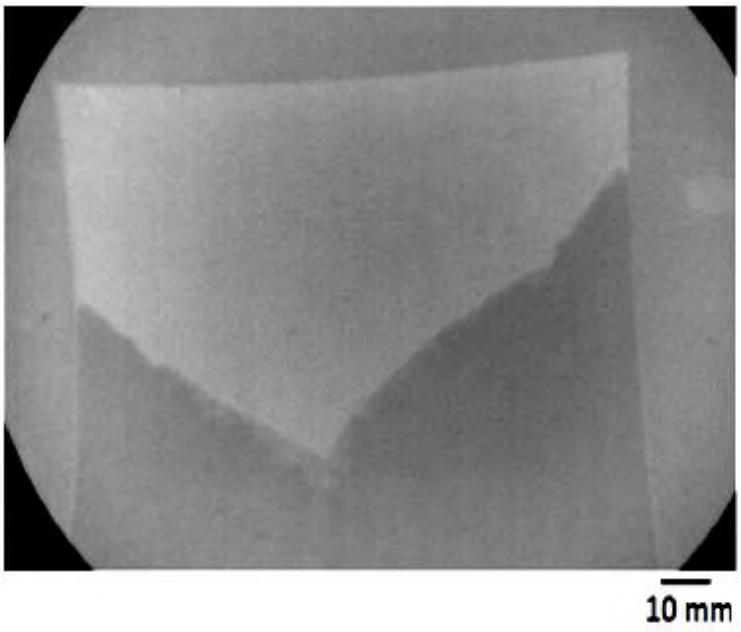

Figure 4-46. Images of real time X-ray observation of LFC with irradiated foam patterns (irradiated with 140 MRad of γ-ray, M_w of 113,000 $gmol^{-1}$).

c) 22 seconds, the stream of liquid metal became smoother with a more stable interface at the end of filling process.

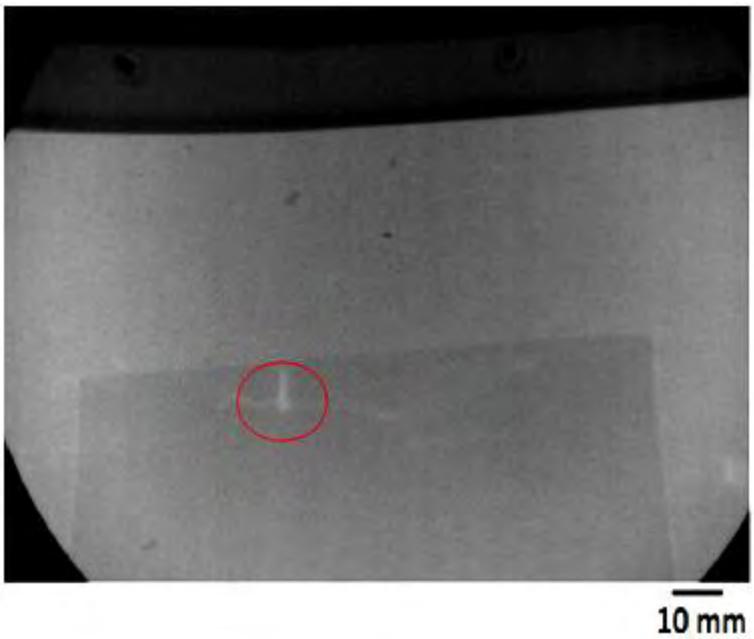

Figure 4-46. Images of real time X-ray observation of LFC with irradiated foam patterns (irradiated with 140 MRad of γ-ray, M_w of 113,000 $gmol^{-1}$).

d) 26 seconds, cold joint failure was occurred at the end of the casting similar to the casting with the foam pattern irradiated with 80 MRad of γ-ray.

It can be concluded that irradiating the foam pattern used in the LFC process increased the velocity of the liquid metal filling the vertically oriented plate, as shown in Figure 4-47.

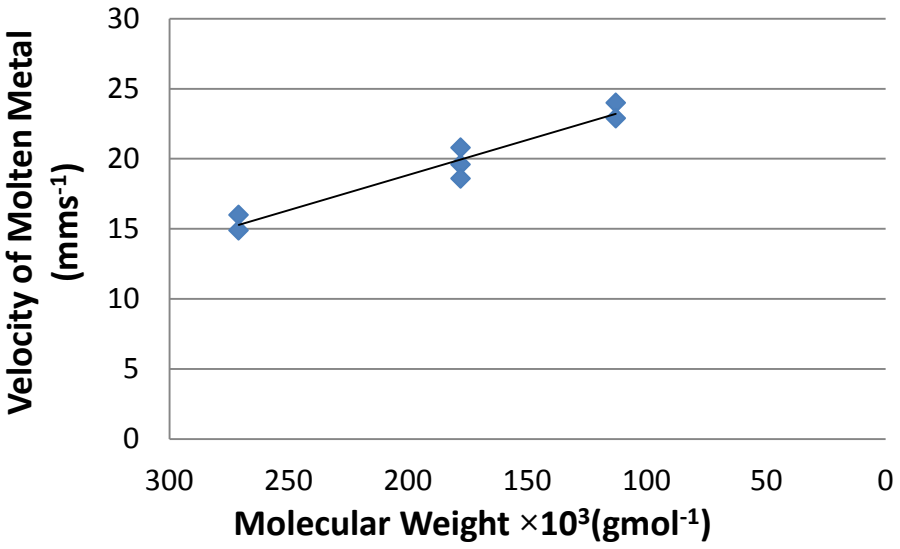

Figure 4-47. Velocity of the molten metal stream filling plates of Probead-30™ with different M_w cast at 820 °C with aluminium 2L99 LFC.

Real time X-ray observation of the filling process with the irradiated and untreated foam patterns revealed that decomposition of the foam pattern was an issue when untreated foam plate was cast and entrapment of the degrading foam pattern inside the flowing metal was observed frequently, but the metal/foam interface was advancing with a more stable shape compared to casting with reduced M_w foam plates.

In the case of casting with irradiated foams, the metal front showed irregularities which increased with reducing molecular weight of the foam plates. Figure 4-48 compares images from the real time X-ray observation taken from foam patterns with different M_w.

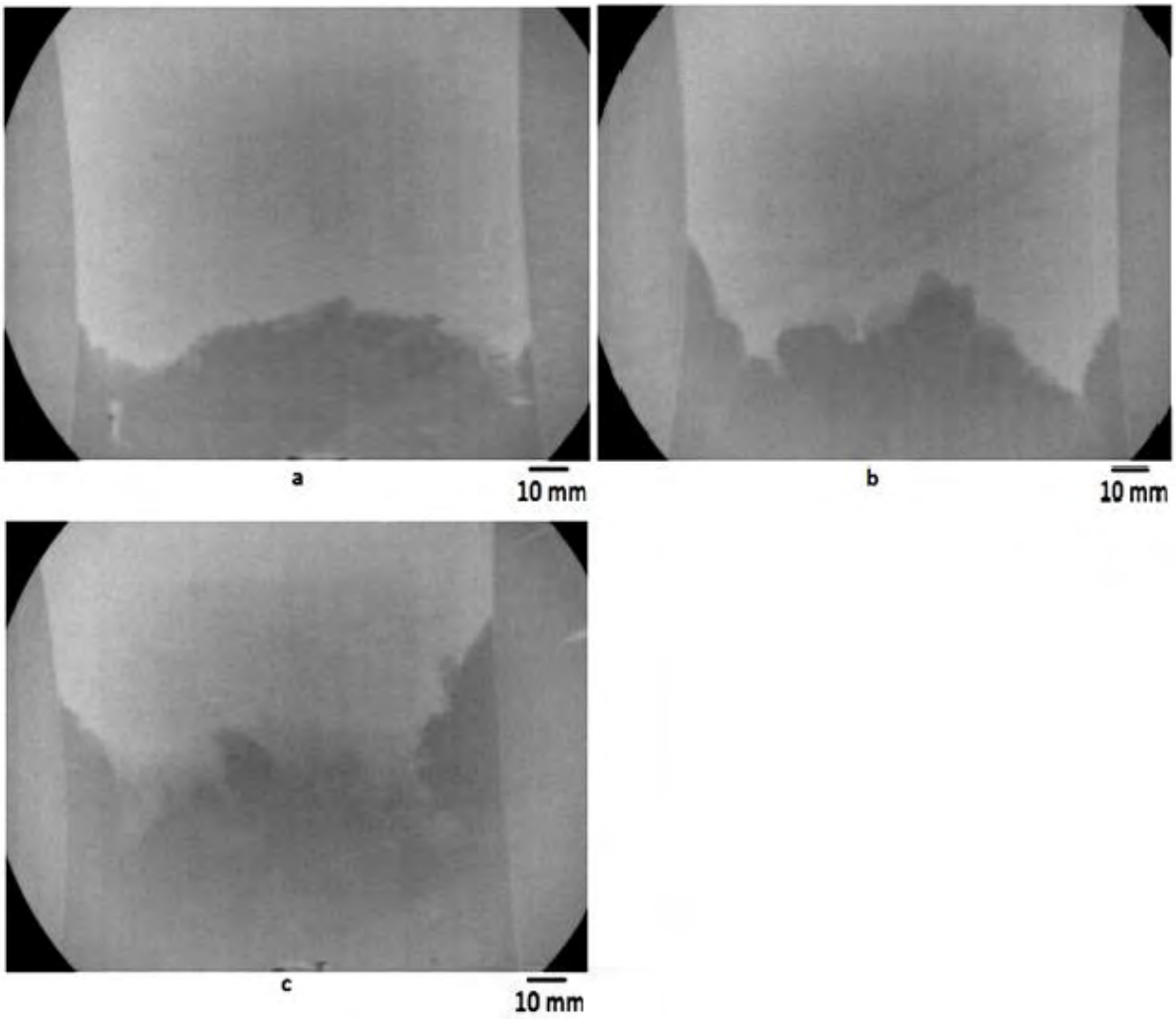

Figure 4-48. Images of real time X-ray, filling plates of Probead-30™ with M_w of a. 271,000 $gmol^{-1}$ (unirradiated), b. 178,000 $gmol^{-1}$ (irradiated with 80 MRad of γ-ray) and c. 113,000 $gmol^{-1}$ (irradiated with 140 MRad of γ-ray) showing that casting with lower M_w foam patterns filled the pattern with more irregularity in the metal/foam interface.

5 DISCUSSION

One of the advantages of LFC over conventional casting is that the pattern remains in the mould and this brings great flexibility in casting design. However, the decomposition of the foam pattern introduces a number of defects, such as porosity and misrun.

A fluidity test was designed to address the role of casting parameters in influencing the fluidity of the molten metal in LFC. A fluidity formula was derived from the results of the fluidity tests by solving the heat balance between the molten metal and the pattern and the mould. In addition, the heat transfer coefficients from the molten metal to the foam and to the mould were also estimated. The fluidity model was used to explain the effect of different casting parameters on the fluidity of LFC.

The current work also showed that the porosity content of LFC was reduced by reducing the M_w of the foam patterns because the decomposition byproducts were more easily removed from the mould when the casting was made with a lower M_w pattern. This reduction in the porosity content resulted in an improvement in the mechanical properties of the castings such as fatigue life.

5.1 The flow behaviour in LFC and the design of the fluidity test

To study the fluidity of LFC and examine the flow behaviour, it is necessary to devise a test that has a single stream of liquid metal rather than two or more streams filling the foam pattern. These might lie vertically, with one stream of metal on top of another, or horizontally, with a single stream of metal splitting into two or more as it flowed along a flat, horizontal channel. Filling of the fluidity test with split liquid metal streams would obscure the fluidity results, because the fluidity length is more easily determined if it consists of a single stream of

molten metal. The X-ray images of the filling of vertically-oriented plates, and thick sections of foam patterns, shown in section 4.1, suggested that the thickness of the pattern in the fluidity test should not be greater than 35 mm, and the width should not exceed more than 50 mm.

The flow regime of the liquid metal (laminar or turbulent) has not been examined in previous studies of LFC. In conventional casting the liquid metal usually exhibits turbulent behaviour ($R_e > 5\times10^5$), but it was found that in LFC all of the Reynolds numbers were well inside the laminar flow region.

Having a high velocity of molten metal in LFC might overcome the misrun issue although it is not recommended because the morphology of the metal/foam interface is strongly affected by the velocity of the molten metal. Increasing the velocity of the molten metal is likely to result in an unstable, finger shape metal/foam interface [69].

The heat transfer and solidification behaviour of LFC differs from conventional empty cavity casting in many aspects. The endothermic nature of the foam pattern decomposition has been proposed to cause a quenching effect on the flowing liquid metal at the metal/foam interface [9]. Secondly, a greater back pressure is produced in LFC compared to other casting methods, due to the decomposition of the foam pattern [43].

While Fleming's model predicts the fluidity length of the empty cavity casting well (within 7%), (see section 4.2.1), it could not predict the fluidity of LFC (35 to 74% shorter, see Table 4-3). Other fluidity models developed for LFC were found to be not as good as Fleming's model, probably because they were derived for particular mould/pattern geometries or based on very simplifying assumptions. For example, the model of Pan and Liao [85] underpredicted the fluidity length by 40%, while the model of Ajdar et al. [11] was grossly in

error, and predicted a fluidity length of 6 mm when the actual fluidity length was 0.2 m (see Table 4-12).

A spiral foam pattern was not an option to examine fluidity of LFC because the heat from the molten metal filling the foam pattern might affect the structure and properties of the foam pattern in the outer radii, and a fluidity test containing a single long straight strip of foam requires a bulky mould. Therefore, it was decided to have a model with different levels of foam strips, in order to produce a robust fluidity test, sensitive to casting conditions, and giving reproducible fluidity results.

The fluidity test developed here, shown in Figure 3-7, was not completely filled at any of the casting conditions with 2L99 alloy, thus, casting the test could produce measurable fluidity lengths. The pattern was, however, completely filled in the case of casting with CP Al. however, this was not considered important because pure Al does not commonly face fluidity issues as it has higher fluidity compared to non-eutectic alloys [74] and CP Al is never or rarely commercially cast. However the fluidity of CP Al can also be tested with this pattern if it is cast at lower casting temperatures (e.g., 680 ^{o}C), when it would not fill the fluidity strips completely.

The test provided a very reproducible examination of the fluidity of LFC, as was shown in Figure 4-5. The standard deviations of the tests varied from 3% to 9% of the mean fluidity lengths of the castings, and were negligible compared to the mean fluidity lengths of the castings.

5.2 A fluidity equation

While some researchers [10, 11, 84] have evolved mathematical models and equations to describe the fluidity of LFC, an inclusive model to explain and relate the fluidity of LFC to various casting parameters is still required.

Fleming assumed skin freezing solidification to develop a fluidity equation for open cavity casting conventional castings. Fleming's equation was derived assuming the molten metal flow stops when the solidified thickness of the metal reached half of the thickness of the casting section [72]. But the results obtained from the cooling curves at different points in the Lost Foam fluidity tests established that solidification occurred at the tip of the liquid metal flow rather than at the beginning of the fluidity channel, probably because of the reduction in the velocity of the molten metal and, in addition, the heat consumed at the liquid metal front by the degrading foam.

To use Fleming's equation for LFC (Equation 2-2), the following assumptions were made;

(i) The liquid metal stops flowing once 22% fraction solid formed at the tip of the advancing liquid metal (the coherency point, estimated in section 4.3.1).

(ii) The interface between the molten metal and the foam pattern is assumed to be a physical gap.

(iii) The heat transfer associated with the degradation of the foam pattern was neglected, and it was assumed that there was no significant heat transfer from the molten metal except to the sand surrounding the foam pattern. To test this assumption, a comparison of the heat fluxes for heat transfer to the foam pattern, and heat transfer to the surrounding sand mould, was carried out for the bottom fluidity strip of casting H2 (fluidity length of 95 mm) using the heat transfer coefficients determined in section 4.4 (h_1~ 485 , h_2 ~ 170 $Wm^{-2}K^{-1}$).

Table 5-1 shows that the heat flux to the foam pattern was an order of magnitude smaller than the heat flux to the mould, which suggests that it could be assumed that most of the heat in LFC is transferred laterally to the mould.

Table 5-1. Comparison between the heat transfer from the molten metal to the mould and to the foam pattern for LFC, (casting H2).

Heat Transfer Through	Material of the Interface	Area of the Interface (mm^2)	Thickness of Interface (mm)	ΔT (K)	The Heat transfer Coefficient of Interface ($Wm^{-2}K^{-1}$)	Heat Flux (Wm^{-2}) $h \times A(T_1 - T_2)$
The pattern/metal interface	Degradation by-products	400	2-4	300	480	97
The Surface of the Casting	Coating	9100	1.3	600	170	927

According to Equations 2-2 and 4-4, the time of freezing is given by;

$$t_f = \frac{\rho_s a(H + c'\Delta T)}{2h(T_M - T_O)} \qquad \textbf{Equation 5-1}$$

The modulus of the mould cross section for the fluidity strips was 0.004 m (the ratio of the volume to the surface area of the fluidity strip) and the coherency point was estimated to be 0.22 (see section 4.3.1). The room temperature was 20 ^oC and the temperature of the metal in the pouring basin was 678 ^oC and the specific heat capacity of the foam was assumed to be 897 J [34].

$$t_f = \frac{2436 \times 0.004 \times (389000 \times 0.22 + 897 \times 60)}{2 \times 170 \times (617 - 20)} = 6.6\,\text{sec}$$

The time of freezing for the bottom fluidity strip of casting H2 was determined in section 4.3.2.5 to have been 15 s; the time of freezing predicted by Fleming's model was about half of the actual value, indicating that Fleming's equation could not be applied for LFC.

A fluidity model was therefore developed that concentrated on the behaviour of the flow front, rather than the behaviour at the beginning of the fluidity channel, and an equation was evolved based on a heat balance equating the heat loss from the molten metal to the foam and to the mould. The heat loss includes the reduction of the temperature of the molten metal from the pouring temperature to the coherency temperature (at which molten metal flow stops), and also to the latent heat of solidification to the coherency point.

To estimate a mean heat transfer coefficient from the molten metal to the foam pattern, the heat flux passing through the metal/foam interface (q/A) was derived from a knowledge of the fluidity length (which depends on the mass of the degraded foam in the fluidity length), this heat flux was equated to $h\,(T_1 - T_1)$ where T_1 and T_2 are the temperatures of the advancing liquid metal front and the collapsing foam. This gave a value of 485 $Wm^{-2}K^{-1}$ for the bottom fluidity strip of casting H2; a value in agreement with values estimated by Liu et al. [93] for metal front velocities of 0.44 cms^{-1} and 1.5 cms^{-1}, 150-350 and 150-370 $Wm^{-2}K^{-1}$ respectively, while the velocity of the molten metal for casting H2 was slightly different (V~0.6 cms^{-1}).

Having determined a heat transfer coefficient for the metal/foam interface, the thermal conductivity of the latter was estimated to be 1-1.5 $Wm^{-1}K^{-1}$ (using Equation 2-11), for a mean thickness of the metal/foam interface of 2-3 mm for the bottom fluidity length casting H2, using the data obtained from the thermocouples inserted in the fluidity strip (the temperature rise at a point was based on the estimation of the interface thickness, see section 4.3.2.4 and Figure 4-23). The thermal conductivity of the metal/foam interface was about 20 times the thermal conductivity of the gaseous decomposition byproducts (the byproducts found in the results of the thermogravimetric analysis of EPS decomposition, shown in section 3.5). Thermal conductivity of butane, air and nitrogen at 330 ^oC are much lower, 0.059, 0.045 and 0.044 $Wm^{-1}K^{-1}$, respectively [114, 115], but this is to be expected because

the metal/foam interface should consist not only of gas but also globules of liquid EPS. Liquid styrene has a thermal conductivity of 1.62 $Wm^{-1}K^{-1}$ at 120 ^{o}C [116]. Therefore a value of 1-1.5 $Wm^{-1}K^{-1}$ is reasonable as being between the thermal conductivity of the gaseous and liquid decomposition byproducts, but closer to the thermal conductivity of liquid styrene which suggests that the metal/foam interface contains predominantly liquid byproducts.

Solving the heat balance for the heat transfer coefficient from the molten metal to the mould suggested the latter to be 170 $Wm^{-2}K^{-1}$, and suggests a thermal conductivity for the low permeability coating of about 0.22 $Wm^{-2}K^{-2}$. This is in agreement with the results of experiments by Molibog et al. [92] which suggested a thermal conductivity of a mica based coating to range from 0.12 to 0.25 $Wm^{-2}K^{-1}$, while the average value was about 0.17 $Wm^{-2}K^{-1}$.

Solving the heat balance from the molten metal to the foam and the mould for the time of freezing resulted in Equation 4-12 which resulted in the derivation of a formula for the time of freezing in LFC. This equation contains the mass of decomposed foam and the mass of metal in the fluidity length. Replacing the latter parameters by the occupied volume (fluidity length × perimeter of the casting channel) multiplied by the density (of the molten metal or the foam) and solving for the fluidity length, the fluidity equation was achieved as shown in Equation 4-13.

5.3 Effect of casting parameters on the fluidity of LFC

The effect of different casting parameters (coating thickness, coating permeability, pouring temperature, head height and foam types) on the fluidity of LFC was discussed briefly in section 4.2. These effects are elaborated on here and were predicted for some of the fluidity tests and compared with the actual fluidity length, using Equation 4-13.

5.3.1 Pouring temperature

Increasing pouring temperature should increase the fluidity length because it would increase the rate of foam pattern degradation and delay solidification. This was confirmed by the results shown in Figure 4-9 which showed that increasing the casting temperature increased the fluidity length in any casting conditions except when the pattern was coated with 0.3 mm of low permeability coating where it had no effect.

It is implied in Equation 4-13 that increasing the pouring temperature would increase the fluidity length due to an increase in the time of freezing. Therefore, castings D2 and H2 were compared here to investigate the effect of casting temperature on the time of freezing and metal velocity during filling, see Table 4-4.

Table 5-2.The mean velocity of the molten metal, time of freezing and fluidity length of casting H2 and D2.

	Casting temperature	Mean velocity (mms^{-1})	Time of freezing (s)	Fluidity Length (mm)
Casting H2	677 (^oC)	5.75	15.6	91
Casting D2	787 (^oC)	11.5	19	225
Increase (%)	15%	100%	22%	147%

Table 5-2 shows that while the time of freezing for the bottom fluidity strip of casting D2 was only 22% more than casting H2, the mean velocity of the molten metal for casting D2 was twice that for casting H2. This means that a 100 ^oC increase in the pouring temperature resulted in a 147% increase in the fluidity length and suggests that the difference in the fluidity length of castings H2 and D2 mostly originates from the difference in the velocity of molten metal, associated with a more rapid rate of foam degradation rather than the time of freezing.

By assuming that the calculated values for the heat transfer coefficients of castings H2 and D2 were similar, the values used for casting H2 were used with Equation 4-12 and Equation 4-13 to predict the time of freezing and filling velocity for casting D2, as shown in Table 5-3. This predicted the fluidity length with about 8% error in the case of casting D2.

Table 5-3. Comparison between the actual and predicted values of the time of freezing and the fluidity length for casting D2.

	Mean velocity (mms^{-1})	Time of freezing (s)	Fluidity Length (mm)
Predicted	-	17.8	204
Actual	11	19	225
Difference (%)	-	6%	8%

In summary, a higher pouring temperature is expected to increase the fluidity of LFC to some extent, although it has been claimed that the role of pouring temperature on the fluidity of

LFC is not very clear [10]. It was suggested that increasing casting temperature increases the temperature gradient between the molten metal and the foam pattern, which increases the rate of foam decomposition. This can increase the volume of the evolved gas and subsequently the back pressure causing a reduction in the velocity of the molten metal, reducing the fluidity length [10]. For example, the fluidity tests showed that when the pouring temperature is increased from 680 ^{o}C to 780 ^{o}C and the foam pattern is coated with 0.3 mm of low permeability coating, the fluidity length was not affected at all. This is in agreement with the results obtained by Wang et al. [69] who reported that the velocity of the molten metal was reduced by 20% when the foam pattern was coated with a low permeability coating and when the pouring temperature was increased from 800 ^{o}C to 820 ^{o}C. However, the permeability and type of coating used was not mentioned.

5.3.2 Metallostatic pressure

The effect of changing the metallostatic pressure on the fluidity length of LFC was shown in Figure 4-6 and Table 4-5. It was concluded from the fluidity lengths of the fluidity strips with different head heights that the effect of metallostatic pressure on fluidity of LFC is negligible.

The following mechanism might explain the interaction between the molten metal and the foam pattern which offset any effect of the head height on the fluidity.

The initial contact between the liquid metal front and the foam pattern in LFC, with large head height, would result in rapid evolution of gas and a large gap might form between the metal front and the foam pattern. The existence of a large metal/foam interface at the beginning of the cast strip is also confirmed by measuring the thickness of the metal/foam interface in the fluidity strips, (see Figure 4-23 and section 4.3.2.4). The heat transfer

coefficient of the molten metal to the foam should be reduced with increasing thickness of the interface, leading to a reduction in the rate of decomposition of the foam pattern.

Figure 5-1 compares the temperature change at point 9 (located at the top fluidity strip of casting "H2") with point 15 (at the bottom fluidity strip of the same casting), both points being 70 mm away from the beginning of the cast strip.

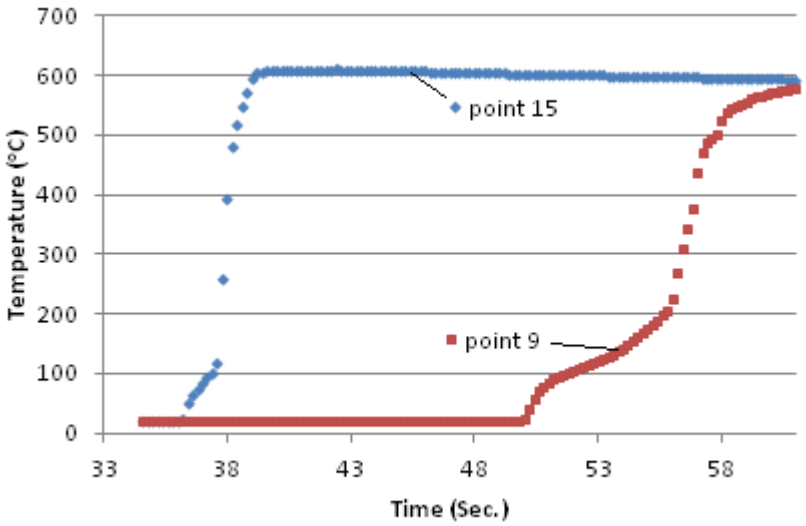

Figure 5-1. Comparison between the temperature rise at point 9 and 15 with different casting head heights, (casting H2).

This shows that the rise in the temperature at point 9 (head height of 110 mm) was more gradual than in the case of point 15 (head height of 260 mm). The comparison of the cooling curves of the points with different casting head heights in other castings (D2 and J) showed a similar effect. This suggests that either the velocity of the molten metal is lower or the metal/foam interface is thicker in the case of the top fluidity strip. However it can be assumed that the velocity of the molten metal was approximately similar at different casting head heights as the fluidity length at different head heights were similar (see Table 4-5). The thickness of the metal/foam interface was probably different at the beginning of the fluidity strip, for different casting head heights (for example it was shown in Figure 5-1 that the temperature rise was different at the beginning of the bottom and the top fluidity strips of

casting H2 which results in different thickness of the metal/foam interface). This difference did not greatly alter the fluidity length. This is probably due to a stabilizing effect between the velocity of molten metal and the metal/foam interface; a thick interface slows down the velocity of molten metal because of greater back pressure and slows down the degradation rate of the foam pattern because of the reduced heat transfer. This should result in reduction in the thickness of the metal/foam interface increasing the velocity of molten metal.

This is also in agreement with reports in the literature. For example, Tschopp [10] indicated that increasing the metallostatic head pressure from 254 mm to 560 mm increased the fluidity by only about 10% when the casting thickness was 3.2 mm. He also concluded that altering the metallostatic pressure to improve the fluidity of LFC had a disadvantage in that it had a minimal effect on fluidity, and a large change in the casting head height was needed to bring about any significant change. Pan and Liao [12] also reached the same conclusion, as they reported that no definite gain in fluidity was obtained after increasing the sprue head height from 100 mm to 150 mm.

5.3.3 Coating thickness

The results of the fluidity tests demonstrating the effect of the coating thickness are shown in Table 5-4. When the molten metal was cast at 680 ^{o}C, and the pattern was coated with a low permeability coating (see Figure 4-7d), reducing the coating thickness by over four times (from 0.3 to 1.3 mm) caused a 50% reduction in the fluidity length. When the molten metal was cast at 780 ^{o}C and the pattern was coated with a low permeability coating, and the coating thickness was increased by the same amount, the fluidity was increased by 20% (see Figure 4-7b). Therefore, the effect of increasing the thickness of a low permeability coating on fluidity was influenced by the pouring temperature.

Table 5-4. The effect of coating thickness on fluidity of LFC.

Coating Thickness (mm)	Low Permeability T (°C)			High Permeability T (°C)	
	680	**780**		**680**	**780**
0.3	180	182		201	274
1.3	91	220		217	260
Difference	-50%	+20%		+8%	-5%

Liquid decomposition byproducts are not thought to be wicked into the coating before the liquid metal stops flowing, only afterwards. Wetting and wicking of the liquid decomposition byproducts into the coating should not therefore occur in the region of the metal/foam interface, because their molecular weight is too high. Interpretation of the fluidity results should not involve the liquid decomposition byproducts, but depend upon the ease of removal of the vapour byproducts. Another argument against liquid decomposition byproducts playing a role in fluidity is that casting with reduced molecular weight foams (which should produce less liquid decomposition byproduct) showed no effect on fluidity (see section 4.2.7).

With a high permeability coating, fluidity length was increased with increasing casting temperature, at both coating thicknesses (0.3 and 1.3 mm); however there was little difference in fluidity length with changes in coating thickness (+8% and -5% for casting at 680 ^{o}C and 780 ^{o}C, respectively). Of course, high permeability coatings would be associated with easier removal of gaseous and liquid byproducts.

The relative resistance against removal of the decomposition byproducts is defined to be the coating thickness divided by the coating permeability. This factor is calculated and shown in Figure 5-2.

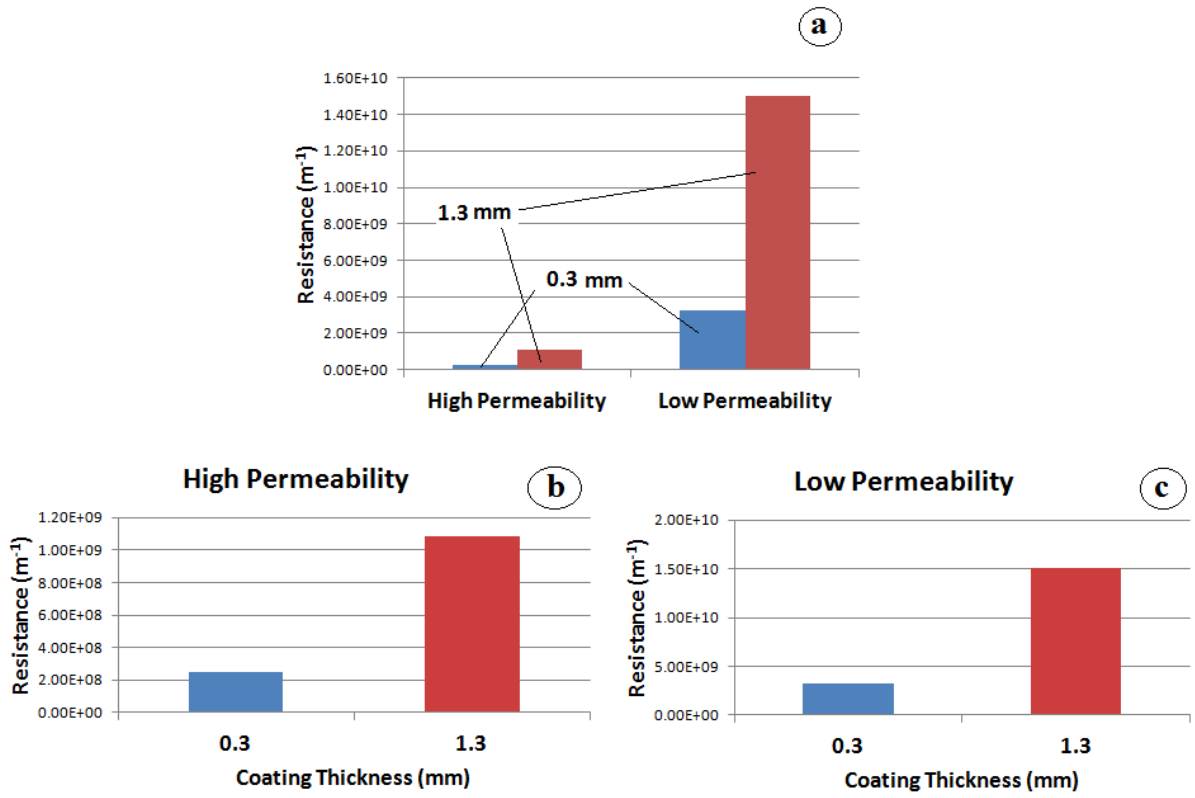

Figure 5-2. The resistance against the removal of the decomposition byproducts for different coating thicknesses and permeabilities. a) comparison between the high and low permeability coatings. b) comparison between different coating thicknesses of high permeability coating. c) comparison between different coating thicknesses of low permeability coatings.

As the coating thickness increases, the rate of heat transfer through the coating decreases assuming they have the same thermal conductivity of coating (0.22 $Wm^{-1}K^{-1}$), estimated from the thermal conductivity calculated in section 4.4.7), therefore the fluidity length should be increased. Increasing coating thickness also increase the back pressure because removal of the vapour byproducts is more difficult through a thicker coating. This reduces the velocity of the molten metal, e.g., the velocity of casting G, cast with the same casting conditions of casting H2, except for the coating thickness (which was 0.3 mm) was 7.5 mms^{-1} while the velocity of casting H2 was 5.7 mms^{-1}. For the high permeability coating there was a little effect of coating thickness on the fluidity length at either high or low temperatures, which suggests that the high permeability coating is effective in allowing the gaseous decomposition byproducts

to escape. The small increase in fluidity with increased casting temperature probably reflects the reduction in heat transfer to the mould with increased coating thickness.

With the low permeability coating, an increase in the back pressure would be expected with an increase in coating thickness (see Figure 5-2a), which would increase the interfacial gap, retard foam degradation, and reduce metal velocity from 7.5 to 5.7 mms^{-1} (by about 25%) and the time of freezing from 22 s to 15 s (about 31%) explaining the 50% reduction in the fluidity length, at 680 ^{o}C, with increased casting thickness (comparing casting H2 and G).

Thus the coating thickness affects both heat transfer from the casting to the mould and also the back pressure in the interface and the metal front velocity. With the high permeability coating, the effect on heat transfer and back pressure and velocity seem negligible. With the low permeability coating heat transfer has a small effect at higher temperatures (780 ^{o}C), giving a 20% increase in fluidity, but back pressure dominated at lower temperatures, (680^{o}C).

5.3.4 Coating permeability

Increasing the permeability of the coating from low to high increased the fluidity of LFC in any casting condition, however the amount of increase differed; for example a 58% increase in the fluidity length was reported when the foam pattern was coated with a 1.3 mm coating and cast at 680 ^{o}C, but the increase was 15% when the casting temperature was 780 ^{o}C), see Figure 4-8.

It is thought that the increase in the fluidity length was due to the increased coating permeability allowing easier removal of the decomposition by-products. The liquid

decomposition by-products are wicked into the high permeability coating more readily as less reduction in the M_w of the liquid decomposition byproducts is required to become absorbed by the refractory coating when the pattern is coated with a high permeability coating [21]. However, it was argued earlier that the liquid decomposition byproducts do not play a role in determining the fluidity, but the vapour byproducts are obviously vented through a high permeability coating more easily [54].

Increasing the permeability of the coating from low to high increased the velocity of the liquid metal from 5 to 8.8 mms^{-1} (shown in Table 4-13), probably because the gaseous byproducts are easier to remove from the mould and the molten metal stream is confronted with less back pressure, resulting in a greater rate of heat transfer from the molten metal to the foam pattern. The heat transfer coefficient from the molten metal to the foam was increased by about 40% (from 365 to 515 $Wm^{-2}K^{-1}$) when the coating permeability was increased (see section 4.4.9). The thickness of the metal/foam interface was not considerably increased, from 1.3 to 1.8 mm, (although the estimated error of this measurement is about ± 0.5 mm), but this change in the thickness would explain the change in the heat transfer coefficient from the molten metal to the foam. The heat transfer coefficient from the molten metal to the mould was assumed to be similar for the high and low permeability coating (see Table 4-13), since the thermal conductivity of the coating should not be greatly affected by its permeability.

In summary, increasing the permeability of the coating reduces the relative resistance against removal of the gaseous decomposition byproducts significantly (see Figure 5-2 a) and this reduces the amount of gas in the metal/foam interface and increases the heat transfer from the molten metal to the foam which leads to an increase in the metal velocity by 76% (see Table 4-13), increasing the fluidity length. Since in any casting condition, increasing the

permeability of the coating increased the fluidity of LFC, this can be used as a key parameter to improve the fluidity of LFC.

5.3.5 Effect of foam pattern type

Foam type

Using a brominated foam pattern instead of conventional EPS did not offer any improvement in the fluidity of LFC (see Figure 4-10). Brominated foam patterns might have a different heat of decomposition compared to conventional EPS, but also offer a different mechanism of foam decomposition by releasing hydrogen bromide at high temperatures(during casting) [28]. This accelerates degradation of the foam pattern and subsequently increases the quality of castings by reducing the formation of folds [25, 29].

Since the fluidity of the castings with untreated EPS and brominated EPS were similar, this suggests that the heat transfer coefficients of h_1 and h_2 were not changed when a brominated foam pattern was used instead of a conventional EPS.

The molecular weight of the Foam pattern

No effect of the molecular weight of the foam pattern on the fluidity of LFC was incorporated in Equation 4-13; however, a lower M_w foam degraded more easily and should have a lower heat of degradation.

However, there was no significant difference between the fluidity length of the castings made with untreated Probead-70™ patterns (M_w of 327,000 $gmol^{-1}$) and irradiated Probead-70™ patterns (M_w of 85,000 $gmol^{-1}$). This shows that although reducing the M_w of the foam pattern

helps the removal mechanism for liquid decomposition byproducts (see section 2.4) it did not change fluidity. It also suggests that the heat of degradation of the pattern is not a significant factor for fluidity.

Foam pattern density

Reducing the density of the foam pattern (from 27 to 16 kgm^{-3}) increased the fluidity length of LFC greatly (with more than an 80% increase when the density was reduced by about 40%). This is also in agreement with Equation 4-12 and Equation 4-13 which state that the time of freezing and the fluidity length depend on the mass of foam degraded.

The amount of gas evolution and rate of foam degradation should also be affected by the density of the foam pattern. The rate of heat transfer from the molten metal to the foam is also influenced by the foam density as the heat required for degradation is lower when a lower density foam is used.

This is in agreement with the work carried out by Tschop [10] who stated that foam density was a parameter which can be reduced to eliminate misrun. This has the disadvantage of reducing the strength of the foam pattern which can result in distortion and damage during compaction of the mould, in addition to increasing the collapse rate of the foam pattern which may be disadvantageous.

5.3.6 Summary of the effect of the casting parameters on the fluidity of LFC

It was shown that, except for the casting head height, parameters, such as pouring temperature, coating permeability, coating thickness and density of the foam pattern, affected the fluidity of LFC of Al alloy (2L99).

Increasing the coating thickness from 0.3 mm to 1.3 mm affected the fluidity of LFC greatly, although only if a low permeability coating was used. Coating thickness did not show a consistent effect on the fluidity of LFC; for example, at higher pouring temperatures (780 ^{o}C), increasing the coating thickness increased the fluidity length by 20%, while when the molten metal was cast at 680 ^{o}C, increasing the coating thickness reduced the fluidity length by 50%, (as was to be expected). This was due to increasing the back pressure and the reduction in the molten metal velocity. It was also concluded that changing the thickness of the high permeability coating does not influence the fluidity length significantly.

Increasing the permeability of the coating from low to high increased the fluidity length in any casting condition, and the increase in the fluidity length differed from 10% to 58% depending on the casting condition.

Similarly, increasing the pouring temperature from 680 ^{o}C to 780 ^{o}C increased the fluidity length in all of the casting conditions except when a thin low permeability coating was used (no improvement in fluidity was reported in this case). It was also considered that increasing the pouring temperature affected the fluidity length by increasing the velocity of the molten metal, mostly by accelerating the degradation of the foam, rather than affecting the time of freezing, as the heat transfer coefficients from the molten metal to the foam and to the mould were not changed significantly.

According to these results, increasing the casting temperature when a low permeability coating is employed, or reducing the permeability of the coating when the molten metal is cast at high temperature, is not recommended as it might reduce fluidity in LFC.

Therefore, three casting parameters of pouring temperature, coating thickness and coating permeability affect fluidity of LFC, and their effect depends on the state of the other two

casting parameters. Figure 5-3 shows the effect of the mentioned casting parameters on the fluidity of LFC.

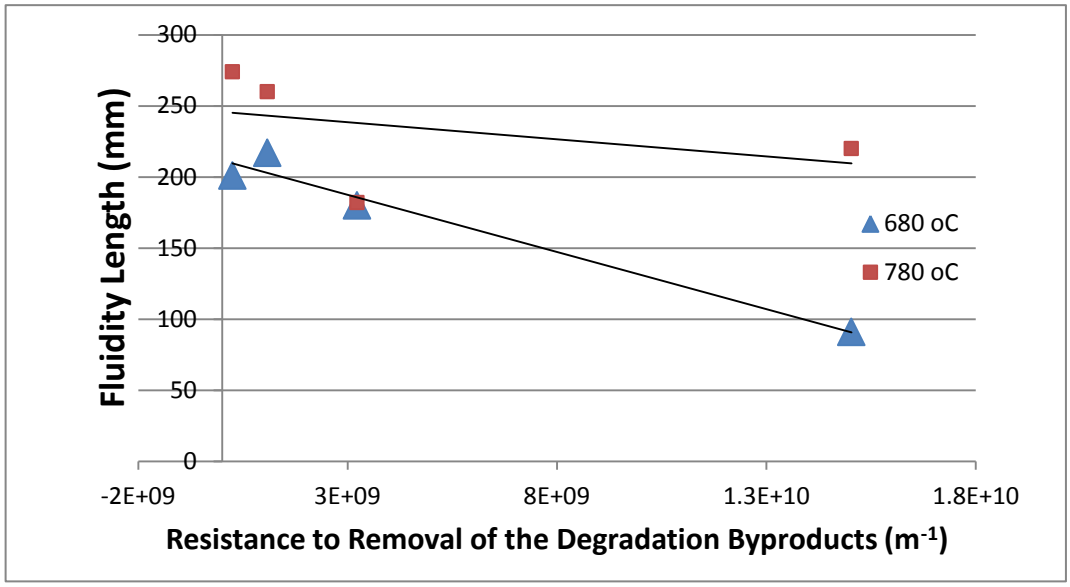

Figure 5-3. Fluidity of LFC vs. the resistance against removal of the degradation byproducts for different coating thicknesses and permeabilities (permeability/thickness) at different temperatures.

This shows that the fluidity of LFC was reduced due to increasing the resistance to the removal of the decomposition byproducts (defined to be the permeability of the coating divided to the coating thickness), i.e. reducing the coating permeability or increasing the coating thickness at both pouring temperatures of 680 ^{o}C and 780 ^{o}C.

The results showed that neither using a low M_w foam pattern or brominated foam pattern had an effect on the fluidity of LFC although they increased the quality of the castings ([25, 29] and section 4.5.6). Instead, reducing the foam pattern density from 27 to 16 kgm^{-3} increased the fluidity length by more than 80%.

5.4 The nature of the metal/foam interface

5.4.1 Observation of the interface

The radius of curvature at the metal front for the bottom fluidity strip of casting H2 was determined to be 18 mm, and the estimation of the length of the metal/foam interface was 2-3 mm (see section 4.3.2.4). This means that the interface is concealed by the curvature of the advancing molten metal and that is probably the reason that no gap was observed between the advancing molten metal and the foam pattern in the real time x-ray observation of the EPS strip castings. The radius of curvature at the molten metal front was greater than the thickness of the metal/foam interface so the interface is concealed by the curvature of the advancing molten metal, (see Figure 5-4). If otherwise, a light zone would have been observed between the metal and the foam pattern and the foam in the real time X-ray (as was observed in the case of castings with vertically positioned plates of irradiated Probead-30™.

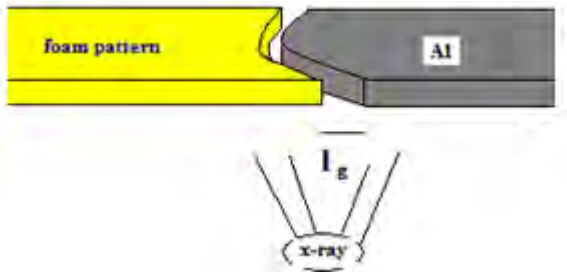

Figure 5-4. The metal/foam interface is not detected in real time X-ray observation if the thickness of the interface is smaller than the radius of the metal flow at front.

The metal/foam interface is sometimes [13] called a "gap". The results of thermogravimetric analysis of EPS decomposition showed that nitrogen and C_8H_8 gas were the decomposition byproducts at 110 ^oC, the temperature at which the EPS foam collapses. It also showed that at a temperature of about 405 ^oC, styrene is the major component of the decomposition

byproducts; this temperature is only reached for the decomposing foam at regions very close to the molten metal front (see Figure 2-7).

The temperature distribution from the molten metal to the foam was shown in Figure 2-7, which shows that the temperature across the interface reduces from more than 400 ^{o}C (temperature of the decomposition byproducts adjacent to the molten metal front) to 100 ^{o}C (temperature of collapsing foam). In this range of temperature both gaseous and liquid decomposition byproducts can exist. Liquid byproducts form at a significant distance from the molten metal front and survive for periods of the order of seconds at lower temperatures (up to 400 ^{o}C) compared to gaseous byproducts [34]. Therefore, the metal/foam interface can be assumed to be a zone containing both liquid and gaseous byproduct in which the amount of liquid byproducts increases with distance from the molten metal to the foam pattern, and the amount of gases reduces in the same direction.

5.4.2 The thickness of the metal/foam interface

As mentioned earlier the thickness of the metal/foam interface was about 6 mm at the beginning of the fluidity strip and this thickness decreased to 1 mm just before solidification (see section 4.3.2.4) for the bottom fluidity strip of casting H2 (this was estimated using the data obtained from the thermocouples in the foam pattern based on the rate of temperature rise at a point). The points located at the entrance of the fluidity strips (Points 12 and 13) were expected to have a thicker interface, as at the initial moment of casting, when the liquid metal enters the fluidity strip, the liquid metal is in direct contact with the foam pattern. This close contact should cause a high heat transfer rate from the molten metal to the foam pattern resulting in a high rate of foam degradation and evolution of gas. The accumulation of gas between the molten metal and the foam pattern reduces the heat transfer from the metal to the

foam, and affects the rate of the foam pattern degradation and the amount of gas evolved. Hence, the interface was estimated to have a length of 1-2 mm on average, in the fluidity strip however a value of 6 mm was also reported for a short length at the beginning of the fluidity strip (for the first 10 mm) (Figure 4-23). This value is in agreement with reports in the literature [63] (see Figure 2-7).

Figure 5-5 compares the temperature rise at the time that the liquid metal reached different points of the bottom fluidity strip of casting H2 (points 12, 13, 14) and this shows that the temperature increased faster at the beginning of the cast strip (point 12). It can be concluded that there is a gap with varying thickness between the molten metal and the foam pattern, as was indicated by the temperatures recorded by thermocouples 12, 13 and 14 (10, 25 and 40 mm away from the beginning of the strip, respectively).

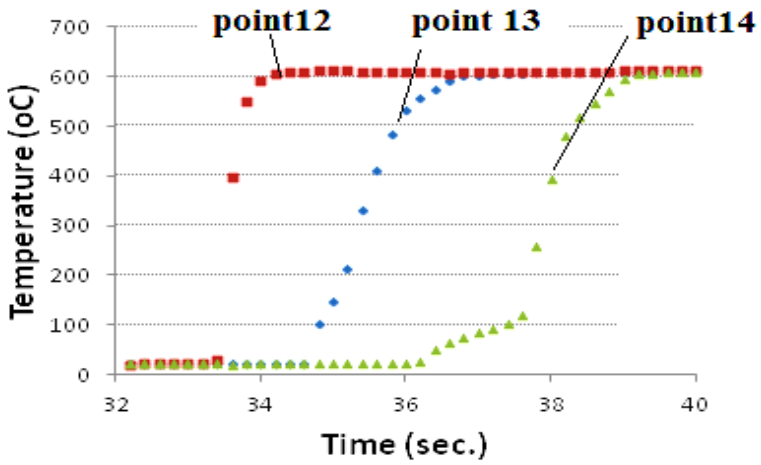

Figure 5-5. Comparison between the temperature rise of point 12, 13 and 14 located at the bottom fluidity length of casting H2.

This is also the case for the upper fluidity strips, as shown in Figure 5-6, which compares the temperature rise for different points located in the top fluidity strip of casting H2 (points 7 and 9). This shows that point 9 located at the very end of the casting strip (70 mm away from the beginning of the cast strip, in which the fluidity length was 85 mm), showed a more gradual

increase in temperature when the liquid metal reached that point, compared to point 7 (located 40 mm away from the beginning of the same cast strip).

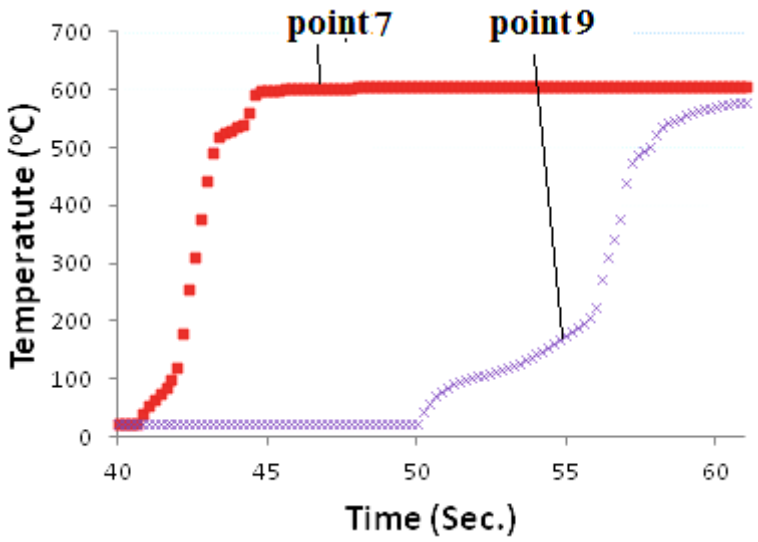

Figure 5-6. Comparison between the temperature rise of point 7 and 9 located at the top fluidity length of casting H2.

This change in the interface thickness can be caused by a higher velocity of the liquid metal and/or faster rate of foam degradation due to a closer contact between the metal and foam pattern, however a large interface was probably formed immediately after the first contact of the liquid metal and foam and the thickness of the interface was reduced further in the casting strip (see Figure 4-23).

5.5 Irradiation processing to increase casting quality

The porosity contents of the castings with different M_w foam patterns were measured and found to be related to the extent of the defects at the base of the castings caused by the globules of the liquid polymer (see Figure 4-37). The results also showed that the porosity content of the castings has reduced with reducing the defects at the base of the castings by using a lower M_w foam pattern. This is support for the wicking and wetting theory of Zhao et al. [42] and Davies and Griffiths [8]. These results confirm that if the liquid degradation byproducts displaced to the casting/coating interface do not reach a critical molecular weight, they can release bubbles of gas into the liquid metal, increasing the porosity content of the casting as shown in Figure 4-35.

Figure 5-7 shows the relationship of the M_w of the foam pattern and the porosity content, related to the critical M_w proposed for wetting of the pattern coating by the liquid polymer residue, and wicking of the liquid polymer residue into the coating, for a high permeability coating [21]. Assuming that the M_w measured in these experiments for the copolymer was comparable to the M_w measurement results from the degraded PS experiments of Davies and Griffiths [8] which was established in section 4.5, the most irradiated foam samples reached a M_w just below the critical value for wicking into the coating. These foam patterns resulted in castings with the least porosity.

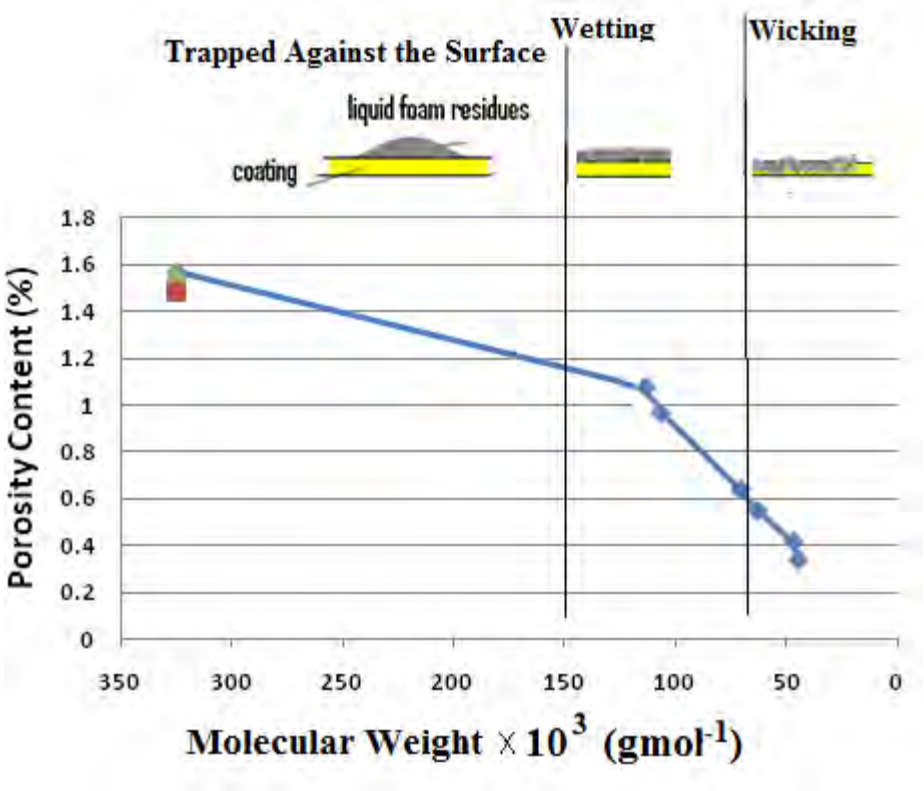

Figure 5-7. Relationship between casting porosity and M_w of the foam patterns related to the M_w at which wetting and wicking can occur, (for a high permeability coating).

It was also shown that the PMMA part of the copolymer foam pattern experienced the major part of the M_w reduction by γ-irradiation. This emphasizes the role of the conjugated aromatic ring in the styrene in increasing the radiation resistance of polystyrene, denoted the protective role of polystyrene in PS-PMMA copolymer [99], thereby decreasing the efficiency of M_w reduction due to increasing cross-linking. The effect of the γ-irradiation is to reduce molecular weight by chain scission. In the case of polystyrene, this chain scission is accompanied by cross-linking, which prevents any reduction in M_w; therefore, irradiation of pure polystyrene foam (PS) had no measurable effect on its molecular weight (see Figure 4-30). PMMA, on the other hand, had its molecular weight reduced progressively by increasing amounts of chain scission with increasing radiation.

Although pure PMMA foam responded better to irradiation with respect to its M_w reduction than the copolymer, casting with low M_w pure PMMA may not result in a good casting because, for example, it may lead to a larger interface between the liquid metal front and the foam pattern (because of the higher decomposition rate for low M_w foams), perhaps resulting in the collapse of the surrounding moulding sand into the metal/foam interface. Furthermore, low M_w foam patterns made from pure PMMA might increase the difficulties associated with making the pattern cluster, as reducing the M_w of the foam may make the patterns unacceptably fragile.

It was also found that, while the E-beam was not quite as effective as γ- radiation in reducing the M_w of the foam patterns, the dose rate of the E-beam irradiation was significantly higher than in the case of γ-irradiation. Therefore, assuming that there is no unwanted heating of the pattern and associated distortion, E-beam irradiation would be the preferred method of M_w reduction.

The hardness of the Al castings (2L99 alloy) was not found to be affected by reducing the M_w of the foam patterns. This is probably because the cooling rates of the castings with untreated and irradiated foam patterns were similar and did not affect the microstructure of the castings.

The reduction in porosity would not be expected to show up clearly in a hardness test as it is a surface property.

As results showed, castings made with a low M_w foam reduced the numbers of defects at the bottom surface of the castings. A surface with less defects and consequently a casting with less porosity content should result in better mechanical properties. This was confirmed as the fatigue properties of the LFC were improved to about double if the M_w of the foam pattern was reduced to about 49,000 $gmol^{-1}$; however, the improvement in the fatigue properties of

the casting was observed to be considerable only when the M_w of the pattern was reduced below the critical value to wick into the refractory coating (see Figure 4-39) and did not show a gradual trend of improvement with gradual reduction in M_w.

The cast iron LFC with reduced M_w foams (Probead-30™) did not show any improvement in their porosity content. However no defects were found at the base of any of the cast iron castings even in the case of castings made with untreated foam patterns. This is probably due to the high temperature of cast iron LFC at which the critical M_w to wick into the coating is reached much faster compared to Al LFC (2L99 alloy), and also less liquid decomposition byproduct is produced, and more quickly vaporized.

The flowing molten metal had a higher velocity when it was filling lower M_w foam. An increase in the velocity of liquid metal changes the shape of the metal/foam interface. As Ainsworth and Griffiths [46] suggested, increasing the velocity of the molten metal (when filling a vertically positioned plate from the bottom) increases the instability in the metal/foam interface. They also concluded that a metal/foam interface with a planar shape can be produced if the foam plate is filled with a velocity of 5 mms^{-1} and less.

The irregularity in the metal/foam interface shown in Figure 4-45, Figure 4-46 and Figure 4-48 could be due to the fact that degradation of a low M_w foam was easier, resulting in the evolution of large amounts of gas, which led to the formation of a large gap ahead of the metal front while decomposition of an untreated foam pattern would take more time and heat. It was shown that in the case of casting with an untreated pattern, the degrading foam became entrapped in the flowing metal where different streams of liquid metal joined together. But in the case of castings with irradiated foam patterns, the flowing metal experienced less resistance in decomposing the pattern which also led to increasing the velocity of the molten

metal (see Figure 4-47), and increasing the instability of the metal/foam interface. Therefore, casting with low M_w foam pattern could benefit the quality of the castings if the velocity of molten metal is controlled in order to avoid formation of unstable metal/foam interface.

Finally, the effect of using brominated and low M_w foam pattern was compared here because both are thought to increase the quality of LFC. In the case of using brominated foam patterns, hydrogen bromide gas is released at high temperatures (during casting) [28] and this speeds up degradation of the foam pattern and subsequently increases the quality of castings [25, 29]. While, in the case of using low M_w foam patterns, the removal mechanisms of byproducts from the mould were assisted, as wicking of the liquid decomposition byproducts of a low M_w foam occur faster because less or no reduction in M_w is required to reach the critical M_w to become absorbed by the coating. Therefore less bubbles are released from the globules of the liquid byproducts waiting to reach the critical M_w which trapped against the casting/coating interface in the case of a low M_w foam.

5.6 Summary

The results of the current work clarify the effect of different parameters on the fluidity of LFC. The advantage of this work is that the effect of different casting parameters at different casting conditions was examined and the fluidity results showed a good degree of consistency, although reproducible LFC fluidity test results are notoriously hard to achieve [71].

It was also aimed at explaining and predicting the effect of different parameters on the fluidity and the time of freezing in LFC (Equation 4-12 and Equation 4-13). The heat transfer coefficients of the molten metal to the foam pattern and to the mould were estimated for a particular casting condition, and were used to predict the fluidity length of some of the

fluidity tests. The prediction of the fluidity tests was reasonably accurate in cases where the estimated heat transfer coefficients were still valid for the casting conditions.

The velocity of the molten metal, the time of freezing, the thickness of the metal/foam interface and the fluidity length were also measured for some of the fluidity tests by employing thermocouples embedded in the pattern and the effect of different casting parameters on these were explained.

In summary the fluidity results showed that to increase the fluidity length the most significant parameters are the permeability of the coating and the pouring temperature. While the pouring temperature is not recommended to be increased in order to increase fluidity, as it would introduce higher solubility for hydrogen in the liquid metal and can increase the porosity of the casting [10] and can also cause loss of alloying elements such as Mg, the coating permeability can be a key parameter to improve the fluidity of LFC as at any casting conditions increasing the coating permeability increased the fluidity length (from 10 to 60%). Another parameter is the density of the foam pattern, although the effect of casting with a very low density foam pattern is not known, but the high collapse rate of low density foam and consequently formation of the a large metal/foam interface might harm the quality of the castings.

In parallel to the fluidity of LFC, the quality and mechanical properties of Al LFC (2L99 alloy) was shown to be improved by employing low M_w foam patterns. The porosity content of the castings was shown to be related to defects on the bottom surface of the horizontally cast flat strips. It was suggested that the liquid byproducts of the foam pattern decomposition become absorbed by the coating only if their M_w has been reduced to a critical value [8]. Reducing the initial M_w of the foam pattern to/or below the critical value for wetting and

wicking into the coating was shown to reduce the porosity of the castings, by encouraging earlier wicking, and this was reflected in improved tensile and fatigue properties associated with irradiated foam patterns.

The porosity content of the cast iron castings made with reduced M_w patterns (Probead-30™) did not show any improvement when compared to the castings with untreated foam patterns probably because wicking to the coating is not an issue in the case of cast iron LFC, due to its much higher casting temperature.

6 CONCLUSIONS

1. A reproducible fluidity test has been devised to determine and compare the fluidity of Al alloys cast using the Lost Foam Casting process. The test was found to be highly reproducible as the standard deviation of different fluidity tests varied from 3% to 8% of the mean fluidity lengths.
2. Lost Foam Casting of Al alloys produces a laminar flow in the bulk liquid.
3. The effect of casting head height was insignificant on the fluidity of Al 2L99 alloy, for the range of head heights used here, from 110 to 260 mm, corresponding to a metallostatic pressure of from 2626 to 6206 Pa.
4. Increasing the thickness of a low permeability coating when using high casting temperatures (780 ^{o}C) increased the fluidity of the Al 2L99 alloy by 20 %, while at a lower casting temperature (680 ^{o}C) the fluidity length was reduced by 50 %. Increasing the thickness of a high permeability coating did not affect the fluidity length significantly. It is not recommended to alter coating thickness in order to improve the fluidity properties of LFC. This is because the coating resistance against removal of the gaseous decomposition byproducts for the high permeability coating was negligible, while with the low permeability coating a high back pressure was produced which reduced the velocity of the molten metal, affecting the fluidity length.
5. The heat transfer coefficient of the molten metal to the mould in the case of Al 2L99 alloy LFC was not influenced significantly by changing the permeability of the coating (the thermal conductivity of the high and low permeability coatings are approximately the same); however the heat transfer coefficient of the molten metal to the foam increased when a high permeability coating was used instead of a low permeability coating (by 40%). This is because the metal/foam interface is thicker in

the case of a low permeability coating and results in a lower heat transfer rate from the molten metal to the foam pattern.

6. The velocity of the molten metal with the high permeability coating was more than that of the low permeability coating (by about 70%). This was also the case for the time of freezing (by about 10%).
7. Reducing coating permeability reduced the fluidity of Al 2L99 alloy LFC in any casting condition (from 10% to 60%), and is the most significant parameter that can be used to alter the fluidity of Al LFC (2L99 alloy). This is because removal of the gaseous decomposition byproducts is easier when a high permeability coating is used and this reduces the back pressure in the interface, and consequently increases the velocity of molten metal.
8. Reducing the density of the foam pattern increased fluidity in Al LFC (2L99 alloy) significantly; however it may have a detrimental effect on the quality of the castings.
9. Using lower M_w foam patterns, nor brominated foam patterns, had no significant effect on fluidity in Al LFC (2L99 alloy).
10. Solidification in Al LFC occurred at the tip of the metal flow rather than at the beginning of the fluidity strip.
11. Thermogravimetric analysis of the decomposition of EPS foam showed that at about 106 ^{o}C nitrogen gas was released, corresponding to the collapse of the foam structure, but a considerable mass loss (over 99%) occurred at about 403 ^{o}C, where styrene is released.
12. Equations to describe the fluidity of LFC and the time of freezing were derived based upon a heat balance between the heat transfer from the molten metal to the mould and

the heat absorbed by the foam to decompose the foam pattern. These were able to predict the fluidity in castings using measured velocity data.

13. The M_w of foam patterns containing poly methyl methacrylate (PMMA) was decreased by γ-irradiation and electron beam irradiation.
14. The reduction in M_w due to irradiation increased in effectiveness with increasing amounts of PMMA in PS-PMMA copolymer foam patterns.
15. Irradiating the copolymer foam patterns up to values of 189 MRad reduced their flexural strength, but they could still be used in the casting process. However, when pure PMMA was given a 100 MRad dose, it became too friable to be used.
16. The porosity content of Al 2L99 alloy castings was reduced by reducing the M_w of the foam patterns used in the casting process.
17. Defects were found at the bottom surface of the castings, due to the entrapment of liquid polymer degradation byproducts at the casting-coating interface. These were decreased, in size and number, when reduced M_w foam patterns were used.
18. The fatigue life of castings was increased by reducing the M_w of the foam patterns used in the casting process, probably because the critical M_w for wicking the liquid pattern degradation byproduct into the permeable coating was more quickly reached. However, the increased fatigue life was obtained only when the M_w of the foam was reduced below the critical M_w for wicking into the coating.
19. Electron beam irradiation is the preferred method of reducing the pattern M_w, as it was found to be about 25 times quicker in delivering the same dosage as γ-radiation However it is approximately 7-10% less effective in reducing the M_w of the foams compared to γ-rays.

20. The quality of cast iron LFC was not dependent on the M_w of the foam pattern; this is because of the high temperature in Lost Foam iron casting which suggests that the decomposition byproducts are mostly or completely vapour, and any liquid byproduct can be rapidly wicked into the coating.
21. Al LFC (2L99 alloy) with low M_w foam pattern benefited from easier decomposition of the foam when the pattern was positioned horizontally, but the metal/foam interface formed an instable, irregular shape which can be detrimental to the quality of castings when the low M_w foam pattern was cast vertically, and filled from below.

7 FURTHER WORK

Considerable progress has been made in understanding the effect of casting parameters on the fluidity of LFC. The quality of Al LFC (2L99 alloy) was also improved by employing irradiation processing to reduce the M_w of the foam pattern. Nonetheless, further research is needed in the following areas:

1. Now that it is known that Al LFC (2L99 alloy) can benefit from low M_w patterns, other starting materials with lower initial M_w such as polylactic acid, or polyglutamic acid might be suitable to foam and carry out LFC process with, to examine the effect of using those foam materials on the filling behaviour of the molten metal and the quality of castings.
2. The UTS of Al 2L99 alloy LFC, using low M_w foams were only about 12% more than castings with untreated foam pattern while the reduction in the porosity content was about 85%. Further mechanical tests showed that the fatigue properties of the casting with reduced M_w foams were twice of the fatigue life in the case of casting with untreated foam patterns. It is also of interest to examine further, the relationship between porosity content of the castings with lower M_w foam patterns, and mechanical properties of the castings such as UTS, to determine why the improvement in the properties is not great. For example the improvement in the mechanical properties of heat treated and as cast castings, due to using low M_w foams can be examined.
3. The size and temperature of the metal/foam interface was studied here but a detailed model of the metal/foam interface (the nature of the interface particularly) is still required. For example, research on the amount of the liquid polymer in the degradation byproducts (compared to the gaseous byproducts) at the metal/foam interface which changes from the foam pattern to the molten metal front. This might

lead to a better understanding of the mechanisms of entrapment of the foam pattern byproducts into the molten metal stream.

4. While reducing the M_w of the foam patterns has benefitted the quality of the castings when the cast strips were positioned horizontally, casting with vertical irradiated foam plates showed that the metal/foam interface formed an unstable interface, probably because of the high velocity of the molten metal when filling a low M_w foam pattern. Therefore, the critical velocity for planar mould filling (from the bottom) using low M_w foam patterns needs to be established. To investigate the critical velocity of the molten metal to prevent irregular metal/foam interface for casting with a certain M_w foam pattern, a bottom filling casting is suggested with the ability of controlling the molten metal velocity in order to establish the optimum and the critical value.

8 REFERENCES

1. Shivkumar, S., L. Wang , and D. Apelian, *The Lost-Foam Casting of Aluminum alloy components.* JOM, 1990 (November): p. 38-44.
2. Niemann, E.H., *Expandable polystyrene pattern material for the Lost Foam process.* AFS Transaction 1988. **33**: p. 793-798.
3. Bast, J., W. Hopf, L. Sacharuk, and T. Hahn, *Optimising mould making for Lost Foam Casting.* AFS Transactions, 2003. **111**: p. 13-11-1319.
4. Austin Group, L.L.C. *Introduction to the Lost Foam Casting Process*. 2003 [cited 2011, 11th September]; Available from: http://www.lostfoam.com/process/pdf/lost_foam_cast_process.pdf.
5. Bennett, S., T. Moody, A. Vrieze, M. Jackson, D.R. Askeland, and C.W. Ramsay, *Pyrolysis defects in Aluminum Lost Foam Castings.* AFS Transactions, 1999. **107**: p. 795-803.
6. Hess, D.R., B. Durham, C.W. Ramsay, and D.R. Askeland, *Observations on the effect of pattern and coating properties on metal flow and defect formation in Aluminum Lost Foam Castings.* AFS Transaction, 2002. **90**: p. 1435-1448.
7. Warner, M.H., B.A. Miller, and H.E. Littleton, *Pattern pyrolysis defect reduction in Lost Foam Castings.* AFS Transaction, 1998. **161**: p. 777-785.
8. Davies, P.J. and W.D. Griffiths, *Wicking of Liquid Polystyrene Degradation Products into the pattern Coating in the Lost Foam Casting Process.* Foundry Trade Journal, 2007. **3642**: p. 62-65.
9. Pan, E.N. and G.L. Sheu, *The filling phenomena of Lost Foam Cast irons and Aluminium alloys.* AFS Transaction, 2003. **87**: p. 1255-1263.
10. Tschopp, M.A., *Fluidity of Aluminum A356 in the Lost Foam Casting process.* AFS Transaction, 2002. **27**: p. 1387-1397.
11. Ajdar, R., C. Ravindran, and A. McLean, *Effect of mold media on solidification of A356 Al-Si alloy in Lost foam casting*. Light Metals 2000 Metaux Legers, Proceedings, ed. J. Kazadi and J. Masounave. 2000, Montreal: Canadian Inst Mining, Metallurgy and Petroleum. 615-633.
12. Pan, E.N. and K.Y. Liao, *Study on flowability of EPC A356 Al alloy.* AFS Transactions, 1998. **106**: p. 233-242.
13. Mirbagheri, S.M.H., N. Varahram, and P. Davami, *3D computer simulation of melt flow and heat transfer in the lost foam casting process.* International Journal for Numerical Methods in Engineering, 2003. **58**(5): p. 723-748.
14. Wang, C.M., W.W. Fincher, and O.J. Huey, *Computational analysis of fluid flow and heat transfer during the EPC process.* AFS Transactions, 1993. **101**: p. 897-904.
15. Sonnenberg, F., *Lost Foam Casting made simple*, in *AFS Lost Foam Book*. 2008, AFS.
16. Goria, C.A., G. Serramoglia, G. Caironi, and G. Tosi, *Coating permeability: A Critical Parameter Of The Evaporative Pattern Process.* AFS Transactions, 1986. **94**: p. 589-600.
17. Tseng, C.H.E. and D.R. Askeland, *Thermal And Chemical Analysis of the Foam, Refractory Coating and Sand in the EPC Process.* AFS Transactions, 1992. **110**: p. 509-518.
18. Sun , W.L., H.E. Littleton, and C.E. Bates, *Real time X-ray investigation on Lost Foam mould filling.* AFS Transactions, 2002. **110**: p. 1347-1355.
19. Tschopp, M.A., Q.G. Wang, and M.J. Dewyse, *Mechanisms of misrun formation in Aluminum Lost Foam Castings.* AFS Transaction, 2002. **110**: p. 1371-???

20. Brighton, C.A., G. Pritchard, and G.A. Skinner, *Styrene polymers: Technology and enviromental aspects*. 1979, Applied science publishers LTD: lONDON.
21. Davies, P.J., *The Role of the Pattern Coating in Lost Foam Casting of Aluminum,* PhD Thesis in Metallurgy & Material 2007, The University of Birmingham: Birmingham. p. 170.
22. Nussbaum, D.A., P. Gaillud, and K. Murphy, *The chemistry of acrylic bone cement and implication for medical use in image-guided therapy* J Interv Radiol, 2004. **15**: p. 121-126.
23. Sonnenberg, F., D. Hajnik, and W. Poole, *Method for improving the expandability of styrenic polymer particles*. 1993: U.S. Patent No. 5,240,967.
24. Jarvela, P., J. Sarlin, and P. Tormala, *A method to measure the fusion strength between expanded polystyrene (EPS) beads* Journal of Materials Science, 1986. **21**(9): p. 3139-3142.
25. Sonnenberg, F., *Recent Innovations with EPS Lost Foam beads.* AFS Transaction, 2003. **06**: p. 1213-1229.
26. Sands, M. and S. Shivkumar, *EPS bead fusion effects on fold defect formation in lost foam casting of aluminum alloys.* J MATER SCI, 2006. **41**: p. 2373-2379.
27. Rossacci, J. and S. Shivkumar, *Bead fusion in polystyrene foams.* Journal of Materials Science, 2003. **38**(2): p. 201-206.
28. Sonnenberg, F., K.M. Taristo, and T.V.J. Johansson, *Treatment for reducing residual carbon in the lost foam process*. 2001: U.S. Patent No. 6,303,664.
29. Hess, D.R., D.R. Askeland, and C.W. Ramsay, *Influence of bead chemistry on metal velocity and defect formation in Aluminum Lost Foam Castings.* AFS Transaction, 2003. **105**: p. 1279-1292.
30. Martinez, O.A., *A supplier's overview of Lost Foam refractory coatings.* AFS Transaction, 1990. **21**: p. 241-244.
31. Penumadu, D., X. Chen, and C. Johnson, *Characterization of rheological properties of Lost Foam Casting coating slurries.* AFS Transaction, 2004. **66**: p. 1113-1130.
32. Parish, J.S., D.J. Jason, and J.L. Meloni, *Practical control of Lost Foam Catings(**?**) in foundry operations.* AFS Transaction, 2003. **153**: p. 1303-1310.
33. Ballmann, R.B., *Assembly and coating of polystyrene foam patterns for the evaporative pattern casting process.* AFS Transaction, 1988. **77**: p. 465-470.
34. Shivkumar, S. and B. Gallois, *Physico-chemical aspects of the full mould casting of Aluminum alloys, Part 1: The degradation of polystyrene.* AFS Transactions, 1987. **95**: p. 791-800.
35. Bates, C.E., J.A. Griffin, and H.E. Littleton, *Expnadable Pattern Casting, Casting Defects Manuals.* AFS Transaction, 1994. **??**: p.??
36. Tschopp, M.A., *???* AFS Transaction, 2002. **110**: p. 1387-?
37. Bennett, S., T. Mooty, A. Vrieze, M. Jackson, D.R. Askeland, and C.W. Ramsy, *????* AFS Transaction, 2000. **108**: p. 795-?
38. Littleton, H.E., B.A. Miller, D. Sheldon, and C.E. Bates, *Lost Foam Casting - Process control for precision.* AFS Transaction, 1996. **124**: p. 335-346.
39. Kocan, G.H., *Incorporating permeability into Lost Foam coating controls.* AFS Transaction, 1996. **96**: p. 565-569.
40. Ji, S., M. Sirvio, J.J. Vuorinen, and J. Orkas, *Measurement of pressure and deformation of LFC patterns in dry sand moulds.* AFS Transaction, 1999. **129**: p. 779-786.

41. Vatankhah, B., D. Sheldon, and H.E. Littleton, *Optimization of vibratory sand compaction.* AFS Transaction, 1998. **162**: p. 787-796.
42. Zhao, Q., J.T. Burke, and T.W. Gustafson, *Foam Removal Mechanism in aluminum Lost Foam Casting.* AFS Transaction, 2002. **83**: p. 1399-1415.
43. Chen, Y.F., R.C. Chen, and W.S. Hwang, *Mold filling study in the EPC process-mathemathical model and flow characteristics.* AFS Transaction, 1997**? 56?**: p. 459-464.
44. Tseng, C.H.E. and D.R. Askeland, *Study of the EPC mould filling process using metal velocity and mass and energy balances.* AFS Transaction, 1992. **??**: p. 520-??
45. Shivkumar, S. and B. Gallois, *Physico-chemical aspects of the full mould casting of Aluminum alloys, Part 2: Metal flow in siple patterns.* AFS Transactions, 1987. **95**: p. 801-812.
46. Ainsworth, M.J. and W.D. Griffiths, *Real-time X-ray of the filling profile in Al alloys Lost Foam Castings* AFS Transaction, 2006. **114**: p. 965-977.
47. Grassie, N., *Chemistry of high polymer degradation process*. 1956, Glasgow: London Butterworths Science Publications.
48. Barone, M. and D. Caulk, *Analysis of mould filling in Lost Foam Casting of Aluminium: Methods.* International Journal of Metalcasting, 2008. **2**(3): p. 29-+**?**
49. Liu, X.J., S.H. Bhavnani, and R.A. Overfelt, *Simulation of EPS foam decomposition in the lost foam casting process.* Journal of Materials Processing Technology, 2007. **182**(1-3): p. 333-342.
50. Mirbagheri, S.H.M., J.R. Silk, and P. Davami, *Modelling of foam degradation in lost foam casting process.* Journal of Materials Science, 2004. **39**(14): p. 4593-4603.
51. Kannan, P., J.J. Biernacki, and D.P. Visco, *A review of physical and kinetic models of thermal degradation of expanded polystyrene foam and their application to the lost foam casting process.* Journal of Analytical and Applied Pyrolysis, 2007. **78**(1): p. 162-171.
52. Molibog, T.V. and H.E. Littleton, *Degradation of Expanded polystyrene Pattern* AFS Transaction, 2002. **101**: p. 1483-1497.
53. Caulk, D.A., *A foam melting model for lost foam casting of aluminum.* International Journal of Heat and Mass Transfer, 2006. **49**(13-14): p. 2124-2136.
54. Fu, J., H.L. Tsai, and D.R. Askeland, *Transport of Foam Decomposition Sand in the Lost Foam Casting Process* AFS Transaction, 1996. **104**: p. 263-270.
55. Shivkumar, S., X. Yao, and M. Makhlouf, *Polymer- melt interactions during casting formation in the Lost Foam process.* Scripta Metallurgica Et Materialia, 1995. **33**(1): p. 39-46.
56. Mehta, S., S. Biederman, and S. Shivkumar, *Thermal degradation of foamed polystyrene.* Journal of Materials Science, 1995. **30**(11): p. 2944-2949.
57. Shivkumar, S., *Modeling of temperature loses in liquid-metal during casting formation expandable pattern casting process.* Materials Science and Technology, 1994. **10**(11): p. 986-992.
58. Sun, Y., H.L. Tsai, and D.R. Askeland, *Investigation of wetting and wicking properties of refractory coating in the EPC process.* AFS Transactions, 1992. **100**: p. 297-308.
59. Hill, M., A.E. Vrieze, T.L. Moody, C.W. Ramsay, and D.R. Askeland, *Effect of Metal Velocity on Defect Formation in Al LFCs.* AFS Transaction, 1998. **106**: p. 365-374.
60. Molibog, T. and H.E. Littleton, *Experimental Simulation of Pattern Degradation in Lost Foam.* AFS Transaction, 2001. **104**: p. 1523-1554.

61. Liu, Y., S.I. Bakhtiyarov, and R.A. Overfelt, *Numerical modeling and experimental verification of mold filling and evolved gas pressure in lost foam casting process.* Journal of Materials Science, 2002. **37**(14): p. 2997-3003.
62. Barone, M.R. and D.A. Caulk, *A Foam Ablation Model for Lost Foam Casting of Aluminum.* International Journal of Heat and Mass Transfer, 2005. **48**: p. 4132-4149.
63. Yang, J., T. Huang, and J. Fu, *Study of gas pressure in EPC (LFC) moulds.* AFS Transaction, 1998. **128**: p. 21-26.
64. Shih, T.S. and A.S. Chang, *Filling of A356 and gray iron in the EPC process.* AFS Transaction, 1997. **37**: p. 377-390.
65. Sands, M. and S. Shivkumar, *Influence of coating thickness and sand fineness on mould filling in the Lost Foam Casting process.* Journal of Materials Science**?**, 2003. **38**: p. 667-673.
66. Liu, J., C.W. Ramsay, and D.R. Askeland, *A Study of foam-metal-coating interaction in the LFC process.* AFS Transaction, 1997. **137**: p. 419-425.
67. Yao, X. and S. Shivkumar, *Mould filling characteristics in Lost Foam Casting process.* Materials Science and Technology, 1997. **13(October)**: p. 841-846.
68. Sun, Y., H.L. Tsai, and D.R. Askeland, *Effects of Silicon content, coating materials and gating design on casting defects in the Aluminum Lost Foam process.* AFS Transaction, 1996. **92**: p. 271-279.
69. Wang, C., C.W. Ramsay, and D.R. Askeland, *Processing variable significance on filling thin plates in the LFC process- The Staggered, nested factorial experiment.* AFS Transaction, 1997. **138**: p. 427-434.
70. Shivkumar, S., L. Wang, and B. Steenhoff, *Metallurgical quality of Aluminum castings produced by the Lost Foam process.* AFS Transaction, 1989. **140**: p. 825-836.
71. Campbell, J., *Castings*. 1991, London: Butterworth-Heinemann.
72. Fleming, M.C., *Solidification Processing*. 1974. p. 219-229.
73. Di Sabatino, M., L. Arnberg, and D. Apelian, *Progress on the understanding of fluidity of Aluminum foundry alloys.* JOM**?**, 2008. **?**: p. 17-26.
74. Niesse, J.E., M.C. Flemings, and H.F. Taylor, *Appication of theory in understanding fluidity of metal.* AFS Transaction, 1959. **67**: p. 685-697.
75. Campbell, J., *Castings*. 1991, London: Butterworth-Heinemann. [Cited from Feliu S (1964).TAFS, 72, 129-137].
76. Li, J.F., H.C. Kou, A.J. Wang, J.S. Li, R. Hu, and H.Z. Fu, *Dendrite coherency point of A357 alloys.* Transactions of Nonferrous Metals Society of China, 2006. **16**: p. 1532-1536.
77. Cabrera, O., M. Ramirez, B. Campillo, and C. Gonzalez-Rivera, *Effect of the presence of SiCp on dendritic coherency of Al-Si-based alloys during solidification.* Materials and Manufacturing Processes, 2008. **23**(1): p. 46-50.
78. Maniara, R., L.A. Dobrzanski, J.H. Sokolowski, W. Kasprzak, and W.T. Kierkus, *Influence of cooling rate on the size of the precipitates and thermal characteristic of Al-Si cast alloys*, in *5th International conference on processing and manufacturing of advanced materials*, T. Chandra, et al., Editors. 2007, Trans Tech Publications Ltd: Zurich. p. 59-64.
79. Ba¨ckerud, L., E. Kro´l, and J. Tamminen, *Solidification characteristics of Aluminium alloys*. Vol. 1: Wrought Alloys, SkanAluminium. 1986, Oslo.
80. Chavez-Zamarripa, R., J.A. Ramos-Salas, J. Talamantes-Silva, S. Valtierra, and R. Colas, *Determination of the dendrite coherency point during solidification by means*

of thermal diffusivity analysis. Metallurgical and Materials Transactions -Physical Metallurgy and Materials Science, 2007. **38A**(8): p. 1875-1879.
81. Veldman, N., A. Dahle, D. StJohn, and L. Arnberg, *Dendrite coherency of Al-Si-Cu alloys.* Metallurgical and Materials Transactions 2001. **32**(1): p. 147-155.
82. Rao, P.N., *Manufacturing technology: foundry, forming and welding*. Vol. 192**? ?**, New Delhi: Tata McGraw-Hill publishing Company.
83. Houzeaux, G. and R. Codina, *Finite element modeling of the lost foam casting process tackling back-pressure effects.* International Journal of Numerical Methods for Heat & Fluid Flow, 2006. **16**(5): p. 573-589.
84. Chvorniov, N., *Theory of casting solidification*. Vol. 27. 1940, Giesseri.
85. Pan, E.N. and K.Y. Liao, *Study on flowability of EPC A356 Al alloys.* AFS Transactions, 1998. **106**: p. 233-242.
86. Streeter, V.L., *Fluid mechanics*. 3 ed, ed. McGraw-Hill. 1962.
87. Batchelor, G.K., *An Introduction to fluid dynamics*. 1967: Cambridge University Press.
88. Truskey, G.A., F. Yuan, and D.F. Katz, *Transport phenomena in biological systems prentice hall*. 2004.
89. Campbell, J., *invisible macrodefects in castings.* Journal de Physique, 1993. **3**: p. 861-873.
90. Shivkumar, S., *Casting characteristics of Aluminum alloys in the LFC process* AFS Transaction, 1993. **101**: p. 513-518.
91. Venkataramani, R. and C. Ravindran, *Effect of coating thickness and pouring temperature on thermal response in Lost Foam Casting.* AFS Transaction, 1996. **104**: p. 281-290.
92. Molibog, T., R.B. Dinwiddie, W.D. Porter, H. Wang, and H.E. Littleton, *Thermal properties of Lost Foam Castings.* AFS Transaction, 2000. **108**: p. 471-477.
93. Liu, X.J., R.C. Bhatz, S.H. Bhavnani, and R.A. Overfelt, *Transport phenomena in the production and use of expanded polystyrene patterns in Lost Foam Casting.* Materials and Manufacturing Processes, 2007. **22**(7-8): p. 811-818.
94. Liu, Z.L., Q.L. Pan, Z.F. Chen, X.Q. Liu, and J. Tao, *Heat transfer characteristics of Lost Foam Casting process of magnesium alloy.* Transactions of Nonferrous Metals Society of China, 2006. **16**(2): p. 445-451.
95. Tsai, H.L. and T.S. Chen, *Modeling of evaporative pattern process, Part 1: Metal flow and heat transfer during the filling stage.* AFS Transaction, 1988. **86**: p. 881-890.
96. Y. Haruvy, ***?*** International Journal of Radiation Applications and Instrumentation. Part C. Radiation Physics and Chemistry 1990. **35** p. 204-212.
97. Silverman, J., ***?*** Journal of Chem. Educ**.?**, 1981. **58**: p.**?**
98. Bradly, R., *Radiation technology handbook*, ed. M. Dekker. 1984, New York.
99. Mellberg, R.S., *Radiation processing* 1979, SRI International Research Report.
100. McLaughlin, W.L., A.W. Boyd, K.W. Chadwick, J.C. McDonald, and A. Miller, eds. *Dosimetery for radiation processing* 1989, Taylor & Francis London.
101. Silverman, J. and A.R. Van Dyken. *Radiat. Phys. Chem **?*** in *The first international meeting on radiation* 1977.
102. Stannett, V.T., J. Silverman, and J.L. Garnet, eds.***?*** Comprehensive polymer Science ed. E.G. C., et al. Vol. 4. 1989, Pragmon Press: Oxford.
103. Charlesby, A., *Atomic radiation and polymer*. 1960, Oxford: Pragmon Press.
104. *Radiation processing of polymers*. Progress in polymer processing, ed. A. Singh and J. Silverman. 1991, New York: Hanser. 377.

105. *British and European Aluminum Casting Alloys*, R. Bartley, Editor. 1996.
106. Schindler, A., *Mass changes and evolved gas analysis of one Polystyrene sample*. 2009, Technical report, NETZSCH: Bavaria, Germany.
107. Young, R.J. and P.A. Lovell, *Introduction to polymers*. second ed. 1991, New York: Chapman & Hall.
108. Holding, S., R. , *Comparison of molecular weight distribustion of poly(styrene-methyl methacrylate) copolymer samples using Gel Permeation Chromatography*. 2009, Smithers Rapra: Shropshire.
109. Gale, W.F. and T.C. Totemeier, eds. *Smithell metals reference book*. 8th ed. 2004, Elsevier and ASM: Amesterdam.
110. Porter, D.A. and K.E. Easterling, *Phase transformation in metals and alloys*. 2nd ed. 1992, Cheltenham: Stanley Thornes.
111. Kurz, W. and D.J. Fisher, *Fundamentals of solidification*. 4th ed. 2005: Trans Tech Publications Ltd.
112. Topping, C., *Effect of electron beam in reducing molecular weight of foam patterns*. 2009: Daventry.
113. Hill, R., *Personal communication*. 2008: Department of Materials, Imperial College, London.
114. Kadoya, K., N. Matsunaga, and A. Nagashima, *Viscosity and thermal conductivity of dry air in the gaseous phase.* J. Phys. Chem. Ref. Data, 1985. **14**: p. 947-968.
115. Younglove, B.A. and H.J.M. Hanley, *The viscosity and thermal conductivity coefficients of gaseous and liquid argon.* J. Phys. Chem. Ref. Data, 1986. **15**: p. 1323-1337.
116. *Styrene*. 1999 [cited 2011, 11th September]; Available from: http://cameochemicals.noaa.gov/chris/STY.pdf.

9 APPENDIX I X-RAY OBSERVATION OF LFC

10APPENDIX II Results of the fluidity tests.

Table 10-1 Results of the fluidity test, cast at 780 ^{o}C using high permeability coating of 0.3 mm thickness (1).

Casting conditions (A1)								
Foam			Type			EPS		
			Density (kgm $^{-3}$)			27		
Coating			Type			High permeability		
			Thickness (mm)			0.33		
Casting Temperature (^{o}C)			784					
Alloy			2L99					
Results detail								
Fluidity Length (mm)								
Level	Head height (mm)	L1	L2	L3	L4	Sum	Mean	Standard Deviation
1	260	295	245	275	295	1180	277	23
2	210	360	285	245	270	1096	274	57
3	160	280	260	255	260	1052	263	11
4	110	280	270	265	255	1068	267	10

Front Curvature –Radius (mm)				
level	R1	R2	R3	R4
1	20	20	20	20
2	20	17	22	22
3	22	22	20	23
4	20	27	20	20

Total length (mm)	4396	Mean (mm)	274
Side1	Mean (mm)	285	
	Total (mm)	2280	
Side2	Mean (mm)	264	
	Total (mm)	2116	

- One of the fluidity strips located at the second level was considerably longer than the others as it was filled completely, highlighted in table.

Table 10-2 Results of the fluidity test, cast at 780 ^{o}C , high permeability coating of 0.3 mm thickness (2).

Casting conditions (A2)								
Foam		Type			EPS			
		Density (kgm $^{-3}$)			27			
Coating		Type			High permeability			
		Thickness (mm)			0.36			
Casting Temperature (^{o}C)		783						
Alloy		2L99						
Results detail								
Fluidity Length (mm)								
Level	Head height (mm)	L1	L2	L3	L4	Sum	Mean	Standard Deviation
1	260	310	320	290	300	1120	305	13
2	210	300	300	280	290	1170	292	9
3	160	280	305	260	250	1095	274	24
4	110	240	260	230	260	1096	247	15

Front Curvature –Radius (mm)				
level	R1	R2	R3	R4
1	12	27	21	15
2	20	19	20	18
3	17	16	22	17
4	26	16	20	25

Total length(mm)	4475	Mean (mm)	280
Side1	Mean (mm)	289	
	Total (mm)	2315	
Side2	Mean (mm)	270	
	Total (mm)	2160	

Table 10-3 Results of the fluidity test, cast at 780 ^{o}C , high permeability coating of 0.3 mm thickness (3).

Casting conditions (A3)								
Foam			Type			EPS		
			Density (kgm $^{-3}$)			27		
Coating			Type			High permeability		
			Thickness (mm)			0.29		
Casting Temperature (^{o}C)			778					
Alloy			2L99					
Results detail								
Fluidity Length (mm)								
Level	Head height (mm)	L1	L2	L3	L4	Sum	Mean	Standard Deviation
1	260	340	255	315	275	1185	296	38
2	210	310	275	280	260	1125	281	21
3	160	260	215	240	250	965	241	19
4	110	250	285	225	270	1030	257	26

Front Curvature –Radius (mm)				
level	R1	R2	R3	R4
1	15	22	25	21
2	22	23	17	20
3	20	22	23	25
4	21	24	26	21

Total length(mm)	4304	Mean (mm)	269
Side1	Mean (mm)	264	
	Total (mm)	2112	
Side2	Mean (mm)	273	
	Total (mm)	2184	

In this test a series of successive thermocouples were inserted into the foam pattern.

Table 10-4 Results of the fluidity test, cast at 780 ^{o}C using high permeability coating of 1.3 mm thickness.

Casting conditions (B)								
Foam		Type			EPS			
		Density (kgm $^{-3}$)			27			
Coating		Type			High permeability			
		Thickness (mm)			1.4			
Casting Temperature (^{o}C)		783						
Alloy		2L99						
Results detail								
Fluidity Length (mm)								
Level	Head height (mm)	L1	L2	L3	L4	Sum	Mean	Standard Deviation
1	260	245	285	295	290	1112	278	22
2	210	230	245	290	265	1028	257	25
3	160	240	260	255	230	984	246	13
4	110	255	260	295	235	1044	261	24

Front Curvature –Radius (mm)				
level	R1	R2	R3	R4
1	25	26	21	14
2	22	22	22	28
3	21	25	20	17
4	22	16	15	22

Total length(mm)	4168	Mean (mm)	260
Side1	Mean (mm)	252	
	Total(mm)	2016	
Side2	Mean (mm)	269	
	Total (mm)	2144	

- The casting strips located in the first level (260 mm head height) have a non-smooth and irregular shape front.

Table 10-5 Results of the fluidity test, cast at 780 ^{o}C using low permeability coating of 0.3 mm thickness (1).

Casting conditions (C1)								
Foam			Type			EPS		
			Density (kgm $^{-3}$)			27		
Coating			Type			Low permeability		
			Thickness (mm)			0.3 (not measured)		
Casting Temperature (^{o}C)			776					
Alloy			2L99					
Results detail								
Fluidity Length (mm)								
Level	Head height (mm)	L1	L2	L3	L4	Sum	Mean	Standard Deviation
1	260	185	180	195	205	764	191	11
2	210	160	170	235	255	820	205	47
3	160	155	190	235	185	764	191	33
4	110	175	170	185	235	764	191	29

Front Curvature –Radius (mm)				
level	R1	R2	R3	R4
1	16	20	18	20
2	25	20	22	22
3	16	25	27	22
4	22	17	16	17

Total length (mm)	3112	Mean (mm)	195
Side1	Mean (mm)	252	
	Total(mm)	2016	
Side2	Mean (mm)	269	
	Total (mm)	2144	

Table 10-6 Results of the fluidity test, cast at 780 ^{o}C using low permeability coating of 0.3 mm thickness (2).

Casting conditions (C2)								
Foam		Type			EPS			
		Density (kgm $^{-3}$)			27			
Coating		Type			Low permeability			
		Thickness (mm)			0.3			
Casting Temperature (^{o}C)		780						
Alloy		2L99						
Results detail								
Fluidity Length (mm)								
Level	Head height (mm)	L1	L2	L3	L4	Sum	Mean	Standard Deviation
1	260	180	186	195	155	716	176	14
2	210	185	163	153	178	679	169	12
3	160	154	189	150	148	641	160	16
4	110	169	176	160	178	683	170	7

Front Curvature –Radius (mm)				
level	R1	R2	R3	R4
1	12	27	21	15
2	20	19	20	18
3	17	16	22	17
4	26	16	20	25

Total length(mm)	2719	Mean (mm)	170
Side1	Mean (mm)	175	
	Total (mm)	1400	
Side2	Mean (mm)	164	
	Total (mm)	1312	

- The filled strips are rough and irregular at the tip.
- The strips at the 3rd and the 4th levels of the casting are not filled vertically at the tip. It might be due to entrapment of some gaseous by-product of the foam degradation.

Table 10-7 Results of the fluidity test, cast at 780 ^{o}C using low permeability coating of 1.3 mm thickness (1).

.Casting conditions (D1)								
Foam			Type			EPS		
			Density (kgm $^{-3}$)			27		
Coating			Type			medium permeability *		
			Thickness (mm)			1.37		
Casting Temperature (^{o}C)			784					
Alloy			2L99					
Results detail								
Fluidity Length (mm)								
level	Head height (mm)	L1	L2	L3	L4	Sum	Mean	Standard Deviation
1	260	190	185	200	360	935	233	84
2	210	170	185	225	195	775	193	23
3	160	190	195	295	195	875	218	50
4	110	200	270	185	205	860	215	37

Front Curvature –Radius (mm)				
level	R1	R2	R3	R4
1	12	27	21	15
2	20	19	20	18
3	17	16	22	17
4	26	16	20	25

Total length (mm)	3445	Mean (mm)	215
Side1	Mean (mm)	198	
	Total (mm)	1585	
Side2	Mean (mm)	232	
	Total (mm)	1860	

- The casting strips located in the first level (260mm head height) have a non-smooth and irregular shape front at the tip.
- The standard deviations of the filled lengths are considerably higher indicating difference in the fluidity lengths of the casting at different levels (head height).
- * The coating used in this test was the medium permeability coating instead of low permeable coating as the low permeable coating was run out.

Table 10-8 Results of the fluidity test, cast at 780 ^{o}C using low permeability coating of 1.3 mm thickness (2).

Casting conditions (D2)								
Foam		Type			EPS			
		Density (kgm $^{-3}$)			27			
Coating		Type			medium permeability *			
		Thickness (mm)			1.45			
Casting Temperature (^{o}C)		787						
Alloy		2L99						
Results detail								
Fluidity Length (mm)								
level	Head height (mm)	L1	L2	L3	L4	Sum	Mean	Standard Deviation
1	260	245	210	225	225(t)	904	226	14
2	210	240	175	255	255	924	231	38
3	160	220	190	210	230	848	212	17
4	110	220	210	250	260	940	235	23

Front Curvature –Radius (mm)				
level	R1	R2	R3	R4
1	17	22	25	21
2	21	26	30	24
3	17	21	17	23
4	25	20	22	27

Total length (mm)	3616	Mean (mm)	226
Side1	Total (mm)	1712	
	Mean (mm)	208	
Side2	Total (mm)	1904	
	Mean (mm)	238	

- The coating used in this test was the medium permeability coating instead of low permeable coating as the low permeable coating was run out.
- In this test a series of successive thermocouples were inserted into the foam pattern.

Table 10-9 Results of the fluidity test, cast at 680 ^{o}C using high permeability coating of 0.3 mm thickness.

Casting conditions (E)								
Foam			Type			EPS		
			Density (kgm $^{-3}$)			27		
Coating			Type			High permeability		
			Thickness (mm)			0.3		
Casting Temperature (^{o}C)			685					
Alloy			2L99					
Results detail								
Fluidity Length (mm)								
level	Head height (mm)	L1	L2	L3	L4	Sum	Mean	Standard Deviation
1	260	205	215	200	200	820	205	7
2	210	240	195	245	190	870	217	29
3	160	195	235	185	170	785	196	27
4	110	190	215	175	170	750	187	20
Front Curvature –Radius (mm)								
level		R1		R2		R3		R4
1		15		22		20		19
2		18		20		15		15
3		15		22		20		16
4		18		25		22		20
Total length (mm)		3225			Mean (mm)		201	
Side1		Mean (mm)			211			
		Total (mm)			1690			
Side2		Mean (mm)			191			
		Total (mm)			1535			

Table 10-10 Results of the fluidity test, cast at 680 ^{o}C using high permeability coating of 1.3 mm thickness.

Casting conditions (F)								
Foam			Type			EPS		
			Density (kgm $^{-3}$)			27		
Coating			Type			High permeability		
			Thickness (mm)			1.3		
Casting Temperature (^{o}C)			681					
Alloy			2L99					
Results detail								
Fluidity Length (mm)								
level	Head height (mm)	L1	L2	L3	L4	Sum	Mean	Standard Deviation
1	260	215	195	215	215	840	210	10
2	210	245	175	210	290	920	230	49
3	160	235	215	210	220	880	220	10
4	110	200	190	200	245	835	208	24
Front Curvature –Radius (mm)								
level	R1	R2	R3	R4				
1	15	22	22	20				
2	17	19	20	25				
3	15	20	18	14				
4	27	25	25	29				
Total length (mm)	3475		Mean (mm)	217				
Side1	Mean (mm)	208						
	Total (mm)	1670						
Side2	Mean (mm)	225						
	Total (mm)	1805						

Table 10-11 Results of the fluidity test, cast at 680 ^{o}C using low permeability coating of 0.3 mm thickness.

Casting conditions (G)								
Foam		Type			EPS			
		Density (kgm^{-3})			27			
Coating		Type			Low permeability			
		Thickness (mm)			0.37			
Casting Temperature (^{o}C)		680						
Alloy		2L99						
Results detail								
Fluidity Length (mm)								
level	Head height (mm)	L1	L2	L3	L4	Sum	Mean	Standard Deviation
1	260	165	190	185	190	730	182	12
2	210	185	185	165	*	535	178	12
3	160	225	185	185	160	755	188	26
4	110	200	200	160	180	740	185	19

Front Curvature –Radius (mm)				
level	R1	R2	R3	R4
1	12	27	21	15
2	20	19	20	18
3	17	16	22	17
4	26	16	20	25

Total length (mm)	2760	Mean (mm)*	180
Side1	Mean (mm)	191	
	Total (mm)	1535	
Side2	Mean* (mm)	175*	
	Total (mm)	1225	

* one of the branches (second level) was not filled at all which might be due to breaking of the foam pattern during the moulding process; therefore the mean fluidity length was calculated based on data from 15 branches.

Table 10-12 Results of the fluidity test, cast at 680 ^{o}C , low permeability coating of 1.3 mm thickness (1).

Casting conditions (H1)								
Foam		Type			EPS			
		Density (kgm $^{-3}$)			27			
Coating		Type			Low permeability			
		Thickness (mm)			1.36			
Casting Temperature (^{o}C)		677						
Alloy		2L99						
Results detail								
Fluidity Length (mm)								
level	Head height (mm)	L1	L2	L3	L4	Sum	Mean	Standard Deviation
1	260	60	30	70	55	216	54	17
2	210	105	85	105	80	376	94	13
3	160	95	100	95	100	392	98	3
4	110	85	100	105	100	388	97	8

Front Curvature –Radius (mm)				
level	R1	R2	R3	R4
1	25	26	21	14
2	22	22	22	28
3	21	25	20	17
4	22	16	15	22

Total length (mm)	1372	Mean (mm)	86
Side1	Mean (mm)	83	
	Total (mm)	664	
Side2	Mean (mm)	88	
	Total (mm)	708	

Table 10-13 Results of the fluidity test, cast at 680 ^{o}C , low permeability coating of 1.3 mm thickness (2)

Casting conditions (H2)								
Foam			Type			EPS		
			Density (kgm $^{-3}$)			27		
Coating			Type			Low permeability		
			Thickness (mm)			1.3		
Casting Temperature (^{o}C)			676					
Alloy			2L99					
Results detail								
Fluidity Length (mm)								
level	Head height (mm)	L1	L2	L3	L4	Sum	Mean	Standard Deviation
1	260	75	95	115	115	400	100	19
2	210	110	90	115	120	435	100	13
3	160	35	105	115	95	350	87	35
4	110	115	85	85	80	365	91	16

Front Curvature –Radius (mm)				
Level	R1	R2	R3	R4
1	15	18	25	22
2	25	20	16	16
3	20	25	25	27
4	28	30	28	24

Total length (mm)	1536	Mean (mm)	96
Side1	Total (mm)	704	
	Mean (mm)	88	
Side2	Total (mm)	840	
	Mean (mm)	105	

- In this test a series of successive thermocouples was inserted into the foam strips.

Table 10-14 Results of the fluidity test, cast at 680 ^{o}C using high permeability coating of 0.3 mm thickness and brominated EPS foam pattern.

Casting conditions (I)								
Foam			Type			Brominated EPS		
			Density (kgm $^{-3}$)			30		
Coating			Type			High permeability		
			Thickness (mm)			0.36		
Casting Temperature (^{o}C)			685					
Alloy			2L99					
Results detail								
Fluidity Length (mm)								
level	Head height (mm)	L1	L2	L3	L4	Sum	Mean	Standard Deviation
1	260	195	195	195	165	752	188	15
2	210	195	175	190	170	732	183	11
3	160	205	210	190	195	800	200	9
4	110	185	220	220	195	820	205	17

Front Curvature –Radius (mm)				
level	R1	R2	R3	R4
1	20	22	23	25
2	21	24	26	21
3	22	23	26	20
4	25	22	23	24

Total length (mm)	3104	Mean (mm)	194
Side1	Mean (mm)	198	
	Total (mm)	1580	
Side2	Mean (mm)	190	
	Total (mm)	1524	

- The fluidity test was carried out using the brominated EPS foam pattern to study the effect of using easily decomposable foam pattern on the fluidity properties of the LFC.
- In this test a series of successive thermocouples were inserted into the foam pattern.

Table 10-15 Results of the fluidity test, cast at 680 ^{o}C using high permeability coating of 0.3 mm thickness and low molecular weight copolymer of (70wt.% PMMA and 30wt.% PS)- 71,000 gmol $^{-1}$.

Casting conditions (J)								
Foam		Type	Probead-70 (70wt.% PMMA and 30wt.% PS)- M_w of 320,000 gmol^{-1}					
		Density (kgm $^{-3}$)	24					
Coating		Type	High permeability					
		Thickness (mm)	0.28					
Casting Temperature (^{o}C)		683						
Alloy		2L99						
Results detail								
Fluidity Length (mm)								
level	Head height (mm)	L1	L2	L3	L4	Sum	Mean	Standard Deviation
1	260	195	180	230	160	765	191	29
2	210	180	235	200	185	800	200	24
3	160	190	205	210	170	775	193	17
4	110	180	200	200	155	735	183	21

Front Curvature –Radius (mm)				
level	R1	R2	R3	R4
1	18	25	21	23
2	25	19	25	17
3	22	25	29	26
4	24	23	20	19

Total length (mm)	3075	Mean (mm)	192
Side1	Mean(mm)	196	
	Total (mm)	1565	
Side2	Mean(mm)	185	
	Total(mm)	1510	

- The fluidity test was carried out using low molecular weight copolymer of (70wt. % PMMA and 30wt. % PS) having the molecular weight of 71,000 gmol $^{-1}$.

Table 10-16 Results of the fluidity test, cast at 680 ^{o}C using high permeability coating of 0.3 mm thickness and low density EPS foam pattern.

Casting conditions (K)								
Foam			Type			EPS		
			Density (kgm $^{-3}$)			16		
Coating			Type			High permeability		
			Thickness (mm)			0.3 (not measured)		
Casting Temperature (^{o}C)			683					
Alloy			2L99					
Results detail								
Fluidity Length (mm)								
level	Head height (mm)	L1	L2	L3	L4	Sum	Mean	Standard Deviation
1	260	360	360	360	360	1440	360	0
2	210	360	360	360	360	1440	360	0
3	160	360	360	360	360	1440	360	0
4	110	360	360	360	360	1440	360	0

Front Curvature –Radius (mm)				
level	**R1**	**R2**	**R3**	**R4**
1	∞	∞	∞	∞
2	∞	∞	∞	∞
3	∞	∞	∞	∞
4	∞	∞	∞	∞

Total length (mm)	5760	Mean (mm)	360
Side1	Mean (mm)	360	
	Total (mm)	2760	
Side2	Mean (mm)	360	
	Total (mm)	2760	

- The fluidity test was carried out using low density foam pattern (EPS). This facilitates studying the effect density of the foam pattern in fluidity of the LFC.

Table 10-17 Results of the fluidity test, cast at 680 ^{o}C using high permeability coating of 0.3 mm thickness and Probead-70™ foam pattern.

Casting conditions (L)								
Foam		Type	Probead-70 (70wt.% PMMA and 30wt.% PS)- M_w of 320,000 $gmol^{-1}$					
		Density (kgm^{-3})	24					
Coating		Type	High permeability					
		Thickness (mm)	0.31					
Casting Temperature (^{o}C)		685						
Alloy		2L99						
Results detail								
Fluidity Length (mm)								
level	Head height (mm)	L1	L2	L3	L4	Sum	Mean	Standard Deviation
1	260	195	195	185	175	825	206	33
2	210	185	230	200	195	820	205	24
3	160	175	195	235	185	790	197	27
4	110	185	215	175	175	750	187	20

Front Curvature –Radius (mm)				
level	R1	R2	R3	R4
1	20	22	15	19
2	23	25	26	24
3	24	26	29	24
4	22	15	26	36

Total length (mm)	796	Mean (mm)	199
Side1	Mean(mm)	205	
	Total (mm)	1645	
Side2	Mean(mm)	192	
	Total(mm)	1540	

11APPENDIX III CONFERENCE PAPAERS

11th INALCO conference 'New Frontiers in Light Metals' June 2010, Eindhoven,

THE EFFECT OF REDUCING MOLECULAR WEIGHT OF THE FOAM PATTERN ON THE POROSITY OF Al ALLOY CASTINGS IN THE LOST FOAM CASTING PROCESS

[1]K. SIAVASHI, [2]C. TOPPING and [3]W. D. GRIFFITHS

1. School of Metallurgy and Materials, College of Engineering and Physical Sciences, University of Birmingham, Birmingham, United Kingdom. B15 2TT. Tel: +44(0)121 414 3443. Email: kxs729@bham.ac.uk, (corresponding author).
2. Isotron, Brunel Close, Daventry, United Kingdom. NN11 8R. Tel: +44(0)132 770 1483. Email: clare.topping@isotron.com.
3. School of Metallurgy and Materials, College of Engineering and Physical Sciences, University of Birmingham, Birmingham, United Kingdom. B15 2TT. **Tel:** +44(0)121 414 5246. **Email:** w.d.griffiths@bham.ac.uk.

ABSTRACT

Lost foam casting offers freedom of design. However the quality of the castings obtained is often reduced by entrapment of degradation byproducts from the foam pattern. These can be absorbed by the permeable pattern coating, once heat from the liquid metal reduces their molecular weight sufficiently, which suggests that starting with a low molecular weight pattern may lead to higher quality castings. The molecular weight of expanded polymethylmethacrylate-polystyrene copolymer foam patterns was reduced by exposure to γ-radiation, and then cast with an Al-7Si-0.3Mg alloy. The porosity of the castings was reduced by as much as 77%, compared to the porosity of castings produced with unirradiated foam patterns.

Introduction

The Lost Foam casting (LFC) process uses an expanded foam pattern, usually expanded polystyrene (EPS) in the case of Al casting, or a copolymer of polystyrene (PS) and polymethylmethacrylate (PMMA) for ferrous castings. The expanded foam shapes are assembled to make a cluster using a hot wax adhesive, given a thin layer of a permeable refractory coating and, once dried, surrounded by vibrated, compacted dry sand in a moulding box. The pattern is not removed, but when the molten metal is poured into the mould it causes the foam pattern to degrade; the liquid metal thus replaces the pattern gradually to fill the mould and achieve the final cast shape.

The pattern decomposition by-products consist of vapour and liquid polymer. The permeable refractory coating on the pattern allows the vapour by-products to escape, and also absorbs the liquid polymer residue. The quality of Lost Foam castings is often reduced due to entrapment of these vapour and liquid by-products in the liquid metal during the mould filling process; therefore study of the degradation by-product removal mechanisms is essential to improve casting quality.

In the case of Al casting, the pattern breaks down predominantly to a viscous liquid residue, which when transported to the metal-coating interface can be wicked into the permeable coating [1]. Davies and Griffiths examined the molecular weight of the liquid polymer degradation by-product, and concluded that a critical molecular weight, and hence critical viscosity, was necessary for its absorption into the pattern coating [2]. Casting experiments showed that when the liquid polymer degradation products are displaced to the metal-coating interface they would form globules of polymer which may remain for some time after the advancing metal front has passed. Once sufficient degradation has occurred the polymer is wicked into the coating [2,3].

This understanding of the behaviour of the liquid polymer residue suggests that low molecular weight (Mw) foams may be a more desirable pattern material than the currently used expanded polystyrene (EPS), (which

typically has a molecular weight of greater than 300,000 $gmol^{-1}$ [2]). Beginning with a low molecular weight (Mw) foam, (perhaps lower than the critical Mw for wicking into the permeable coating), may assist the removal mechanisms of the pattern decomposition by-products.

Chain scission is the breaking of a molecular bond causing the loss of a side group or shortening of the overall chain [4]. This can be achieved by γ-irradiation, in the case of polymethylmethacrylate (PMMA), while irradiation of polystyrene does not have the same effect on Mw, due to the stabilising presence of the aromatic ring which promotes cross-linking reactions. Polymethylmethacrylate is more susceptible to reductions in Mw when exposed to high doses of radiation, due to the predominance of chain scission over cross-linking reactions [5].

Pure PMMA was not available in foamed form; hence a foamed copolymer of polystyrene (PS) and PMMA was used in these experiments instead. The work reported here was aimed at exploring the effect of using γ-irradiation to reduce the molecular weight of this copolymer foam pattern material, and determining the effect of using these low molecular weight foam patterns on the quality of Al alloy castings.

Experimental Procedure

Foam patterns consisting of a copolymer of 70wt.% PMMA and 30wt.% PS in the shape of rectangular plates, of dimensions 450 x 180 x 10 mm, were exposed to γ-irradiation (using a cobalt-60 source) in order to reduce their molecular weight. The foam patterns were exposed to dosages of up to about 190 MRad. Before irradiation, the foam patterns were sealed in polythene bags under a vacuum of 0.5 bar to attempt to minimize the presence of oxygen and reduce cross-linking. In addition to γ–irradiation of the copolymer foam patterns, the effects of different parameters such as irradiation with or without vacuum, irradiation of a copolymer or of pure foam PMMA, and irradiation using γ-rays or an electron beam, (E-beam), were also compared.

Following the irradiation procedure**,** the Mw of the irradiated foam patterns was measured using Gel Permeation Chromatography (GPC) by Rapra Technology (Shrewsbury, UK). The GPC system used for this work was calibrated with polystyrene calibrants and all of the results were expressed as 'polystyrene equivalent' Mw. It should be appreciated that there could be considerable differences between these polystyrene equivalents and the true Mw of the samples which is common in conventional GPC, although comparisons between results obtained in this work would still be valid.

Strips of dimensions 10 x 40 x 300 mm were cut from the irradiated foam patterns, coated with a high permeability coating of thickness 0.3 mm, and cast horizontally with 2L99 aluminium alloy (Al-7wt.%Si-0.3wt.%Mg) with a pouring temperature of 780°C and 150 mm head height. All castings filled completely.

The quality of the castings made in this way were characterised by measurement of their porosity content, obtained by image analysis of samples cut from the centre line of the castings, ground and polished to 1 μm. The defects of particular interest were internal porosity, and surface concavities thought to be associated with the entrapment of liquid polymer degradation byproducts at the casting-coating interface. The internal porosity was characterised by measurement of their total area, while the surface concavities, which were only found on the bottom casting surface, were characterised by measurement of their total length and frequency.

To examine the effect of irradiation of the foam patterns on mechanical properties of the castings obtained, test bars were taken from the centre line of the castings, (of dimensions 8 x 8 mm cross-section and 70 mm gauge length), and subjected to tensile testing at a strain rate of 1 mm min^{-1}. In addition, 3 point bending was used to determine what effect the γ-irradiation had on the mechanical properties of the irradiated copolymer foams. This was carried out on samples of dimensions 80 x 50 x 10 mm, subjected to a 30 kg load applied at 5 mm min^{-1}.

Results

The results showed that γ-irradiation reduced the Mw of the foam patterns significantly, (by up to 85%). The original foam patterns had a Mw of about 325,000 $gmol^{-1}$, which was reduced according to the amount of irradiation received, to values as low as about 45,000 $gmol^{-1}$, as shown in Figure 1.

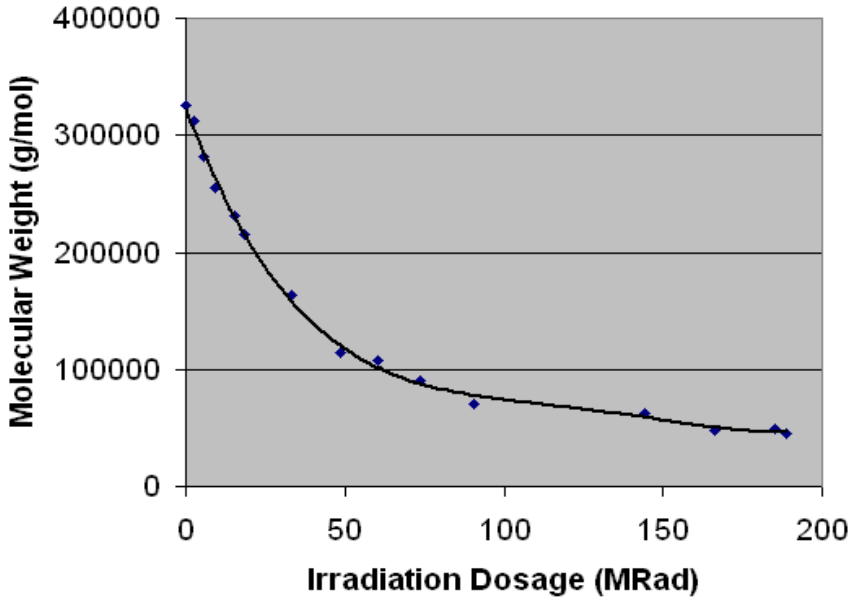

Figure 1. The effect of γ-irradiation on molecular weight.

Figure 2 shows micrographs of defects found at the base of the horizontal strip castings, thought to be due to the occurrence of globules of liquid polymer degradation products trapped at the casting-coating interface. The Figure shows the globules to be associated with porosity in the casting immediately above, showing that at least some of the casting porosity was caused by gas evolved from the trapped globule, travelling upwards through the liquid metal.

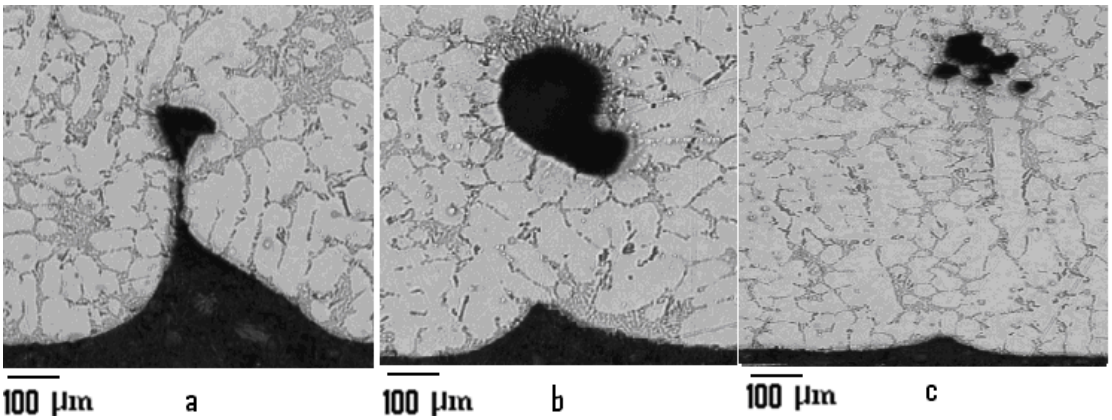

Figure 2. Defects occurring at the base of the castings. (a) Casting made with unirradiated foam pattern, (b) and (c) castings made with irradiated foam patterns, (30 and 75 MRad respectively).

Figure 3 shows the porosity content of the castings made with irradiated foam was reduced as the foam pattern molecular weight was reduced, from about 1.6% in the casting made with the unirradiated foam, to about 0.4% in the casting made with the most irradiated foam (189 MRad, Mw of about 45,000 $gmol^{-1}$. In other words, the porosity content of the castings was decreased by up to 85% due to irradiation of the foam patterns. A Fisher test confirmed that the porosity content of the castings made with unirradiated foam and with the most irradiated foam were statistically different at the 99% confidence limit.

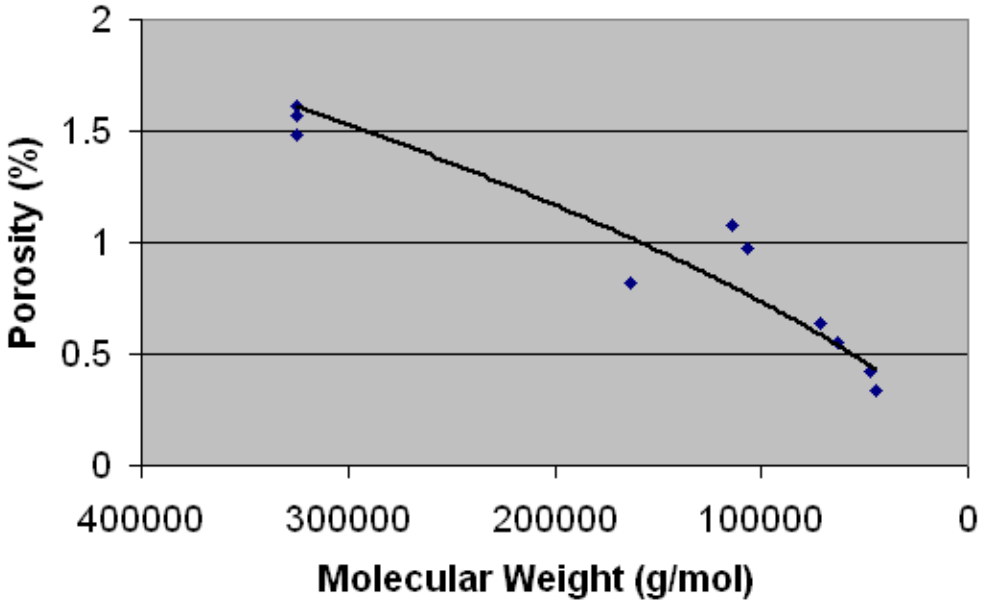

Figure 3. Graph showing porosity content of the castings reduced by decreasing the Mw of the foam pattern.

Figure 4 shows a correlation of the total length of the globular defects found at the base of the castings, measured on a length of 25 mm, with casting porosity content. Figures 2 and 4 therefore suggest that porosity content of the castings increased with size of the globular defects at the base of the castings, and that the total area of the porosity associated with the liquid globules trapped during mould filling decreased with γ-irradiation of the foam pattern.

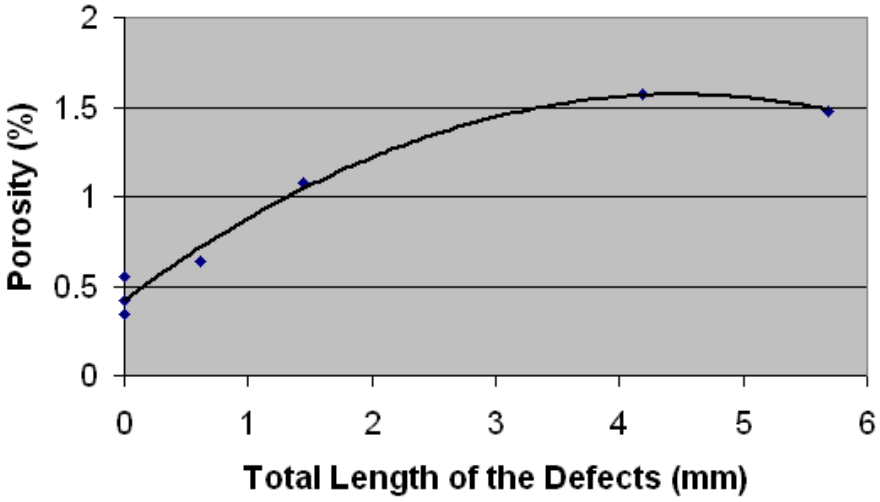

Figure 4. Graph showing relationship between porosity content of the castings made with foam patterns of different Mw, related to the total length of the defects found on the surface of the base of the horizontally cast plates.

The UTS of the castings made with γ-irradiated foam patterns increased slightly with decreasing molecular weight, as shown in Figure 5. A Fisher test confirmed that the UTS of the castings made with the unirradiated foam, and made with the most irradiated foam (189 MRad), were statistically different at the 99.9% confidence limit.

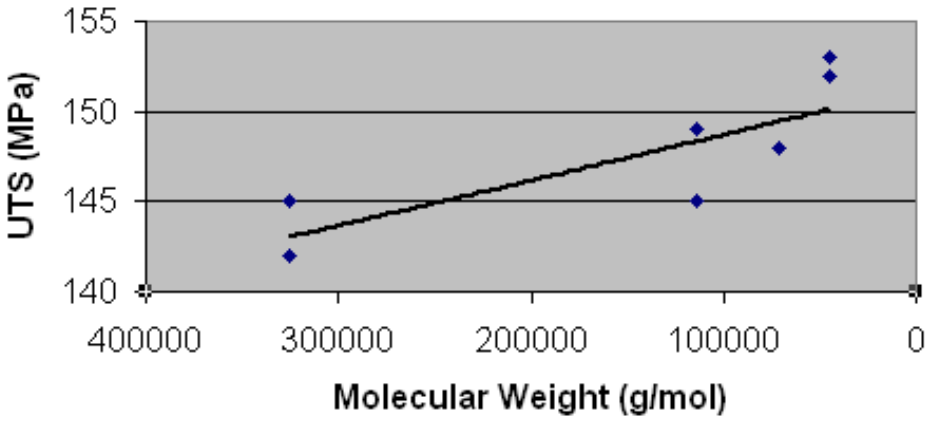

Figure 5. Graph showing Ultimate Tensile Strength of test bars of Al-7Si-0.3Mg alloy related to the Mw of the patterns used.

To determine whether irradiation of the foam would cause a decrease in foam mechanical properties, and therefore make the foam patterns unacceptably fragile during mould preparation, the maximum load at fracture of irradiated foam samples was determined using a 3-point bend test. This is plotted against Mw of the foam patterns in Figure 6, and shows a reduction in maximum load at failure with increasing irradiation and decreasing Mw. The maximum reduction of foam strength was about 60%, which occurred in the most irradiated foam (189 MRad).

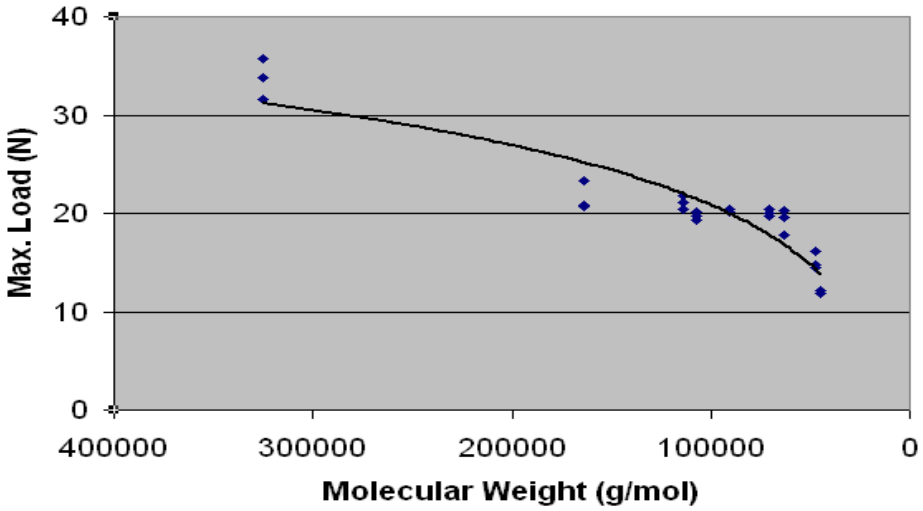

Figure 6. Results of 3 point bending tests on the irradiated foam patterns, showing that foam strength was reduced by reduction of its molecular weight by γ-irradiation.

Irradiating the copolymer foam patterns using the E-beam process, to deliver 80 MRad exposure, reduced the Mw of the foam sample by 67%, compared to its original Mw. In contrast, when the same exposure was delivered by γ radiation, a 74% reduction in Mw was obtained, (extrapolated from Figure 1). This implies that the effect of the E-beam was slightly less than that of γ irradiation. This is due to the difference in the residence time of the samples in front of the radiation sources, as obtaining 80 MRad from the E-beam process can be achieved much more quickly than by irradiation with γ sources (by about 25 times). A shorter irradiation time

reduces the amount of ozone initiated oxidation and therefore the opportunity for chain scission and cross-linking reactions.

To compare with the effect obtained with the foamed PMMA-PS copolymer, pure PMMA powder and pure EPS were both exposed to 100 MRad of γ radiation. The pure PMMA powder showed a marked reduction in Mw (by 95%) while pure EPS did not experience any reduction in Mw. This illustrated that the foamed PPMA-PS copolymer owed its reduction in Mw to the effect of radiation on the PMMA.

Finally, the amount of reduction in Mw of the foam patterns when irradiated under normal atmospheric conditions was found to be the same as that obtained when irradiation occurred under 0.5 bar pressure.

Discussion

The correlation between porosity and the defects at the base of the castings, shown in Figures 2 and 4, is support for the wicking and wetting theory of Zhao et al. [3] and Davies and Griffiths [6]. These results confirm that if the liquid degradation products displaced to the casting-coating interface do not reach the critical Mw, they can release bubbles of gas into the liquid metal, increasing the porosity content of the casting.

The GPC analysis, measuring Mw of the irradiated foams, showed an obvious reduction in Mw (by 85% for an irradiation of 189 MRad); therefore the Mw below the critical value for wicking into the coating suggested by Davies and Griffiths, (about 70,000 g/mol for a high permeability coating) [2], was achieved. Figure 7 shows the distribution of foam pattern Mw and the porosity content, related to the critical Mw proposed for wetting of the pattern coating by the liquid polymer residue, and wicking of the liquid polymer residue into the coating, (for a high permeability coating). Assuming that the Mw measured in these experiments for the copolymer is comparable to the Mw measurement results from the degraded PS experiments of Davies and Griffiths [2,6], the most irradiated foam samples reached a Mw just below the critical value for wicking into the coating. These foam patterns resulted in castings with the least porosity. However, the desirable Mw for patterns for Lost Foam casting is yet unknown. Very low Mw foam patterns may cause some other defects in the casting process, for example, a more rapid evolution of gas from the more rapidly-degrading foam.

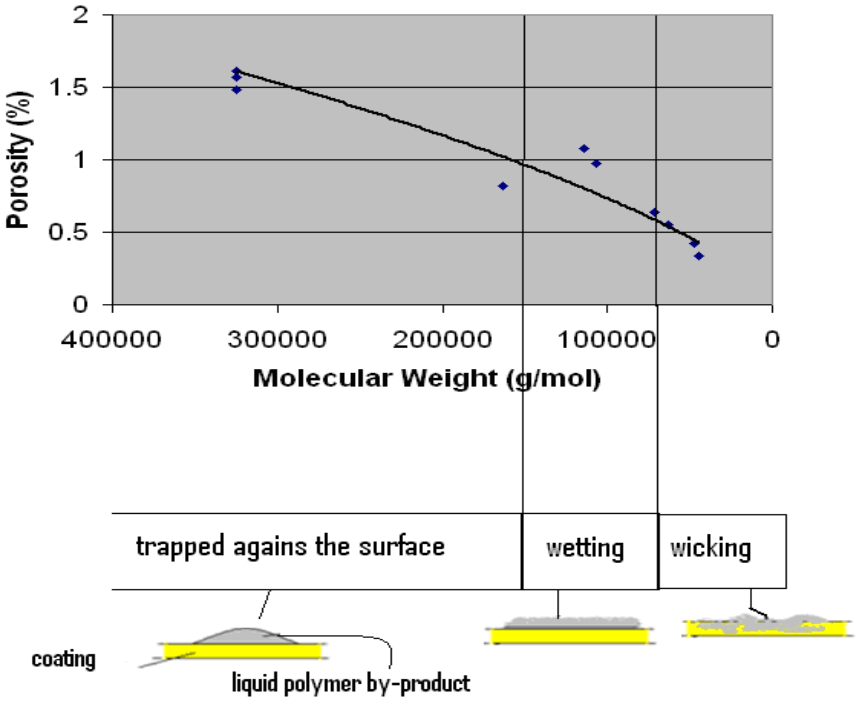

Figure 7. Relationship between casting porosity and Mw of the foam patterns related to the Mw at which wetting and wicking can occur, (for a high permeability coating).

The results also found that the PMMA part of the copolymer foam pattern probably experienced the major part of the Mw reduction by γ-irradiation. This emphasizes the role of the conjugated aromatic ring in the styrene in increasing the radiation resistance of polystyrene, thereby decreasing the efficiency of Mw reduction due to increasing cross-linking.

Although pure PMMA foam responded better to irradiation with respect to its Mw reduction than the copolymer, casting with low Mw pure PMMA may not result in a good casting because, for example, it may lead to a larger gap between the liquid metal front and the foam pattern, perhaps resulting in the collapse of the surrounding moulding sand into the gap. Furthermore, low Mw foam patterns made from pure PMMA might increase the difficulties associated with making the pattern cluster in the LFC process, as reducing the Mw of the foam may make the patterns unacceptably fragile, as suggested by Figure 6.

It was also found that, while the E-beam was not quite as effective as γ rays in reducing the Mw of the foam patterns, the dose rate of the E-beam irradiation was significantly higher than for γ irradiation. Therefore, assuming that there is no unwanted heating of the pattern, and associated distortion, E-beam irradiation would be the preferred method of Mw reduction.

While the statistical test showed that the tensile properties of the castings made from reduced Mw foam patterns were improved, compared to conventional LFC, the amount of improvement was small (6%). It would be of interest to examine the fatigue lives of castings made with low Mw foam patterns, as less porous samples should give much improved fatigue properties.

Conclusions

1. The molecular weight of PMMA-PS copolymer foam patterns is reduced by γ- and E-beam irradiation.

2. The porosity content of Al alloy castings produced by the Lost Foam casting process was reduced by using reduced molecular weight foam patterns.

3. γ-irradiation of the foam patterns reduced their fracture strength in 3-point bending, and may make more difficult the cluster making process.

4. Pure PMMA foam was associated with a greater reduction in molecular weight than the PS-PMMA copolymer, while pure EPS did not show any reduction in molecular weight with γ-irradiation.

5. E-beam irradiation would be the preferred method of molecular weight reduction compared to γ irradiation, due to its higher irradiation rate.

References

1. Sun, Y., Tsai H. L., Askeland D. R., Investigation of Wetting and Wicking Properties of Refractory Coating in the EPC Process, AFS Trans.100(1992) 297.

2. Davies P.J., Griffiths W.D., The Role of the Pattern Coating in the Lost Foam Casting of Aluminium, 12th International Metallurgy and Materials Congress, Istanbul, Turkey, September 2005.

3. Zhao, Q., Burke J. T., Gustafson T. W., Foam Removal Mechanism in Aluminium Lost Foam Casting, AFS Trans.110 (2002) 1399.

4. Singh A., Silverman J., Radiation Processing of Polymers, Hanser, New York, 1991.

5. Hill R., Personal Communication, Department of Materials, Imperial College London, UK, 2008.

6. Davies P.J., Griffiths W.D., Wicking of Liquid Polystyrene Degradation Products into the Pattern Coating in the Lost Foam Casting Process, 67th World Foundry Congress, Harrogate, UK, June 2006.

Shape casting, 4th International Symposium, 2011, San Diego, California

THE EFFECT OF REDUCING MOLECULAR WEIGHT OF THE FOAM PATTERN ON THE PROPERTIES OF CASTINGS IN THE LOST FOAM CASTING PROCESS

[1]K. SIAVASHI, [2]C. TOPPING and [1]W. D. GRIFFITHS

1 School of Metallurgy and Materials, College of Engineering and Physical Sciences, University of Birmingham, Birmingham, United Kingdom. B15 2TT
2 Isotron, Brunel Close, Daventry, United Kingdom. NN11 8RB

Keywords: Aluminium alloys, lost foam casting, mechanical properties, ɣ radiation, molecular weight.

ABSTRACT

In Lost Foam casting heat from the cast liquid metal causes the foam pattern to degrade and results in the evolution of gas and formation of liquid polymer byproducts. These can cause cause a reduction in the casting quality if they become entrapped in the liquid metal. However, the liquid polymer byproducts can be absorbed by the permeable pattern coating, once their molecular weight (Mw) is sufficiently reduced by the action of heat. Therefore using a lower molecular weight (Mw) pattern may lead to higher quality castings because less reduction in Mw will be required before absorption of the liquid polymer byproduct into the pattern coating. The Mw of expanded copolymers foam patterns can be reduced by exposure to γ-radiation. The properties of castings made with irradiated foam patterns, such as porosity content and fatigue properties, were compared with the properties of castings made from unirradiated foam, to show the advantages of using the former.

Introduction

In the Lost Foam casting process the pattern is constructed of polystyrene (PS) foam, coated with a permeable refractory layer, typically about 500 μm in thickness. This is placed into a moulding box and surrounded by loose, unbonded silica sand, which is compacted by vibration. The mould is then cast, with the polystyrene (PS) pattern being degraded by the heat from the liquid metal, to form the desired cast shape.

The process confers great freedom of design compared to conventional casting processes. Complex patterns can be made by joining together simpler shapes and cored features can be formed *in situ*, reducing machining costs. However, the degradation of the polystyrene pattern produces liquid and gaseous byproducts, and if these become entrapped in the liquid metal during mould filling, the quality of the final casting can be considerably reduced.

Significant effort has been put into studying the thermal decomposition of the foam pattern and the removal mechanisms of the degradation byproducts over the last 20 years, for example, by Zhao et al. [1], Shivkumar et al. [2], Liu et al. [3], Caulk [4], Barone et al. [5], Molibog et al. [6], Sun et al. [7] and Hill et al. [8]. Previous research has suggested that an important feature of the process is the permeable pattern coating, through which the pattern degradation products must pass. In the case of casting with liquid Al alloys, the pattern tends to degrade to form a mostly liquid residue. It has been proposed that the permeable pattern coating absorbs the liquid polystyrene residue by a wicking action [7], although alternative suggestions have been put forward [1]. Detailed investigation suggested that once the liquid polystyrene residue degraded to reach a critical molecular weight (Mw), (and hence critical viscosity), absorption into the pattern coating occurs. For example, for a coating permeability of 1.2×10^{-12} m^2, the polystyrene, with initial Mw of 325,000 $gmol^{-1}$, is wicked into the coating once the liquid degradation byproduct reaches a Mw of about 70,000 $gmol^{-1}$ [9].

This suggests that improved Lost Foam castings could be obtained if the material used for the pattern possessed a lower initial molecular weight. The liquid polystyrene residue might then reach the critical Mw for wicking into the pattern coating more quickly, and be removed more easily. This would presumably reduce the likelihood of it being entrained in the casting, improving casting properties.

Apart from polystyrene, foam patterns are also made out of a copolymer of PS and polymethylmethacrylate (PMMA). The Mw of the latter can be reduced by γ-radiation, (which does not have the same effect on

polystyrene) [10]. The results presented in this paper show how using irradiated foam patterns can produce improved castings.

Experimental Procedure

Rectangular plates of a copolymer of 70wt.% PMMA and 30wt.% PS (PROBEAD-70) with a thickness of 10 mm, and length and width 180 x 450 mm, respectively, were irradiated by a cobalt-60 γ-ray source in order to reduce their Mw. The foam plates were exposed to dosages of up to about 190 MRad. In addition to this, the effect of foam type, (the copolymer or pure PMMA*)*, and irradiation source*, (*γ-rays or an electron beam), were also compared. The resulting foam patterns were cast with an Al-Si-Mg alloy, and the quality of the resulting castings characterised. Another copolymer *(PROBEAD-30, COPOL 1.3) (*30wt.% PMMA and 70wt.% PS*),* was also exposed to an electron beam to reduce its Mw with dosages of up to about 180 *MRad.* The effect of irradiating the foam patterns was established by measuring their Mw and polydispersity using *Gel Permeation* Chromatography (GPC), carried out by Rapra Technology (Shrewsbury, UK). The results of the GPC measurements were expressed as 'polystyrene equivalent' Mw, rather than absolute values of Mw, but comparisons between results obtained within this work would still be valid.

In order to ascertain the effect of γ–irradiation on the mechanical properties of the irradiated foams, *a* 3 point bending test was carried out on samples of dimensions 80 x 50 x 10 mm, subjected to a 30 kg load applied at 5 mm min^{-1}.

Foam strips were then cast of dimensions 10 x 40 x 300 mm, with a 0.3 mm layer of a high permeability coating (1.2×10^{-12} m^2) and cast horizontally with 2L99 alloy (Al-7wt.%Si-0.3wt.%Mg) at 780°C and 150 mm head height. All castings filled completely.

To characterize the quality of the castings obtained, their porosity was measured by image analysis, carried out on polished samples taken from the centre line of the castings. Defects such as internal porosity and surface cavities are considered to be associated with the entrapment of liquid polymer degradation byproducts at the casting-coating interface. The internal porosity was characterised by measurement of the total porosity area, while the surface cavities, which were only found on the bottom casting surface, were characterised by measurement of their total length and frequency.

To establish the effect of using reduced Mw foam patterns on the mechanical properties of lost foam Al alloy castings, a fatigue test was used. Test bars, of dimensions 10 x 40 x 300 mm, were taken from the centre line of the strip castings, and given a T6 heat treatment, (solutionised at 535°C for 12 hours, aged at 135°C for 6 hours). These samples were subjected to a high cycle fatigue test using 4 point bending, with maximum and minimum forces of 2.5 and 0.25 kN, frequency of 67 Hz, and loading span on the top and bottom of the specimens of 20 mm and 60 mm, respectively. The samples were placed in the fatigue test with their as-cast surfaces intact, arranged so that the base of the casting faced downwards. This meant that the surface containing the cavities were suspected of being associated with liquid polymer degradation byproducts trapped at the casting-coating interface, experienced the maximum stress.

Results

In Figure 1 the Mw of the foam pattern is plotted against the irradiation dosage received. The foam pattern (PROBEAD-70) had an original Mw of about 325,000 $gmol^{-1}$, which was reduced according to the amount of irradiation received, to values as low as about 45,000 $gmol^{-1}$ with the maximum γ-irradiation, (a dosage of 189 MRad). The other copolymer type, which is usually used for ferrous castings, (COPOL 1.3) also showed a reduction in its Mw due to the effect of the electron beam irradiation. The original Mw of the COPOL 1.3 was 271,000 $gmol^{-1}$ and it was reduced to about 86,000 $gmol^{-1}$ by exposure to 160 MRad.

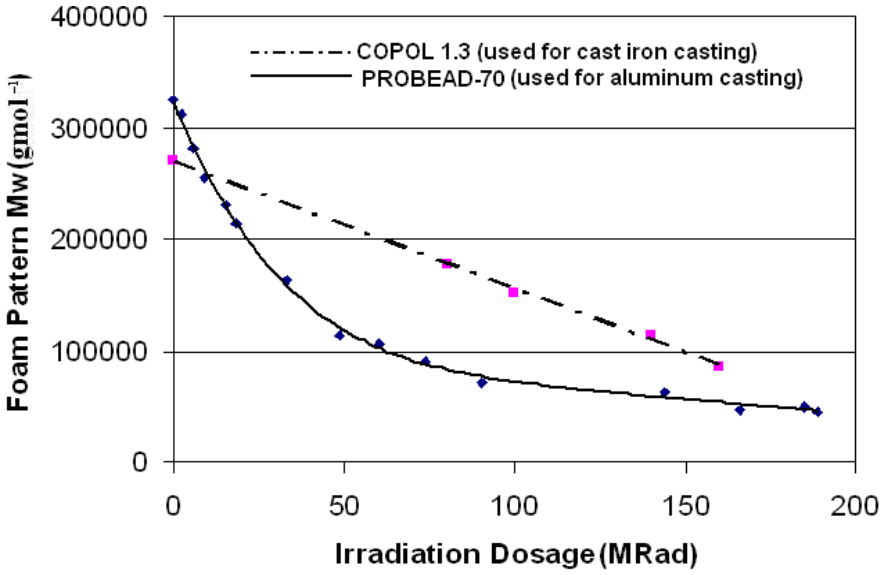

Figure 1. The effect of γ-irradiation on Mw of different types of foam pattern .

As the Mw of the foam pattern was reduced by irradiation, the mechanical properties of the foam pattern decreased. The maximum load at fracture plotted against Mw of the foam pattern, has been shown in Figure 2. The maximum reduction of foam strength in the most irradiated foam pattern (189 MRad), was about 60%.

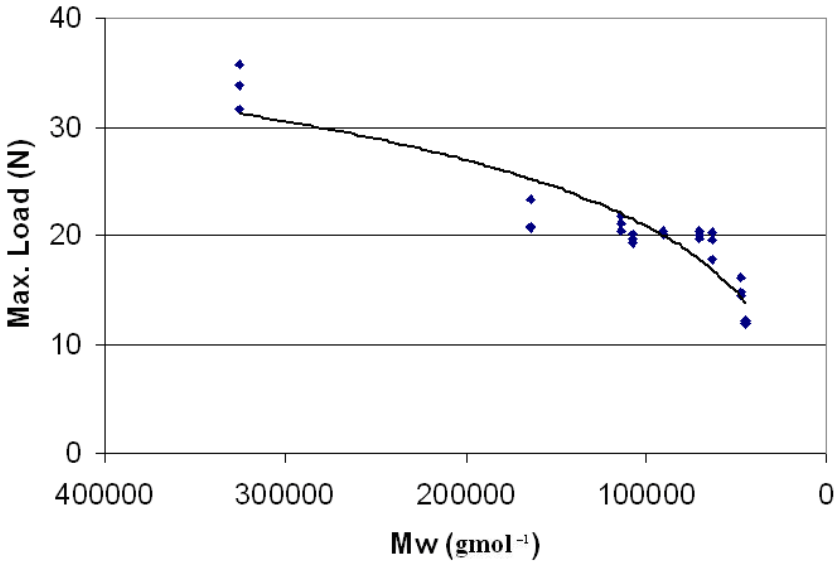

Figure 2. Results of 3 point bending tests on the irradiated foam patterns (PROBEAD-70), showing that foam strength was reduced by reduction of its Mw by γ-irradiation.

Figure 3 shows how the porosity content of the aluminium alloy castings made with the irradiated foam patterns was reduced as the Mw of the foam pattern was reduced. The porosity content of the casting made with an unirradiated foam pattern (Mw of 325,000 $gmol^{-1}$) was about 1.6%, and was reduced to about 0.4% in the casting made with the most irradiated foam (Mw of about 45,000 $gmol^{-1}$). In other words, the porosity content of the castings was decreased to about 25% of the original porosity, by irradiation of the foam patterns. A Fisher test confirmed that the porosity content of the castings made with unirradiated foam and with the most irradiated foam were statistically different at the 99% confidence limit.

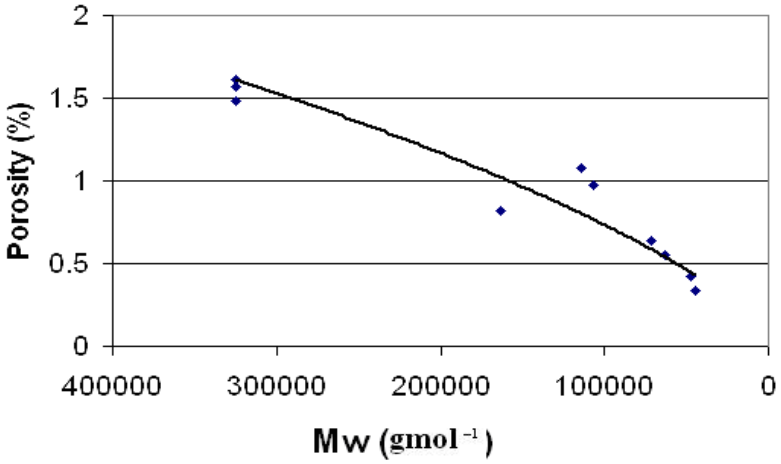

Figure 3. Graph showing porosity content of the aluminium castings reduced by decreasing the Mw of the foam pattern (PROBEAD -70).

The castings showed defects (cavities) at the base of the cast strips, thought to be associated with globules of liquid polymer degradation byproduct trapped at the casting-coating interface. This is shown in Figure 4, where the surface cavities were associated with porosity immediately above them, indicative of gas released by the liquid polymer degradation product rising up through the liquid metal above and becoming trapped in the solidifying casting. Figure 5 shows the total length of defects found at the base of the horizontal casting strips decreased with decreasing Mw of the foam pattern used, in agreement with the reduction internal casting porosity.

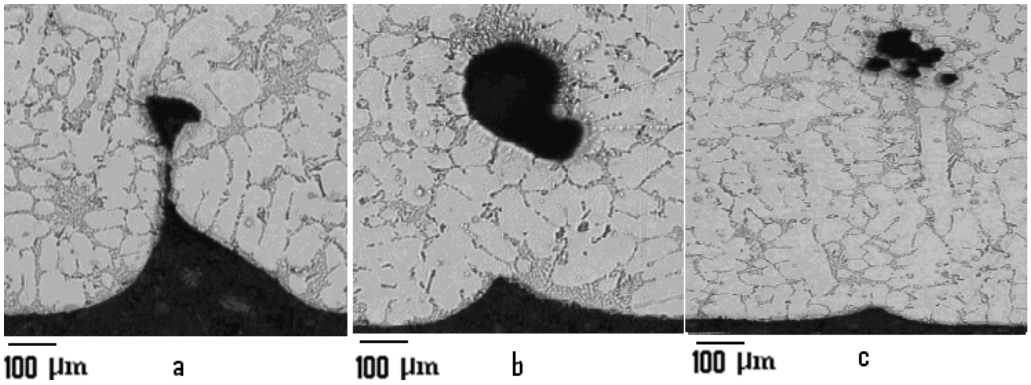

Figure 4. Defects occurring at the base of the castings. (a) Casting made with unirradiated foam pattern, (b) and (c) castings made with irradiated foam patterns, (30 and 75 MRad respectively).

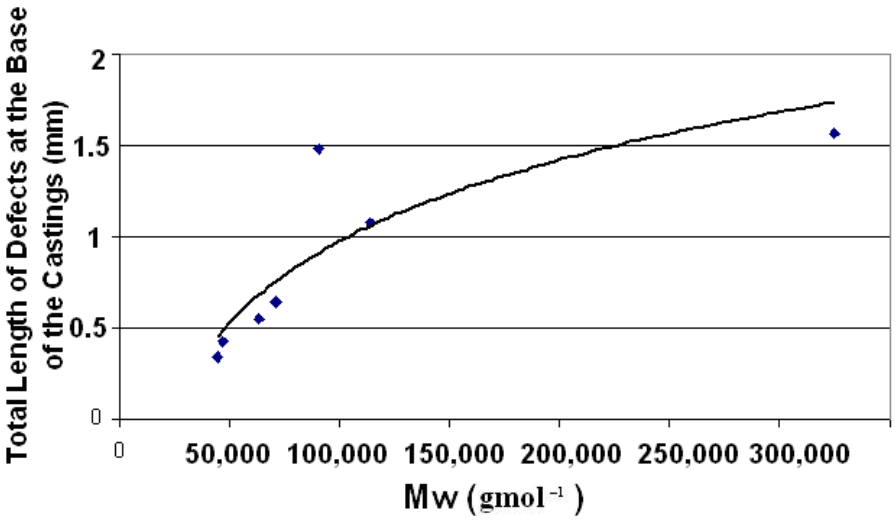

Figure 5. Graph showing the relationship between Mw of the foam patterns (PROBEAD-70) related to the total length of the defects found on the bottom surface of the horizontally cast plates.

Figure 6 illustrates how, when the Mw of the initial foam pattern was lower than the critical value, (which was about 70,000 $gmol^{-1}$ in the case of the high permeability coating used here), the fatigue properties of the castings were much higher than when the castings were made with the unirradiated foam pattern (with an initial Mw of 32500 $gmol^{-1}$). The castings made with the foam pattern exposed to about 144 MRad of γ-radiation, (Mw of 63,000 $gmol^{-1}$), had a fatigue life increased to nearly twice that of castings made with the conventional, unirradiated patterns.

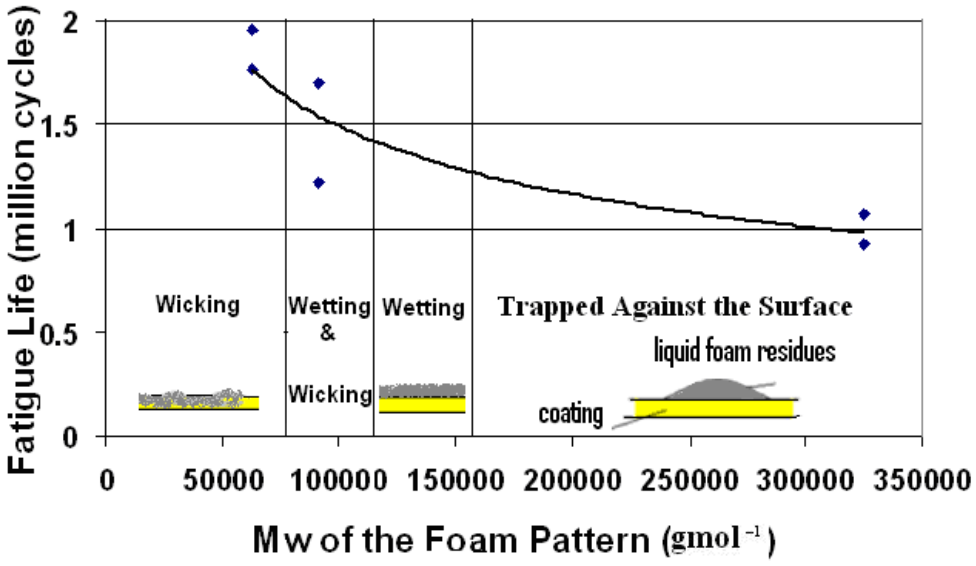

Figure 6. Results of fatigue test showing that fatigue properties of the heat treated samples improved by irradiation of the foam patterns used in the casting process.

The SEM results of the fracture surface of the specimens illustrated that the failure of the castings made with an irradiated foam pattern with Mw of 63,000 $gmol^{-1}$, occurred due to a small surface-breaking defect on the bottom surface of the casting (see Figure 7b). However the initiation of the fatigue failure of the casting made with an unirradiated foam pattern was due to a near-surface pore with a diameter 4 times greater than that of the former defect (Figure 7a).

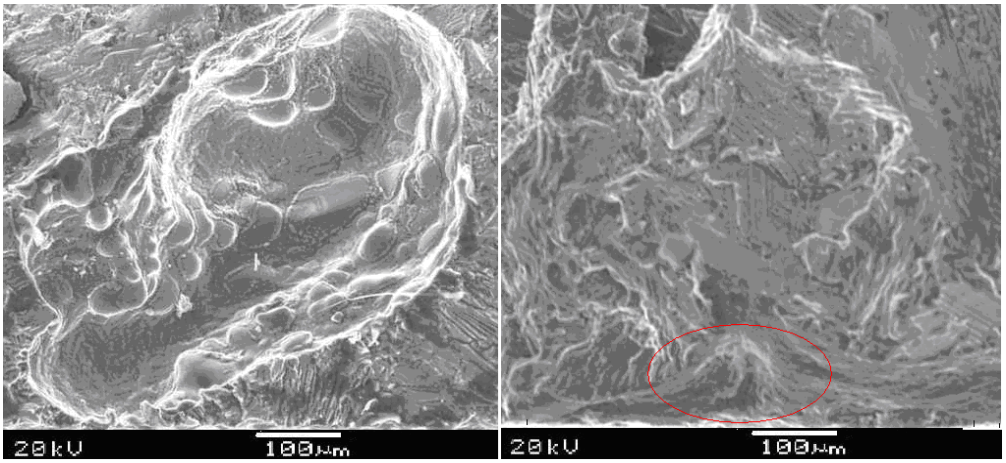

Figure 7. Graph showing the SEM results of the fracture surface from fatigue test. (a) casting with unirradiated foam pattern (Mw of 32563,000 $gmol^{-1}$) and (b) casting with the irradiated foam pattern (144 MRad, Mw of 63,000 $gmol^{-1}$).

Discussion

Irradiation of the copolymer foam patterns reduced the Mw significantly, and this was observed in the case of both copolymer types, containing 70% PMMA / 30% PS and 30% PMMA / 30% PS. The reduction in Mw, for any dose of γ-radiation, was greatest in the case of the 70% PMMA copolymer, than in the case of the 30% copolymer, (see Figure 1). Irradiation of pure polystyrene foam (PS) had no measurable effect on molecular weight. These results were obtained by γ-irradiation, but a faster alternative would be to use an E-beam irradiation method, where electrons are driven through the polymer foam structure instead of γ-irradiation. This is substantially faster, about 25 times, (and was used here to prepare the patterns used for cast iron Lost Foam casting).

Irradiation of pure PMMA foam reduced the Mw significantly, (by up to 95%), i.e., the effect of irradiation increased in effectiveness with increasing amounts of PMMA in the foam patterns. However, the foam structure was obviously damaged by the radiation dose, with the pattern becoming friable and unusable for moulding. In the case of the copolymers, irradiation reduced mechanical properties, as shown by the 3-point bending test results in Figure 2, but the foam patterns were still readily useable.

The effect of the γ-irradiation is to reduce molecular weight by chain scission. In the case of polystyrene, this chain scission is accompanied by cross-linking, which prevents any reduction in Mw; PMMA, on the other hand, has its molecular weight reduced progressively by increasing amounts of chain scission with increasing radiation [10,11].

Measurement of the porosity content of the Lost Foam aluminium castings showed that this was related to defects on the bottom surface of the horizontally cast flat strips, (see Figure 5). Reducing the initial Mw of the foam pattern to, or below, the critical value to cause wicking of the liquid polymer byproduct into the coating reduced casting porosity, (see Figure 3). Since the casting porosity is thought to be associated with the surface defects caused by entrapment of the liquid polymer byproducts at the casting-coating interface, it follows that reducing the initial Mw of the pattern reduces the extent of these surface defects, (for example, as shown in Figure 7), and this is reflected in the improved fatigue properties associated with irradiated foam patterns, Figure 6.

Conclusions

1. The Mw of foam patterns containing polymethylmethacrylate (PMMA) was decreased by γ-irradiation and electron beam irradiation.
2. The reduction in Mw due to irradiation increased in effectiveness with increasing amounts of PMMA in the foam patterns.

3. Irradiating the copolymer foam patterns up to values of 189 MRad reduced their flexural modulus, but they could still be used in the casting process. However, when pure PMMA was given a 100 MRad dose, it became too friable to be used.
4. The porosity content of the castings was reduced by reducing the Mw of the foam patterns used in the casting process.
5. The defects at the bottom surface of the castings, due to the entrapment of the liquid polymer degradation byproducts at the casting-coating interface, were shorter than in the case of conventional Lost Foam casting, when reduced Mw foam patterns were used.
6. The fatigue life of the castings was increased by reducing the Mw of the foam patterns used in the casting process, probably because the critical Mw for wicking the liquid pattern degradation byproduct into the permeable coating was more quickly reached.
7. Electron beam irradiation is the preferred method of reducing the pattern Mw, as it was found to be about 25 times quicker in delivering the same dosage as γ-radiation.

References

1. Zhao Q., Burke J.T. and Gustafson T.W., Foam Removal Mechanism in Aluminium Lost Foam Casting, AFS Trans., 110, 2002, pp. 1399-1414.
2. Shivkumar S. and Gallois B., Physico-Chemical Aspects of the Full Mold Casting of Aluminum Alloys, Part I: The Degradation of Polystyrene, AFS Trans.**,** 95, 1987, pp. 791-800.
3. Liu X.J., Bhavnani S.H. and Overfelt R.A., Simulation of EPS Foam Decomposition in the Lost Foam Casting Process, J. Mat. Proc. Technol., 182, 2007, pp. 333-342.
4. Caulk D.A., A Foam Melting Model for Lost Foam Casting of Aluminum, Int. J. Heat and Mass Trans., 49, 2006, pp. 2124–2136.
5. Barone M. and Caulk D., Analysis of Mold Filling in Lost Foam Casting of Aluminum: Method, Int. J. Metalcasting, 2008, 2, (part 3), 29-43.
6. Molibog T.V. and Littleton H., Degradation of Expanded Polystyrene Patterns, AFS Trans., 110, 2002, pp. 1483-1496**.**
7. Sun Y., Tsai H.L. and Askeland D.R., Investigation of Wetting and Wicking Properties of Refractory Coating in the EPC Process, AFS Trans., 1992, 100, pp. 297-308.
8. Hill M., Vrieze A.E., Moody T.L., Ramsay C.W. and Askeland D.R., Effect of Metal Velocity on Defect Formation in Al LFCs, AFS Trans., 106, 1998, pp. 365-374.
9. Griffiths W.D. and Davies P.J., Wetting and Wicking of Liquid Polymer Degradation Byproducts into the Pattern Coating during Lost Foam Casting of Al Alloys, Int. J. Cast Met. Res., in press.
10. Hill, R., Imperial College, pers. comm., 2009.
11. Wilson, J.E., Radiation Chemistry of Monomers, Polymers and Plastics, Marcel Dekker, New York, (1974).